1995

Field study of a steel plate-girder bridge, Final Report, Vol. II of PennDOT Project 86-05, May 1995

Ben T. Yen

Ti Huang

David A. VanHorn

COMMONWEALTH OF PENNSYLVANIA

Department of Transportation

Office of Research and Special Studies

Research Project No. 86-05
Field Testing of a Steel Bridge and a Prestressed Concrete Bridge

FINAL REPORT
Vol. II
FIELD STUDY OF A STEEL PLATE-GIRDER BRIDGE

by

Ben T. Yen
Ti Huang
David A. VanHorn

Prepared in cooperation with the Pennsylvania Department of Transportation and the U.S. Department of Transportation, Federal Highway Administration.

LEHIGH UNIVERSITY

Office of Research and Sponsored Program
Bethlehem, Pennsylvania

May 1995

Fritz Engineering Laboratory Report No. 519.2

Table of Contents

(continued)

Table of Contents (continued)

1. INTRODUCTION

Two highway bridges have been monitored for the determination of (1) stresses and deflections developed during construction, and (2) stresses under traffic loads after completion. The primary purpose of this study was to use stress data based on measured strains to evaluate the adequacy of several commercially available finite element programs which are being used for the analysis and design of bridge superstructures. This report describes the study conducted on a steel plate girder bridge which carries the east bound traffic on the I-78 highway over the Delaware River near Easton, Pennsylvania. A separate report describes the study of the second bridge in this project, a prestressed concrete beam bridge across the Susquehanna River at Milton, Pennsylvania[1].

The research reported herein was conducted by Lehigh University under the Pennsylvania Department of Transportation Research Project 86-05. The tasks completed by Lehigh University included the field measurement of plate girder deflections and strains during the casting of the reinforced concrete deck slab, the measurement of strains under various vehicular loading conditions, the comparison of stresses based on measured strains with those obtained from four commercially available computer programs, and field observation of the behavior of the webs of the plate girders during construction as well as under traffic load.

The computer program results were supplied by Modjeski and Masters, Inc. of Camp Hill, Pennsylvania, under a separate contract with the Pennsylvania Department of Transportation. The Lehigh University researchers had no direct interaction with the providers of the various

computer-based analysis and design programs. The specific tasks performed by Lehigh University on the I-78 Bridge are as follows:

1. Measurement of the dead load stresses in the plate girders caused by the sequential casting of the reinforced concrete deck slab.
2. Measurement of the deflections of the plate girders caused by the sequential casting of the reinforced concrete deck slab.
3. Measurement of lateral deflection of some web panels of the plate girders caused by formwork and the casting of reinforced concrete deck slab.
4. Measurement of strains in girders and deck for determination of the structural response of the bridge superstructure to simulated AASHTO and PennDOT design vehicular loads.
5. Measurement of strains in girders and deck for determination of the structural response of the bridge superstructure to normal in-service traffic loads.
6. Comparison of the stresses based on field measurements with corresponding stress values obtained from four commercially available finite element computer programs.
7. Evaluation of the fatigue life of the web panels.
8. Evaluation and recommendation of supporting methods for the formwork for the overhanging portion of the deck slab, and development of design recommendations to ensure the appropriate behavior of web panels with respect to fatigue.

2. GENERAL DESCRIPTION OF THE STRUCTURE AND INSTRUMENTATION

2.1 Description of the Bridge

The bridge under study is a seven-span structure near Easton, Pennsylvania. It carries the Interstate Highway I-78 across the Delaware River. The bridge has a total length of 1222 ft., and is divided into two separate, identical structures carrying the east-bound and west-bound traffic. All of the field study was conducted on the east-bound structure. The overall deck slab width, from outside to outside of the parapet wall, is 51 ft. 6 in. The span lengths are 100 ft., 169 ft., 228 ft., 228 ft., 228 ft., 169 ft. and 100 ft. Fig. 2.1 shows the plan and elevation of the east bound structure.

The main superstructure elements of this bridge consist of four welded plate girders, spaced at 14 ft. 3 in. center to center. The depth of the web plate (inside to inside of the flange plates) varies from 82 inches in the end spans to 90 inches in the three longest spans. The web depth for the 169-ft. spans is tapered.

Figure 2.2 shows the variation of the plate girder dimensions. As indicated, the flange plate size, the web plate thickness, and the grade of steel all change over the length of the bridge. Typically, the top flange plate of the steel girder is smaller than the bottom flange plate, since the top flange will eventually be completely encased in the concrete slab.

Figure 2.3 shows a typical cross-section of the bridge. The deck slab is symmetrically placed over the four plate girders. However, the 36 ft. wide vehicular roadway, comprising three operating traffic lanes, is

slightly shifted inward (towards the twin structure), leaving shoulder widths of 4-ft. and 8 ft. respectively. As a result, the fascia girders are expected to carry a relatively small portion of the truck loads.

The plate girders were initially fabricated in segments of 100 ft. to 120 ft. lengths. These segments were then spliced in the field with high-strength bolts, and diaphragms were installed. Stay-in-place metal deck forms were then placed, shear stud connectors were attached to the top flange plates, deck reinforcing bars were placed, and the concrete deck slab was cast. By this method of construction, the entire dead load, including the self-weight of the girders and the concrete deck, is supported by the steel plate girders. The concrete deck is effective only for loads applied after the hardening of the deck slab.

The placing of the concrete deck was done in segments symmetrically located with respect to the mid-span section of central span over a period of 20 days from Oct. 15 to Nov. 3, 1987. The positive moment regions were cast first, then the segments near the points of inflection in the longest spans. The negative moment regions over the interior piers were cast at last. This sequence of casting minimizes dead load stresses in the deck concrete. Figure 2.4 shows the sequence of slab casting.

Two phenomena were observed during the construction of this bridge, and led to supplemental tasks in this study. These are listed as items 3, 7 and 8 on page 2, Chapter 1. The metal deck formwork for the overhanging portion of the deck slab was supported by struts bearing against the web plate of the fascia girder, approximately 38 in. below the top flange. (See Fig. 2.5) The force in these struts caused the web plate to deflect inwards, resulting in a relatively large magnitude of out-of-flatness.

This condition could be related to the separation of the metal deck formwork that was observed at one location in the westbound structure.

Large magnitudes of out-of-flatness (or bulges) were also observed on some web panels of the interior plate girders, although these panels were not subjected to thrusts from formwork struts. In addition, the magnitudes of these deflections were observed to change with time. It was suspected that many factors may contribute to these bulges, including the sequence of deck slab placement, the shrinkage of deck concrete, the fixity of the bridge bearings and the thermal fluctuations of the ambient condition. Under vehicular loads, these deflections, or bulges, exhibit lateral (horizontal) movements. There was concern that the stresses associated with these lateral movements may cause fatigue damage along the web panel boundaries.

Fig. 2.6 shows the bridge structure under construction. The plate girders in spans 1 through 5 are in place. The metal deck forms have not yet been placed.

2.2 Description of Instrumentation

2.2.1 Strain Gages on Girder Flanges

Flexural strains in the steel plate girders were monitored using ¼ in. long, temperature-compensated, electric resistance strain gages mounted on the top and bottom flanges. The general layout of the strain gage locations is given in Fig. 2.7. Nine cross-sections, near quarter span points in spans 2,3 and 4, were instrumented. A total of 72 strain gages were used, all oriented in the longitudinal direction. At each

instrumented section of each plate girder, two gages were mounted on the upper surface of the top flange, and one gage on the upper surface of the bottom flange. The top flange gages were placed near the edges of the flange plate. The bottom flange gage was placed as close as convenient to the web plate. As a rule, the bottom flange gages on girders 1 and 2 were placed on the north side of the web, while those on girders 3 and 4 were on the south side. Tables 2.1 to 2.4 give the precise location of each gage.

Each of the flange gages is identified by an alphanumeric code which describes the location of the gages. For example, gage 243TS is located in span 2 (from the west end of the structure), on girder number 4 (from the south side), near the 3rd quarter point of the span (from the west end of the span, in this case pier 1), on the top flange, and near the south edge. This code system is used throughout this report.

2.2.2 Strain Gages on Concrete Deck Slab

Twenty four strain gages were mounted on the concrete deck slab, along three transverse cross-sections at midspan of the spans 2 and 3, and directly above pier 2 (sections 2x2, 3x0, and 3x2). The locations of these cross sections, and those of the gages on each section, are depicted in Figures 2.7 and 2.8.

The twenty four deck slab gages are arranged into twelve 90-degree rosettes, with individual gages placed in the longitudinal and transverse directions, respectively. Each gage is given an alphanumerical code to designate its location and direction. For example, the gage 342SL is located in span 3, to the South of girder No. 4, at the 2nd quarter span

point (midspan), and in the Longitudinal direction.

In view of the unsatisfactory results regarding the deck slab strain gages on the Milton bridge [1], a different procedure was adopted for the I-78 bridges. Polyester mold gages, with a gage length of 60 mm (approx. 2½ in.)(total length approx. 5 in.) were used. (See Fig. 2.9). While these gages are originally designed for embedment inside of concrete, on this research project they were attached to the top surface of the deck slab using epoxy glue, which also provided protection against weather and traffic. The result was a resounding success. All but one of the twenty four gages functioned satisfactorily throughout the study period.

2.2.3 Strain Gages on Plate Girder Webs and Diaphragms

During and after the construction of the bridge superstructure, several web panels of the plate girders were observed to deflect laterally. In a fascia girder (No. 1 or No. 4), the formwork of the overhanging portion of the deck slab was supported by struts which bore against the web plate approximately 34 in. below the top flange. The thrust in these struts under the weight of wet concrete clearly contributed to the lateral deflection of these web panels. In one case, near the third quarter point of span 7 of the west bound structure (approximately 25 ft. from the East abutment), the metal deck slab form separated from the girder flange. Very likely, the lateral deflection of the web plate here was a contributing factor. Significant web deflections were also observed in the interior girders. Such lateral deflections caused concern regarding the behavior of the structure under traffic load and the potential of fatigue damage along the web panel boundaries.

In order to examine the stresses associated with the lateral deflection of the plate girder web panels caused by the weight of the concrete slab, and by traffic load, thirteen electric resistance strain gages were installed on the web plates at the midspan section of girder 4 in span 2, and of girders 3 and 4 in span 4 (sections 242, 432, and 442). These gages are in the vertical direction and are placed within one inch of the top flange. The designation of each gage indicates the section location, and whether it is on the south (S) or north (N) face of the web plate. A listing of these gages is given in Table 2.5. Figures 2.10 and 2.11, show detailed arrangements and location of these gages.

Recent experience in plate girder bridge structures has shown that the differential deflections between adjacent girders could induce severe bending deformations and stresses in the web plates at the diaphragm connection regions. Under live load, the fluctuations of these stresses could cause fatigue cracks to develop. The structural design of the superstructure of the I-78 bridge over the Delaware River contains several unusual features, such as the small number of main girders and the larger spacings of the very flexible section design afforded by the computer analysis and design procedure. In order to assess the diaphragm action stressed in this bridge, eighteen strain gages were mounted on various diaphragm elements at two transverse sections of the superstructure.

The two instrumented diaphragms are the third diaphragm in span 3 from its west end (pier 2), and the second diaphragm in span 2 from its east end (pier 2). (See Figure 2.9). Gages were attached to the diagonal angles, stiffener connecting plates, web plate in the gap of the stiffener

cope area, and bottom flange of the plate girder. The bottom flange gages are on the upper surface of the flange plate, near its outer edges, and oriented in the longitudinal direction of the girder. All other diaphragm gages measured strains in the plane of the diaphragm (transverse to the girder direction). The alphanumeric designation of each gage reflect the member (Diagonal, Stiffener, Web or Bottom flange), the span (2 or 3), the nearest plate girder (3 or 4), and the gage's position relative to the girder (Top or Bottom, North or South). The diaphragm gages are listed in Table 2.6. Their locations and arrangements are shown in Figures 2.10 and 2.12.

2.2.4 Instrumentation for Deflection Measurements

One of the tasks in this research project was the determination of the vertical deflections of the plate girders caused by the weight of the concrete deck slab. The elevations of girders 3 and 4 were measured by an automatic level at each quarter span point for the west half of the bridge (from the west abutment to the midspan of span 4). These measurements were taken before and after each stage of the placement of concrete. In Figure 2.4, the deflection measurement sequence and its relationship with the deck casting sequence is given. A more detailed description of the deflection measurements is given in Chapter 3 of this report.

In order to coordinate elevation readings before and after a target point has been concealed by concrete, a pedestal is attached to the top of the top flange of the plate girder. Each pedestal consisted of a No. 4 reinforcing bar with a square base-plate. Each pedestal was cut to such a length that its top extended to about 1 in. (varying from 3/8 in. to 1-¼

in. of the top surface of the concrete slab. Figure 3.2 shows a typical pedestal attached to the top flange of a plate girder.

2.2.5 Instruments for Strain Measurement

For the measurement of girder strains during bridge construction, the primary concern was the steadiness of reference for static strains. Static strain indicators and switch boxes were located in a trailer under the bridge, and were permanently connected throughout the period of concrete placement (Oct. 15 to Nov. 3, 1987). The electrical resistances of the lead wires of the strain gages were recorded and incorporated into the evaluation of strains. Repeated reading of the strain indicators demonstrated that an accuracy of 2 micro inches per inch. was achieved at all times.

For the measurement of strains due to vehicular loads, a high-precision, analog, magnetic tape recorder was used. This recorder was capable of monitoring 21 gages simultaneously. The most important quantity to be determined was the time variation of strain at each gage as the test vehicle(s) moved at various speeds on the bridge. The magnetic tape recorder permitted continuous recording of strains. The recorded live load strains were plotted as strain-time diagrams, and separately analyzed by computer for live load stress evaluation.

3. GIRDER DEFLECTIONS DUE TO PLACEMENT OF DECK SLAB

3.1 Instrumentation and Procedure

The deflections due to the placement of the deck slab concrete were measured by the standard levelling process. The level used was a Lietz B1 Automatic Level, and the standard level rod was graduated in intervals of 0.01 ft. All readings were taken to the nearest 0.005 ft.. In the determination of deflections, elevations of two of the four girders, one exterior and one interior, were determined at 15 longitudinal locations: (1) at the midspan and quarterpoints of spans 1, 2, and 3, (2) at the midspan and West quarterpoint of span 4, (3) at piers 1, 2, and 3, and (4) at the West abutment. See Fig. 2.7. A three-digit notation was used to identify the 30 locations. The first digit signifies the span (1, 2, 3, or 4); the second indicates which of the two girders (3 or 4); and the third identifies the longitudinal quarter point (0, 1, 2, or 3) in that span. Thus, location 243 indicates span 2, girder 4, three-quarter point. Location 240 indicates the "zero" - quarter point of the same span and beam (which is actually at pier 1).

The primary objective of this phase of this project was to determine the actual deflections of the two girders due to the weight of the deck slab, with the entire deck slab in place. However, the slab concrete was placed in 19 segments on 14 days, over a period of 20 days. Therefore, 13 sets of deflections were determined, one after each of the days of slab placement (with one exception). The locations of the slab segments, the placement dates, and the dates and times when elevations were recorded are all shown in Fig. 3.1.

The first set of elevations was recorded on October 14 in the period 4:15-6:00 p.m., with all slab forms in place. The second set was recorded in approximately the same time period on October 15, following the placement of slab segments 1 and 2W earlier that day. The only deviation from this procedure occurred after the placement of slab segment 7E on October 27. A heavy rain in the late afternoon on that day made it impossible to take the elevation readings that day. Therefore, the readings were resumed on October 28, after the placement of segment 7W.

In taking the 14 sets of elevation readings over the 20-day period from start to finish of the placement of concrete for the entire bridge deck, it was necessary to take readings at two different levels at each of the 30 points. All of the initial readings (on day 0), were taken on the top surface of the girders. After the slab concrete was placed in segments 1 and 2W on day 1, readings were taken on the girders at all points except 332, 432, 342, and 442, which were inaccessible because of the fresh concrete at those locations. On day 5, segment 2E (in the eastern half of the bridge) was cast. Therefore, the readings (set no. 2) were taken on the girders at all points except 332, 432, 342, and 442, where they were taken on the top surface of the slab. As the placement of the slab segments proceeded from day-to-day, each of the other 26 points was eventually covered with slab concrete, and subsequent readings were taken on the top surface of the slab.

The conversion of top-of-the-slab elevations to top-of-the-girder elevations was accomplished through the use of steel pedestals attached to the top of the girders prior to placement of any of the slab concrete. The pedestals were attached at 28 locations, all except the two abutment

locations where elevations of the abutment were used (points 130 and 140). Each pedestal consisted of a No. 4 re-bar welded to a square base plate, then coated with an epoxy paint, and attached to the top of the girder with an epoxy glue. See Fig. 3.2. Each pedestal was fabricated to extend to within ¼-inch of the top surface of the slab at its location.

To convert the top-of-the-slab elevation to top-of-the-girder elevation at each point, the slab thickness was needed. The slab thickness was equal to the known length of the pedestal plus the actual clearance from the top of the pedestal to the top surface of the slab. To obtain the actual clearance at each point, a small prism of concrete directly above the top of each pedestal was chipped away and the clearance was measured directly. Of the 28 pedestals, only one (340) was not located. Two (142 and 330) were found to be slightly tilted. All of the others appeared to be intact.

In order to provide a measurement of time-dependent and environmental effects, a set of elevations (Reading No. 14) was taken on 12 August 1988, 283 days after the deck slab had been completed (3 November 1987). The readings were taken in the period 3:20-5:00 p.m., which was in the same time interval used for all previous readings.

3.2 Results

A complete listing of all measured deflections, 14 sets of readings at 30 locations, is given in Tables 3.1 and 3.2. The variation in measured deflection at each of the points over the 14 sets of readings is presented in Fig. 3.3-3.6. This information would enable a comparison of measured deflections with theoretical values at 13 stages of the placement

of the deck slab, and at a time approximately 9 months after the slab was completed.

A comparison of measured deflections with theoretical values, at completion of the slab (Reading No. 13), is given in Fig. 3.7. A larger scale comparison is given in Figs. 3.8 and 3.9. Numerical values of the measured and theoretical deflections are given in Table 3.3. Since theoretical values at the intermediate stages were unavailable, (if computed at all), no other comparisons can be shown.

3.3 Discussion

The comparison of measured deflections with theoretical values is most vividly shown in Fig. 3.7. In spans 1 and 2 the measured values are reasonably close to the theoretical deflected shapes. Only three of the twelve measured values deviate from theoretical values by more than 0.1 in. On the other hand, the deviations in spans 3 and 4 are considerably greater, ranging from 0.7 in. greater to 1.8 in. less than theoretical values. It can be seen that in span 3, all of the measured values are less than theoretical values, while the opposite occurs in span 4. It is also noted that there is a very good consistency between the deviations in girders 3 and 4. Interestingly, the measured deflections indicate that the actual deflections in span 3 are nearly the same as the deflections in spans 4, for both girders 3 and 4.

Regarding the deflected shapes of spans 3 and 4, as shown in Fig. 3.7, it appears that manipulation of the joint rotations at piers 2 and 3 could bring the analytical values much closer to the measured values. That is, if the rotation at both piers 2 and 3 was less than shown (less

clockwise at pier 2 and less counter-clockwise at pier 3), the analytical values would be closer to the measured values.

It is understood that in the analysis which yielded the theoretical values, the supports at piers 3 and 4 were considered to be hinged, while the supports were considered to be rollers at piers 1, 2, 5, and 6, and at the abutments. In span 4, the hinged end condition would produce horizontal restraint at the bottom surface at the ends of the girders, yielding additional negative moments at the ends of span 4, which would reduce the theoretical deflections. The flexibility of piers 3 and 4 would allow horizontal movement of these hinges away from the centerline of the bridge, reduce the negative moments at the ends of the span, and result in actual deflections which are greater than the theoretical values. On the other hand, the horizontal movement of the pier 3 hinge to the left, together with some unaccounted-for restraint to horizontal movement at pier 2, would develop additional negative moments at both ends of span 3. Therefore, the actual deflections would be less than the theoretical values.

Another factor which may account for some of the differences between the actual and theoretical values is that the 19 slab segments were placed on 14 different days, thereby altering the flexural stiffnesses of the girders from day-to-day. It is understood that the theoretical analysis was based on a one-time application of the weight of the entire slab. Therefore, some difference between actual and theoretical values would be expected, even if the supports behaved as assumed in the analysis.

4. STRESSES IN GIRDERS AND WEB DEFLECTIONS DURING CONSTRUCTION

4.1 Stresses in Girders

4.1.1 Flange Stresses

A. Measured Stresses

The strains in the steel girder flanges and in a couple of web panels due to deck casting were measured after each stage of casting. Eighty strain gages were connected to strain recorders in this period. The results are listed in Appendix A. For each gage, the reading was first adjusted to account for the effect of the electrical resistance of the connecting cable to yield the strain values, which were then converted to stresses by simple multiplication by the modulus of elasticity (E_s = 29,000 ksi). The strain correction factors for the gages are listed in App. A and the stresses at several flange gage locations are given in Tables 4.1 to 4.3.

The casting of the deck took twenty calendar days (from Oct. 15 to Nov. 3, 1987) to complete, and the development of composite action between the deck concrete and the steel girders progressed as the concrete gained strength. As a result, the effective cross-sectional properties changed with time during this period. In particular, the centroidal axis of the effective girder section shifted from that of the bare girder (slightly lower than mid-height) to a position significantly higher. For example, at the cross section 432, assuming the effective deck width specified by the AASHTO Specifications[2] is applicable, the centroidal axis

shifted from about two-fifth the depth from the bottom to about four-fifth the depth. These positions are depicted in Fig. 4.1.

At this cross-section, before the casting of concrete deck, under the action of the weight of the steel girder, deck formwork and slab reinforcing steel, there existed longitudinal stresses in the flanges. These stresses could not be detected by the strain gages. The computed values from the four computer programs are all essentially identical and are shown in Fig. 4.2 as "initial" stresses (also refer to section 4.1.1 E, p.4.11). The strain gage readings before and after the casting of deck segments 1 and 2W on day 1 indicate incremental stresses in the top and bottom flanges, as shown in Fig. 4.2 for day 1. These are combined with the initial stresses to produce the cumulative stresses at the end of day 1. Similar incremental and cumulative stresses at several subsequent days are illustrated in Fig. 4.2. It is clear that the neutral axis of the composite section moved considerably with the progress of deck casting. At several stages, the entire girder was under compression. It should be pointed out that dependent upon the presence or absence of any longitudinal restraining force in the girder, the neutral axis does not necessarily coincide with the centroidal axis.

To examine the variation of stresses in the girder flanges at different locations of the bridge during concrete deck casting, the stresses converted from measured strains are plotted in Figs. 4.3, 4.4 and 4.5 for girder 3 in spans 3 and 4. Figure 4.3 shows the change of "measured" stresses in the cross section at the middle of

span 3, 332. The placement of concrete on day 1 at middle of span 4 and span 3, directly over this cross section, induced about 5.7 ksi tension in the bottom flange and about 8.5 ksi compression in the top flange of the steel girder. Relatively minor changes took place in days 5.6 and 7 (see Fig. 2.4 for casting sequences). When concrete slab was casted on days 8 and 9 in the middle of the adjacent spans 2 and 4, the tensile stress in the bottom flange (at 332B) decreased noticeably. On day 10, when segment 6W in span 3 and near the cross section was cast, the tensile stress in the bottom flange increased by about 6.8 Ksi. The change of stress was much less in the top flange in days 8, 9 and 10. After day 10 (casting of segment 6W) both flanges experienced only minor stress changes.

The change of flange stresses in cross section 432 at the middle of span 4, as shown in Fig. 4.4, was more pronounced during the stages of deck concrete casting. Several factors could possibly contributing to these results, including that (1) the span is the middle of the three longest spans of 228 ft., and (2) the span has "fixed" (non-expansion) bearings at both ends. The casting of 40 feet of deck directly above the cross section (segement 1) on day 1 caused a 4.7 ksi tension stress in the bottom flange and a 9.1 ksi compressive stress in the top flange of the plate girder. On day 9, the placement of two 33 foot segments of the deck near the cross section (segments 5E and 5W) induced an incremental tensile stress of nearly 9.0 ksi in the bottom flange while the compressive stress in the top flange only increased by about 1.6 ksi. In fact, after

the casting of concrete in the middle of this span and the adjacent spans in Days 1 and 5, the top flange compressive stress changed within a relatively narrow range, while the bottom flange stress fluctuated much more severely with each casting.

Over pier 2 at the western end of span 3, in the region of negative bending, the top flange of cross section 330 was subjected to increasingly more compression during the deck casting stages. The magnitudes of the "measured" stresses in the flanges of this cross section are shown in Fig. 4.5. The casting of deck segments 4W and 6W in adjacent regions on days 8 and 10, generated negative bending moments in the section, and caused the stresses in the flanges to increase. The placement of deck segment 8W directly above the pier and this cross section, on day 16, further increased the stresses. The measured deadload stress due to the completed deck is 11.3 ksi in the top flange and 11.9 ksi in the bottom flange.

Comparison of the stress variations in Figs. 4.3, 4.4 and 4.5 indicates that the stress generated by the concrete deck is about the same in the top and bottom flanges of cross section 330 over a pier, somewhat higher in the top flange than in the bottom flange of cross section 332 at the middle of span 3, and substantially higher in the top flange of cross section 432 at the middle of span 4. This phenomenon will be discussed later.

B. Comparison with Computed Values

The measured variation of flange stresses are compared with

the corresponding computed values provided for this study. The computer programs used are STRESS, CURVBURG, DESCUS, and BSDI. The material properties and the deck casting sequence were incorporated into the computer analyses. Several computer runs, with a variation of parameter values were made by the contracting agency, Majeski and Masters[3]. The results of computation utilized for comparison in this report are based on the following assumptions. (1) The steel girder component plates have the specified minimum yield strength of the respective material (ASTM A588, A572, Gr 50, and A36), (2) The deck concrete has a 28 day strength of f'_c = 4,500 psi. (3) Full composite behavior of cross sections is achieved before the next stage of deck casting. (4) The modulus of elasticity of concrete during the deck-casting period is taken to be that corresponding to the 28-day strength. (In one set of computations, this modulus was reduced by 20%, with negligible effects). In general, the stresses comouted by the programs using two-dimensional (2D) structural models (STRESS, CURVBRG and DESCUS) agree very well with one another. Those generated by the three-dimensional model of BSDI also agree well, although some stress values in some cross sections were different from the 2D results.

Figures 4.6 to 4.11 are examples of the comparison among the computed stresses, and between the computed and measured values. The stresses in the top and bottom flanges of cross section 332 are shown in Figs. 4.6 and 4.7, respectively. For the top flange, all computed stresses are in good agreement with each other, while the measured values are much higher after Day 1. The maximum deviation

is about 5.0 ksi from the measured value of 14.6 ksi. For the tensile bottom flange, the BSDI values are slightly higher than the 2D values while the measured values are lower.

In cross section 432 at the middle of span 4, the difference among the measured, 2D and BSDI values are quite drastic, as is depicted by the curves in Figs. 4.8 and 4.9. The computations severely underestimated the compressive stresses in the top flange, and overestimate the tension in the bottom flange. The maximum deviation is about 10 ksi from the measured value of 18 ksi in the compression (top) flange, and 9.7 ksi from the measured value of -1.0 ksi in the tension (bottom) flange. Since the fixed (hinged) bearing conditions at both ends of span 4 have been incorporated into the computer structural models, some other factors must have contributed to the stresses in the flanges.

The stresses in the top and bottom flange of the girder cross section 330, in the negative moment region over pier 2, agree better than the two cross sections in the adjacent positive moment regions. Figure 4.10 shows that there is only minor difference among the computed and measured tensile stresses in the top flange. The measured compressive stresses in the bottom flange are slightly lower than the computed values. (Fig. 4.11)

C. Results of Analysis Incorporating Shrinkage

One of the factors which could have a pronounced effect on the stresses in the girders during construction, is the shrinkage of the

concrete deck. In order to examine the influence of this factor, a three dimensional finite element model of the bridge was established.[4] The stresses in the flanges of the girders were first computed ignoring the shrinkage of concrete (LU) for comparison with the available computed values, and then including the shrinkage (LUSH). Some results are summarized here.

Figures 4.12 to 4.19 show the computed stress variation in the flanges of cross sections 342, 332, 330, and 430 without considering shrinkage in the computation. These cross sections are at the middle of a fascia girder and of an interior girder in span 3, at one end of an interior girder over a pier in span 3, and at the middle of an interior girder in span 4. Because the results of the three two-dimensional (2D) programs are nearly identical, and even the 3-D program BSDI gives very similar results, only results from one of the 2D program (STRESS) are chosen for comparison. Also included in the figures for comparison are the stresses from the measured strains.

From the curves of Figs. 4.12 to 4.19, it is clear that, without incorporating the shrinkage of concrete, the three-dimension finite element model (LU) provides computed flange stresses which are generally in good agreement with the 2D values. There are some deviation in the computed top flange stresses in cross sections 332 and 432, and in the bottom flange at 432. Without detailed information on the forces at the fixed bearings of span 4, the general agreement between the 2D and LU values is considered satisfactory for the utilization of the LU model for shrinkage

effects.

The results of analysis which incorporates the effects of concrete shrinkage are presented in Figs. 4.20 to 4.25. (These figures are directly corresponding to Figs. 4.14 to 4.19, which do not include shrinkage effects). For cross section 332, the consideration of shrinkage reduced the deviation of computed top flange stresses from the measured values. For cross section 330 over a pier, in the negative moment region where the concrete slab was casted on day 16, little difference is expected between the LU and LUSH values. That this is so is depicted in Figs. 4.22 and 4.23. There is some deviation between the measured and computed compressive stresses in the bottom flange. (This deviation is, in essence, incurred from day 1).

In the flanges of cross section 432 at middle of span 4, incorporation of shrinkage in the computation of stresses leads to a better correlation between the computed and measured compressive stresses in the top flange. However, little improvement is gained regarding the tensile stresses in the bottom flange. Other factors, such as thermal effects and pier flexibility, could account for some of the duration of this specific span.

Overall, incorporating the effect of concrete shrinkage when the period of casting the continuous deck of a long multispan bridge is more than a few days, appears to improve the structural model.

D. Cross Sectional Stress Profiles and Neutral Axes

As it has been pointed out earlier, the cross sectional

properties of the girders changed as the concrete of the deck developed its strength. The centroidal axis of a girder cross section, therefore, shifted from the position of the bare steel girder to that of the composite girder. However, the width of the deck slab which effectively participated with the steel girder cannot be accurately estimated by the simple rules for "effective width" provided by the AASHTO design specifications.[2]. Furthermore, the gradual development of concrete strength and the continuity of the deck make it very difficult to determine the effective cross section of the composite section. On the other hand, the measured stresses in the steel girder flanges provide an direct indication of the approximate location of the neutral axis, so far as the stresses are within the proportional limit.

The profile of cross sectional stresses at location 332 on days 1, 9 and 20 of deck casting are plotted in Fig. 4.26, assuming a linear variation of stress between the top and the bottom flange. The segment of concrete deck in this region was casted on day 1 (see Fig. 2.4). The incremental stresses on day 1, therefore, were carried by the bare girder. The good agreement between the location of zero stress and the computed centroidal axis of the bare girder attests to this condition. Between day 8 and day 9, the concrete had already developed most of its strength. The neutral axis of the cross section should be at the upper part of the web. The stress profile in fig. 4.26 does seem to indicate so, although the magnitudes of incremental stresses are small due to the deck segment 5E and 5W in the adjacent span. Very small incremental stresses

were introduced in cross section 332 when concrete was placed in the region over pier 3 at the end of the span on day 20.

Figure 4.27 for cross section 432 at the middle of span 4, shows again the same phenomenon of the neutral axis shifting toward the top flange. On day 1, the bare girder carried the bending moment induced by the wet concrete directly above. The computed centroidal axis agrees well with the neutral axis indicated by the stress profile. Between day 8 and day 9, when two other segments of deck were placed in the span and near the cross section, the composite girder carried the induced moment and the neutral axis was near the deck. The bottom flange had a higher increase of stress. On day 20, when concrete was casted over pier 3 at the west end of the span, the bending moment induced at the middle of the span was very small. The presence of compessive stress over the whole depth indicates that some axial force had been generated.

Location 330 over pier 2 had its concrete deck cast on day 16. The steel girder alone carried all bending moment of the cross section up to that time. The cross section is relatively stocky and the incremental stresses due to each casting are not high. Therefore, the profiles of incremental stresses do not provide very reliable indications of the location of the neutral axis. Figure 4.5, which shows the variation of flange stresses in this cross section, shows that the position of the neutral axis did not move very much.

E. Cumulative Stresses

While Figs. 4.26 to 4.28 present the profiles of the measured incremental stresses in the cross sections for the examination of the progressive change of neutral axis location, comparison of the computed and measured stress values is more revealing by using the accumulated stresses induced by the deck segments. Figure 4.29 shows the cumulative stress profiles for cross section 432. As before, only the values from one of the computer programs are plotted (2D), and the results of analysis with shrinkage effects are also shown (LUSH). When the bare girder carried all the weight of the wet concrete deck above, on day 1, all the computed values agree well with the measured values. On day 9, when the concrete deck had already gained most of its strength and the shrinkage effects were in progress in different concrete deck segments, the analytical results incorporating shrinkage provide a very good estimate. The 2D computed results, which ignores shrinkage, are different from the measured ones, by about 3 ksi in both flanges. On day 20, the casting of deck was complete. The computed stress profiles are substantially different from the measured results. As discussed earlier, a more refined analysis incorporating pier flexibility and thermal effects might improve the computed results, but it is beyond the scope of this study.

To examine the total dead load stresses at each cross section, the initial stresses due to the weight of the steel girders, deck reinforcing bars, and formwork must also be included. These initial stresses are quite consistent among the four computer programs

utilized for this project. By using the same set of initial stresses, the profiles of total accumulated dead load stresses at days 1, 9 and 20 of cross sections 332, 432 and 330 are constructed in Figs. 4.30, 4.31 and 4.32, respectively.

From comparing Fig. 4.31 and Fig. 4.29, it can be seen that the difference in values between the computed and measured stresses is the same for each day, but the proportion of difference is lower when the total dead weight of the steel girders, rebars, formwork and the concrete deck are all included. The maximum difference is in the bottom flange.

In examining the total stresses from measurement, again it shows that cross section 432 was subjected to "unusual" stress distribution when compared with other cross sections. Almost the entire cross section was in compression at the completion of the deck concrete placement, as well as during many other stages of deck casting. This is depicted in Fig. 4.2. This "unusual" stress distribution could have lead to the relatively large magnitude of web deflection at location 432, which was discovered after the completion of the bridge.

4.1.2 Web Stresses Perpendicular to Top Flange

Two strain gages were installed on the web at location 242, just below the top flange, for the measurement of vertical strains due to placement of deck concrete. These are gages 242WS1 and 242WS2 on the inside surface of the fascia girder. (See Fig. 2.11a). It was not possible to attach strain gages on the outside face of the web without

very extensive rigging.

The stresses, converted from the measured strains without incorporating Poisson's effect, are plotted in Fig. 4.33. Strain gage 242 WS2 at the centerline of the panel had stresses higher than those in gage 242WS1, and neither changed much after day 8. Relatively large changes occurred on day 1 and day 8, when concrete deck segments were casted in span 3 and directly above the cross section, respectively (see Fig. 2.4). Because the strain gages are on only one side of the web plate, it is not possible to determine whether the web plate was subjected to lateral deflection and plate bending stresses.

Figure 4.34 shows the variation of stresses at the sides of the top flange. The shifting from tension to compression on day 8, due to the casting of deck segment in the region, was accompanied by the reversal of differential bending stress between the two sides of the flange. This implies that the top flange shifted from deflecting inward to deflecting outward, that is, north and away from the bridge. The minor change in web stresses in the vertical direction, combined with the Poisson's effect from the average compressive flange stress of 15 ksi, suggests that the web plate lateral bending was minor. This will be further examined later.

4.2 Lateral Deflection of Web Panels

While the vertical deflections of the bridge girders were readily measured by using a level, and the stresses in the bridge components by strain gages, the measurement of lateral deflection of girder web panels was not easily achievable. This was because of (1) the difficulty in

accessing the locations where large web deflections are expected, and (2) the difficulty in establishing a stable reference line. With great effort, vertical reference lines were fastened to the top and bottom flanges of an exterior girder in two regions near the midspan section of the first and second spans (sections 142 and 242) before the placement of the deck concrete. Within each region three reference lines were established as shown in Fig. 4.35. Lines A and C were opposite the diagonal struts of supporting brackets for the formwork of the deck overhang. Line B was half way in between.

The web panel at region 142 has no transverse stiffeners between diaphragms, which are 25 ft. apart. Because of the large lateral deflection of the web and the separating of the metal deck form at the corresponding location of the west bound bridge (W742), the web panel at spans 1 and 7 of the eastbound bridge, including panel 142, were braced laterally during construction, by placing wooden beams between adjacent girders. Measurements of the web profiles were made by offset from the reference lines before and after casting of the concrete deck directly above and also after the removal of the deck overhang formwork, the supporting bracket and the wooden bracing beams. The largest magnitude of deflections occurred at line B. The web profiles at line B are sketched in Fig. 4.36. Before the casting of the concrete deck, with the deck formwork and the web bracing in place, the web panel 142 showed a double curvature lateral deflection (out-of-flatness). The placement of deck concrete caused the web to deflect further inward, in spite of the presence of the wooden bracings between adjacent girders. The removal of the deck overhang formwork, the supporting bracket and the wooden bracing

members resulted in a very small decrease of lateral deflection in the upper portion of the web, and a small increase in the lower portion. The web deflection shape is essentially of single curvature. The maximum residual out-of-flatness is at mid-depth and is about 0.34 in.

In the second span, at the region 242, the transverse intermediate stiffeners between the cross diaphragms are spaced at 100 in. The corresponding web profiles before and after casting of the concrete deck directly above, and after removal of the overhang supporting bracket are also presented in Fig. 4.36. Here no wooden bracing of the web was applied and no unexpected event occurred. This web panel had an initial lateral deflection of about 0.32 in. (before casting of slab concrete but with all formwork in place). The placing of the concrete deck caused an increase of the lateral deflection to about 0.8 in. After the removal of formwork and props, the residual permanent deflection was about 0.6 in.

Obviously, bracing of the web plate by the wooden beams in panel 142 had a strong influence on the final out-of-flatness when compared with that of panel 242, even when the web panel length of 142 is three times that of 242.

For further comparison, the final out-of-flatness of the corresponding web panels in the west bound bridge were also measured. The profile of web panel W742, where metal deck form separation occurred and wooden column shoring and horizontal bracing were used, is shown in Fig. 4.37. The web profile of the corresponding location of the other exterior girder, W712, where no shoring was made, is also shown for comparison. It is interesting to observe the following.

1. The out-of-flatness of all four web panels of these exterior girders are inward. No doubt this is caused by the thrust in the strut of the overhang supporting brackets.
2. The permanent lateral deflection of the web is smaller at the girder of deck form separation (W742) than at the other exterior girder (W712). The magnitudes are about 0.5 in. and 0.9 in., respectively. This difference possibly is because that the top flange of panel W742 was shored whereas that of panel W712 was not.
3. Bracing of the web panel 142 before casting of concrete resulted in a smaller permanent out-of-flatness than that of web panel W712, which was braced after the casting of the deck concrete.
4. The web panel at 242, with a length of 100 in., has a smaller permanent out-of-flatness than that of web panel W712, which has a length of 300 in. Other conditions being the same, obviously closer spacing of transverse stiffeners results in smaller out-of-flatness of the web.

The maximum out-of-flatness of the web panels are summarized in Table 4.4. The final or permanent deflections are also expressed in terms of the web thickness in the table. Some of these final out-of-flatnesses are higher than the permitted magnitude at fabrication according to AWS specification.[5] There is no existing provisions with regard to the permissible permanent out-of-flatness of girder webs. Further discussion of web plate deflection will be made later in this report.

5. TEST TRUCK LOADING AND BRIDGE RESPONSE

5.1 Test Trucks and Test Runs

5.1.1 Test Trucks

Before the bridge was opened to regular traffic, a series of live load tests using trucks with known axle loads and configuration were conducted to establish the response of the bridge superstructure. Ideally, the vehicles used for such tests should conform to the configuration of (1) the AASHTO HS-25 standard, and (2) the 204-kip Pennsylvania special permit truck. However, trucks of these configurations are not available. Six four-axle vehicles, each weighing approximately 67.5 kips, were used to simulate the HS-25 and 204 k loads. The axle spacings and axle weights of these trucks are summarized in Fig. 5.1.

To simulate HS-25 standard live load, two test trucks were placed in tendon in each operating traffic lane, as illustrated in Fig. 5.2 and Fig. 5.3. For a simple span of 228 ft. (spans 3, 4 and 5), the two-truck combinations in the three traffic lanes would generate maximum bending moment of 6503, 6488 and 6561 k-ft., respectively. In comparison, the standard HS-25 live load would generate a moment of 6481 k-ft. (controlled by lane loading).

Similarly, the effect of a 204-k permit vehicle was simulated by placing trucks 3, 5 and 6 in succession, as shown in Fig. 5.2. For a simple span of 228 ft., this three-truck combination would cause a maximum bending moment of 9113 k-ft. This compares to the moment of 9870 k-ft. caused by a 204-k permit truck.

5.1.2 Test Runs

The I-78 bridge has a curb-to-curb roadway width of 48 ft. which contains three 12-ft wide normal operating traffic lanes, and shoulders of 8 ft. and 4 ft., as shown in Fig. 5.3. The test trucks were operated within these traffic lanes.

Seven runs at crawl speed (about 5 miles per hour) and three at moderate speed (about 50 miles per hour) were made by the test trucks. Each run included a forward (eastbound) travel of the trucks from span 1 to span 7, followed by a backward travel to span 1. Table 5.1 lists the run designations and the configuration, location and speed of the test trucks for each run. For example, run C1 had a simulated HS 25 live load in lane No. 1, traveling at crawl speed, while run S23 had simulated HS 25 loads in both lanes 2 and 3, simultaneously traveling at moderate speed.

Only 21 strain gages could be monitored at one time by the magnetic tape recorder being used. As the total number of gages far exceeded this number, each test run was repeated six times while different groups of gages were monitored. Table 5.2 shows the groupings of the gages. It is noted that two girder flange gages (332B and 342B) were included in all six groups. Also, two deck gages (332ST and 342NL) were included in both groups 4 and 5, which contained all deck gages. These common gages were used to correlate the recorded responses of gages in different groups.

5.2 Stresses in Bridge Components due to Test Trucks

5.2.1 Strain Variations in Girders

A. Strain-Time Traces

As trucks travelled on the bridge, strains were generated in the bridge components. The magnetic tape of the monitoring equipment recorded the continuous variation of strains at each strain gage. The variation can be plotted out as strain-time traces (see Appendix B). Figures 5.4, 5.5 and 5.6 are examples of such traces for eight strain gages. These plotted strains were caused by one simulated HS 25 truck in traffic lane 3 alone (run C3), one simulated truck in lane 2 alone (run C2), and two simulated trucks side-by-side in lanes 2 and 3 (run C23), respectively.

For each strain-time trace the horizontal axis represents time (from left to right) and the vertical dimension is the uncorrected or apparent strain. The time scale of all traces in all figures is the same and is indicated (2 seconds for each smallest division), while the vertical scale varies from figure to figure. In Figs. 5.4 and 5.5 the full scale of each strip of trace is 250 micro inches per inch (FS 250), corresponding to 7.5 ksi in stress if a value of 30,000 ksi is used for the modulus of elasticity. (This value is used here for the sake of simplicity.) The full scale of strain in Fig. 5.6 is 500 micro inches per inch (FS 500), or 15 ksi. In all figures of strain-time traces, the test truck run condition and the position of traffic lanes are indicated.

Each of the continuous strain-time traces has upward excursion, downward excursion, or both, representing the variation of strain due to passing of the truck load. These are live load strains (stresses). A

downward excursion corresponds to live load tension whereas an upward one represents live load compression. The bottom trace in Fig. 5.4, for example, shows that strain gage 342B was subjected first to a small compression (0.8 ksi), then a tension of higher magnitude (about 5.3 ksi), and again to compression (1.1 ksi) as the test truck crawled forward in lane 3. Gage 342B is in span 3, on girder 4, at midspan (second quarter point) and on the bottom flange. The strain-time trace resembles the influence line of strain for this point of the multispan continuous bridge structure. In fact, all strain-time traces in Figs. 5.4, 5.5 and 5.6 are directly related to the influence lines for stresses at various points in girder flanges.

B. Stresses in Girders due to Simulated HS Trucks

By examining the strain-time traces generated by the simulated HS trucks, a wealth of information can be deduced, including the magnitudes of stresses in different girders and their components. The first three strips of Figure 5.4 are the strain time traces of gages 332 TN, 332B and 332TS, which are located in the same cross section of girder 3 in span 3, at midspan. When the simulated HS 25 truck crawled from West to East in traffic lane 3 (see Fig. 5.3) the bottom flange (gage 332B) was primarily subjected to tension with a maximum live load stress of about 3.4 ksi. The stresses in the top flange of the steel girder (gages 332TN and 332TS) were quite low, being only about 0.5 ksi in compression. The simulated test truck took about 40 seconds to traverse span 3 which is 228 ft. in length; the travel speed was therefore less than 4 mph, and the dynamic effect was negligible. The stress reversal caused by the simulated HS 25 truck run resulted in a total live load stress range of about 4.4 ksi. in

the bottom flange.

At the girder cross section one quarter span to the east, cross section 333, the top and bottom flanges' response can be similarly examined. The maximum live load tension in the bottom flange (gage 333 B) was 2.2 ksi, and the maximum compression was 1.5 ksi. Again, the top flange stress was low, as is indicated by the strain-time traces of gages 333TN and 333TS. Because the cross section 333 is at 3/4 span and closer to pier 3, the peak response occurred about 10 seconds later than that of the midspan cross section 332, and the stress magnitude was lower (3.4 ksi vs. 2.2 ksi). These "static" stresses from the crawl run of the simulated HS 25 truck are in full agreement with the nature of the influence lines of stresses in girder flanges.

In Fig. 5.4, the last one and the first three strain-time traces are for strain gages at the same cross section of the bridge, cross section 3x2. The maximum response of girders 3 and 4 occurred at the same time. The maximum live load tension in girder 4 (at gage 342B) was 5.3 ksi while that of girder 3 (at gage 332B) was 3.4 ksi. This indicates that girder 4 carried more of the test truck load than girder 3, as would be expected because the simulated HS 25 truck was in lane 3, much closer to girder 4 than to girder 3, (see Figs. 5.3 and 2.7). When the test truck was in traffic lane 2, away from girder 3 and further away from girder 4, the stresses in the flanges of these girders were correspondingly lower. This is depicted by the second and the last strain-time traces in Fig. 5.5. Gage 332B indicates a maximum live load tension of 2.7 ksi, and gage 342B, 1.9 ksi.

By examining the instantaneous stresses at the strain gage locations of the girders, the "static" response of the bridge and the distribution of truck loads among these girders can be deduced. The results will be presented later in this section and in Section 5.3 of this report.

Figure 5.6 shows the strain-time traces of the same eight strain gages of Figs. 5.4 and 5.5 when two simulated HS 25 trucks were crawling side-by-side, one in traffic lane 3 and one in lane 2. The scale for strain in this figure is twice of those in Figs. 5.4 and 5.5. The shapes of the corresponding strain-time traces in these three figures are identical, and the sum of the strain magnitudes of each gage in Figs. 5.4 and 5.5 is the corresponding strain magnitude of Fig. 5.6. This result confirms the expected linear elastic behavior of the bridge and the applicability of the principle of superposition. Further presentation of results of superposition will be given later.

C. Girder Stresses Induced by a Simulated 204 K Permit Trucks

The live load stresses in the bridge's components due to a simulated 204K permit truck were higher than those induced by the simulated HS 25 trucks at the same position on the bridge. Figure 5.7 shows strain-time traces of the same eight strain gages of Fig. 5.4 when the 204K permit truck was in lane 3. The shape of all corresponding strain-time traces are identical. The strain scale of Fig. 5.7 is FS 500, or about 15 ksi for the full width of each "strip chart". The maximum live load tension in the bottom flange at midspan of girder 4 (gage 342B) was 6.9 ksi, higher than the 5.3 ksi tension induced by the HS 25 truck (as shown in Fig. 5.4). The corresponding live load tension at the

midspan of girder 3 (gage 332B) was 4.5 ksi due to this simulated permit truck, as compared to 3.4 ksi by the HS 25 truck.

Similar strain-time traces due to the simulated 204 K permit truck are presented in Appendix B. By comparing the corresponding strain records from the simulated 204 K truck and those from a simulated HS 25 truck, it is evident that the former always generates higher stresses in the girders than the later but the shape of strain-time trace remains the same. This condition indicates the repeatability of live load stress variations and the linear elastic nature of the bridge behavior.

D. Stress Distribution in Bridge Cross Sections

As indicated earlier, by examining the instantaneous strains or stresses in the girders the stress distribution in girder cross sections and among the four continuous girders can be deduced. Table 5.3 summarizes the instantaneous strains and stresses in the midspan cross section of the four girders in span 2 due to the test trucks. These are the maximum strains and stresses converted from the maximum readings of the strain-time record with correction for the electrical resistance of the strain gage cables. Because the four cross sections (2x2) are at the same position along the length of the bridge, the maximum stresses due to a test truck occur at the same time. Results from the crawl runs C1, C2, C3, C23 and C123 of the simulated HS 25 trucks and P2 and P3 of the simulated 204 K permit truck are all listed.

When a test truck was in lane 1 (run C1), it was located above girder 1 and girder 2, and the stresses in the midspan cross section of these

girders were higher than those in girder 3 and girder 4. The maximum bottom flange stress of girders 2, 3 and 4 were 3.52 ksi, 1.91 ksi and 0.23 ksi, respectively, in tension. This indicates a decreasing share taken by the girders away from the truck. The corresponding stresses in the top flanges were in compression and the magnitudes were quite low, but the decrease of magnitude from girder 1 to girder 4 was the same. Similarly, when a test truck was in lane 3 (run C3 and P3), it was located above girder 4 and girder 3. The stresses were highest in girder 4 and decreased towards girder 1. For example, the stress in the top flange gages 242TS, 232TS, 222TS and 212TS were, respectively. -0.97 ksi, -0.95 ksi, -0.57 ksi and 0.32 ksi when the 204 K permit truck was in lane 3 (P3). (Note the reversal of stress in girder 1).

These results clearly demonstrate the stress or load distribution character among the girders and the behavior of the four girder bridge under live load. Further demonstration is provided by the corrected instantaneous strains in the midspan cross sections of the girders in span 3. The strains are listed in Table 5.4. Strains in the concrete deck, where available, are also listed. Once again, the results show that girders directly under or near the truck load have higher live load stresses and carry a large share of the truck load (test runs C1, C2 and C3). When a truck was near one edge of the deck, (test runs C3 and P3), the girder on the other side of the bridge cross section endured a "negative bending". This behavior of "cross bending" of the bride, not indicated by bridge design specifications, has been a well known phenomenon to bridge engineers.

The strains in each girder cross section as summarized in Table 5.4 also provide information of strain (and stress) distribution over the depth of a cross section. For example, in girder section 332, during test truck run C3, the maximum strains in the top flange of the steel girder were 16.6 and 19.6 micro inches per inch in compression. Simultaneously, the strains registered at the top level of the concrete deck were 24.0 and 35.5 micro inches per inch in compression, and the strain in the bottom flange of the steel girder was 129.5 micro inches per inch in tension. These strain magnitudes form almost a straight line across the depth of the girder, and indicate that the girder cross section behaved compositely and that the neutral axis of the cross section was close to the steel top flange. More extensive examination of cross sectional stresses will be made in Section 5.3.

E. Combination of Stresses due to Truck Loads

It has been shown earlier in this section that superposition of loads and stresses can be confirmed by combining the stresses or strains from test truck runs in two different traffic lanes separately and compare the values with those from the trucks traveling side-by-side in these lanes. The cross-sectional strains and stresses presented in Table 5.3 and Table 5.4 can be used for this purpose. As an example, the stresses at strain gage 232B on the bottom flange of girder 3 in span 2 was 1.91 ksi, 2.82 ksi and 3.57 ksi, respectively for test truck runs C1, C2 and C3 (see Table 5.3). The sum of the values for C2 and C3 is 6.39 ksi, which is almost the same as that directly measured during test truck run C23, 6.48 ksi. Similarly, at the same location, the sum of stresses from runs

C1, C2 and C3 is 8.30 ksi, and the stress from run C123 is 8.10 ksi. Again, the values are very nearly the same.

For girder cross section 342, Table 5.4 gives the bottom flange strains of 27.4, 68.4 and 193.8 micro inches per inch from test truck runs C1, C2 and C3, respectively. The sum of C2 and C3 is 262.2 micro inches per inch, which is the same as that from test run C23. The sum of C1, C2 and C3 is 289.2 micro inches per inch, and C123 gives 283.9 micro inches per inch. The difference is less than 2%.

Considering the accuracy and precision of the strain measurements, the results illustrated above can be viewed as conclusive confirmation of the applicability of the principle of load and stress superposition to the bridge. More extensive discussions will be made later.

5.2.2 Stresses in Diaphragm Members

The cross diaphragms between the bridge girders served to stabilize the girders during the construction stage. After the completion of the bridge, these diaphragms are utilized to transmit lateral forces due to wind loads. Generally, no consideration of traffic load induced forces in the diaphragms is made. Experience with girder bridges have pointed to the existence of diaphragm action under traffic load and occasional local distress at the connections between diaphragm members and the girders. Because this bridge has a large spacing between girders, the diaphragm action could be relatively strong. In order to examine the magnitude of forces in the diaphragm members of the bridge, six strain gages were placed on these members. (See Fig. 2.12.) (After test truck runs, two additional strain gages were attached to diaphragm members with additional

strain gages on the girders. These will be discussed later in Chapter 6).

The recorded strain variation in the six diaphragm gages due to the passage of test trucks were examined to obtain the magnitudes of stress in these members. Figure 5.8 is an example of strain-time traces, which were induced by a simulated HS 25 truck crawling forward in traffic lane (run C1). The strain-time record of the bottom flange of girder 3 and girder 4 at middle of span 2 (332B and 342B), are also plotted for reference of time. The stresses in the diaphragm members were primarily tension or compression with minor reversal, and the maximum stresses occurred when the truck was in the span of the diaphragm. With the test truck in lane 1 (between girder 1 and girder 2), the top strain gages D23TS, D33TS and D24TS near the top of girder 3 and girder 4 were in tension while the corresponding bottom strain gages D23BS, D33BS and D24BS were in compression. This condition of opposite stresses in the opposite members of the cross diaphragm implies that girder 2 had a downward deflection larger than that of girder 3, and girder 3 larger than girder 4. In other words, a truck load on one side of the bridge deck centerline caused differential deflection of the girders and induced diaphragm action between girders.

The magnitudes of maximum stress in the diaphragm members due to test truck run C1 are listed in Table 5.5, together with those from other test truck runs. The highest stress in the diagonal cross members during run C1 was 4.3 ksi, in D23TS. This is of the same order of magnitude of stress in the bottom flange of the girder (3.52 ksi, see Table 5.3). Assuming a uniform stress distribution within the 4x4x5/8 angle section of the diaphragm member, the total live load force in the member would be 4.3

ksi x 2.83 sq in = 12.2 kips.

Examination of the maximum stresses listed in Table 5.5 reveals a number of behavioral conditions of the bridge and diaphragms.

(a) As pointed out earlier, when a truck was off the bridge deck centerline, in the outside lanes, the top and bottom members of cross diaphragms had opposite stresses. This is indicated by the opposite sign of stresses in the top and bottom gages during test truck runs C1, C3, P3 and S3. Because of the highly statically indeterminate configuration of the cross frames, the stresses were not of the same magnitude in the two diagonal members of the cross diaphragms.

(b) The magnitude of stresses in the top and bottom members of cross diaphragms at interior girders were more even when a truck was in the middle lane, (test truck runs C2 and P2).

(c) The principle of superposition is valid, as is confirmed by comparing stress magnitudes from C2+C3 with C23 and C1+C2+C1 with C123. For example, at gage D23TS, the magnitudes are 3.5 - 2.1 = 1.4 ksi versus 1.5 ksi, and 4.3 + 3.5 - 2.1 = 5.7 ksi versus 5.2 ksi, respectively.

(d) The highest magnitude of stress in a cross diaphragm member was not necessarily generated when there were trucks in more than one lane.

Further examination of diaphragm action and related stresses will be made later.

5.2.3 Stresses from Speed Runs

During the time of test truck runs, the construction of approach roadway at the east end of the bridge was not yet complete. The

test trucks could travel at crawl speed at ease, but had to slow down beyond span 4 in the speed runs. Furthermore, it was not easy to maintain the desired distance between the two trucks which simulated the HS 25 truck. These conditions limited the travel speed to about 50-55 mph and very likely diminished the effects on the bridge structure. Nevertheless, the measured stresses from the speed runs of the test trucks provided some information on the dynamic behavior of the bridge.

Figure 5.9 shows examples of strain time record at selected locations due to one simulated HS truck in traffic lane 2 traveling at about 55 mph. The locations of strain measurements are the same as those of Fig. 5.5, which shows in different scales the corresponding strain-time record under a crawl run of a simulated HS 25 truck in the same lane. Comparison of the traces in these two figures reveals the dynamic effects of the speed run. While the strain-time traces of Fig. 5.5 are analogous to static influence lines, those in Fig. 5.9 include the dynamic or vibrational response of the bridge components to the fast moving test trucks. By taking into consideration the difference of scale for time and for strain, the traces in Fig. 5.9 could be visualized as the corresponding ones in Fig. 5.5, superimposed by fluctuations caused by the bridge vibration. The frequency of the vibration, as measured from the traces, was about 4 Hz. The vibration started when the test truck came onto the bridge, and continued well beyond the time when the truck got to the other end of the bridge. Examination of the traces in Fig. 5.9 shows that all three girders 4, 3 and 2 vibrated, with the fluctuation of stresses quite prominent in the steel bottom flanges but hardly measurable in the top

flanges just below the concrete deck. Examination of strain time traces of other speed runs (given in Appendix B), showed that in most cases the fast moving test trucks induced similar vibrations, but the amplitudes were much smaller.

The consequence of the vibration or dynamic behavior is an increase of the magnitude of maximum live load stresses, usually referred to as "impact load stresses". The strain time traces of Fig. 5.9 (and those in the Appendix) show that the impact stresses in this bridge are quite small, being less than 0.5 ksi.

Table 5.6 lists, for a few locations, the measured stress ranges from the test truck loads (after incorporating the electric resistance of the strain gage cables). These live load stress ranges are calculated as the algebraic differences between the maximum and minimum values of the stress-time traces. Included in the table are the results from speed runs S3 and S2, when a simulated HS 25 truck was traveling at moderate speed in lane 3 and in lane 2, respectively. Also listed are the corresponding results from the crawl runs C3 and C2. The magnitude of stress ranges due to the speed runs were not always higher than those of the corresponding crawl runs. For comparison, the measured stresses in a diaphragm are also listed and the results are similar. (See also Table 5.5.) This condition is most likely due to the characteristics of dynamic response of the bridge and the situation that the test trucks were not the same during the test runs and the lateral position of these trucks in the lane might be also not the same.

Irrespective of the above, the following conclusions could be drawn from examining the stresses from the test truck speed runs. (1) A

simulated HS truck, at a speed of about 55 mph, induced noticeable vibration of the bridge at a frequency of about 4 Hz. (2) The "impact stresses" due to the simulated HS 25 truck loads were not high, even when bridge vibration was induced. No result of dynamic analysis was provided for this study. The dynamic behavior of the bridge under truck loads of regular traffic will be presented in Chapter 6.

5.3 Comparison of Stresses from Measurement and Computation

5.3.1 Cross Sectional Stresses

For the comparison of stresses from computation and from measurements, the maximum values of test truck induced stresses in a few girder cross sections are plotted. Figures 5.10 to 5.17 show the stress profiles with an assumed linear stress distribution. Figures 5.10 and 5.11 are for the midspan section of a fascia girder in spans 2 and 3, respectively; Figure 5.12 refers to the midspan section of the interior girder 3 in span 3; and Fig. 5.13 shows the stress profile of girder 3 over pier 2 at the west end of span 3, all due to a simulated HS 25 truck in Lane 3. As before, because the computed values from the three 2D computer programs are nearly the same, results from only one program are shown with those from the 3D finite element program (BSDI) and those from measurements. It is obvious from the stress profiles in these figures that all the computed results for a simulated HS 25 truck load agree very well with the corresponding measured stresses. Regardless of the lateral position of the girder, that is, interior or exterior, the neutral axis is within one-sixth of depth from the top at the middle of a span, and about four-fifth of the web depth from the bottom over a pier. These very high

positions of the neutral axis are consistent with full composite action of the steel girders with the concrete deck slab, even in the negative moment regions over the piers. This is also true when the bridge is under a simulated 204-kip permit truck, as is depicted by Figs. 5.14 to 5.17, which show the results from computation and measurements corresponding to those in Figs. 5.10 to 5.13. Again, the computed results of flange stresses agree very well with the measured values. The observed agreement between computed and measured stresses was not restricted to the girder section and test truck runs depicted in Fig. 5.10 to 5.17. In fact, for all cross sections and all test truck runs, the results agreed very well.

It should be noted that the computed stresses were based on assumed material properties, while the measured values reflect the actual materials as built. Nevertheless, the effect of these differences on the comparison of computed and measured stress values is not likely to exceed a few percent. Therefore, the observed agreement between the computed and measured stresses can be accepted as indeed valid.

As previously stated in Section 4.1.1 in the discussion of girder stresses due to deck construction, it is difficult to determine the cross sectional properties of individual composite girders. The girders are composite with the deck slab which is transversely continuous over the four girders, as well as longitudinally continuous over the piers. Under live load, the entire deck and all the girders participate in transmitting the live load down to the bearings, piers, and abutments. The entire bridge structure must be analyzed as a whole in order to estimate correctly the stresses in the various components[4]. Effects such as shear lag and differential displacement also need to be considered.[6] The live

load distribution factors, and the criteria for effective flange width of composite girders given by the AASHTO Bridge Specifications[2] provide satisfactory guidelines for the designing of composite girder bridges. However, these provisions are not suitable for the analysis of the behavior of bridge structures under given loads. The computer programs[3] enable fairly accurate analyses of finite element models which approximately represent the real structure. Three of the four included programs (STRESS, DESCUS and CURVBRG) model the bridge structure by a horizontal grid system, where the properties of the longitudinal elements incorporate the effect of the composite deck slab as well as the offset of the beam axis from the plane of the deck. From the information received,[3] the effective cross section properties of these composite beams are calculated based on an effective width of the deck slab equal to twelve times its thickness, same as the AASHTO specifications provide for design[2]. In the three-dimensional structural model used by the fourth program (BSDI), the steel girders and the concrete deck slab are represented by separate elements, and the selection of an "effective flange width" for the composite beam is not necessary. Nevertheless, the computed results in reference 3 included cross-sectional properties identical to those listed for the two-dimensional model programs. It is not known what was the significance of these cross-sectional properties in the 3-D model analysis, and how they affected the computed bending moments and stresses. Without knowing the input parameters and the details of these computerized analyses, the only observation possible from the comparison of computed and measured stresses is that, given the field measurement results, all four computer programs can be used to generate

very close estimates of the girder stresses under specified vehicular loads. The "goodness of fit" is clearly demonstrated in Figures 5.10 to 5.17.

Tables 5.7, 5.8, and 5.9 list the computed and measured stresses of three cross sections in the bridge for more comparison. Very good agreement exists for almost all girder cross sections.

5.3.2 Load Distribution Among Girders

One aspect of the behavior of girder bridges that has been studied extensively for the development of design rules is the lateral load distribution among bridge girders when a truck is on the deck at various transverse locations.[7] In view of the large spacing (14'-3") between girders in this bridge, and the slender design of the plate girders, it is uncertain that the traditional lateral load distribution of more conventional configurations is applicable. An extensive computerized analysis of the superstructure system for standard vehicular live loads in various traffic lanes would allow the determination of the live load distribution among the longitudinal girders. This, however, is beyond the scope of this research project. On the other hand, an examination of the measured girder stresses under a few selected loading conditions can provide qualitative insight to this very important aspect of the behavior of this bridge.

Figure 5.18 shows the stresses in the flanges of the four plate girders at the middle of span 3 (section 3X2), when the test trucks were in lane 3 and very close to girder 4. (See Fig. 5.3 for the positioning of traffic lanes and test trucks). For both simulated HS-25 truck (test

run C3), and the simulated 204-K permit truck (run P3), the stresses were clearly lower in girders successively farther away from the load. In fact, the farthest girder (No. 1) was subject to negative bending. Because the overhanging portion of the deck slab is only slightly narrower than one half the spacing between adjacent girders and there are the cast-in-place parapets, all four girders may be reasonably assumed to have approximately the same "effective composite cross section". Therefore, the comparison of flange stresses in the girders provides an indication of the distribution of live load moments among the girders. The distribution is seen to be approximately linear.

The stress distributions shown in Fig. 5.19 are for the bridge cross section at the end of span 3 and over pier 2 (section 3X0) when the simulated test trucks were in lane 3. The condition of linearly decreasing participation of girders away from the trucks is also evident.

When a test truck was in lane 2, slightly off the centerline of the bridge deck, the two interior girders developed nearly equal stresses and the exterior girders had slightly lower stresses. This condition is depicted in Figs. 5.20 and 5.21 for the middle and the end of span 3, respectively. This pattern of distribution is again in agreement with results from earlier studies on girders with more conventional spacing[7].

5.3.3 Superposition of Loads

The instantaneous stresses in girders due to test trucks can also be used for examining the effects of multiple vehicles in different lanes of the bridge. Under permissible live loads, the bridge is expected to respond linear-elastically, and the principle of superposition should

apply. The stresses in the girders due to more than one truck at specific positions should equal to the sum of the corresponding stresses due to the individual trucks at the respective positions.

Figure 5.22 shows the stresses in the flanges of the girders at the middle of span 3 due to simulated HS-25 trucks in both lane 2 and lane 3 simultaneously (C23), and the sums of stresses due to one HS-25 in lane 3 and one in lane 2, separately, (C2+C3). The two sets of stresses are almost identical. This confirms the applicability of superposition. For comparison, the computed stresses, by the three-dimensional computer program (BSDI) for the same two trucks in lanes 2 and 3, are also superimposed and plotted (3D) in Fig. 5.22. The computed stresses also agree very well with the measured (C23) and superimposed-measured (C2+C3) values.

To examine this further, the superposition of trucks in all three lanes is shown in Fig. 5.23. The girder flange stresses from measurement when three simulated HS-25 trucks travelled side-by-side in lanes 1, 2, and 3 (C123) are plotted. These values agree very well with the corresponding stresses which are the sums of measured stresses due to the three trucks individually (C1+C2+C3). The agreement with the computed stresses (3D) is also quite good.

Examination of the measured stresses in other girder cross sections, as listed in Tables 5.3, 5.7, 5.8 and 5.9, shows that in all cases, the sum C2+C3 is very close to C23, and C1+C2+C3 to C123. Superposition of loads and the corresponding stresses is therefore applicable for this bridge.

For the possible but unlikely condition that a 204K permit truck and two HS-25 trucks occupy the three lanes simultaneously, the maximum live load stresses in the girders can be estimated by summation. For example, the maximum live load stress at cross section 342 would be, from Table 5.8, P3+C2+C1 = 7.57 + 1.98 + 0.79 = 10.34 ksi (tension) in the bottom flange and -1.57 - 0.42 - 0.18 = -2.17 ksi (compression) in the top flange. These values are in very good agreement with the 3D computed values of 10.81 ksi and -2.19 ksi, respectively.[3] It should be mentioned that the computed values from the 3D computer program are based on trucks in the three lanes positioned to produce maximum effect in girder 4 according to AASHTO design specifications[2,3], while as shown in Fig. 5.3, the test truck in lane 2 was not as such a position; it was near the south edge of the lane instead of the north edge. The agreement between the computed and measured results is expected to improve if this difference in truck position were eliminated. Table 5.10 provides additional comparisons of measured and computed girder stresses.

5.3.4 Deck Strains

While the stresses in the steel girders can be converted directly from the measured strains, the state of stresses in the concrete bridge deck are two-dimensional in nature and cannot be calculated so easily. The difference between the elastic moduli of steel and concrete further complicates direct comparison of girder and slab stresses. On the other hand, the measured longitudinal strains are directly comparable. An examination of the longitudinal strains on the deck surface provides an insight to the participation of the deck slab in longitudinal bending.

If the concrete deck slab is fully composite with the steel girders, and the bridge structure behaves linear-elastically, the strain distribution would be linear between the bottom flange of the girder and the top surface of the deck. With the girder flange strains known from measurements, the longitudinal strain at deck top can be calculated by means of extrapolation.

The longitudinal strains at the top surface of the deck slab across the middle of span 3 are summarized in Table 5.11. Strains directly above the girders are obtained from extrapolation, while those at the longitudinal deck gage locations are directly measured. Results from all test truck crawl runs are presented.

The strain data from the simulated HS-25 truck in lane 3 (C3), and from the simulated 204K permit truck in lane 3 (P3), are plotted in Fig. 5.24. A number of observations can be made from this figure. (1) The measured longitudinal strains at deck gage locations are consistent with those obtained from extrapolation, although there appear to be shear lag or local effects over the girders. (2) The variation of deck strains for the HS-25 and 204K permit trucks are similar. This is consistent with the distribution of girder stresses across the bridge cross section as shown in Fig. 5.18. (3) When a truck is close to the edge of the roadway on one side of the bridge, negative bending could occur at the other side of the roadway deck, as it is indicated by the strain over girder 1 under test truck run C3.

Figure 5.25 shows the deck strain across the same bridge cross section at the middle of span 3 due to three different test runs: one HS-25 truck in lane 3 (C3), one in lane 2 (C2), and one each in lane 3 and

lane 2 simultaneously (C23). When the truck was in lane 3, near girder 4, the strain in the deck decreased continuously from girder 4 to girder 1 away from the truck. When the truck was in the middle of the roadway, the strain distribution was by and large uniform across the deck. When two trucks were at the cross section at the same time, the strains generally decreased from the north edge (above girder 4) to the south edge (above girder 1), similar to the situation when a single simulated truck was in lane 3, but the magnitudes were higher. Examination of the tabulated values show that the principle of superposition applied very well to the concrete deck strains, as with the steel girder strains.

The effect of lateral position of trucks can be further deduced from Fig. 5.26, which shows the strains when three trucks were on the bridge (C123). While one truck was near girder 4 and produced strains decreasing from girder 4 towards girder 1, the truck in lane 1 between girders 1 and 2 did the opposite, and the truck in lane 2 induced nearly equal strains above all girders. The result is an approximately uniform strain distribution across the bridge deck, as indicated in the figure by the line designated C123. Summation of the deck strains from separate runs by three simulated trucks (C1+C2+C3) shows essentially the same variation. The results again confirm the applicability of load and strain superposition.

No computed deck stress or strain was provided for comparison with the measured values. From the fact that good agreement exists between the computed and measured stresses in the plate girders, it is anticipated good agreement of stresses or strains would also exist in the deck. The consistency of the measured and extrapolated deck strain values appears to

support this expectation.

5.4 Stresses and Deflection of Web Panels

5.4.1 Web Deflection

A. Initial Out-of-Flatness

While girder stresses and the vertical deflections are routinely evaluated, the stresses and lateral deflections of girder webs are rarely computed, on account of the unknown initial lateral deflection or out-of-flatness of the web plates due to fabrication and the weight of the bridge. Qualitatively, it is well known that larger initial lateral deflections will result in larger lateral deflections under live loads and possible fatigue damage.[8] Because of the different geometry of the girder web panels and the different condition to which some panels were subjected during construction of the bridge, it was expected that the long panels of web in the end spans of the exterior girders would have the largest initial deflections. (See Section 4.2)

After the completion of the bridge deck, and prior to load testing using test trucks, it was found in the summer of 1988 that the web panels of an interior girder, girder 3, at the middle of span 4 had large, noticeable lateral deflection. Consequently, measurement of the initial deflections were made at two web panels in girder 3, panels 432P1 and 432P2 (See Fig. 2.11b). The results are plotted in Fig. 5.27. These adjacent panels have lateral deflections in opposite direction, with the maximum out-of-flatness at about the midpanel.

Table 5.12 summarized all measured initial deflections of web panels. The interior girder web panels 432P1 and 432P2 have the largest

lateral deflections, about 1.1 in. in magnitude, which is about twice the web thickness. Two web panels in an exterior girder which have similar geometrical conditions but were subjected to lateral forces from the deck form struts during construction, both deflected inward, with a maximum deflection of about half an inch, or about the thickness of the web. The initial deflections of web panels 432P1 and 432P2 were about twice as large. Visual examination of other web panels of the interior girders in spans 3 and 4 showed that all sustained noticeable initial deflections, though not as severely as panels 432P1 and 432P2. The deflections in adjacent panels are mostly in opposite directions, similar to the situation of panels 432P1 and 432P2. This type of deflection pattern suggests a correlation with the compressive flexural stresses in the girder. Further discussion will be made later.

B. Web Deflection due to Test Truck Loads

The lateral deflection, or movement, of the web plate in panel 432P1 was measured using a "clip gage" during the test trucks runs. The gage is a spring-mounted device with electrical resistance strain gages, which can be continuously monitored. The recorded strain-time variation during the test truck runs is converted to deflection-time traces for evaluation. Figure 5.28 shows such a trace (the fifth trace) for a test truck crawl run in Lane 3 (C3). The pattern of the deflection-time trace remains the same regardless of the lane position of the test trucks, and is analogous to the pattern of influence line for bending moment in that panel. This analogy confirms the suspicion that the relatively large initial deflection was related to the dead load moments in the girders.

Table 5.13 shows the total lateral movement (sum of deflections in opposite directions) of panel 432P1 due to each test truck run, after the corrections to account for the resistance of strain gage cables. The largest total movement was 0.21 in., occurring during test truck run C123 when three simulated HS25 trucks travelled side by side in the three lanes. The largest deflection in one direction was +0.17 in. Adding this to the initial deflection of 1.13 in., the largest out-of-flatness of the web plate was 1.30 in. When a single test truck was traversing the bridges, the total lateral movement of the web was 0.11 in. or less, less than one-tenth of the initial deflection. Such a magnitude of lateral movement of the web was not detectable by eye during the test truck runs.

5.4.2 Web Plate Bending Stresses Under Test Truck Loads

Lateral deflection of web plates generates web (out-of-plane) bending stresses, particularly bending perpendicular to the plate boundary in the flexural compression zone of the girder. Strain gages in back-to-back pairs were mounted on the web, perpendicular to the top flange of girders in panels 432P1 and 432P2, and on the inside surface of panel 242, as shown in Fig. 2.11a. (Gage 242WN2 on the outside surface of exterior girder 4 was added later when a vehicle for inspection, snooper, was made available).

Examples of the strain-time traces from some of these web plate gages during the test truck runs are shown in Figs. 5.28 and 5.29. Figure 5.28 from test run C3 includes the strain variations at the two strain gages on the inside surface of web in pane 242, the clip gage for web deflection in panel 432 (as described in Section 5.4.1), and several

reference strain gages in spans 2 and 3. The strain traces of gages 242WS1 and 242WS2 both show tension on the inside surface, implying that the web was deflecting outward. The spikes in the traces correspond to live load compression generated by the axles of the test trucks almost directly over the gages. The general similarity between the shape of trace of these two gages and that of gages 222B and 222TS on the girder flanges indicates that the web plate bending is directly associated with the girder bending.

Figure 5.29 shows the corresponding strain-time traces of the three strain gage pairs in panel 432P1 and 432P2, from test run C3. For each pair, the back-to-back gages showed stresses of about the same magnitude but of opposite sign. For gages 432WS1 and 432WN1, the condition of tension on the south (inner) face and compression on the north (outer) indicates that the web plate was deflecting north (outward), which is in agreement with the deflection pattern from measurement (See Fig. 5.27).

The live load stresses at the web gages from the test truck runs are summarized in Table 5.14. The highest magnitude was 4.0 ksi in a panel of the interior girder and 5.3 ksi in a panel of the exterior girder, both occurred when three simulated HS25 trucks were traveling side by side (run C123). These magnitudes were higher than the primary flexural bending stresses in the respective top flange of the girders. For each pair of gages, during any test truck run, the recorded stresses were always of opposite sign, and of about the same magnitude, indicating out-of-plane bending of the web plate. In other words, the web plates always deflect laterally when the bridge was under live load. It is, therefore, prudent to consider web plate bending stresses when the initial lateral deflection

of web plates are relatively large.

6. LIVE LOAD STRESSES DUE TO REGULAR TRAFFIC

6.1 Live Load Stresses in Girder Flanges

6.1.1 Stress Variations in Girders

After the bridge was opened to regular traffic late in 1989, strain variations at some locations due to truck loads were measured in June, August and September of 1990. The purpose of these measurements was to detect noticeable changes of behavior of the bridge and to obtain stresses for assessing the fatigue life of certain structural details which are prone to fatigue cracking under live load stresses. Because live load stresses and the behavior of the bridge have already been examined using the results from test truck runs, comparison of live load stresses from regular truck traffic with those from test trucks would provide indication of noticeable behavioral changes. Additional strain gages were mounted on web panels and cross diaphragms for fatigue life assessment. These gages are shown in Fig. 2.11 but not included in the six groups of Table 5.2.

The first set of measurements included practically all strain gages on the bridge which had shown measurable strains, except the gages on the concrete deck, which had to be removed before the bridge was opened to traffic. Examination of the stress magnitudes and distribution of stresses from this set confirmed that there was no change in the behavior of the bridge between the test truck runs and trucks of regular traffic. During two subsequent sets of measurements, attention was directed to the web and cross diaphragm strain gages for fatigue life assessment.

That the bridge under regular truck traffic behaved as it did under the test truck loads, can be concluded upon comparison of the strain-time traces in Figs. 6.1 to 6.6 with those in Figs. 5.4 to 5.7 and 5.9.

Figures 6.1 to 6.6 show the strain-time traces of strain gages on sample girder flanges and web plates. Figures 6.1 to 6.3 show responses to a regular 18-wheel semi-trailer (3S2) in Lane 2 of the bridge deck (R2), travelling at about 60 mph, followed by two similar trucks 17 and 24 seconds later in the same lane and at about the same speed. The first truck generated highest stresses in the bridge components. The shapes of the strain-time traces of gages 332B and 342B, in Fig. 6.1 due to the first truck, for example, are the same as those shown in Fig. 5.9 from test truck run S2, which is due to a simulated HS25 truck traveling in lane 2 at about 55 mph. The magnitudes of stress ranges, however, are different, being lower for this regular truck of unknown weight and configuration (2.24 ksi and 1.95 ksi) than for the simulated HS25 test truck (4.81 ksi and 2.57 ksi, respectively as listed in Table 5.6).

The magnitudes of live load stress ranges at some locations due to the first truck of Figs. 6.1 to 6.3 are listed in Table 6.1. The magnitudes of stress ranges are not high. For a truck in lane 2, girders 2 and 3 are expected to be stressed slightly more highly than girders 1 and 4. Gages 322B and 332B indeed recorded slightly higher stresses than gages 312B and 342B. It is also important to note that all four gages recorded stress ranges less than 3 ksi.

Similarly, the stress ranges at all locations due to two regular trucks travelling side by side in lane 2 and lane 3 (R23) are lower than those due to the test trucks in the same lanes (S23 or C23). Figures 6.4 to 6.6 show the strain time traces of the same gages as those in Figs. 6.1 to 6.3. The shape of strain-time records of gages 332B and 342B, for example, are analogous to those corresponding ones in Fig. 5.6 for two

trucks crawling side by side (C23). The stress ranges from measurement at some gages of Figs. 6.4 to 6.6 are also listed in Table 6.1. Again, the magnitude of stress ranges due to regular trucks are lower than those due to the simulated HS25 test trucks at crawl speed, (see Table 5.8 for C23).

It is interesting to note that the distribution of stresses among the four girders under two regular 3S2 trucks (R23) was similar to that under two simulated HS-25 trucks in lanes 2 and 3 (test truck run C23). Considering that the regular truck responses included dynamic (impact) effect, comparison of the stress values listed in Tables 6.1 and 5.8 suggests that the effects of these regular 3S2 trucks is approximately that of a simulated HS-20 vehicle.

Further comparison and confirmation that there was no change of bridge behavior can be made by examining the shape or pattern of strain-time traces at various points along girders and by evaluating the distribution of stresses across bridge cross sections. For example, the variation of shape of strain-time traces for gage 340B, 341B, and 342B in Figs. 6.1 to 6.6 due to regular trucks (R2 and R23) are identical to those of S2 and S23 (or C2 and C23) due to the test trucks (see Appendix B). This condition indicates that the behavior of the bridge under truck traffic is similar to that under the test trucks. There had been no change in the structural characteristics.

Figure 6.7 summarizes the stress ranges in the four girders at the middle of span 3, during the assage of the distribution of stresses across the first truck of Fig. 6.1 to 6.3 (R2). For comparison, the stresses caused by a simulated HS 25 truck in lane 2 (C2) are also shown. The qualitative similarity of the two distributions among the four girders is

evident. Additional comparison is given in Fig. 6.8, which shows the stress distribution at the middle of span 3 for the test truck run C23 and the regular truck record (R23) from Figs. 6.4 to 6.6. Again the distribution of stresses agrees well.

All these comparisons confirm that the bridge behaved the same under the test truck loads and individual regular truck traffic load. The response of the bridge under continuous truck traffic with multiple presence of closely spaced trucks on the bridge is examined next.

6.1.2 Stresses due to Multiple Presence of Trucks

Each of the twin bridges has three traffic lanes. During the three periods of field measurement of live load stresses, it was observed that the bridge traffic was moderately heavy in some intervals of time. Because of the rightward curve of the roadway from the west approach around a stone wall, the eastbound truck traffic often travelled in the middle lane (lane 2) instead of the right lane (lane 1). Figures 6.1 to 6.3 (R2) show that, for that particular set of strain records, three 3S2 trucks were all in lane 2, travelling at about 60 mph. Figures 6.4 to 6.6 (R23) show two trucks side by side in lanes 2 and 3, also travelling at about 60 mph. It was observed that often high speed trucks travelled in lane 3 to pass other trucks in lane 2. This would cause higher magnitude of stresses in girders 3 and 4 below lane 2 and lane 3. Therefore, the examination of stresses at gages on girders 3 and 4 is appropriate.

The three trucks represented in Figs. 6.1 to 6.3, did not induce overlapping of individual strain-time traces. With a safe distance between trucks (about 500 and 600 ft.) respectively, each truck caused an

excursion of the strain-time trace independent of the preceding or following vehicle. Only when two or more trucks following each other at very close distances would the effects of strain variation overlap. Figures 6.9 and 6.10 are strain-time records from a number of strain gages while four trucks were travelling in tandem, at about 60 mph. The second, third and fourth trucks were about 4, 7 and 10 second behind the first, corresponding to a headway of about 350 ft., 260 ft., and 260 ft. between successive trucks. These distances are more than the length of the bridge spans, and there was almost no effect of any truck on the induced stresses of another truck.

When trucks travelled in different lanes, either side by side or almost side by side, their effects on the stresses at various locations of the bridge would overlap and superposition of stresses occurred. Figures 6.4 to 6.6 show the result of two trucks side by side, the effects are analogous to those of a single vehicle of heavier weight. This condition of stress superposition has been examined and discussed in Chapter 5 with reference to test truck runs. It suffices to mention here that random examination of strain variation on site during the strain measurement periods confirmed that two trucks side-by-side generated higher stresses than when the two trucks were staggered. Figures 6.11 and 6.12 show another set of strain-time traces caused by a series of trucks with two 3S2 trucks side-by-side among them. The shape of the strain-time traces from these two trucks is practically identical to that of a single truck, only the magnitudes of stresses differ.

From these examinations, it is clear that the bridge structure behaved linearly under normal truck traffic. It is extremely unlikely

that trucks following each other would be close enough to cause overlapping stress effects. When several vehicles travel side by side in different lanes, the effects can be estimated by simple superposition, as reported in Chapter 5.

6.2 Stresses at Web Boundaries

It has been reported earlier, in Section 5.4.2, that web plates with initial out-of-flatness deflected laterally under test truck loads and generated plate bending stresses perpendicular to the web boundary. Under random truck load of regular traffic, it was expected that web plate bending stresses would similarly occur. These stresses were measured at several selected locations.

Figure 6.12 includes the strain-time traces of three pairs of strain gages on the webs of the girder panels with the largest initial lateral deflection (see Table 5.12 and Fig. 2.11b). These strains (stresses) were induced by two trucks side-by-side in lanes 2 and 3 (R23). The stresses recorded by each pair of back to back strain gages, for example, 432WN2 and 432WS3, were always opposite in sign, indicating out-of-plane bending. The web plate deflected toward the side of compressive bending stress. The magnitude of the stress ranges are listed in Table 6.2, in the column with reference to Fig. 6.12. The magnitude of stresses are much smaller than those generated by two simulated HS 25 trucks travelling in the same lanes, (S23). These later magnitudes are also listed in Table 6.2 for comparison.

Because only a limited number of strain gages could be monitored at any one time while trucks of regular traffic were random and not repeated,

it was not possible to examine the stresses at all web plate gages due to the same truck. Table 6.2 lists several sets of measured live load stress ranges at web plate gages. The corresponding strain-time traces are included in Figs. 6.3, 6.6, 6.11, 6.13 and 6.14. For each of these cases, the lane position of the truck is indicated if it is known. The web plate bending stresses due to trucks of regular traffic, as listed in Table 6.2, are consistent with those due to the test trucks, summarized in Table 5.14.

From the results in Table 5.14 and 6.2, it can be deduced that, for web plates of interior girders, truck loads always increase the lateral deflection of the web. Depending on the direction of the initial lateral deflection, the web plate bending stress at the top edge was always compressive on the surface in the direction of deflection and tensile on the opposite surface of the web. For the web plates of exterior girders, however, the recorded web plate bending stresses were always in tension on the inside surface of the web, signifying that the web plate always deflected outward when the bridge was under truck loads. This direction of web deflection was opposite to the direction of the initial lateral deflection of the webs of the exterior girders. The inclined struts of the formwork for the deck overhang (Fig. 2.5) have caused the initial lateral deflection to be inward.

Regardless of the direction of web deflection under truck loads, the magnitudes of web plate bending stresses were always less than those generated by the test trucks, as shown in Table 6.2. The assessment of potential for fatigue cracking at web plate boundary will be made later in Chapter 7.

6.3 Stresses at Cross Diaphragms

The stresses in cross diaphragm members differ in sign and magnitude as trucks traveled in different lateral positions (or lane) across the bridge deck. This result has been presented in Section 5.2.2 with the help of Table 5.5 which summarizes the cross diaphragm member stresses under test truck loads. It has also been pointed out that the diaphragm member stresses were not necessarily higher when simulated HS trucks were present in more than one lane at a bridge cross section. During the periods when stresses due to regular traffic were monitored, the position and the weight of individual trucks were not known, yet similar differences of signs of stresses in diaphragm members were observed again and again. This occurred not only to a pair of top and bottom members on one side of a girder but also to top or bottom members on opposite sides of a girder. Figures 6.13 to 6.18 include examples of strain-time traces of strain gages on cross diaphragm members and on girder webs at the connection of these members to the girders.

The tensile and compressive stresses in the members of the cross diaphragms signify corresponding forces in these members. These forces push or pull the diaphragm connection plates (or stiffeners) which connect the diaphragm members to the girder web. The forces act on the plate girder and may bend the girder web at the cope or gap at the web-to-flange weld. Fatigue cracks have been observed to develop in these gaps of existing bridges where the connection plates were not positively attached to the flanges.[9.10] In the I-78 bridge over the Delaware River, the diaphragm connection plates are welded to the flanges. The plate bending stresses in the web at the cope were not expected to be high, but the

large distance between girders (14 ft-3 in.) and the relatively thin webs caused some concern. This was amplified by the detection of large lateral deflections of the web panels. For this reason, the strain gages on the web at the cross diaphragms were added and the strain measurements were made.

The strain-time traces in Figs. 6.13 to 6.18 include examples of the maximum responses of the diaphragm member strain gages to trucks of regular traffic during the period of monitoring. The maximum stress valuesare listed in Table 6.3. The web plate bending stresses at the connections plate were found to be higher than those in web panels at midspan of girders (Table 6.2). The maximum magnitude was about 6.4 ksi in range of stress, being approximately the same as the flexural stresses in the flanges of the girders (Table 6.1). Further examination of these stresses with regard to fatigue will be made later.

6.4 Stresses due to Vibration

The strain-time traces of cross diaphragm members due to regular traffic, as shown in Figs. 6.13 to 6.18, are similar in shape to those shown in Fig. 5.8 from a test truck traveling at crawl speed. Although the regular traffic vehicles were traveling at high speed and were expected t induce significant impact effect, there was no vibrational response of the cross diaphragm members. In contrast, the girder flange gages showed noticeable vibrational response, as shown in Fig. 5.9.

During test truck runs at high speed of 50-55 mph, the bridge girders were found to vibrate at about 4Hz when one simulated HS truck came onto the bridge. The vibration continued even when the truck got to

the other end of the bridge, lasting for more than twenty seconds before being damped out. This phenomenon was again observed under regular traffic when one truck came onto the bridge traveling at a speed of about 60 mph. Example of strain-time traces with such vibrational effects in the girder flanges are shown in Figs. 6.1 to 6.3 and 6.14. When two trucks traveled side-by-side, it was equivalent to a single truck and the vibration was similarly observed. Fig. 6.4 to 6.6 show examples of strain vibration in this situation.

When there were subsequent trucks following the first one which induced the bridge vibration, the dynamic effect of the subsequent trucks interrupted or changed the vibrational response of the bridge. This is depicted by the flange strain records of Figs. 6.1 to 6.3, 6.9 to 6.11, and 6.16 to 6.17. The interruption could by and large eliminate the vibration, as was the case of Figs. 6.1 to 6.3; could superimpose and extend the vibration, as shown by the strain traces of Figs. 6.9 to 6.11; or induce a new vibration, as indicated by the strains of gage 342B in Figs. 6.16 and 6.17. In all this situations, the important phenomenon is that the bridge girders vibrated, and induced vibrational cyclic stress variations (stress ranges) in the bridge girders.

Vibration of the girders led to the lateral vibration of the girder webs in web panels. This can be deduced from the strain variation in the two web plate gages, 242WN1 and 242WS1 in Fig. 6.11, the three pairs of web gages in Fig. 6.12, and gages 242 WS1, 242WS2 and 242WN2 in Fig. 6.14. The magnitudes of the cyclic stresses were not high, being less than 0.5 ksi. In terms of the total live load stress range due to a truck, this is about 20 to 25 per cent, about the same as that for the girder flanges.

Examination of the strain variation at the strain gages on the web at the cross diaphragm connection plate, such as those included in Figs. 6.13 to 6.16, reveals that those gages too were influenced by the vibration, but the effect was only minor.

The vibration of multigirder bridges due to random traffic loads is a fairly complicated behavioral phenomenon; the analysis of the lateral vibration of the web plates is even more complex. Although monitoring of flexural vibration and girder stresses using strain gages could be conducted with effort, [11, 12] it was beyond the scope of the intended study of this report. What must be kept in mind is that the bridge does vibrate due to truck traffic and, as a consequence, is subjected to large number of cyclic stresses of relatively low magnitude.

7. DISCUSSIONS

7.1 Assessment of Fatigue Life of Girders

7.1.1 Web Panels

One of the objectives of this study is to evaluate the fatigue life of girder web panels. The fatigue strength of a structural member is dictated by the strength of its details, which are represented by a set of curves correlating stress ranges and number of expected stress cycles (S-N curves). For the lateral or out-of-plane bending of web plates, the fatigue strength is currently represented by the Category C curve of the AASHTO specifications for bridge design.[2, 13] This curve is a straight line in the stress range versus cycles diagram of logarithmic scale, as shown in Fig. 7.1. The curve is applicable for stress cycles of constant amplitude. However, at any structural detail in a bridge, the stress ranges induced by the vehicular traffic of trucks and cars, are not of constant amplitude. Based on current knowledge, if the magnitude of all stress cycles is lower than the constant amplitude fatigue limit (CAFL), which is 10 ksi for Category C, no fatigue damage would be expected of this structural detail.[9, 13]

As has been mentioned earlier in this report, large initial lateral deflections of the web plate result in higher web plate bending stresses. The measurement of these stresses in a few selected web panels with relatively large initial deflections yields stress ranges of about 1 to 2 ksi for most of the trucks, up to about 2-4 ksi occasionally, but always lower than 10 ksi, the constant amplitude fatigue limit. (See Section 6.2) Consequently, based on these results, no fatigue cracking would be expected of the web panels of the girders.

Two aspects concerning stress magnitudes and the vibration of the web plates need to be examined. Because the measurement of web plate bending stresses was carried out only for limited periods of time, it is uncertain whether the occurrence of the highest possible live load stress range has been captured. This is a question of traffic characteristics and probability and cannot be definitively answered without an extensive traffic survey. More important is the question of stress range magnitude. Examination of Table 5.14 reveals that the highest stress range recorded, due to three simulated HS25 trucks crawling side by side in the three lanes, was 5.3 ksi in an exterior girder panel, and 4.0 ksi in the interior girder panel 432 which exhibited the largest initial lateral deflection.

During the periods of measurement of regular traffic load stresses, it was not known whether these heavy trucks ever occurred abreast in all three lanes. It was not known what vehicle configuration and position caused the largest recorded web bending stress of 3.7 ksi at gage 242WN2 (on an exterior girder). Nevertheless, as illustrated in Chapter 6, the bridge behaved linear-elastically under traffic load, as under test truck runs. An estimate of the maximum range of the stress cycle can be obtained according to the principle of superposition. For the condition of three HS-25 trucks traveling abreast, and applying a magnification factor of 1.2 to reflect the dynamic effect, the maximum web bending stress range would be 5.3 x 1.2 = 6.4 ksi. For the improbable condition of an HS-25 in lane 3 overtaking a slow-moving 204-k permit truck, the corresponding stress range would be 3.7 x 1.2 + 1.6, or 6.0 ksi. These estimated stress ranges would still be considerably lower than the

constant amplitude fatigue limit of 10 ksi. As was previously pointed out, regardless of the large number of cycles of low-amplitude stresses due to the effect of bridge vibration, no fatigue cracking along the web to top flange boundary is expected because the largest stress range live load is lower than the fatigue limit.

It should be pointed out that the relatively large live load out-of-plane bending stresses induced in the web plates of the interior girders are the results of relatively large initial lateral deflection of the web plates. More discussion on the initial deflection will be made in Section 7.3

7.1.2 Diaphragm Connections

The diaphragm action of the cross members induce push and pull between the diaphragm connection plates and the web plate, resulting in web plate bending stresses in the region. Many fatigue cracks have been found at this structural detail in existing bridges when the diaphragm connection plates are not positively connected to the girder flange [9,10,14]. In the I-78 bridge under study, the diaphragm connection plates are welded to both the top and the bottom flanges at every cross diaphragm. This arrangement permits the transfer of forces from the cross diaphragm member through the connection plates to the flanges as well as to the web, and alleviates the development of high web plate bending stresses.

However, possibly as a result of the large spacing between girders and the relatively thin web plates, the measured web plate bending stresses at the copes of diaphragm connection plates of this bridge were

not low. They are actually higher than those at the middle of web panels (See Section 6.3). The highest measured web plate bending stress at diaphragm connection plates was 6.4 ksi in the web of an exterior girder. The type, weight, and position of the truck which produced this stress are unknown. By the examination of concurrent stresses at other strain gages, it is estimated that the truck was in Lane 2, traveled at about 60 mph.

Whether this magnitude of 6.4 ksi represents the highest possible stress under regular traffic is uncertain. Examination of Table 5.5 reveals that trucks in Lane 2 generated highest cross diaphragm member forces at exterior girders. These forces in turn produce the highest web plate bending stresses at the connection plates. Assuming that this vehicle was equivalent to an HS-20 truck, and that HS-25 trucks will be permitted on the bridge, the highest magnitude of web plate bending stress may be extrapolated to be 6.4 x (25/20) = 8.0 ksi. This is less than the constant amplitude fatigue limit of 10 ksi. Therefore, no fatigue cracking would be expected of the web at diaphragm connection plates.

7.1.3 Girder Flanges

The flanges of girders contain both bolted field splices at about quarter spans, and butt-welded joints with transition of width and thickness of the flange plates. In the middle half of each span, the girder flanges are single prismatic plates with continuous fillet weld connecting the plates to the webs. The fatigue strength of the bolted splices and the continuously welded flanges is that of category B, with a constant amplitude fatigue limit (CAFL) of 16 ksi. The butt-welded joints have a fatigue strength of category C and CAFL of 10 ksi.

The butt-welded joints of the bottom flanges are in the negative moment region near the piers and are subjected to compressive live load stresses; those of the top flanges are only subjected to very low tensile stresses (always below 2ksi) because of the composite action between the steel girders and the concrete deck. (See Table 5.9 for the stresses from measurement). Therefore, there should be no expected fatigue cracking at the butt-welded joints.

The highest live load stresses due to trucks of regular traffic was measured to be 6.2 ksi in an exterior girder at the middle of span 3 when two trucks traveled side-by-side in lanes 2 and 3. The stresses in the bottom flanges of girders in Span 4 was slightly lower. If these trucks were equivalent HS 20 trucks, the expected live load stress due to two HS 25 trucks would be 6.2 x (25/20) = 7.8 ksi. This is less than that due to the superimposing of test truck speed runs S2 and S3, 2.57 + 7.27 = 9.84 ksi by Table 5.6, or that from the incorporation of dynamic effects to the crawl run C123 of three simulated HS 25 trucks, 8.23 x 1.20 = 9.88 ksi by Table 5.8. If a 204 kip permit truck is traveling in Lane 2 and a HS 25 speeds by in Lane 3, the combined flange stress would be 2.78 + 5.62 x 1.20 = 9.53 ksi from Table 5.8. All these live load stresses are well below the CAFL of 16 ksi for the flanges. Therefore, there should be no danger of fatigue cracking at the flange to web welds of the girders.

No doubt, the consideration of fatigue strength of the flanges has been incorporated in the process of designing the bridge. The above results from measurement and interpretation confirm the adequacy of the girder flanges with respect to fatigue strength. With the flanges, web panels, and diaphragms all having sufficient fatigue strength under HS 25

loading, it can be stated with confidence that the bridge is not expected to develop fatigue crack in its components. As long as the bridge is adequately maintained, the girders should have indefinite life with respect to fatigue.

7.2 Transverse Cracks in Concrete Deck

Whereas the bridge structure is assessed to be satisfactory in fatigue strengths under traffic load, cracks were detected in the concrete deck before the bridge was opened to traffic. It was found that many transverse cracks existed in the deck across its widths and at some locations continued up the cast-in-place parapet. These cracks were at the middle of spans in the positive moment region much more than in the negative moment region over the piers. The width of some cracks was more than 0.05 in. on the deck surface. Under the bridge deck, where stay-in-place metal forms prevent visual examination of the lower surface of the concrete slab, corrosion of the metal form was noticed at several locations, indicating that water had seeped through the deck at these places. This was detected before the monitoring of stresses due to regular traffic. Visual observation of the exterior girders at that time revealed discoloration of the bottom flange at some places along the bridge. These "white" spots are directly under the overhang of the concrete deck where there is no stay-in-place metal form and water can drip onto the bottom flange. Transverse cracks in the deck could be found above the discolored spots. There appeared to be more white spots in spans 2, 4, and 6.

The larger cracks have been patched and no new transverse cracks

have been reported. Continued monitoring of the discoloration of the bottom flange of exterior girders and corrosion of stay-in-place deck forms appear advisable, together with the detection of any additional cracking of the deck slab. On he other hand, a preliminary examination of the genesis of these cracks would be useful.

As the transverse cracking of the deck slab was not originally included in the tasks of this study, there was no comprehensive surveillance of the deck slab at the very early stage when these cracks developed. Nevertheless, with the small amount of information available, it is possible to suggest two plausible causes for these cracks.

It is well known that the hydration process of cement generates heat, and causes the temperature of fresh concrete to rise. The amount of heat generated, and the temperature rise, depend upon many parameters, including the type of cement, the composition of concrete. The curing procedure, the ambient environment, and the dimensions of the member. For highway bridge deck slabs, it is not unusual for a 50°F temperature increase to occur in the initial stage when concrete is still plastic. Subsequent cooling to the ambient temperature would cause hardened concrete to contract, and cracking could occur if the contraction is prevented from taking place. In the case of the bridge deck, longitudinal restraint is provided by the stud connectors on the top flange of the steel girders. The thermal contraction of concrete corresponding to a 50°F temperature drop would be approximate 270 microinches per inch. Even if a part of this contraction is relieved by the deformation of steel, the concrete tensile strength (particularly at the very early age) can be easily reached and cracks would develop. It is noted that in the

transverse direction, the steel structure is far more flexible, hence longitudinal cracks do not form on the concrete deck.

The sequential casting of the concrete deck in segments may also be inducive to the transverse cracking of concrete deck. As indicated in Fig. 2.4, the continuous deck was cast in segments. The cross sections at the middle of spans 4 and 3 received the segments 1 and 2W, respectively in day 1. As other segments were subsequently cast on portions of the girders in other spans, segments 1 and 2W hardened gradually and the middle of spans 4 and 3 gradually developed into composite girders. When deck segment 2E was cast in span 5 on day 5, strains were in the concrete of segment 1 and 2W. Assuming that the deck concrete at those locations had hardened sufficiently to carry strain and that the strain variation was linear throughout the depths of the girder cross sections, the magnitude of the strains at the top fiber of the concrete deck could be estimated by extrapolating from those in the girder flanges. These estimated top fiber strains of the concrete deck at locations 432 and 332 are listed in Tables 7.1 and 7.2. Also listed in the table are the measured strains in the girder flanges and the changes of strains from day 1 when the deck concrete had been placed, but not yet set. The assumption is that there was no stress-related strain in the concrete deck at 432 and 332 before casting of segment 2E on day 5.

The estimated strain in the top fiber of the deck at 332 in span 3 was compressive on day 5. This is consistent with the theoretical condition that application of loads in one span here (span 5) of a continuous beam induces positive bending two spans away (in span 3), hence compressive strain in the top fiber. However, cast 2E in span 5 also

induced compressive strain in the top fiber of the deck at location 432 in span 4. In fact, the entire cross section at 432 was subjected to compressive strain due to the casting of segment 2E. This state of strain included the combined effects of weight of segment 2E, construction loads on the bridge, bearing conditions at piers 3 and 4 at the ends of span 4 as well as at all supports, concrete shrinkage and change of temperature due to hydration, and all other unknown causes. Many of these effects cannot be adequately estimated. Therefore, evaluation of the deck strains during construction of the bridge can only be reasonably made through the use of measured strains in the girder flanges.

Table 7.1 shows that the estimated strain at the top fiber of the deck at 432 was -233 micro in. per in. For the next three days, days 6, 7 and 8, the top fiber was subjected to reduction of strains due to the casting of other segments (3E, 3W, 4E and 4W) of the concrete deck. The magnitude of strain reduced from -233.1 to -227.5 to -169.5 to -149.8 micro in. per in., with a total of 83.3 micro in. per in. Whether this magnitude of strain reduction in three days in the lightly compressed and slowly hardening concrete would produce the transverse cracks at location 432, is not certain. No information is available in literature providing similar conditions for judgment. The suspicion is that hair cracks might develop, and these hair cracks would grow wider as hardening and shrinkage of concrete continued. Between days 13 and 15, the magnitude of strain again reduced, from -271.3 to -205.5 to -186.8 micro in. per in. for a total of 84.5 micro in. per in. This was about the same amount as that between days 5 to 8. It is suspected that additional transverse cracks in the deck formed in these later days.

The estimated strains at the top fiber of concrete at location on 332 reduced from -132.6 to -70.7 between days 6 and 9, as shown in Table 7.2. The total reduction of 61.9 micro in. per in. was less than that at location 432. Thereafter, the top fiber strains became continuously more compressive. This is consistent with the observation that there were fewer transverse cracks in the deck in this region than in span number 4.

At cross section 232 in span 2, the concrete deck segment 4W directly over this portion of the steel girders was cast on day 8. Assuming that the concrete hardened sufficiently to carry stresses on day 9, the estimated strains at the top of the concrete deck have been computed and are listed in Table 7.3. From these estimated strain values there was a minor reduction of compressive strain between days 10 and 13, and between days 14 and 15. Between days 16 and 22, compressive strain was continuously decreasing, changing from -125.5 to +97.0 micro in. per in., for a total of 222.5 micro in. per in. This magnitude would no doubt induce cracking of the deck in span 2.

In summary, two contributing factors are suggested for the development of transverse cracks in the concrete deck slab. Other factors may include the change of thermal gradient of the composite girders, and the seasonal changes of ambient temperature. An understanding of the true cause of these cracks, and the control of them, can be achieved through future research. At the current time, one such study is being conducted under the auspices of the National Cooperative Highway Research Program, as Project 12-37.

7.3 Flange Stability and Web Deflection During Construction

7.3.1 Web Deflection

From the results of measurements presented in Section 4.2, 5.4 and 6.2, the following phenomena and observations can be summarized.

(1) Web panels had initial out-of-flatness or lateral deflection of the web plates when the girders were erected.

(2) Adding of concrete deck on top of the plate girders increased the magnitude of lateral deflection in web panels of both interior and exterior girders. This increase of lateral deflection is sometimes referred to as "buckling".

(3) The inclined struts of the formwork for the overhanging portion of the deck caused the web plate of the exterior girder to deflect inward.

(4) As a general rule, the web plates in adjacent web panels of interior girders "buckled" or deflected in opposite directions.

(5) The magnitudes of lateral deflection of web plates were relatively large under the weight of the bridge. The largest measured value was 1.13 in. in a 100 in. x 90 in web panel at location 432 of an interior girder, corresponding to twice the thickness of the web plate. In exterior girders, the largest measured deflection was 0.89 in. or 1.6 times the web thickness in a 300 in. x 82 in. panel which was braced during construction, and 0.60 in. or 1.1 times the web thickness in a 100 in. x 86 in. panel which was not.

(6) Under live loads on the deck, the lateral deflection increased slightly in web panels of interior girders, and decreased slightly in exterior girder web panels. The decreasing of web deflection in exterior girder web panels corresponded to the condition that the live loads caused

the web plates to deflect outward, against the inward permanent deflection due to dead load.

(7) The magnitudes of web plate bending stresses due to live loads were not high, being less than 6 Ksi in all cases of measurement. Even with additional dynamic effects and combination of high loads, no fatigue damage is anticipated.

Based on the foregoing observations, it is concluded that, although the web deflections are relatively large, there is no problem of web behavior under live loads, nor is there a problem of girder strengths under these loads. It is the behavior of the bridge girders during construction that needs to be examined. The examination is made in the following sections with respect to the web panels of interior girders and of exterior girders, separately.

A. Web Panels of Interior Girders

The web panels of interior girders had initial lateral deflection after fabrication. The maximum permissible out-of-flatness is specified by the AWS Codes.[5] For the 100 in. x 90 in. web panels, the limit is 90/67 = 1.34 in. and for the 300 in x 82 in. panels 82/150 = 0.53 in. These values are comparable with the measured "permanent" lateral deflections, under the total dead load of the bridge structure (see Table 5.12), which are much larger than the corresponding deflection at fabrication time. It is clear that the girders of this bridge satisfied the AWS limits when fabricated.

Although not specifically required, the out-of-flatness of web plates due to fabrication is usually measured with the girders in the upright position and continuously supported. The deadweight of a girder

is not acting on the girder in this condition. When girders are erected on site, the sequence of field splicing, the arrangement of bearings, the attachment of diaphragm and bracing members, etc., dictate the distribution of girder weights and create different web panel forces. The out-of-flatness or lateral deflection of the web plates changes accordingly and takes on "initial" deflection profiles such as those shown in Fig. 4.36. For girders with relatively stocky cross section and moderate length, these "initial" lateral deflections of web plate panels under the girder's own weight are usually not large, and usually not noticeable. For this bridge, the girders are relatively slender, the span length of 228 ft. is fairly long, and the "initial" lateral deflection of the web under the girder weight was larger than usual and was visible. Unfortunately, the examination of web lateral deflections of the interior girders was requested late during the construction, and measurement of the "initial" deflections under the girder's own weight could not be made. Because the slenderness and flexibility of the girders caused some concern on their overall lateral stability, presumably the strength of the bare girders during erection was evaluated. But current design practice does not impose an upper limit of the lateral deflection of the web plates for the girders under their own weight; measurement of web deflection by the construction engineers was not expected.

When the bridge deck was cast, the lateral deflection of web plates in girder web panels increased. Because there was initial out-of-flatness from fabrication and initial lateral deflection under the girders' weight, these increases are not "buckling" of the web plate in the narrow sense of sudden snapping or "bifurcation". It was just a gradual change of lateral

deflection of the web plates in response to the increase of dead weight of the bridge. Classical analysis of web panels with perfectly flat web plate provides the theoretical "buckling load" of the plate under various boundary and loading conditions. [8, 15]. However, little information is available in the literature on the magnitude of lateral deflection of web plates with initial out-of-flatness. Computation of lateral deflection by procedures such as using finite element models is necessary and requires definite information of the initial lateral deflection. Furthermore, for this continuous composite girder bridge, the sequential placement of concrete deck segments, their gradual development of composite action with the steel girders below, the fixed bearing at both ends of span 4, and other factors made accurate computation of web deflections impossible.

On the other hand, it is well known from analyses of specific cases of plate panels with and without initial lateral deflection that the behavior of perfect plates can be viewed as an upper bound of the behavior of imperfect plates and that plate panels with larger initial lateral deflection will have larger lateral deflection under load. A quantitative sketch is shown in Fig. 7.2. The maximum capacity of the plate panel to carry load is not limited by the buckling load. The significant postbuckling strength of plates has been recognized and are incorporated in both the allowable stress design procedure and the load factor design procedure of AASHTO provisions[2]. The condition which is important for the evaluation of web plates in this girder bridge is that web panels with relatively large initial lateral deflection and relatively low buckling strength would have larger lateral deflection when web panels are under relatively high loads.

For the 100 in. x 90 in. x 9/16 in. web plate at location 432, under a triangular loading condition corresponding to that of Day 20 in Fig. 4.2, the buckling stress of a perfectly flat plate with simply supported boundary is estimated to be about 8.0 ksi.

$$f_{cr} = K \frac{\pi^2 E}{12(1-\nu^2)} \left(\frac{t}{D}\right)^2$$

$$= 7.8 \frac{\pi^2 (29,000)}{12(1-0.3^2)} \left(\frac{9/16}{90}\right)^2 \qquad (7.1)$$

$$= 8.0 \; ksi$$

The stress in the top flange of the girder at this location 432, was 22.70 ksi as shown in Fig. 4.2 The relatively large lateral deflection of the web plate was consistent with this loading condition and load magnitude. The measured lateral deflections of the two adjacent web panels were 1.13 in. and 1.06 in., respectively, nearly twice the plate thickness, as listed in Table 5.12.

To examine further the buckling stresses of the web panel at location 432, the contribution of the vertical, gravity load of the concrete deck is considered. Figure 7.3 shows schematically the loading condition of a perfectly flat web plate with all edges approximated as simply supported. By using the classical method which employs the energy concept and a trigonometric series representation of web deflection, the buckling stresses of the web plate panels at location 432 are computed for various ratios of top and bottom flange stresses. The results are plotted in Fig. 7.4. The influence of the vertical edge load (estimated as 0.17

kips per in.) is seen to be not strong on the buckling of the web plate; it amount to only a few per cent. Of interest is the comparison between the analytical buckling stress and the actually measured stress at different days of deck concrete placement. On day 1, after the casting of concrete deck segments 1 and 2W (see Fig. 2.4), the measured stress was below the buckling curve, as it is shown in Fig. 7.4. The computed (theoretical) stress condition due to the deck segment 1 alone is also shown for reference (point TH). The fact that both points 1 and TH lie below the buckling curves indicates that perfectly flat plate would not "buckle" under these loading conditions. The data points corresponding to the measured flange stresses of days 5, 6, 9 and 20 all lie above the buckling curve in Fig. 7.4. It is therefore most likely that the web plate of the 100 in. x 90 in. panels in the interior girder at the middle of span 4 undertook relatively large magnitudes of lateral deflection at these stages of deck concrete placement.

No measurement was made on the initial deflection of the web at location 132 or 122 under the girders' own weight, nor the deflection under the weight of the concrete deck. These 300 in. x 82 in. x 9/16 in. web plates were braced laterally against each other and against the webs of the exterior girders at locations 142 and 112. Had these long web panels been unbraced, the lateral deflection of the web plate after completion of the deck would be expected to be large. It is important to note that, all other conditions being the same, longer web panels generally have larger initial out-of-flatness and larger lateral deflections under load. The AWS codes [5] place a more stringent limitation on out-of-flatness from fabrication for unstiffened web panels.

But there is no provision in the AASHTO specifications [2] for a permissible lateral deflection of webs under load. It appears from examination of web deflections of test girders [8, 16, 17, 18, 19, 20, 21] that the simplest approach to control lateral deflection is to limit the aspect ratio (such as 1.5) for web panels. More discussion on this will be made with respect to exterior girders.

B. Exterior Girder Webs subjected to Lateral Loads

The computation of lateral deflection of webs in the exterior (fascia) girders of the bridge is even more complicated than that for the interior girders because of the inclined struts of the triangular wooden frames which support the formwork for the overhang of the concrete deck. The inclined struts, as shown schematically in Fig. 2.5, introduce lateral thrust forces on the web plate and cause the web plate to deflect inward.

The lateral force applied onto the web plate by each strut was not known. Before the casting of deck concrete, this force was due to the weight of the formwork for the deck overhang, the reinforcing bars in this region, and the rail and supports for the concrete deck paving machine. Regardless of the actual magnitude of the force in a strut, it pushed the web plate inward. This was observed at all exterior girder web panels of the bridge during construction. The deflections at this stage of construction were measured at locations 142 and 242, and the results are shown in Table 4.4 and Fig. 4.36. When deck concrete was cast directly above, the weight of the concrete produced higher forces in the struts and also increased the girder bending moment at the web panel. Therefore, the computation of the web deflection of a girder web panel requires knowing not only the initial lateral deflection of the web plate (due to the

weight of the girder) and the thrusts in the struts acting in the panel, but also the primary bending stresses acting along the boundary of the panel. The actual web plate profiles at sections 142 and 242, from measured deflections at this stage are shown in Fig. 4.36.

To explore the influence of the forces from the inclined struts on the lateral deflection of the web in a panel, several simplified analyses were made. The first is to consider the lateral deflection of perfectly flat web plates subjected to lateral forces from the struts in the panel. Assuming the triangular wooden frame (Fig. 2.5) to be a truss with hinged supports at the lower end of the inclined strut and at the anchor at the tip of the flange, the horizontal force at the lower end of the strut can be estimated. This force is applied at each triangular frame to the web plate of the girder panel at location 142 and 242. The resulting lateral deflection by a finite element model is about 1.7 in. for the web panel at 142 and 0.8 in. at 242. The magnitude at location 242 is in very good agreement with the measured deflection, as listed in Table 4.4. The web panel at 142 was braced against the web at the interior girder at 132, and the actual lateral deflection was much less than the computed value which did not take the bracing into account.

The second analysis is an examination of the effect of the vertical position of the inclined struts. A horizontal force is applied from each strut at different assumed distance from the top flange of the girder panel. This force is estimated from the truss model of the triangular supporting frame as described above, but having the assumed distance of the strut. Fig. 7.5 shows the maximum lateral deflection of the web panel 242 as a function of the strut position. These computed lateral

deflections can only be considered as very rough estimates. However, the trend that the lateral deflection decreases as the strut position is lowered is unmistakable. It confirms the belief that placing the struts at the lower part of the web would reduce the lateral deflection of the web. One very good theoretical solution to the problem of lateral deflection of the web due to the deck form support at the overhang would be to place the lower end of the inclined strut at the junction of the bottom flange to the web.

A third series of analyses was used to examine the effects of web panel aspect ratio (length to depth), d/D. By using the same model as used in the first analysis of the web panels at 142 and 242, but assuming different values of the aspect ratio, the magnitude of lateral deflection of web were computed. The results are shown in Fig. 7.6. Panel 242 has a web depth of 86 in. and a web slenderness ratio of D/t = 153. For panel 142, D is 82 in., and D/t ratio is 146. Since panel 242 is slightly more slender, it has slightly larger lateral deflection for the same aspect ratio of the web. The magnitude of web deflection consistently increases as the aspect ratio increases. This indicates that longer panels would have larger web deflections. A reduction of the aspect ratio from 3 to 1 would result in a decrease of lateral deflection by approximately 50%. Therefore, reducing the distance between intermediate transverse stiffeners would be an effective solution to the problem of lateral deflection of web at exterior girders with inclined struts for the deck form support.

With two possible ways of controlling the lateral deflection, a comparison is warranted. Before doing so, it should be noted that in both

series of analyses, the web plate is assumed to be perfectly flat and the primary bending moment of the web panel is not considered. With these conditions in mind, the following comments can be made with regard to the control of lateral deflection of webs of exterior girders when triangular support frames for deck overhand are utilized.

(1) Without imposing new rule or changing existing rules on the design or fabrication of girders, the simplest procedure of avoiding development of large lateral deflection of exterior girder webs would be to place the inclined strut at or near the lower edge of the web plate. The advantage of this approach is that only one party, the contractor, would be involved in the decision as to the position of the strut. However, to achieve an effective deflection control, the contractor would need to make supporting frames of different sizes, incurring added cost of construction. At the present time, the triangular support frames are more or less standardized to have the inclined struts about 30 in. to 45 in. from the top flange of a girder, which is typically less than half of the web depth of modern long span girders. Furthermore, even when such a statement of strut position is included in the construction contract and rigidly enforced, the exterior web may still exhibit relatively large and noticeable (and aesthetically disturbing) lateral deflections because of the possible large initial out-of-flatness, high girder moments, likely large panel length of web of modern girders, and the strut forces if the struts are not at the junction of the web and the bottom flange.

(2) The reduction of the maximum permitted spacing between intermediate transverse stiffeners on girder webs can be easily accomplished. The current AASHTO limit is three times the web depth, or

3D,[2] which was determined on the basis that when the load carrying capacity in shear is adequate, transverse stiffeners at 3D spacings would provide some undefined control of the out-of-flatness of the web plate, and that the diaphragms are often placed at these spacings. In other words, this limit of 3D is based more on girder capacity (strength) and only marginally on girder behavior under load. In earlier AASHTO Specifications, the maximum permitted stiffener spacing was 1.5 times the web depth. That earlier limit of 1.5D was adopted with consideration of lateral deflection of the girder web under load, possible fatigue damages at web panel boundary, and the lateral flexibility of the entire girder during erection.[22, 23, 24] From the curves of Fig. 7.6, it is obvious that web panels having lengths of 1.5D have smaller lateral deflection than panels having lengths of 3D, when both are subjected to the same lateral force from the inclined struts. At 1.5D, the lateral deflection of the web after the completion of the bridge would most likely be less than about 1.5 times the web thickness. No plate girder web has been found to develop fatigue crack under traffic load with this magnitude of initial lateral deflection and an aspect ratio less than 1.5D. [8, 24, 25] Other advantages of imposing this upper limit of 1.5D for stiffener spacing include that the likely smaller initial out-of-flatness from fabrication, the subsequent less visible permanent lateral deflection under dead load, and not having to rely on the contractor to control these possible unsightly permanent deflection. The addition of a few transverse intermediate stiffeners during fabrication and a very slight increase of girder weight appear to be minor disadvantages. For example, for this bridge system of eight continuous girder in the twin bridges, only one

midspan panel in the end span of each girder exceeds the 1.5D limit. Imposing the 1.5D limit would only add four stiffeners and about 320 lbs. of weight to each girder. The increase of fabricational cost would be very small in comparison with the total cost of the bridge.

Based on the above discussion, it is believed that the better approach to control the permanent lateral deflection of girder webs is to impose a more stringent limit for the distance between transverse stiffeners. It is recommended that the following equation, which was in the AASHTO Specifications up to 1983, be re-adopted.

$$d_o \leq D \left(\frac{260}{D/t_w}\right)^2 \leq 1.5D \qquad (7.2)$$

7.3.2 Flange Stability During Construction

While there were unexpectedly large lateral deflections of web plates and high compressive stresses in the top flanges of girders, no damage of any web panel or flange in the interior girders of the bridge was detected during construction of the bridge superstructure. A single mishap occurred at the top flange of an end span of one exterior girder at location W742. The stay-in-place metal form for the concrete deck and the supporting angle separated from the flange. The tack welds between the supporting angle and the edge of the top flange were torn, and about 40 in. of the metal form dropped, spilling the wet concrete. This event led to the shoring of the overhanging part of the concrete deck and bracing of the unstiffened web plates at similar locations of other girders. No

subsequent difficulty was encounted at these places.

To explore the cause which triggered the separation of the metal form from the top flange, an examination of the loads and conditions of the girder panel is necessary. The web panel of the girder at W742 and other similar web panels in the end spans has no transverse intermediate stiffeners between cross diaphragms, and is 300 in. long, 82 in. deep and 9/16 in. thick (see Fig. 2.2). The top flange is a 12 in. x 5/8 in. plate and is not braced between the cross diaphragms. When the concrete deck segment over the end of the girder was placed, the girder panel was subjected to in-plane bending moment and shear, vertical gravity load of the wet concrete through the top flange, and horizontal out-of-plane forces which were the component forces of the triangular formwork supporting the deck outside of the girder.

A schematic of a "compression flange beam-column" representing the top flange is shown in Fig. 7.7. The vertical forces, q_o and q_i, are from the outside and inside formworks of the deck, respectively; q_c is the weight of the portion of wet concrete and reinforcing bars directly above; and q_w is the balancing or resisting force from the web. The horizontal forces, p, are the reactions from the triangular supporting frame of the deck overhang. The twisting moment, m, is associated with the lateral bending and deflection of the web plate. The magnitude of any of these forces must be estimated to enable an evaluation of the behavior of this beam-column. There could also be horizontal forces above the flange plate, induced by the interaction between the reinforcing bars and the shear connectors, but these forces are judged to be negligible because the ties at the shear connectors are not "positively connected".

The breaking of the tack weld along the inner edge of the flange could be due to inferior quality of a few adjacent welds, or due to excessive deflection of the flange plate. Assuming that the tack welds were appropriately made, attention is here focussed on the possible deflection of the top flange. The flange plate could deflect vertically down towards the web plate, rotate or twist with respect to the junction between the web and the flange, or move sideways with the attached web.

(1) The vertical, downward deflection of the top flange is associated with the lateral deflection or the broader sense of buckling of the web plate. An exaggerated configuration is sketched in Fig. 7.8. Lateral deflection of the web causes reduction of the distance between the flanges and thus the vertical deflection of the top flange. If the magnitude of vertical deflection of the flange plate is small and gradual from one end of the panel to the other, the metal stay-in-place form and the attachment angle along the inside edge of the flange would move down with the flange. No separation of the attachment angle would take place. Breaking of the tack welds and separation would occur only when there is a sudden and drastic change of slope, that is, large curvature of the flange profile, which is not compatible with the vertical bending rigidity of the attachment angle.

Referring to Fig. 7.8, the vertical deflection of the flange is dependent upon the vertical web force q_w which in turn is related to the lateral deflection of the web plate. Accurately determining the distribution of q_w is not currently possible. It is, however, qualitatively known that q_w is not uniform along the panel length, and that this resisting force is smaller where the lateral deflection of the web is

larger. Referring to the ideal case of a perfectly flat web plate and an uniform q_w, the maximum vertical stress which could be applied on the web along the top flange without causing web plate "buckling", and thus large deflection and curvature of flange, has been estimated.[8, 22] This stress is calculated by the formula

$$f_m = \frac{\pi^2 E}{12(1-\nu^2)} [2.0(\frac{t_w}{D})^2 + 4.0(\frac{t_w}{d})^2] \qquad (7.3)$$

where d is the length of the flange between stiffeners. For the web panel at W742, d = 300 in. and the magnitude of the estimated maximum stress is f_m = 2.59 ksi. The estimate value of q_o, q_i and q_c are 22.8, 72.9, and 10.4 lb per in. respectively, resulting in an applied vertical stress q_w of (22.8 + 72.9 + 10.4) + (9/16) = 189 psi. Since the applied force is much smaller than the estimated strength, no large downward deflection of the flange would be expected to take place.

It is important to note that Eq. 7.3 indicates that a smaller d would provide a higher verticle buckling load of the web plate, and consequently smaller downward deflection of the flange due to the vertical load. This means that closer spacings between stiffeners would reduce the risk of vertical buckling of web plates. Adding an intermediate stiffener between the diaphragm connection plates at W742 would reduce d to 150 in., and the web buckling strength according to Eq. 7.3 would become 3.70 ksi. Examination of literature shows that the strength of vertical buckling of flange into the web usually is not the governing condition of failure.[8, 16,18, 22] The significant benefit of adding an intermediate stiffener is

the reduction of vertical-load-induced lateral deflection of the web which had strong influence on other modes of girder panel failure.

(2) The twisting of top flange plate could lead to the breaking of the tack welds between the flange and the attachment angle. For a flange plate subjected to compression without vertical loads, the flange local buckling stress corresponding to twisting is estimated by using the classical equation for long plates.

$$f_{cr} = K \frac{\pi^2 E}{12(1-\nu^2)} \left(\frac{t_f}{b}\right)^2 \qquad (7.4)$$

In the equation, b is the outstanding width of the flange plate and t_f is its thickness. The length of the plate does not appear in the equation because the buckling is of a local nature. If the constraint to flange twisting is equivalent to a fixed support along the flange-to-web junction, the coefficient, K, has a value of 1.277[8]. Because the flange plate at the location of consideration is relatively stocky, the flange local buckling strengths is very high, thus is not governing.

With the vertical loads q_o, q_i, and q_c, and the twisting moment m, as shown in Fig. 7.7, the twisting phenomenon is much more complicated. There is no simple, readily available solution to the mathematical problem. The twisting of flange is associated with the vertical bending of the outstanding width of flange plate between supports which are the vertical intermediate stiffeners or the diaphragm connection plate of the web. Without knowing the twisting moment m, no attempt has been made to estimate the twisting of the flange at location W742.

It is, however, again obvious that the spacing of vertical stiffeners plays an important role. The closer is the distance between stiffeners, the higher would be the resistance to flange twisting. Physically, this is borne out by the negligible difference in flange stresses at the northern and southern tip of the flange at location 242 after day 8 (see Fig. 4.34), when the concrete deck segment 4W was placed over the girder. The low magnitude of web plate bending stresses in the vertical direction, as shown in Fig. 4.33, indicates that the lateral deflection of the web was also small. The distance between intermediate stiffeners is 100 in. at this location.

(3) The lateral deflection of the top flange under longitudinal compression and lateral load from the supports of the deck overhang, is equivalent to the condition of a beam column. Neglecting the effects of the vertical loads and the twisting moment of Fig. 7.7, the maximum lateral deflection of the top flange can be estimated by the formula:[8]

$$W_{max} = \frac{5pd^4}{384EI}\left[\frac{12\ (2\ Sec\lambda - 2 - \lambda^2)}{5\lambda^2}\right] \qquad (7.5)$$

where $\lambda = \frac{\pi}{2}\sqrt{P}/P_e$

P = *flange compressive force* $= f_b\ A_{flange}$

P_e = *Euler buckling load of the flange column*

p = *Uniformly distributed lateral load on the flange*

d = *Length of the flange column*

I = *Lateral moment of inertia of the flange column*

The beam column is assumed to be 300 in. long and the lateral force p is estimated by the models of section 7.3.1 B; then the maximum deflection can be computed for various load ratios P/P_e. The results are plotted in Fig. 7.9. For location W742, the load ratio is computed to be 0.55 when the deck concrete was placed. The estimated lateral deflection of the flange is about 0.7 in. This magnitude of deflection would be sufficient to cause breaking of the tack welds and separation of the metal deck form from the flange.

Equation 7.5 indicates the very strong influence of the length of the flange beam-column. At locations W742, 142, etc., of the end spans of the I78 bridge under study, the restraint to lateral movement of the girders are at the cross diaphragms, which are 300 inches apart. Whether the length of the hyperthetical beam-column in the continuous top flange at location W742 is 300 in., is subjected to interpretation. The direct influence of the flange moment of inertia against lateral deflection must be kept in mind. Sufficient rigidity with respect to lateral deflection must be provided against not only the maximum computed flange force P, but also the maximum lateral force p from the supports of the deck overhang.

In the discussion above, the contribution of the twisting moment m, (see Fig. 7.7), has been ignored. The inward forces at the ends of the inclined struts and the inward deflection of the web plate would produce a twisting moment on the flange beam-column, which would increase the outward deflection of the flange. The control of the twisting moment is, therefore, beneficial against the lateral deflection of the top flange. As indicated a few times before, a closer distance between transverse stiffeners would reduce the lateral deflection of the web, and thus would

control the twisting moment. The adoption of a more stringent limit of maximum spacing between transverse stiffeners, as given by Eq. 7.2, is recommended.

8. Summary and Recommendations

The results of this study are the following:

(1) The elevation of the top flanges of the girders in the spans moved up or down as expected as successive segments of the concrete deck were cast.

(2) The measured girder deflections after the completion of the deck are in good agreement with the theoretical values (from the design drawings) in spans 1 and 2, the measured deflections are greater than the theoretical values for span 3, but slightly lower for span 4. Both ends of span 4 are supported on fixed bearings. However, the high piers would provide some flexibility and allow the distance between bearings to change. This is suspected to be the reason of the observed discrepancy.

(3) During the period of concrete deck placement, the measured stresses in the girder flanges increased and decreased as consecutive segments of the deck were cast. The fluctuations of flange stresses were more pronounced in girder span 4 than in other spans and over the piers.

(4) The measured and computed flange stresses in the girder spans differ rather substantially. In span 3, it is 5 ksi out of 14.6 ksi for the top flange. In span 4, it is 10 ksi out of 18 ksi for the top flange and about 10 ksi versus -1.0 ksi for the bottom flange.

(5) An in-house analysis of the bridge using a finite element model and incorporating the shrinkage of concrete yielded flange stresses which are in good agreement with the values from measurement, except for the bottom flange of span 4. Fixed bearings were assumed in this analysis. Consideration of shrinkage and pier flexibility in analyzing continuous girder bridges is important and is recommended.

(6) Profiles of incremental stresses at girder cross sections confirmed the shifting of the neutral axis of the cross section, from that of a bare steel girder to that of a composite section as concrete hardened. Additional shifting of neutral axis of the composite section afterwards implies the existence of axial forces in the girders at certain locations. This is believed to be the effect of fixed bearings at the ends of span 4.

(7) Comparison of profiles of cumulative stresses in girder cross sections further revealed the difference between measured and computed stresses and the importance of considering concrete shrinkage in analysis.

(8) In an exterior girder panel with a 100 in. x 86 in. web plate, the measured web plate bending stresses in the vertical direction perpendicular to the top flange were small when concrete deck was cast directly above.

(9) The web plate of exterior girder panels deflected inward under the action of the inclined strut of the formwork for deck overhang. The magnitude of deflection increased when concrete was cast over the panel. For a 100 in. x 86 in. x 9/16 in. web plate, the magnitude of deflection before and after the casting was 0.32 and 0.80 in., respectively. After removal of formwork, the permanent deflection was 0.6 in.

(10) The permanent lateral deflection of three 300 in. x 82 in. x 9/16 in. web plates of exterior girder panels, one braced before casting of concrete deck above, one braced after, and one braced and shored, were 0.34, 0.89 and 0.54 in., respectively.

(11) Two adjacent web panels in an interior girder were found to have large, noticeable permanent lateral deflections after completion of the bridge deck. The web plates are 100 in. x

90 in. x 9/16 in. in dimension and the lateral deflections were about 1.1 in. in opposite directions. Many web panels of the interior girders in the middle of spans 3 and 4 have similar pattern of lateral deflection.

(12) Test trucks simulating HS25 loading and 204 kip permit load crawling along the bridge generated strain-time records which are in full agreement with the nature of influence lines of stresses at various points of the flanges.

(13) The sum of stresses in a girder flange due to individual test trucks traveling in different lanes agrees very well with that due to these trucks traveling side by side in their lanes simultaneously. This result confirms the linear elastic nature of the behavior of the bridge, and the applicability of the principle of superposition.

(14) When a test truck was on the bridge, instantaneous stresses at different locations indicated the load distribution among the four widely spaced girders of the bridge. The girder directly under or near the truck carried a larger share of the load. When a truck was near one edge of the roadway, the girder on the other side of the bridge cross section endured a negative bending. These results are similar to those from earlier studies on bridges with more conventional spacing between girders.

(15) The computed stresses in girder cross sections due to test truck loads agree well with those from measurements. The computed stresses, provided for comparison, are from analyzing the entire bridge structure with trucks at specific position and not from utilizing the load distribution factor of the AASHTO design specifications.

(16) Measured strains at the top surface of the roadway deck are consistent with those strains extrapolated from the steel girders assuming full composite action between the girders and the deck. The principle of superposition is applicable to the deck strains, as revealed by an examination of the summation of deck strains due to various test truck combinations.

(17) The highest magnitude of lateral movement of the web plate with the largest permanent lateral deflection was measured to be 0.21 in., occurring when three simulated HS25 trucks traveled side-by-side in the three lanes. The maximum total lateral deflection under this loading condition was 1.3 in.

(18) The measured vertical stresses in two web panels along the top flange connection indicate out-of-plane bending of the web plate, in full agreement with the measured lateral deflection. The highest range of web plate bending stress was 4.0 ksi corresponding to the maximum movement of the web.

(19) The highest measured range of web bending stress was 5.3 ksi in the web panel of an exterior girder, due to three simulated HS25 trucks travelling side by side.

(20) Test trucks travelling at a moderate speed of 50-55 mph generated vibrations of the bridge girders, at a frequency of about 4 Hz. The impact stresses corresponding to the vibration were not high, being less than 0.5 ksi in the girder flanges, or about 20-25 percent of the live load stresses generated by the trucks.

(21) When the bridge was subjected to regular traffic, the phenomenon of vibration was again detected. Subsequent trucks following one which caused the vibration to start were observed to interrupt, prolong, or eliminate the bridge vibration.

(22) The behavior of the bridge under truck loads of regular traffic is found to be consistent with that under test truck loads. The strain-time relationship for all locations of the bridge and the distribution of stresses in bridge cross-sections are all similar for similar test truck and regular truck runs.

(23) The stress ranges (live load plus impact stresses) due to regular traffic are lower than those due to the test trucks simulating HS25 loading. The stresses due to trucks of regular traffic were more nearly represented by those due to HS 20 trucks.

(24) The magnitude of live load stresses in the girder flanges, even when projected for the most severe condition of a HS25 truck speeding pass a 204 kip permit truck at the most critical position, are below the fatigue limit of the structural details in the flanges. No fatigue cracking of the flange is expected.

(25) Similarly, the projected maximum range of web plate bending stresses at web panel boundaries along the top flange of girders are below the fatigue limit of this structural detail, even with the large permanent lateral deflection of the web plates. No fatigue crack is expected along these web boundaries.

(26) Measurements at cross diaphragm members between girders showed that the magnitude of live load stresses in these members were about the same as those in the girder flanges. The tensile and compressive forces in the diaphragm members induced web plate bending stresses at the junction of diaphragm connection plates to the girder flanges. The maximum measured stress range was 6.4 ksi. This magnitude of live load stress is not expected to cause fatigue damage at the diaphragm connections

even if heavier truck loads of HS25 are allowed on the bridge in the future.

(27) Transverse cracks as wide as 0.05 in. were found in the concrete deck after the completion of the bridge. One possible cause of these cracks is the thermal change due to hydration of concrete and subsequent cooling. The variation of girder and deck strains during the sequential casting of concrete deck segments may also have a strong influence. Low compressive strains in concrete deck were computed to decrease by 100 to 200 micro in. per in. while the hardening process was in progress.

(28) From a careful review of the well known concept of buckling of perfectly flat plates, the gradual increase of lateral deflections of initially out-of-flat plates, the AWS tolerance of web plate out-of-flatness caused by fabrication, the AASHTO rules regarding the placing of transverse stiffeners, and the measured stresses in the girder flanges during construction of the deck, it is concluded that the large magnitude of web deflection in the interior girder panels of span 4 were the results of high compressive stresses in the top flange with near zero tensile stress in the bottom flange. Control of the flange stresses during construction can be achieved through careful arrangement of deck casting length and sequence. The simplest way to reduce web lateral deflection is to limit the panel aspect ratio of stiffener spacing to web depth to 1.5.

(29) For webs of exterior girder panels, which support the inclined struts of the formwork of deck overhang during construction, the magnitudes of lateral deflection can be reduced by lowering the position of the struts toward the bottom flange. Supporting the struts at the junction of the bottom flange and the web would minimize the lateral bending of the web plates.

(30) By evaluating analytically the lateral deflection of webs supporting the inclined struts as a function of the web panel aspect ratio, and comparing with the measured deflection of exterior web panels, it is concluded that limiting the web panel aspect ratio (or stiffener spacing) would be an effective solution to the problem of large magnitude of lateral deflection of exterior girder webs. It is recommended to re-adopt the AASHTO 1983 provision that limited the aspect ratio to 1.5.

(31) The mishap at the west bound girder, location W742, could be associated with large vertical deflection of the top flange, twisting of the flange plate, or large lateral deflection of the flange, all related to the lateral deflection of the web. An examination of the forces and stresses from simplified loading conditions of a compression flange beam-column suggested that the lateral deflection of the flange was the primary cause. That in turn was affected by the large unbraced length of the top flange, the relatively high compressive stresses in the flange, the lateral forces from the supports for the deck overhang, and the large lateral deflection of the web. The addition of intermediate stiffeners between the diaphragms would have provided control of the lateral deflection of the web and decreased the chance of the mishap.

Based on the above observations, the following recommendations are made:

(1) The computer programs associated with this study were adequate as tools in the design process of highway bridges.

(2) For multispan composite girder bridges with continuous concrete deck, the stresses in the steel girder flanges should

be carefully examined considering the length and sequence of casting concrete deck segments, the effects of shrinkage of concrete, and the influence of bearing fixity and pier flexibility.

(3) Consideration of the above factors as well as the thermal variation due to hydration of concrete and the change of ambient temperature is recommended for the investigation of transverse cracks in the concrete deck.

(4) The inclined struts of the formwork supports for the deck overhang should be placed as close to the lower flange as possible.

(5) The spacing of transverse stiffeners of girder webs should be limited to the following.

$$D\left(\frac{260}{D/t_w}\right)^2 \leq 1.5D$$

(6) Consideration of the forces from the formwork for deck overhang should be made in evaluating the strength of the steel flange of exterior girders during deck construction.

(7) Continued monitoring of the small transverse cracks in the deck of this bridge is recommended.

9. References

(1) Yen, Ben T., Huang, Ti, and VanHorn, David A.
Field Study of A Prestressed Concrete Bridge Final Report. Vol I, PennDOT Research Project No. 86-05, Fritz Engineering Laboratory Report No. 519.1, Lehigh University, January 1993.

(2) American Association of State Highway and Transportation Officials (AASHTO), Standard Specifications for Highway Bridges, 15th Edition, 1993.

(3) Modjeski and Masters, Inc., Consulting Engineers
I-78 Bridge over Delaware River; Moments and Stresses for SimulatedHS-25 Truck and Simulated 204 K vehicle at Specific Locations Using Computer Programs, 1989.

(4) Deppert, Glenn
The Case Study of a Composite Steel I-Girder Bridge under Construction Loads, M.S. Thesis, Lehigh University, Bethlehem, PA. 1990.

(5) American Welding Society
Structural Welding Code (ANSI/AWS D1.1), 1994.

(6) Bae, Doobyong
Effective Slab Width in Multi-Girder Composite Bridges, Dissertation in Partial Fulfillment of the Requirements for the Ph.D. Degree, Department of Civil Engineering, Lehigh University, 1991.

(7) NCHRP
Cheng-Shung Lin and David A. VanHorn
The Effect of Midspan Diaphragms on Load Distribution in a Prestressed Concrete Box-Beam Bridge, Philadelphia Bridge, Lehigh University, Fritz Engineering Laboratory Report No. 315.6, 1968.

(8) Structural Stability Research Council, Editors
"Guide to Design Criteria for Metal Compression Member, 4th Ed., John Wiley, New York 1988.

(9) Yen, Ben T., Huang, T., Lai, Lung-Yang; and Fisher, John W.
Manual for Inspecting Bridges for Fatigue Damage Conditions, Final Report, PennDOT Research Project 85-02; Department of Civil Engineering Report No. 511.1, Lehigh University, January 1990.

(10) Fisher, John W.
Fatigue and Fracture of Steel Bridges, Case Studies, John Wiley and Sons, 1984.

(11) Lai, L. Y.
Traffic Induced Stress Range Cycles in Bridge Main Members, Ph.D. Dissertation, Lehigh University, Bethlehem, PA, 1988

(12) Yen, B.T. and Lai, Leon Y.
Evaluation of Bridge Vibration through Field Measurement of Strains TRB Transportation Research Record 1223, 1989.

(13) Keating, P.B. and Fisher, J.W.
Evaluation of Fatigue Tests and Design Criteria on Welded Details NCHRP Report 286, Sept. 1986.

(14) Demers, C. E. and Fisher, J. W.
A Survey of Localized Cracking in Steel Bridges, 1981-1988. Federal Highway Administration Research Report, FHWA-RD-89-166, July 1989.

(15) Timoshinko, S.P. and Woinowsky-Krieger, S.
Theory of Plates and Shells, McGraw-Hill Book Company, 2nd Edition, 1959.

(16) Basler, K., Yen, B.T., Muller, J.A. and Thurlimann, B.
Web Buckling Tests on Welded Plate Girders, Welding Research Council, Bulletin No. 64, September 1960.

(17) Ostapenko, A. and Chen, C.
Ultimate Strength of Longitudinally Stiffened Plate Girders under Combined Loads, Proc. IABSE, Colloquium on Design of Plate and Box Girders for Ultimate Strength, London, 1971.

(18) Rockey, K. C., El-Gaaly, M.A.
Ultimate Strength of Plates when Subjected to In-plane Patch Loading, Proc. IABSE, Colloquium on Design of Plate and Box Girders for Ultimate Strength, London, 1971.

(19) Yen, B. T., and Muller, J. A.
Fatigue Tests of Large-Sized Welded Plate Girders, Welding Research Council Bulletin No. 118, November 1966.

(20) Lew, H. S. and Toprac, A. A.
Fatigue Strength of Hybrid Plate Girders Under Constant Moment, Highway Research Record 167, 1967.

(21) Hall, L. R. and Stallmeyer, J. E.
Thin Web Girder Fatigue Behavior as Influenced by Boundary Rigidity, University of Illinois Structural Research Series No. 278, January 1964.

(22) AISC
Specification for the Design, Fabrication and Erection of Structural Steel for Buildings, 1963.

(23) Yen, B.T. and Basler, K.
Static Carrying Capacity of Steel Plate Girders, Highway Research Board, Proc., Vol. 41, 1962.

(24) Vincent, George S.
Tentative Criteria for Load Factor Design of Highway Bridges, American Iron and Steel Institute (AISI) Bulletin No. 15, March 1969.

(25) Corrado, J.A., Mueller, J.A., and Yen, B.T.
Fatigue Tests of Welded Plate Girders in Bending, Lehigh University Fritz Engineering Laboratory Report No. 303.9, May 1965.

Table 2.1 Instrumentation Section Locations

Span	Section	Distance from West End of Span
2	2 X 2	84' - 6"
	2 X 3	126' - 9"
3	3 X 0	2' - 0"
	3 X 1	59' - 0"
	3 X 2	116' - 0"
	3 X 3	169' - 0"
	3 X 4	226' - 0" (2' - 0" from east end)
4	4 X 1	53' - 8"
	4 X 2	112' - 0" (2' - 0" from midspan)

Table 2.2 Flange Gages - Span 2

Gage	Location of Gage	Position
212TN	1/2" from edge of flange	North
212TS	1/2" from edge of flange	South
212B	3/4" from web	North
222TN	13/16" from edge of flange	North
222TS	1" from edge of flange	South
222B	7/8" from web	North
232TN	11/16" from edge of flange	North
232TS	13/16" from edge of flange	South
232B	3/4" from web	South
242TN	1/4" from edge of flange	North
242TS	1/2" from edge of flange	South
242B	3/4" from web	South
233TN	1/2" from edge of flange	North
233TS	7/16" from edge of flange	South
233B	13/16" from web	South
243TN	1/2" from edge of flange	North
243TS	1/2" from edge of flange	South
243B	5/8" from web	South

Note: All flange gages are on the top surface of the flange plate. Position gives gage location in relation to girder web.

Table 2.3 Flange Gages - Span 3

Gage	Location of Gage	Position	Gage	Location of Gage	Position
310TN	5/8" from edge of flange	North	322TN	11/16" from edge of flange	North
310TS	5/8" from edge of flange	South	322TS	1/2" from edge of flange	South
310B	13/16" from web	North	322B	13/16" from web	North
320TN	3/8" from edge of flange	North	332TN	1 1/2" from edge of flange	North
320TS	7/8" from edge of flange	South	332TS	3/4" from edge of flange	South
320B	13/16" from web	North	332B	15/16" from web	South
330TN	1/2" from edge of flange	North	342TN	9/16" from edge of flange	North
330TS	5/8" from edge of flange	South	342TS	9/16" from edge of flange	South
330B	1" from web	South	342B	3/4" from web	South
340TN	9/16" from edge of flange	North	333TN	5/8" from edge of flange	North
340TS	1/2" from edge of flange	South	333TS	1/2" from edge of flange	South
340B	7/8" from web	South	333B	1" from web	South
331TN	3/4" from edge of flange	North	343TN	1/2" from edge of flange	North
331TS	1" from edge of flange	South	343TS	3/4" from edge of flange	South
331B	1 1/8" from web	South	343B	1 1/8" from web	South
341TN	1/2" from edge of flange	North	334TN	3/4" from edge of flange	North
341TS	5/8" from edge of flange	South	334TS	3/4" from edge of flange	South
341B	1 1/8" from web	South	334B	7/8" from web	South
312TN	1/2" from edge of flange	North	344TN	5/8" from edge of flange	North
312TS	1/2" from edge of flange	South	344TS	7/16" from edge of flange	South
312B	5/8" from web	North	344B	7/8" from web	South

Note: All flange gages are on the top surface of the flange plate. Position gives gage location in relation to girder web.

Table 2.4 Flange Gages - Span 4

Gage	Location of Gage	Position
431TN	1/2" from edge of flange	North
431TS	3/8" from edge of flange	South
431B	3/4" from web	South
441TN	1/2" from edge of flange	North
441TS	5/16" from edge of flange	South
441B	13/16" from web	South
432TN	9/16" from edge of flange	North
432TS	7/16" from edge of flange	South
432B	5/8" from web	South
442TN	7/16" from edge of flange	North
442TS	1/2" from edge of flange	South
442B	13/16" from web	South

Note: All flange gages are on the top surface of the flange plate. Position gives gage location in relation to girder web.

Table 2.5 Web Gage Locations

Section	Gage Designation	Web Surface	Distance from midspan
242	242WS1	South	1'- 4" West
	242WS2	South	0' - 0"
	242WN2	North	0' - 0"
432	432WS1	South	4' - 2" West
	432WS2	South	3' - 2" West
	432WS3	South	4' - 2" East
	432WN1	North	4' - 2" West
	432WN2	North	3' - 2" West
	432WN3	North	4' - 2" East
442	442WS1	South	4' - 2" West
	442WS2	South	4' - 2" East
	442WN1	North	4' - 2" West
	442WN2	North	4' - 2" East

Table 2.6 Diaphragm Gages

Diaphragm Element	Gage Designation	Fig. No.
Diagonals	D23TS	Fig. 2.12 (a)
	D23BS	
	D24TS	
	D24BS	
	D33TN	Fig. 2.12 (b)
	D33BN	
	D33TS	
	D33BS	
Stiffeners	S33T	Fig. 2.12 (c)
	S34T	
Bottom Flange	B33N	
	B33S	
Web	W33TN1	
	W33TN2	
	W33BN1	
	W33BN2	
	W34TS1	
	W34TS2	

Table 3.1 Measured Deflections - Girder 3

	Section	Reading No.	0	1	2	3	4	5	6	7	8	9	10	11	12	13		14	
		Day No.	0	1	5	6	7	8	9	11	12	14	15	16	19	22		303	Δ (14-13)
Abutment	130		0	0	-5	0	0	-5	0	-5	0	0	-5	-5	-5	(B)		0	---
	131		0	-5	-10	(A)	-40	-25	-20	-35	-30	-45	-50	-45	-50	-55		-45	10
	132		0	(B)	(B)	-70	-65	-10	-5	-20	-20	(A)	-45	-40	-45	-50		-35	15
	133		0	-10	-15	-50	-40	10	10	0	0	(A)	-5	-5	-15	-15		-5	10
Pier 1	230		0	20	20	20	20	10	15	10	10	(A)	15	10	10	15		25	10
	231		0	25	30	60	55	(A)	-140	-115	-115	-95	-100	-110	-90	-70		-65	5
	232		0	45	60	85	80	(A)	-195	-135	-135	-110	-115	-135	-115	-95		-90	5
	233		0	40	55	50	60	-95	-125	-50	-40	-25	-35	(A)	-40	-30		-15	15
Pier 2	330		0	10	10	10	5	0	-5	-10	-5	-5	-10	(A)	-25	-25		-5	20
	331		0	-95	-115	-125	-115	-10	60	-105	-190	-185	-195	-205	-180	-190		-185	5
	332		0	(A)	-170	-170	-160	-55	80	-255	-310	-300	-310	-320	-280	-300		-320	-20
	333		0	-45	-80	-85	-65	-15	120	-105	-160	-155	-160	-165	-130	-155		-155	0
Pier 3	430		0	5	0	0	-5	-10	-10	-15	-20	-15	-15	-15	-10	-10		30	40
	431		0	-70	-30	-15	-40	-95	-325	-195	-135	-125	-120	-115	-145	-165		-130	35
	432		0	(A)	-90	-75	-115	-180	-510	-390	-290	-255	-250	-255	-305	-300		-270	30

(A) Fresh concrete

(B) Equipment on bridge

Deflections are in ft. x 10^{3}

Table 3.2 Measured Deflections - Girder 4

	Section	Reading No.	0	1	2	3	4	5	6	7	8	9	10	11	12	13		14	
		Day No.	0	1	5	6	7	8	9	11	12	14	15	16	19	22		303	Δ (14-13)
Abutment	140		0	0	0	5	0	0	0	0	0	0	0	0	0	0		0	0
	141		0	0	-5	(A)	-30	-5	-5	-20	-15	-30	-35	-30	-30	-30		-35	-5
	142		0	(B)	(B)	-75	-65	-10	-10	-20	-25	(A)	-45	-40	-50	-50		-40	10
	143		0	-10	-15	-50	-40	5	10	-15	0	(A)	-20	-20	-25	-25		-15	10
Pier 1	240		0	15	5	5	5	-5	-5	-10	-5	(A)	0	0	0	5		20	15
	241		0	30	40	65	60	(A)	-120	-90	-90	-75	-75	-85	-65	-50		-45	5
	242		0	45	65	95	85	(A)	-200	-140	-130	-110	-110	-130	-105	-90		-85	5
	243		0	35	50	60	55	-100	-130	-55	-45	-30	-35	(A)	-40	-35		-25	10
Pier 2	340		0	0	5	0	0	-10	-10	-20	-20	-15	-20	(A)	(C)	(C)		(C)	---
	341		0	-90	-105	-115	-105	0	70	-140	-175	-175	-180	-185	-160	-170		-170	0
	342		0	(A)	-165	-165	-155	-50	95	-240	-285	-280	-285	-300	-255	-265		-285	-20
	343		0	-40	-75	-75	-65	-10	135	-95	-150	-145	-150	-150	-120	-140		-125	15
Pier 3	440		0	0	-5	-5	-5	-15	-15	-20	-25	-20	-25	-20	-15	0		40	40
	441		0	-80	-30	-15	-40	-95	-330	-205	-155	-130	-135	-125	-150	-170		-135	35
	442		0	(A)	-90	-60	-100	-175	-505	-395	-295	-260	-260	-250	-300	-295		-275	20

Deflections are in ft. x 10^{3}

(A) Fresh concrete

(B) Equipment on bridge

(C) Location obliterated

Table 3.3 Deflections due to Total Slab Weight

Span	Tenth Point	Girder 3		Girder 4	
		Theoretical in.	Measured in.	Theoretical in.	Measured in.
1	0	0.00	0.00	0.00	0.00
	1	-0.25		-0.23	
	2	-0.45		-0.41	
	2.5		-0.66		-0.36
	3	-0.56		-0.51	
	4	-0.58		-0.52	
	5	-0.55	-0.60	-0.49	-0.60
	6	-0.46		-0.41	
	7	-0.31		-0.27	
	7.5		-0.18		-0.30
	8	-0.13		-0.12	
	9	-0.03		-0.02	
2	0	0.00	0.18	0.00	0.06
	1	-0.28		-0.27	
	2	-0.63		-0.60	
	2.5		-0.84		-0.60
	3	-1.02		-0.97	
	4	-1.17		-1.11	
	5	-1.08	-1.14	-1.01	-1.08
	6	-0.74		-0.67	
	7	-0.31		-0.26	
	7.5		-0.36		-0.42
	8	0.06		0.08	
	9	0.16		0.17	
3	0	0.00	0.30	0.00	
	1	-0.93		-0.91	
	2	-2.30		-2.25	
	2.5		-2.28		-2.04
	3	-3.80		-3.75	
	4	-4.78		-4.74	
	5	-5.05	-3.60	-5.01	-3.18
	6	-4.50		-4.45	
	7	-3.33		-3.27	
	7.5		-1.86		-1.68
	8	-1.85		-1.78	
	9	-0.67		-0.64	
4	0	0.00	-0.12	0.00	0.00
	1	-0.18		-0.16	
	2	-0.88		-0.83	
	2.5		-1.98		-2.04
	3	-1.97		-1.91	
	4	-2.84		-2.78	
	5	-3.23	-3.60	-3.17	-3.54

Table 4.1 Strains and Stresses in Girder Flanges at Location 332

Gage	332TN			332B			332TS		
Correction Factor	140/120			139/120			139/120		
Day	Reading	Strain (μin/in)	Stress (ksi)	Reading	Strain (μin/in)	Stress (ksi)	Reading	Strain (μin/in)	Stress (ksi)
0	0.0	0.0	0.00	0.0	0.0	0.00	0.0	0.0	0.00
1	-286.0	-333.7	-9.68	170.0	196.9	5.71	-217.0	-251.4	-7.29
5	-358.0	-417.7	-12.11	181.0	209.7	6.08	-299.0	-346.3	-10.04
6	-380.0	-443.3	-12.86	154.0	178.4	5.17	-327.0	-378.4	-10.97
Zero Balance	0.0	-443.3	-12.86	0.0	178.4	5.17	0.0	-378.4	-10.97
7	28.0	-410.6	-11.91	27.0	209.7	6.08	27.0	-347.1	-10.07
8	31.0	-407.1	-11.81	-28.0	146.0	4.23	28.0	-346.0	-10.03
9	37.0	-400.1	-11.60	-100.0	62.6	1.81	31.0	-342.5	-9.93
10	-19.0	-465.5	-13.50	101.0	295.4	8.57	-21.0	-402.7	-11.68
12	-15.0	-460.8	-13.36	116.0	312.8	9.07	-20.0	-401.6	-11.65
13	-20.0	-466.6	-13.53	83.0	274.5	7.96	-29.0	-412.0	-11.95
14	-25.0	-472.5	-13.70	109.0	304.7	8.84	-22.0	-403.9	-11.71
15	-44.0	-494.6	-14.34	103.0	297.7	8.63	-33.0	-416.6	-12.08
16	-43.0	-493.5	-14.31	101.0	295.4	8.57	-34.0	-417.8	-12.12
19	-52.0	-504.0	-14.62	68.0	257.2	7.46	-40.0	-424.7	-12.32
20	-84.0	-541.3	-15.70	47.0	232.8	6.75	-73.0	-463.0	-13.43
22	-96.0	-555.3	-16.10	10.0	190.0	5.51	-86.0	-478.0	-13.86

Table 4.2 Strains and Stresses in Girder Flanges at Location 432

Gage	432TN			432B			432TS		
Correction Factor	175/120			175/120			171/120		
Day	Reading	Strain (μin/in)	Stress (ksi)	Reading	Strain (μin/in)	Stress (ksi)	Reading	Strain (μin/in)	Stress (ksi)
0	0.0	0.0	0.00	0.0	0.0	0.00	0.0	0.0	0.00
1	-221.0	-322.3	-9.35	112.0	163.3	4.74	-215.0	-306.4	-8.89
5	-301.0	-439.0	-12.73	0.0	0.0	0.00	-448.0	-638.4	-18.51
6	-325.0	-474.0	-13.75	-52.0	-75.8	-2.20	-430.0	-612.8	-17.77
Zero Balance	0.0	-474.0	-13.75	0.0	-75.8	-2.20	0.0	-612.8	-17.77
7	34.0	-424.4	-12.31	31.0	-30.6	-0.89	43.0	-551.5	-15.99
8	29.0	-431.7	-12.52	40.0	-17.5	-0.51	76.0	-504.5	-14.63
9	-14.0	-494.4	-14.34	252.0	291.7	8.46	42.0	-552.9	-16.04
10	-11.0	-490.0	-14.21	160.0	157.5	4.57	43.0	-551.5	-15.99
12	-6.0	-482.8	-14.00	102.0	73.0	2.12	17.0	-588.6	-17.07
13	-17.0	-498.8	-14.46	67.0	21.9	0.64	-19.0	-639.9	-18.56
14	-1.0	-475.5	-13.79	128.0	110.9	3.22	61.0	-525.9	-15.25
15	-6.0	-482.8	-14.00	85.0	48.2	1.40	78.0	-501.6	-14.55
16	-19.0	-501.7	-14.55	47.0	-7.3	-0.21	39.0	-557.2	-16.16
19	-26.0	-511.9	-14.85	95.0	62.7	1.82	-5.0	-619.9	-17.98
20	-32.0	-520.7	-15.10	28.0	-35.0	-1.01	-77.0	-722.5	-20.95
22	-29.0	-516.3	-14.97	-17.0	-100.6	-2.92	-57.0	-694.0	-20.13

Table 4.3 Strains and Stresses in Girder Flanges at Location 330

Gage	330TN			330B			330TS		
Correction Factor	130/120			130/120			130/120		
Day	Reading	Strain (μin/in)	Stress (ksi)	Reading	Strain (μin/in)	Stress (ksi)	Reading	Strain (μin/in)	Stress (ksi)
0	0.0	0.0	0.00	0.0	0.0	0.00	0.0	0.0	0.00
1	46.0	49.8	1.44	-9.0	-9.8	-0.28	56.0	60.7	1.76
5	53.0	57.4	1.66	-18.0	-19.5	-0.57	55.0	59.6	1.73
6	63.0	68.3	1.98	-35.0	-37.9	-1.10	67.0	72.6	2.11
Zero Balance	0.0	68.3	1.98	0.0	-37.9	-1.10	0.0	72.6	2.11
7	7.0	75.9	2.20	25.0	-10.8	-0.31	9.0	82.3	2.39
8	114.0	191.8	5.56	-83.0	-127.8	-3.71	112.0	193.9	5.62
9	65.0	138.7	4.02	-51.0	-93.1	-2.70	70.0	148.4	4.30
10	239.0	327.2	9.49	-200.0	-254.6	-7.38	236.0	328.3	9.52
12	276.0	367.3	10.65	-230.0	-287.1	-8.32	277.0	372.7	10.81
13	266.0	356.5	10.34	-236.0	-293.6	-8.51	270.0	365.1	10.59
14	270.0	360.8	10.46	-232.0	-289.2	-8.39	272.0	367.3	10.65
15	261.0	351.1	10.18	-234.0	-291.4	-8.45	272.0	367.3	10.65
16	367.0	465.9	13.51	-305.0	-368.3	-10.68	382.0	486.4	14.11
19	288.0	380.3	11.03	-313.0	-377.0	-10.93	297.0	394.4	11.44
20	292.0	384.6	11.15	-345.0	-411.6	-11.94	297.0	394.4	11.44
22	305.0	398.7	11.56	-312.0	-375.9	-10.90	308.0	406.3	11.78

Table 4.4 Maximum Permanent Web Deflection - *w*

Location		142	242	W712	W742
d/D		300/82	100/86	300/82	300/82
D/t		146	153	146	146
Condition		Braced*	Normal	Braced	Shored and Braced
w (in.)	Before Casting of Deck	0.16	0.32	---	---
	After Casting of Deck	0.38	0.80	---	---
	After Removal of Formwork	0.34	0.60	0.89	0.50
w/t		0.6	1.1	1.6	0.9

* Braced before casting of concrete deck

Table 5.1 Test Truck Runs

Designation	Simulated Live Load	Lane(s)	Speed
C1	HS - 25	1	Crawl
C2	HS - 25	2	Crawl
C3	HS - 25	3	Crawl
C23	HS - 25	2 and 3	Crawl
C123	HS - 25	1, 2 and 3	Crawl
S2	HS - 25	2	Moderate
S3	HS - 25	3	Moderate
S23	HS - 25	2 and 3	Moderate
P2	204 ^{k}	2	Crawl
P3	204 ^{k}	3	Crawl

Table 5.2 Strain Gage Groupings During Test Truck Runs

	1	2	3	4	5	6
1	242TN	344TS	332TN	322TN	242SL	D23TS
2	242B	441TN	332TS	322B	242ST	D23BS
3	242TS	441B	333TN	322TS	340SL	D33TS
4	243TN	441TS	333B	212TN	340ST	D33BS
5	243B	442TN	333TS	212B	342SL	D24TS
6	243TS	442B	334TN	212TS	342ST	D24BS
7	340TN	442TS	334B	310TN	232NL	242WS1
8	340B	232TN	334TS	320TS	232NT	242WS2
9	340TS	232B	431TN	310TS	330NL	432WS1
10	341TN	232TS	431B	312TN	330NT	432WN1
11	341B	233TN	431TS	312B	332NL	432WS2
12	341TS	233B	432TN	342NT	332NT	432WN2
13	342TN	233TS	432B	242NL	232SL	432WS3
14	342TS	330TN	432TS	242NT	232ST	432WN3
15	343TN	330B	222TN	340NL	330SL	CL2
16	343B	330TS	222B	340NT	330ST	222B
17	343TS	331TN	222TS	342NL	332SL	222TS
18	344TN	331B	320TN	---	332ST	320TN
19	344B	331TS	320B	332ST	342NL	320B
20	332B	332B	332B	332B	332B	332B
21	342B	342B	342B	342B	342B	342B

Table 5.3 Strains and Stresses due to Test Trucks Middle of Span 2

Gage	212TS			212B			212TN		
Correction Factor	146.9/120			146.8/120			146.7/120		
Run Designation	Reading	Strain (μ in/in)	Stress (ksi)	Reading	Strain (μ in/in)	Stress (ksi)	Reading	Strain (μ in/in)	Stress (ksi)
C1	-44	-53.8	-1.56	---	---	---	-26	-31.8	-0.92
C2	-29	-35.5	-1.03	---	---	---	-17	-20.8	-0.60
C3	10	12.2	0.36	---	---	---	3	3.7	0.11
C23	-21	-25.7	-0.75	---	---	---	-13	-15.9	-0.46
C123	-50	-61.2	-1.78	---	---	---	-33	-40.3	-1.17
P2	-36	-44.1	-1.28	---	---	---	-22	-26.9	-0.78
P3	9	11.0	0.32	---	---	---	4	4.9	0.14

Gage	222TS			222B			222TN		
Correction Factor	146.7/120			136.3/120			136.0/120		
Run Designation	Reading	Strain (μ in/in)	Stress (ksi)	Reading	Strain (μ in/in)	Stress (ksi)	Reading	Strain (μ in/in)	Stress (ksi)
C1	-24	-29.3	-0.85	107	121.5	3.52	-27	-30.6	-0.89
C2	-20	-24.5	-0.71	90	102.2	2.97	-24	-27.2	-0.79
C3	-13	-15.9	-0.46	37	42.0	1.22	-16	-18.1	-0.53
C23	-29	-35.5	-1.03	126	143.1	4.15	-35	-39.7	-1.15
C123	-43	-52.6	-1.52	233	264.6	7.68	-51	-57.8	-1.68
P2	-26	-31.8	-0.92	117	132.9	3.85	-30	-34.0	-0.99
P3	-16	-52.6	-0.57	52	59.1	1.71	-20	-22.7	-0.66

Table 5.3 (Con't) Strains and Stresses due to Test Trucks Middle of Span 2

Gage	232TS			232B			232TN		
Correction Factor	135.3/120			134.1/120			143.9/120		
Run Designation	Reading	Strain (μ in/in)	Stress (ksi)	Reading	Strain (μ in/in)	Stress (ksi)	Reading	Strain (μ in/in)	Stress (ksi)
C1	-15	-16.9	-0.49	59	65.9	1.91	---	---	---
C2	-19	-21.4	-0.62	87	97.2	2.82	---	---	---
C3	-23	-25.9	-0.75	110	122.9	3.57	---	---	---
C23	-34	-38.3	-1.11	200	223.5	6.48	---	---	---
C123	-44	-49.6	-1.44	250	279.3	8.10	---	---	---
P2	-22	-24.8	-0.72	115	128.5	3.73	---	---	---
P3	-29	-32.7	-0.95	140	156.5	4.54	---	---	---

Gage	242TS			242B			242TN		
Correction Factor	148.4/120			133.8/120			142.8/120		
Run Designation	Reading	Strain (μ in/in)	Stress (ksi)	Reading	Strain (μ in/in)	Stress (ksi)	Reading	Strain (μ in/in)	Stress (ksi)
C1	-3	-3.7	-0.11	7	7.8	0.23	-2	-2.4	-0.07
C2	-12	-14.8	-0.43	55	61.3	1.78	-6	-7.1	-0.21
C3	-23	-28.4	-0.83	169	188.4	5.47	-14	-16.7	-0.48
C23	-33	-40.8	-1.18	220	245.3	7.11	-16	-19.0	-0.55
C123	-37	-45.8	-1.33	234	260.9	7.57	-18	-21.4	-0.62
P2	-15	-18.6	-0.54	70	78.1	2.26	-9	-10.7	-0.31
P3	-27	-33.4	-0.97	216	240.8	6.98	-16	-19.0	-0.55

Table 5.4 Strains in Deck and Girders Test Truck Crawl Runs (μ in./in.)

Run	312TS	312TN	312B	322TS	322TN	322B
Designation						
C1	---	-22.2	132.9	-13.8	-13.9	120.2
C2	---	-13.5	78.6	-9.2	-17.4	99.6
C3	---	2.5	-11.6	-4.6	-7.0	43.5
C23	---	-4.9	64.7	-11.5	-20.9	152.3
C123	---	-29.6	216.1	-26.4	-8.1	269.1
P2	---	-18.5	111.0	-8.0	-20.9	131.7
P3	---	6.2	-10.4	-5.7	-33.6	71.0

Run	332TS	332TN	332SL	332NL	332B
Designation					
C1	-10.6	-6.9	-21.8	-14.3	72.2
C2	-15.4	-10.4	-37.1	-22.0	103.1
C3	-16.6	-19.6	-24.0	-35.5	129.5
C23	-29.6	-30.1	-60.0	-61.6	233.7
C123	-40.2	-37.0	-76.4	-80.3	302.5
P2	-17.7	-12.7	-43.7	-29.7	131.8
P3	-20.1	-26.6	-31.7	-55.0	171.9

Run	342TS	342TN	342SL	342NL	342B
Designation					
C1	-8.4	-3.6	-7.6	-6.6	27.4
C2	-16.8	-12.0	-22.9	-26.5	68.4
C3	-48.1	-37.3	-60.9	-63.0	193.8
C23	-60.1	-45.7	-84.9	-88.5	262.2
C123	-71.2	-51.7	-92.5	-94.0	283.9
P2	-21.6	-16.8	-30.5	-35.4	95.8
P3	-60.1	-48.1	-87.1	-82.9	261.1

Table 5.5 Maximum Stresses in Diaphragms
Test Truck Runs (Ksi)

Run	Gage Locations					
Designation	D23 TS	D23 BS	D33 TS	D33 BS	D24 TS	D24 BS
C1	4.7	-2.1	3.9	-1.8	0.8	-0.8
C2	3.8	2.8	2.9	1.8	3.1	-3.6
C3	2.3	1.0	-2.2	0.8	0.7	1.8
C23	1.6	3.6	0.7	3.0	2.7	-2.0
C123	5.7	1.6	4.1	0.8	3.1	-3.0
P2	4.8	2.7	3.5	2.0	3.7	-4.1
P3	-2.4	2.0	-2.6	1.7	-0.3	0.7
S2	3.3	2.1	2.4	2.1	2.5	-2.7
S3	-2.0	1.0	-2.1	1.1	-0.3	1.6
S23	1.6	3.7	0.7	3.3	2.7	-2.0

Table 5.6 Bottom Flange Stress Ranges
due to Test Truck (Ksi)

Location	Speed Runs		Crawl Runs	
	S3	S2	C3	C2
242B	7.53	2.92	7.69	2.84
340B	3.41	1.10	3.17	1.30
341B	5.37	2.01	5.37	1.85
342B	7.27	2.57	7.18	2.74
343B	6.39	2.20	6.57	2.56
344B	2.58	1.03	2.98	1.19
332B	4.98	4.81	4.81	3.95
333B	4.41	3.07	4.15	3.54
334B	1.80	1.60	1.80	1.40
431B	5.19	3.11	4.56	3.85
432B	5.84	(Off)	5.24	4.54
D33TS	(-)2.08	2.41	(-)2.19	2.85
D33BS	1.09	2.07	0.76	1.75

Table 5.7 Stresses due to Test Truck Crawl Runs Middle of Span 2 (ksi)

Location	Designation	2 - D		3 - D		Measured	
		Top	Bottom	Top	Bottom	Top	Bottom
212	C1	-0.51	3.53	-0.52	3.58	-1.24	---
	C2	-0.27	1.84	-0.25	1.70	-0.82	---
	C3	0.06	-0.44	-0.01	0.10	0.23	---
	C23	-0.21	1.40	-0.26	1.80	-0.60	---
	C123	-0.72	4.93	-0.78	5.38	-1.47	---
	P2	---	---	-0.33	2.31	---	---
	P3	0.08	-0.58	-0.02	0.12	0.23	---
222	C1	-0.35	2.99	-0.42	3.64	-0.87	3.52
	C2	-0.28	2.38	-0.34	2.88	-0.75	2.97
	C3	-0.14	1.21	-0.13	1.10	-0.49	1.22
	C23	-0.42	3.59	-0.47	3.98	-1.09	4.15
	C123	-0.77	6.58	-0.89	7.62	-1.60	7.68
	P2	---	---	-0.44	3.74	---	---
	P3	-0.19	1.63	-0.17	1.47	-0.61	1.71
232	C1	-0.19	1.64	-0.19	1.65	-0.49	1.91
	C2	-0.28	2.38	-0.34	2.85	-0.62	2.82
	C3	-0.36	3.11	-0.41	3.55	-0.75	3.57
	C23	-0.64	5.49	-0.75	6.40	-1.11	6.48
	C123	-0.83	7.13	-0.94	8.05	-1.44	8.10
	P2	---	---	-0.44	3.74	---	---
	P3	-0.45	3.89	-0.49	4.23	-0.95	4.54
242	C1	-0.05	0.37	-0.06	0.38	-0.09	0.23
	C2	-.027	1.84	-0.25	1.70	-0.32	1.78
	C3	-0.71	4.87	-0.78	5.37	-0.65	5.47
	C23	-0.97	6.71	-1.03	7.07	-0.87	7.11
	C123	-1.02	7.08	-1.09	7.45	-0.97	7.57
	P2	---	---	-0.33	2.30	---	---
	P3	-0.88	6.09	-0.92	6.38	-0.76	6.98

Table 5.8 Stresses due to Test Truck Crawl Runs Middle of Span 3 (ksi)

Location	Designation	2 - D		3 - D		Measured	
		Top	Bottom	Top	Bottom	Top	Bottom
312	C1	-0.75	3.73	-0.79	3.92	-0.64	3.86
	C2	-0.40	1.99	-0.40	1.99	-0.39	2.28
	C3	0.07	-0.35	-0.01	0.04	0.07	-0.34
	C23	-0.33	1.64	-0.41	2.03	-0.14	1.88
	C123	-1.08	5.37	-1.20	5.95	-0.86	6.27
	P2	-0.58	2.85	-0.57	2.82	-0.54	3.22
	P3	0.09	-0.47	-0.01	0.06	0.18	-0.30
322	C1	-0.60	3.21	-0.65	3.53	-0.40	3.49
	C2	-0.47	2.55	-0.52	2.78	-0.39	2.89
	C3	-0.24	1.29	-0.23	1.24	-0.17	1.26
	C23	-0.71	3.83	-0.75	4.02	-0.47	4.42
	C123	-1.31	7.04	-1.40	7.55	-0.87	7.80
	P2	-0.63	3.40	-0.69	3.70	-0.42	3.82
	P3	-0.34	1.81	-0.32	1.71	-0.20	2.06
332	C1	-0.31	1.68	-0.32	1.70	-0.26	2.09
	C2	-0.47	2.55	-0.51	2.77	-0.37	2.99
	C3	-0.60	3.21	-0.65	3.48	-0.53	3.76
	C23	-1.07	5.76	-1.16	6.25	-0.86	6.78
	C123	-1.38	7.44	-1.48	7.95	-1.12	8.77
	P2	-0.63	3.39	-0.69	3.70	-0.44	3.82
	P3	-0.80	4.33	-0.86	4.65	-0.68	4.98
342	C1	-0.10	0.50	-0.09	0.45	-0.18	0.79
	C2	-0.40	1.99	-0.40	1.98	-0.42	1.98
	C3	-1.03	5.08	-1.09	5.41	-1.24	5.62
	C23	-1.43	7.07	-1.49	7.39	-1.53	7.60
	C123	-1.53	7.57	-1.58	7.84	-1.80	8.23
	P2	-0.58	2.85	-0.57	2.81	-0.56	2.78
	P3	-1.38	6.81	-1.47	7.27	-1.57	7.57

Table 5.9 Stresses due to Test Truck Crawl Runs over Pier 2 (ksi)

Location	Designation	2 - D		3 - D		Measured	
		Top	Bottom	Top	Bottom	Top	Bottom
310	C1	0.50	-1.69	0.54	-1.82	0.68	---
	C2	0.28	-0.93	0.29	-0.97	0.36	---
	C3	-0.05	0.17	0.01	-0.03	-0.23	---
	C23	0.23	-0.75	0.30	-1.00	0.20	---
	C123	0.73	-2.44	0.84	-2.82	0.96	---
	P2	0.37	-1.25	0.41	-1.38	0.53	---
	P3	-0.07	0.23	0.01	-0.04	-0.31	---
320	C1	0.35	-1.40	0.39	-1.57	0.46	-1.78
	C2	0.29	-1.15	0.32	-1.28	0.38	-1.53
	C3	0.15	-0.62	0.16	-0.64	0.22	-0.65
	C23	0.44	-1.76	0.48	-1.92	0.67	-2.09
	C123	0.79	-3.17	0.87	-3.49	1.16	-3.58
	P2	0.39	-1.57	0.45	-1.79	0.55	-2.12
	P3	0.22	-0.86	0.23	-0.90	0.33	-0.97
330	C1	0.20	-0.81	0.22	-0.86	0.20	-1.00
	C2	0.29	-1.15	0.32	-1.25	0.24	-1.40
	C3	0.37	-1.47	0.40	-1.61	0.44	-1.68
	C23	0.66	-2.62	0.72	-2.86	0.74	-3.02
	C123	0.86	-3.43	1.12	-3.72	0.97	-3.98
	P2	0.39	-1.57	0.45	-1.19	0.38	-1.93
	P3	0.51	-2.04	0.57	-2.26	0.66	-2.33
340	C1	0.07	-0.22	0.07	-0.22	0.08	-0.19
	C2	0.28	-0.93	0.29	-0.97	0.30	-0.94
	C3	0.65	-2.20	0.72	-2.42	1.08	-2.35
	C23	0.93	-3.13	1.01	-3.39	1.18	-3.30
	C123	1.00	-3.35	1.08	-3.61	1.23	-3.42
	P2	0.39	-1.30	0.41	-1.38	0.34	-1.13
	P3	0.91	-3.05	1.01	-3.40	1.36	-3.55

Table 5.10 Comparison of Maximum Live Load Stresses Cross Section 342 (ksi)

HS - 25 Loading in All Lanes

	2 - D	3 - D	Measured C123
Top	-2.21	-2.13	-1.80
Bottom	10.92	10.51	8.23

204^{k} + Two HS - 25

	2 - D	3 - D	Measured C123
Top	-2.19	-2.19	-2.17
Bottom	10.21	10.82	10.34

Table 5.11 Longitudinal Strains on Deck Surface
Test Truck Crawl Runs (μ in./in.)

Run	312 *	322 *	332SL	332 *	332NL	342SL	342 *	342NL
Designation								
C1	-44.6	-33.1	-21.8	-20.4	-14.3	-7.6	-10.8	-6.6
C2	-26.8	-29.5	-37.1	-29.6	-22.0	-22.9	-26.4	-26.5
C3	4.5	-12.9	-24.0	-39.3	-35.5	-60.9	-76.7	-63.0
C23	-15.0	-40.4	-60.0	-67.7	-61.6	-84.9	-98.4	-88.5
C123	-65.1	-58.4	-76.4	-108.2	-80.3	-92.5	-111.3	-94.0
P2	-37.2	-35.4	-43.7	-36.3	-29.7	-30.5	-35.8	-35.4
P3	-12.8	-32.7	-31.7	-51.4	-55.0	-87.1	-99.6	-82.9

* Extrapolated

Table 5.9 Stresses due to Test Truck Crawl Runs over Pier 2 (ksi)

Location	Designation	2 - D		3 - D		Measured	
		Top	Bottom	Top	Bottom	Top	Bottom
310	C1	0.50	-1.69	0.54	-1.82	0.68	---
	C2	0.28	-0.93	0.29	-0.97	0.36	---
	C3	-0.05	0.17	0.01	-0.03	-0.23	---
	C23	0.23	-0.75	0.30	-1.00	0.20	---
	C123	0.73	-2.44	0.84	-2.82	0.96	---
	P2	0.37	-1.25	0.41	-1.38	0.53	---
	P3	-0.07	0.23	0.01	-0.04	-0.31	---
320	C1	0.35	-1.40	0.39	-1.57	0.46	-1.78
	C2	0.29	-1.15	0.32	-1.28	0.38	-1.53
	C3	0.15	-0.62	0.16	-0.64	0.22	-0.65
	C23	0.44	-1.76	0.48	-1.92	0.67	-2.09
	C123	0.79	-3.17	0.87	-3.49	1.16	-3.58
	P2	0.39	-1.57	0.45	-1.79	0.55	-2.12
	P3	0.22	-0.86	0.23	-0.90	0.33	-0.97
330	C1	0.20	-0.81	0.22	-0.86	0.20	-1.00
	C2	0.29	-1.15	0.32	-1.25	0.24	-1.40
	C3	0.37	-1.47	0.40	-1.61	0.44	-1.68
	C23	0.66	-2.62	0.72	-2.86	0.74	-3.02
	C123	0.86	-3.43	1.12	-3.72	0.97	-3.98
	P2	0.39	-1.57	0.45	-1.19	0.38	-1.93
	P3	0.51	-2.04	0.57	-2.26	0.66	-2.33
340	C1	0.07	-0.22	0.07	-0.22	0.08	-0.19
	C2	0.28	-0.93	0.29	-0.97	0.30	-0.94
	C3	0.65	-2.20	0.72	-2.42	1.08	-2.35
	C23	0.93	-3.13	1.01	-3.39	1.18	-3.30
	C123	1.00	-3.35	1.08	-3.61	1.23	-3.42
	P2	0.39	-1.30	0.41	-1.38	0.34	-1.13
	P3	0.91	-3.05	1.01	-3.40	1.36	-3.55

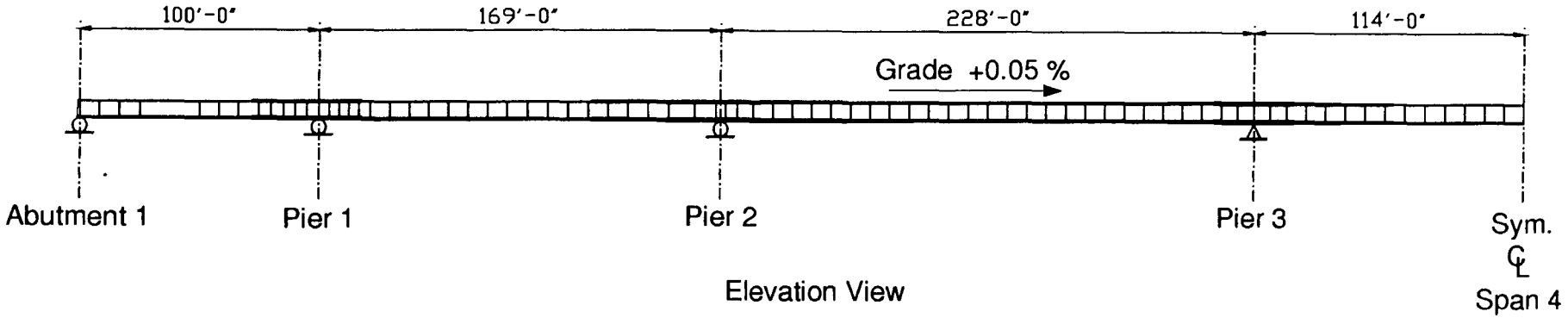

Elevation View

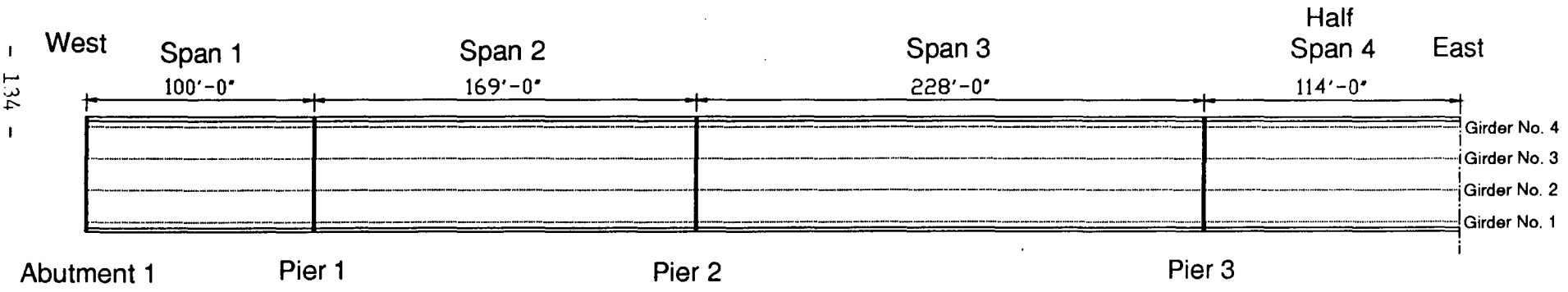

Plan View

Fig 2.1 Plan and Elevation of East-Bound Structure
(Abutment to midspan of Span 4)

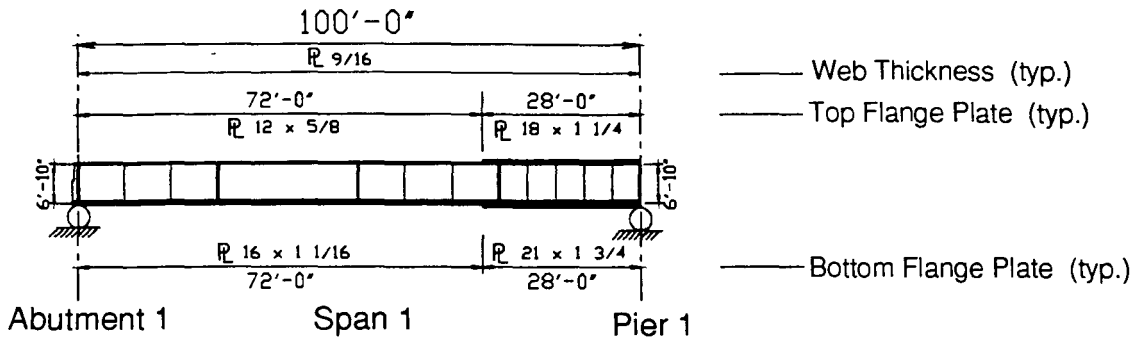

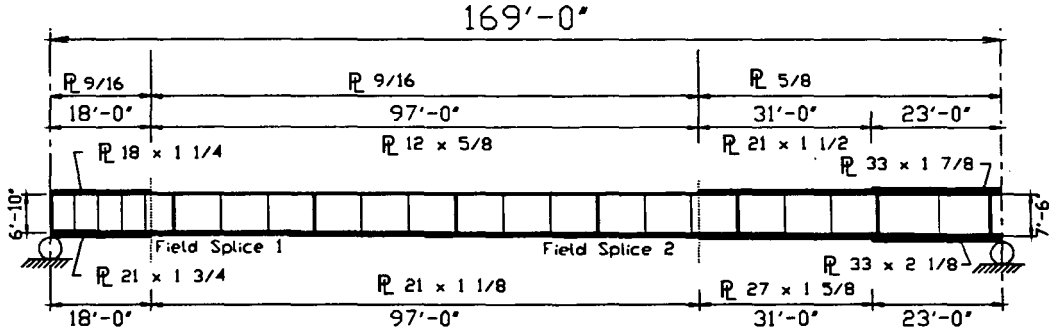

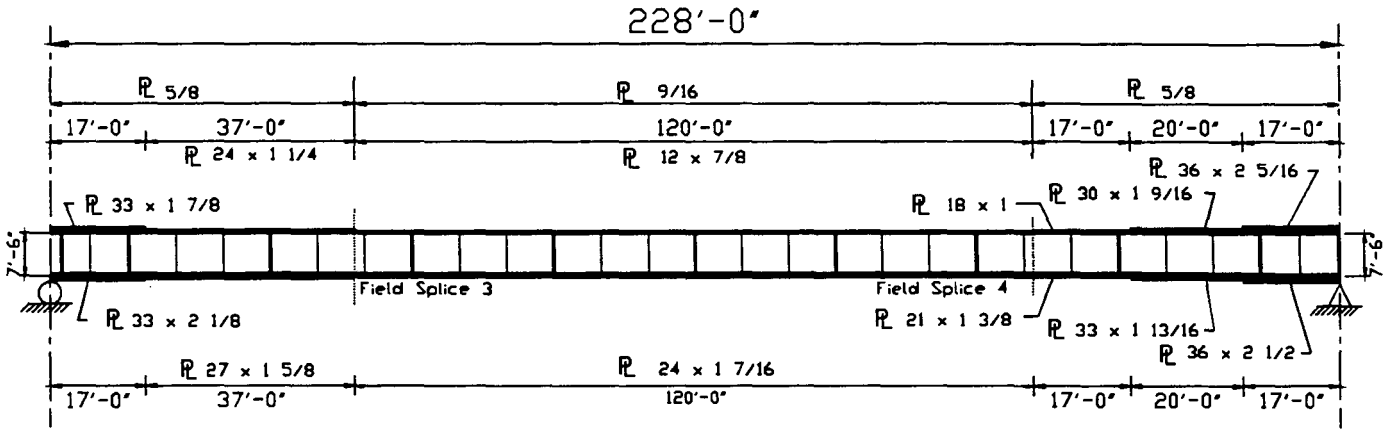

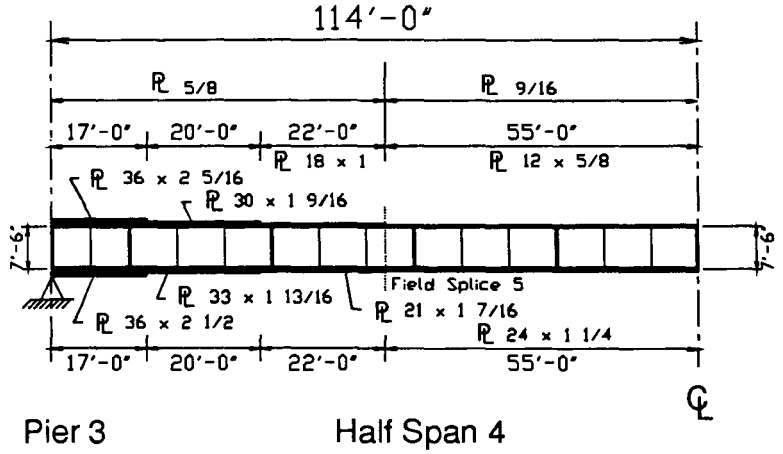

Fig 2.2 Variation of Plate-Girder Dimensions

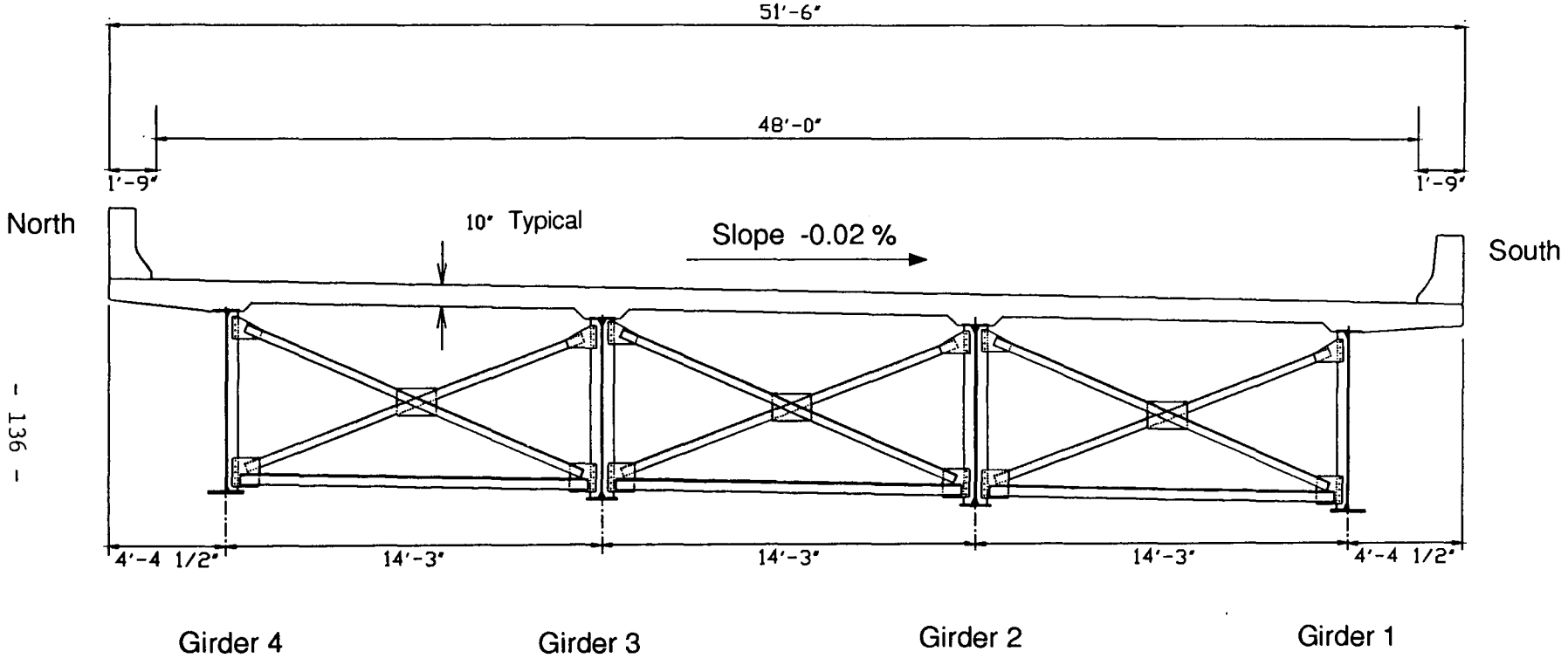

Fig. 2.3 Typical Cross Section of Bridge Superstructure

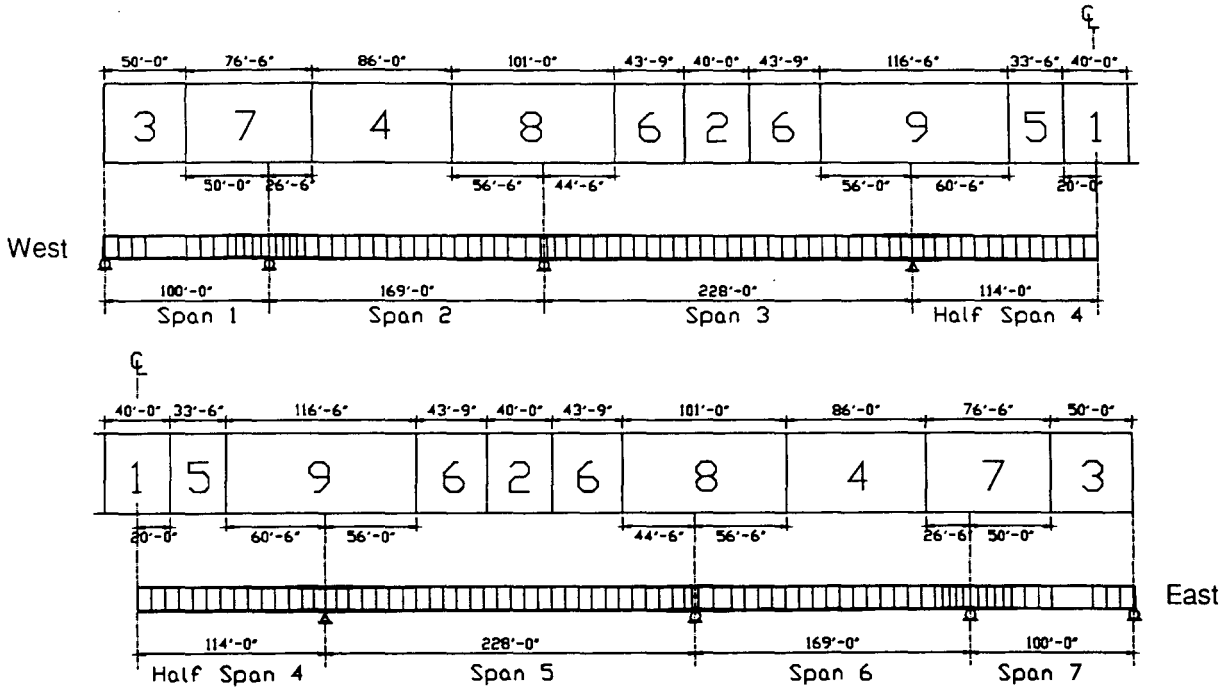

Casting Sequence	Day No.	Casting Date	Deflection * Measurement No.
1,2W	1	10/15/87 (Th)	0
2E	5	10/19/87 (M)	1
3E,3W	6	10/20/87 (Tu)	2
4E	7	10/21/87 (W)	3
4W	8	10/22/87 (Th)	4
5E,5W	9	10/23/87 (F)	5
6W	10	10/24/87 (Sa)	6
6E	12	10/26/87 (M)	7
7E	13	10/27/87 (Tu)	8
7W	14	10/28/87 (W)	
8E	15	10/29/87 (Th)	9
8W	16	10/30/87 (F)	10
9E	19	11/2/87 (M)	11
9W	20	11/3/87 (Tu)	12
			13
			14

* For measurement dates refer to Fig. 3.1

Fig. 2.4 Deck Casting Sequence

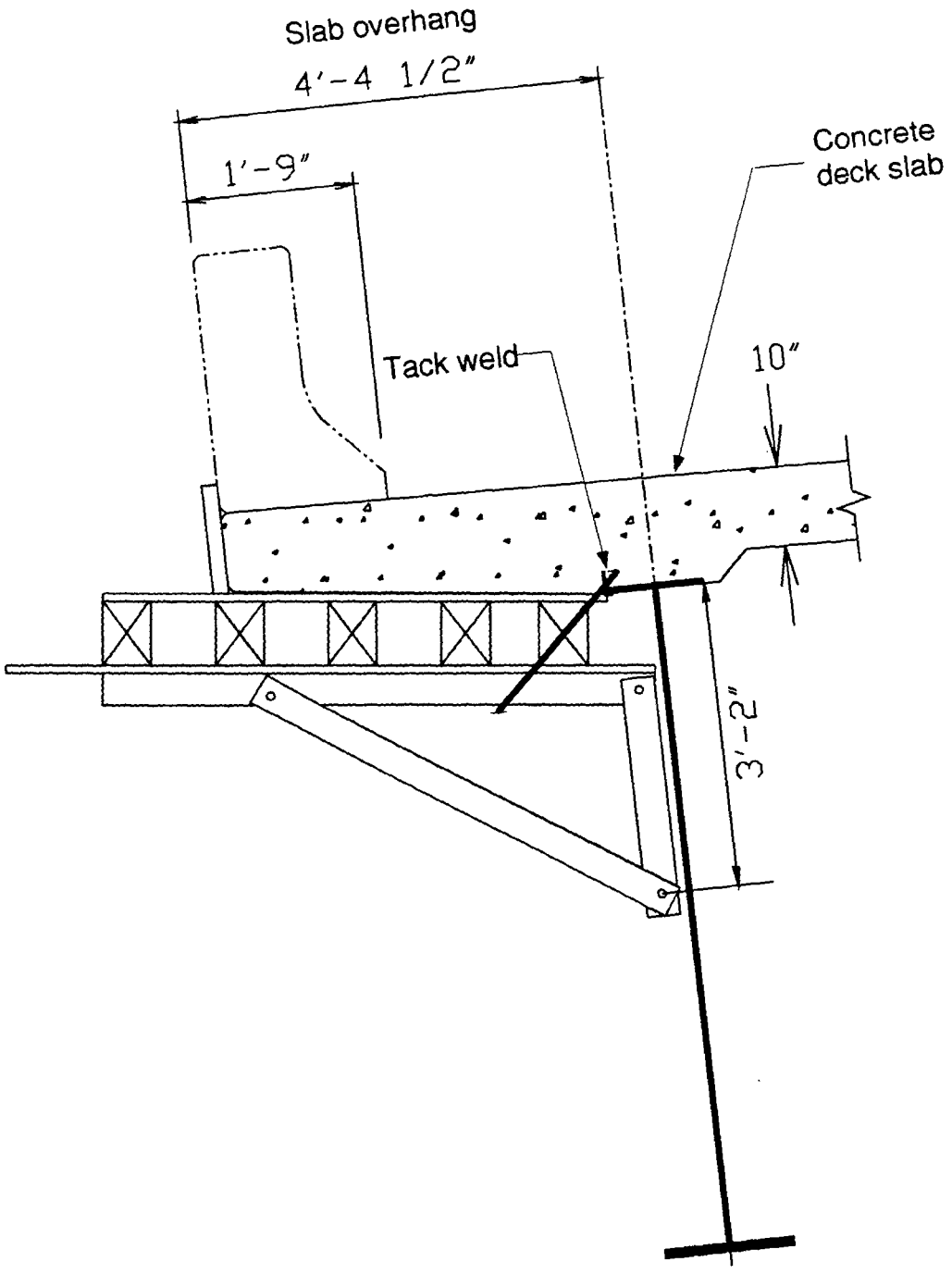

Fig. 2.5 Concrete Deck Slab Edge Formwork

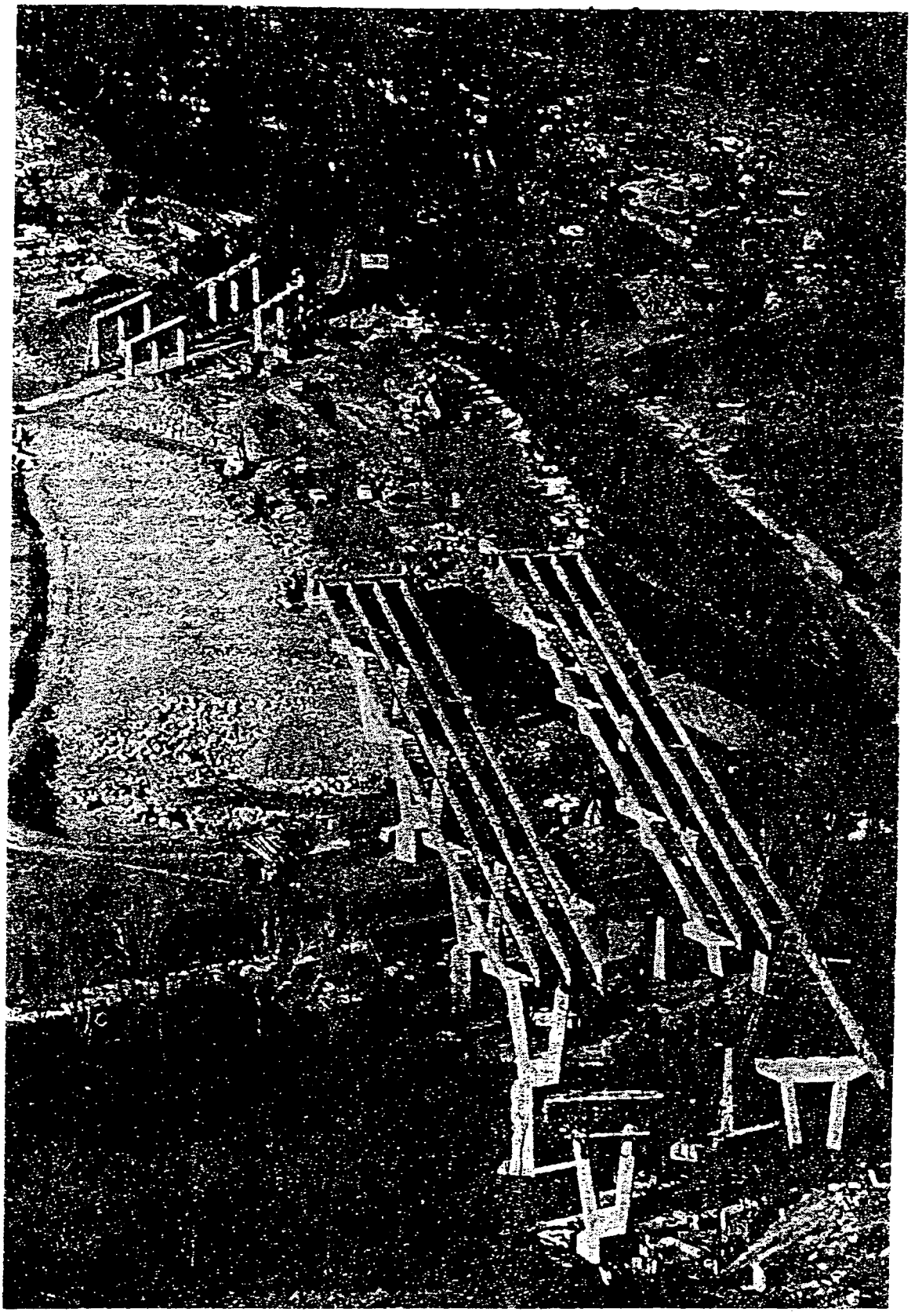

Fig. 2.6 Bridge under Construction (Newspaper photograph)

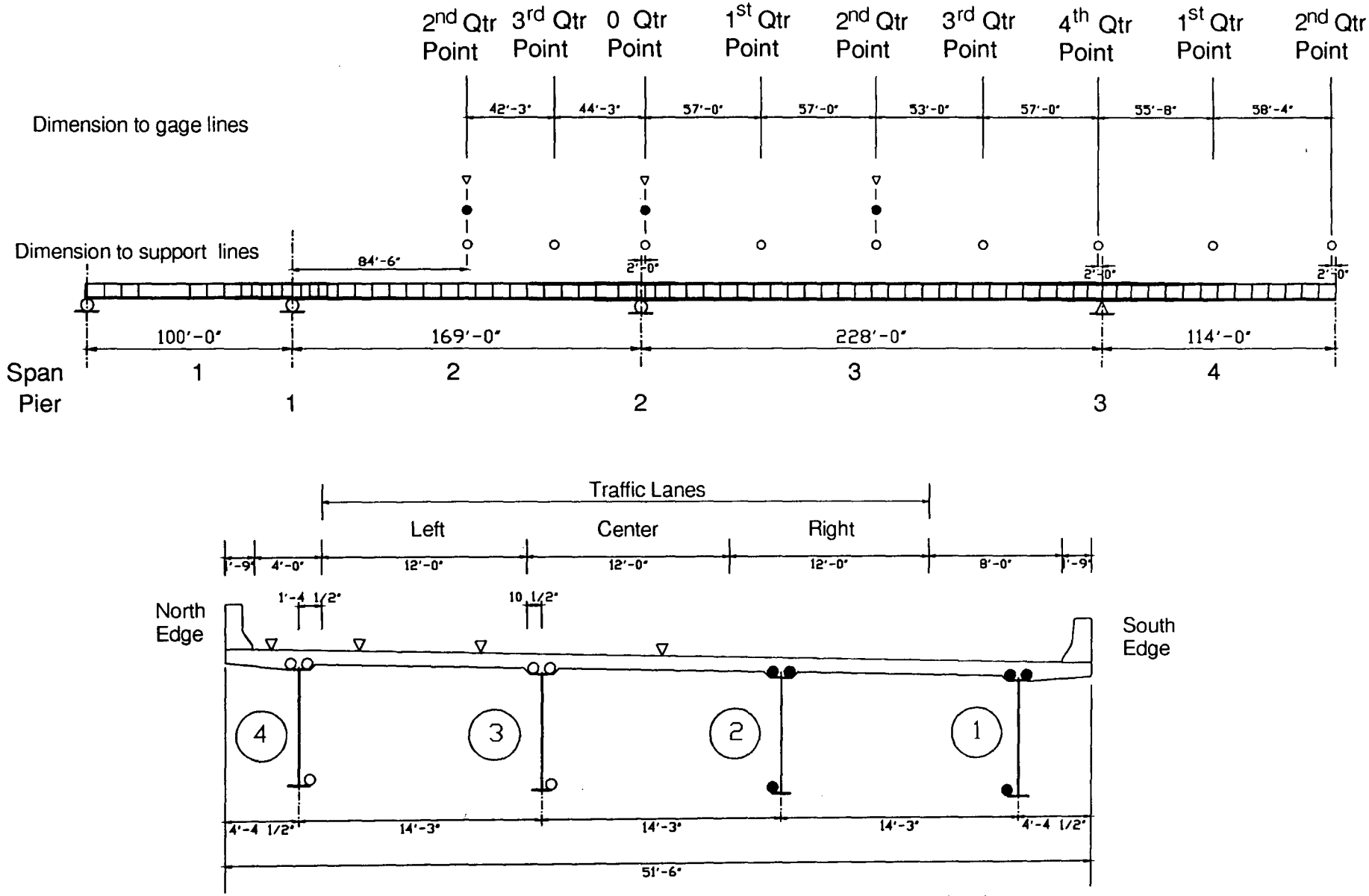

o Longitudinal Gages on Girders 3 and 4 (9 cross-sections)

● Longitudinal Gages on Girders 1 and 2 (3 cross-sections)

▽ Two Gage 90° Rosettes on Slab (3 cross-sections) (refer to Fig. 2.8)

Fig 2.7 Plate Girder and Deck Slab Strain Gages

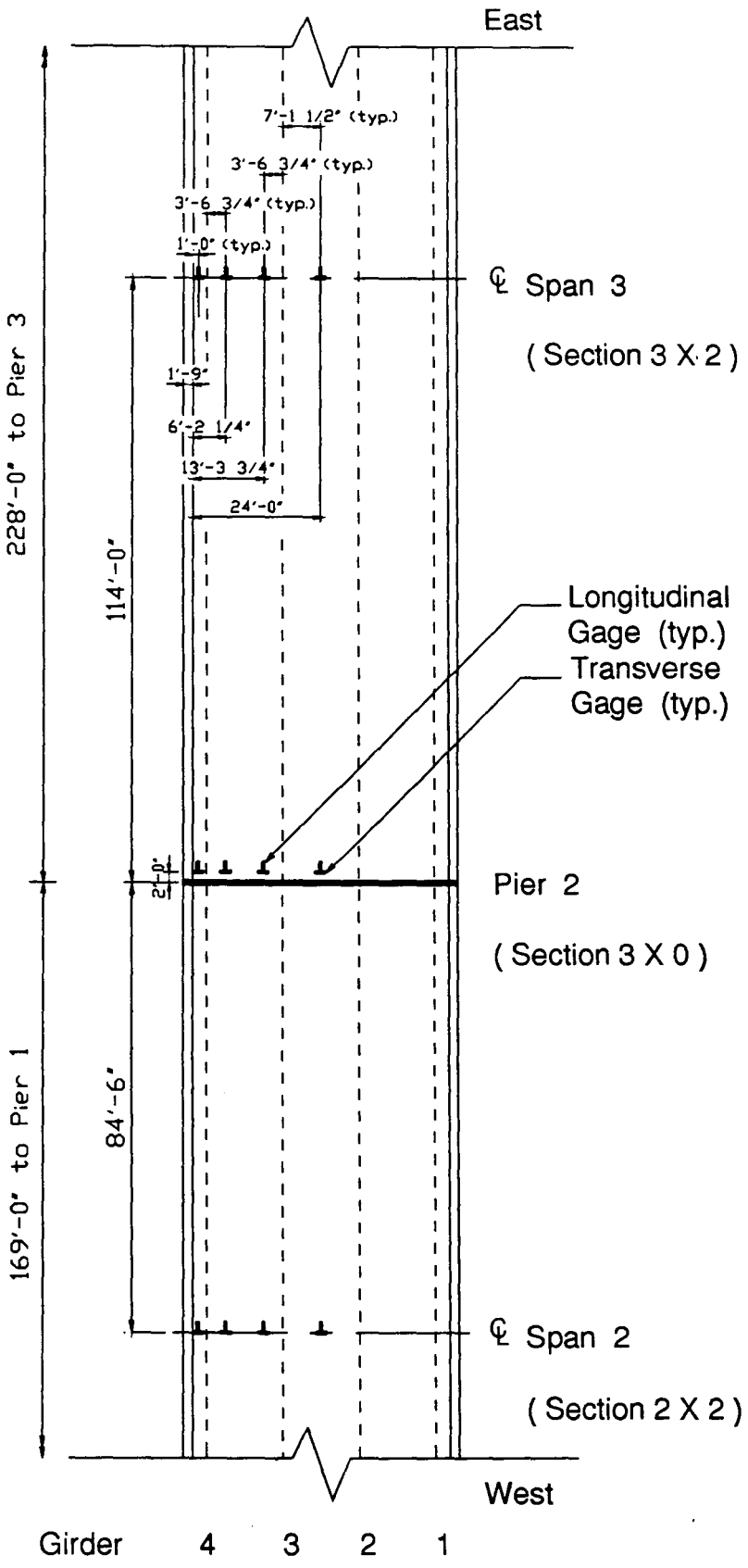

Fig. 2.8 Strain Gages on Deck Slab

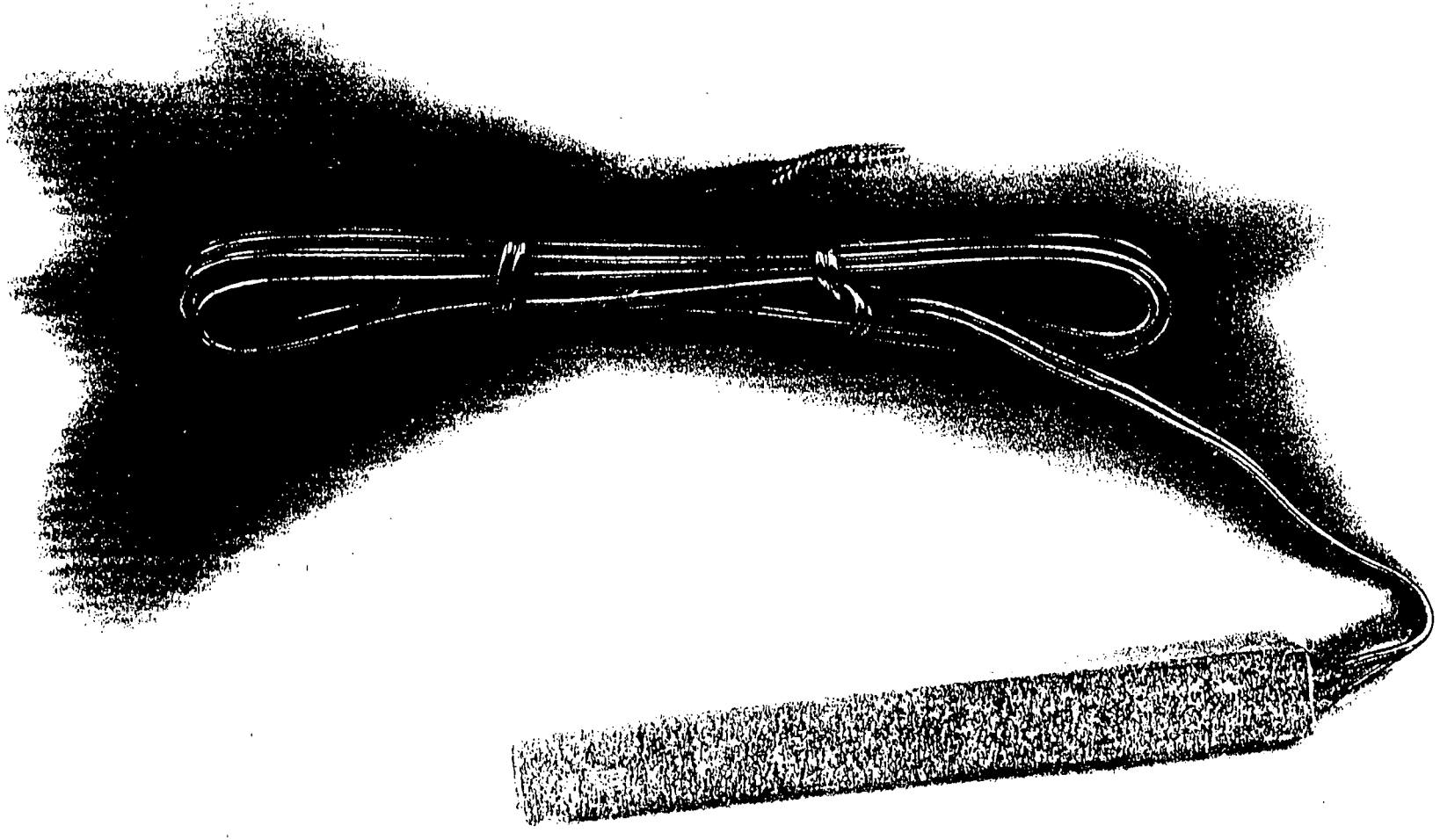

Fig. 2.9 Polyester Mold Gage

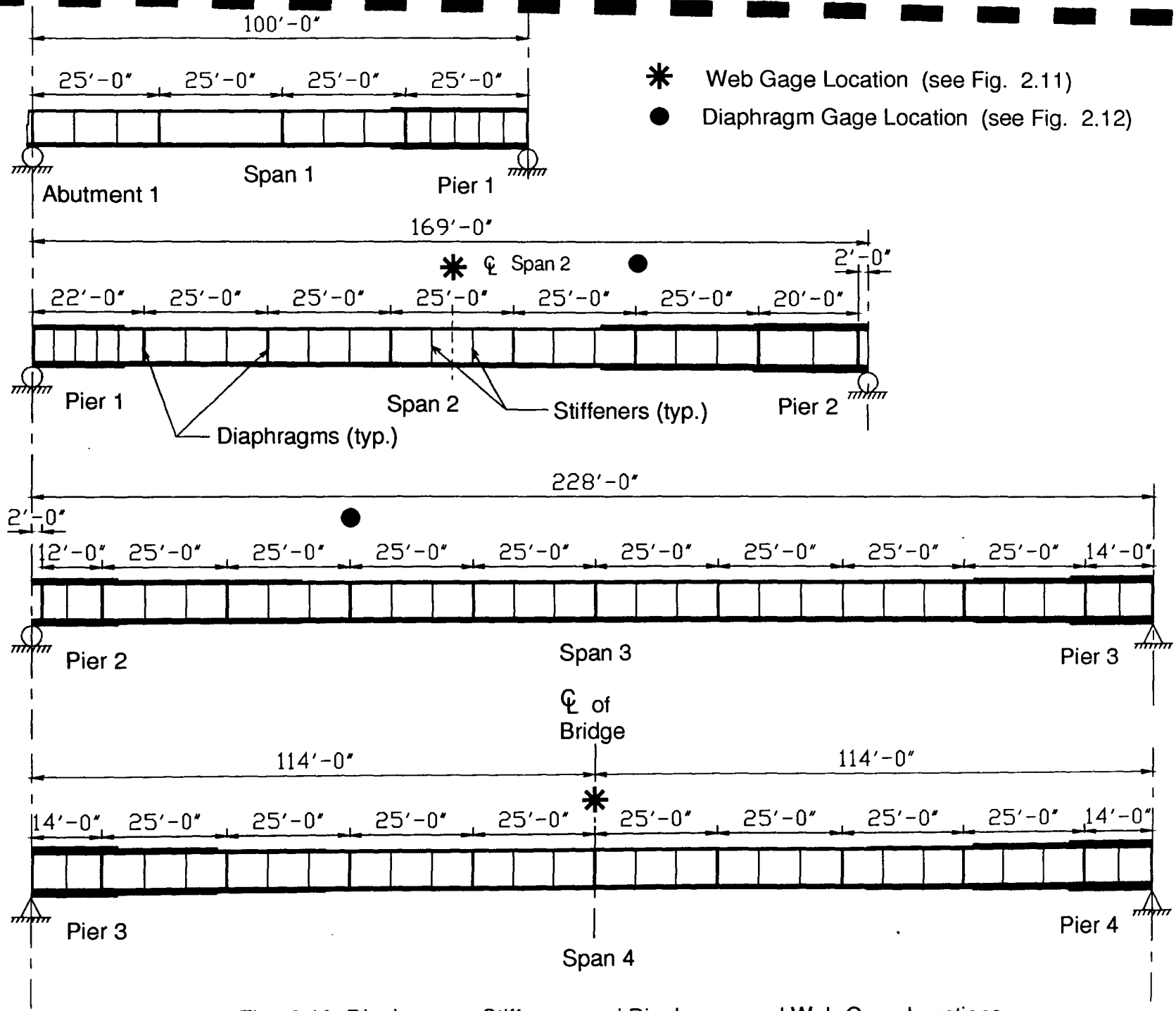

Fig. 2.10 Diaphragms, Stiffeners and Diaphragm and Web Gage Locations

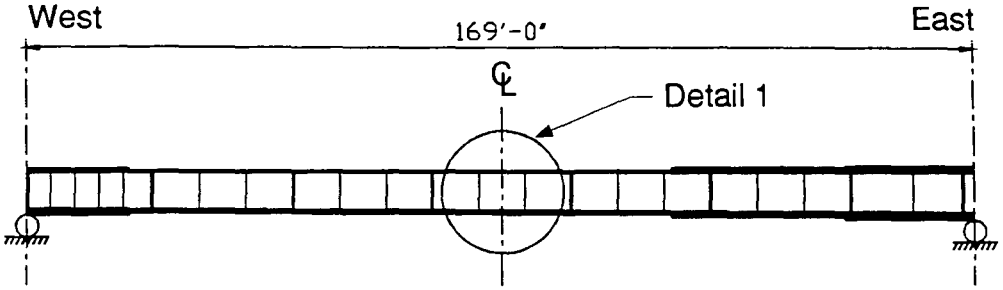

Girder 4 in Span 2

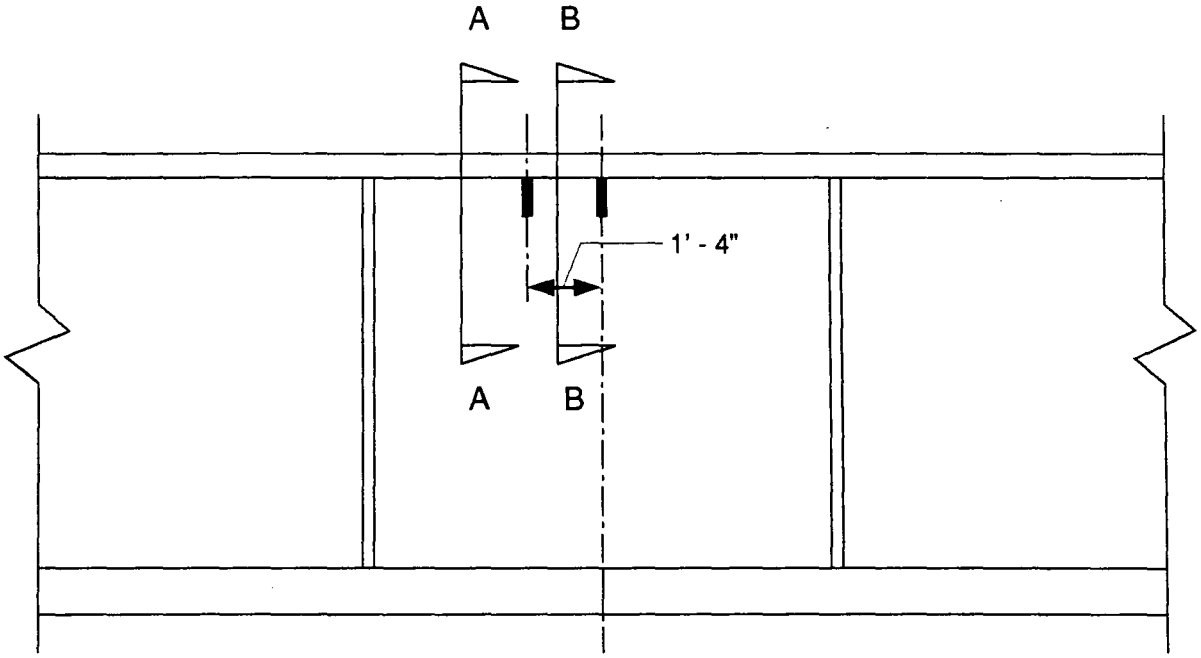

Detail 1

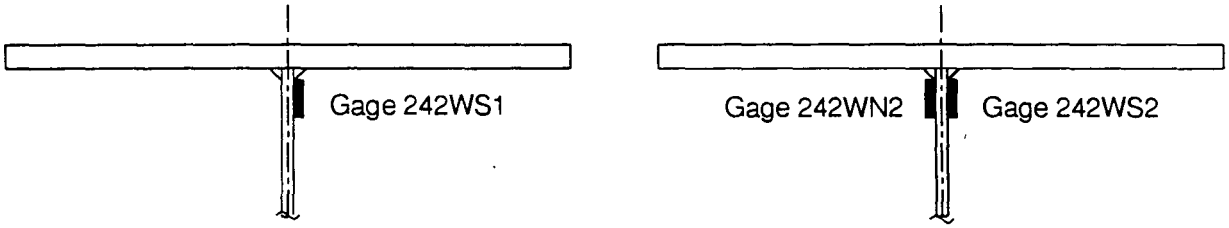

Section A - A

Section B - B

Fig. 2.11 (a) Web Gage Locations - Span 2

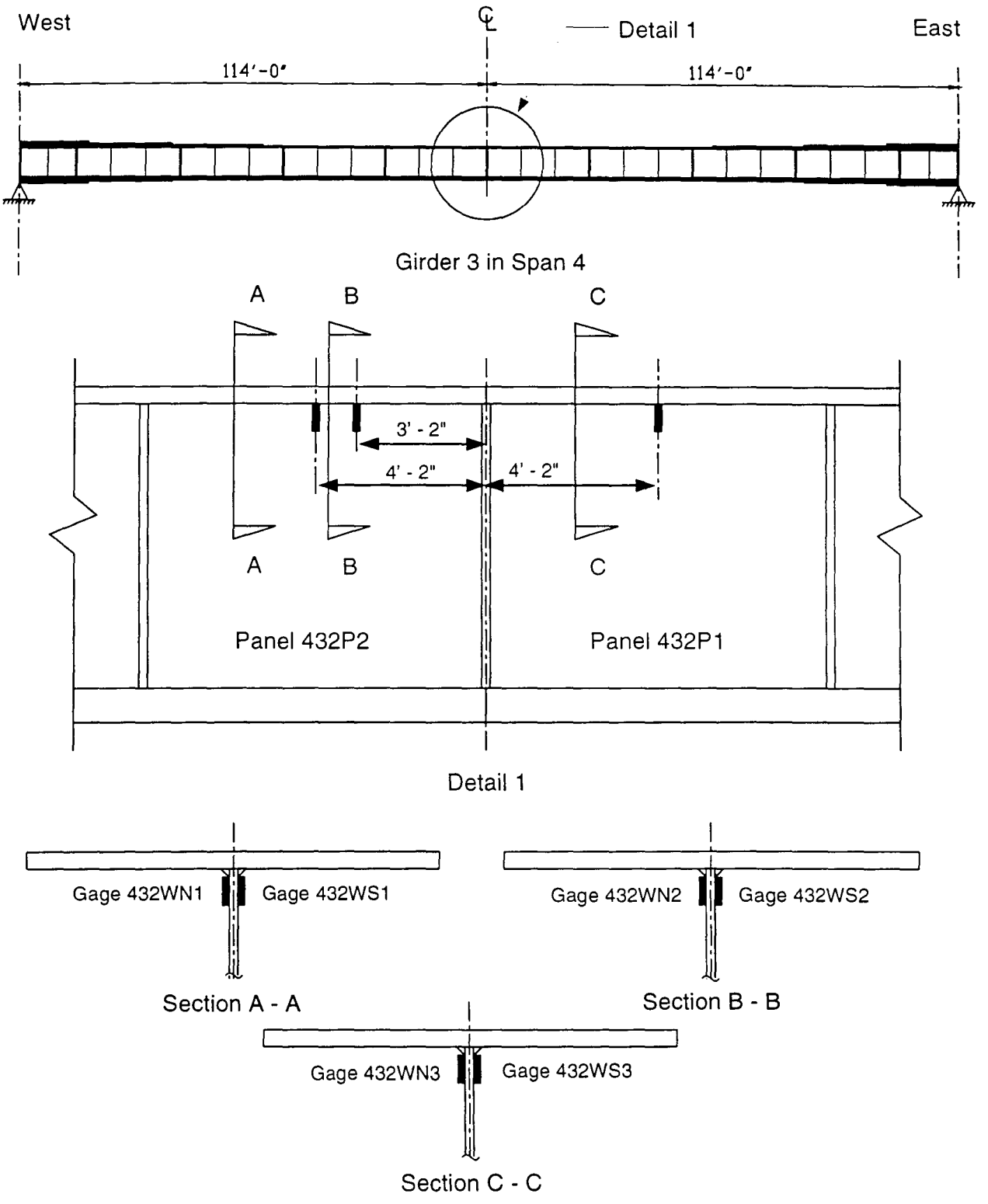

Fig. 2.11 (b) Web Gage Locations - Span 4

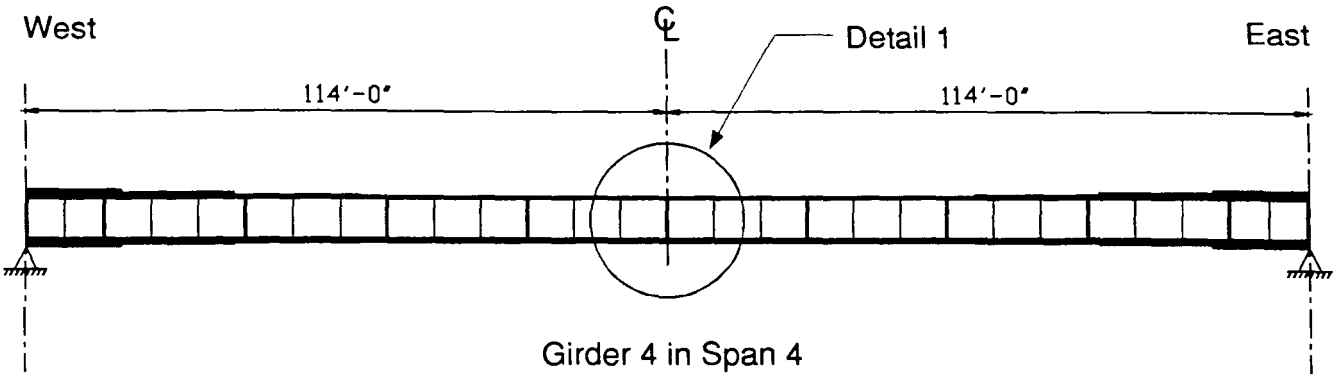

Girder 4 in Span 4

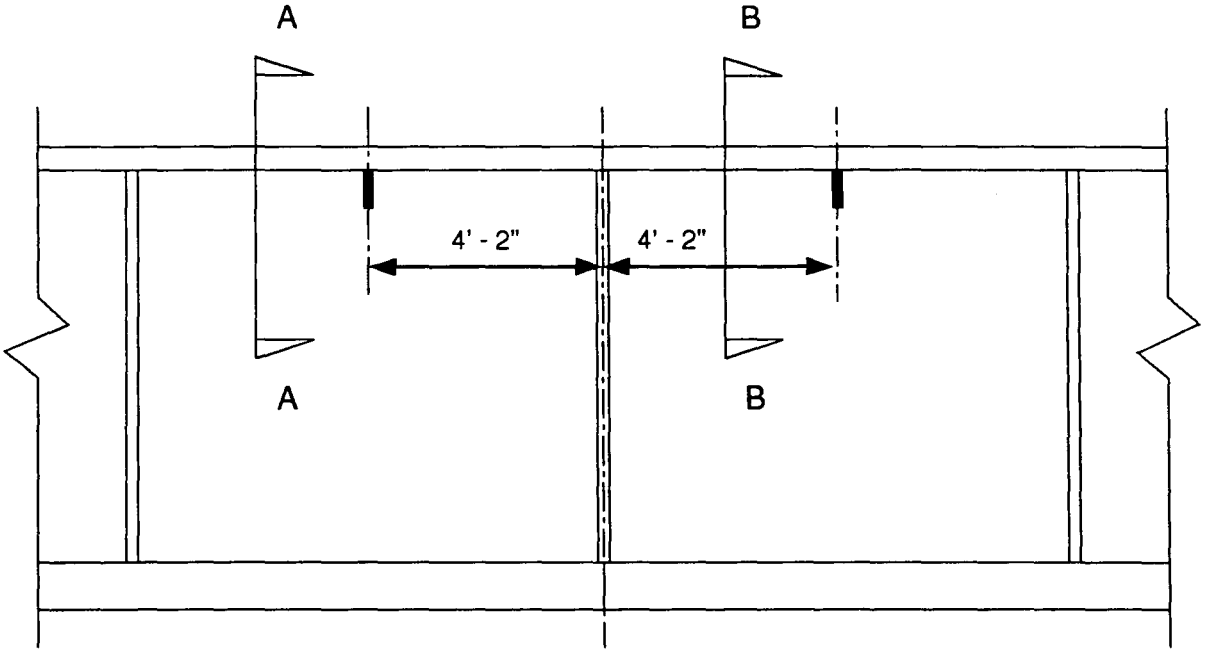

Detail 1

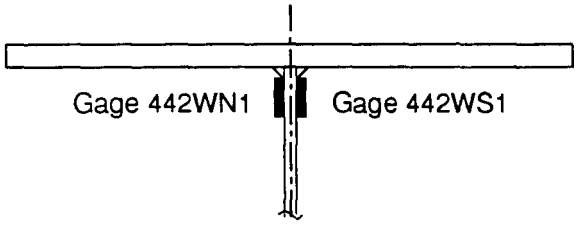

Section A - A

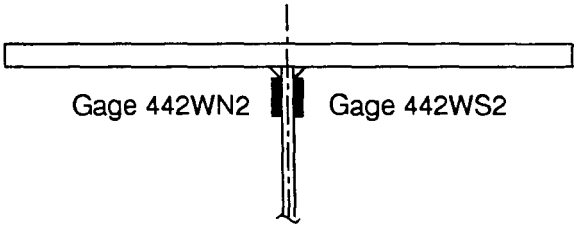

Section B - B

Fig. 2.11 (c) Web Gage Locations - Span 4

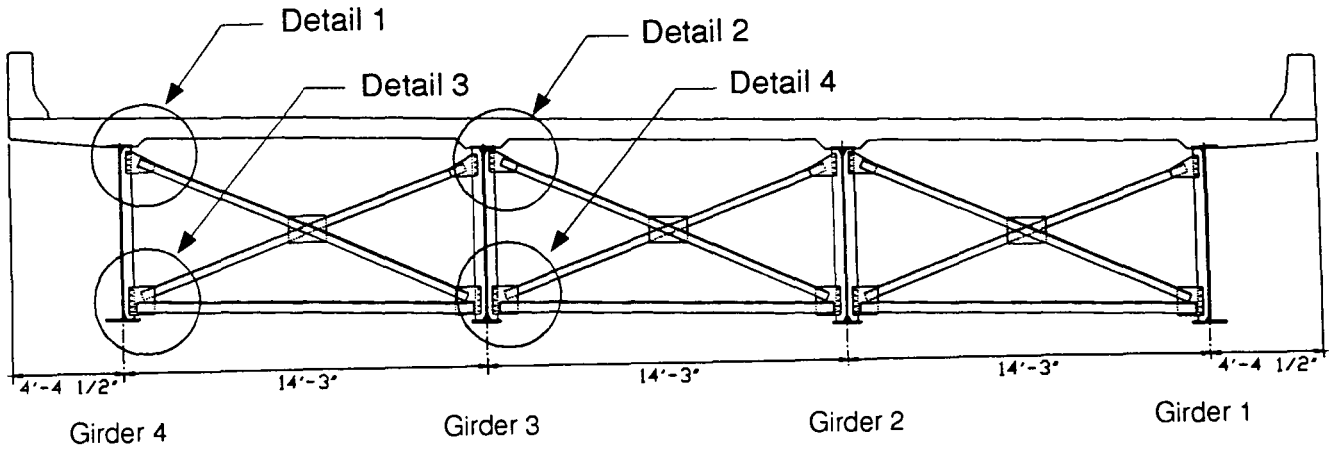

Diaphragm 5 in Span 2

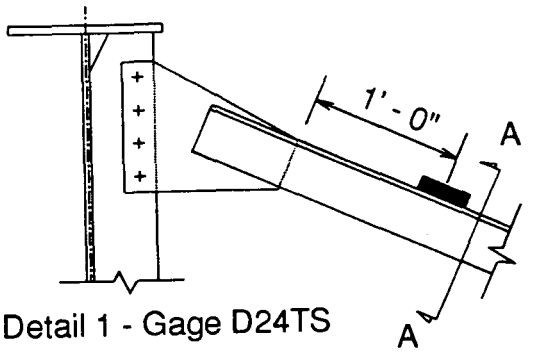

Detail 1 - Gage D24TS

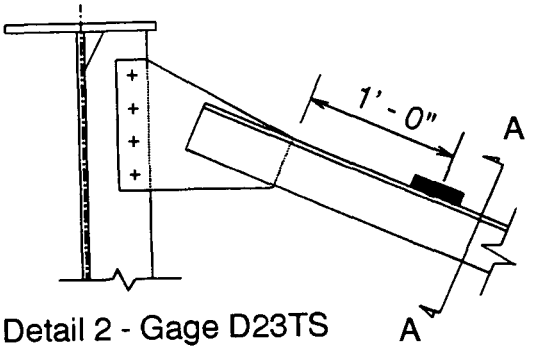

Detail 2 - Gage D23TS

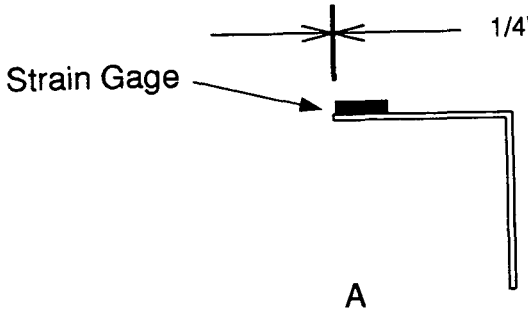

Section A - A
(typ.)

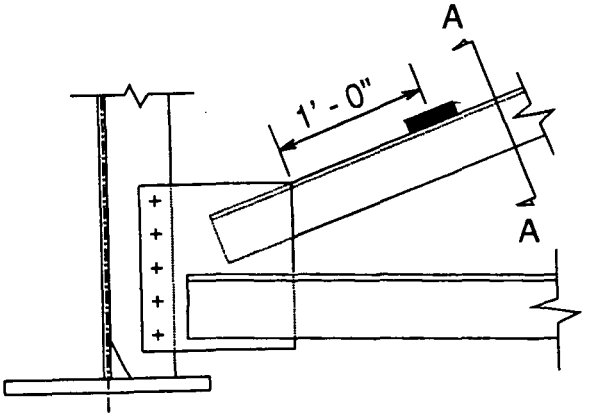

Detail 3 - Gage D24BS

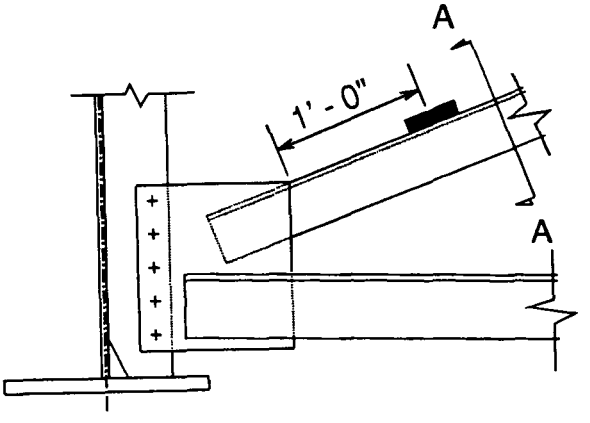

Detail 4 - Gage D23BS

Fig. 2.12 (a) Diaphragm Gage Locations - Span 2

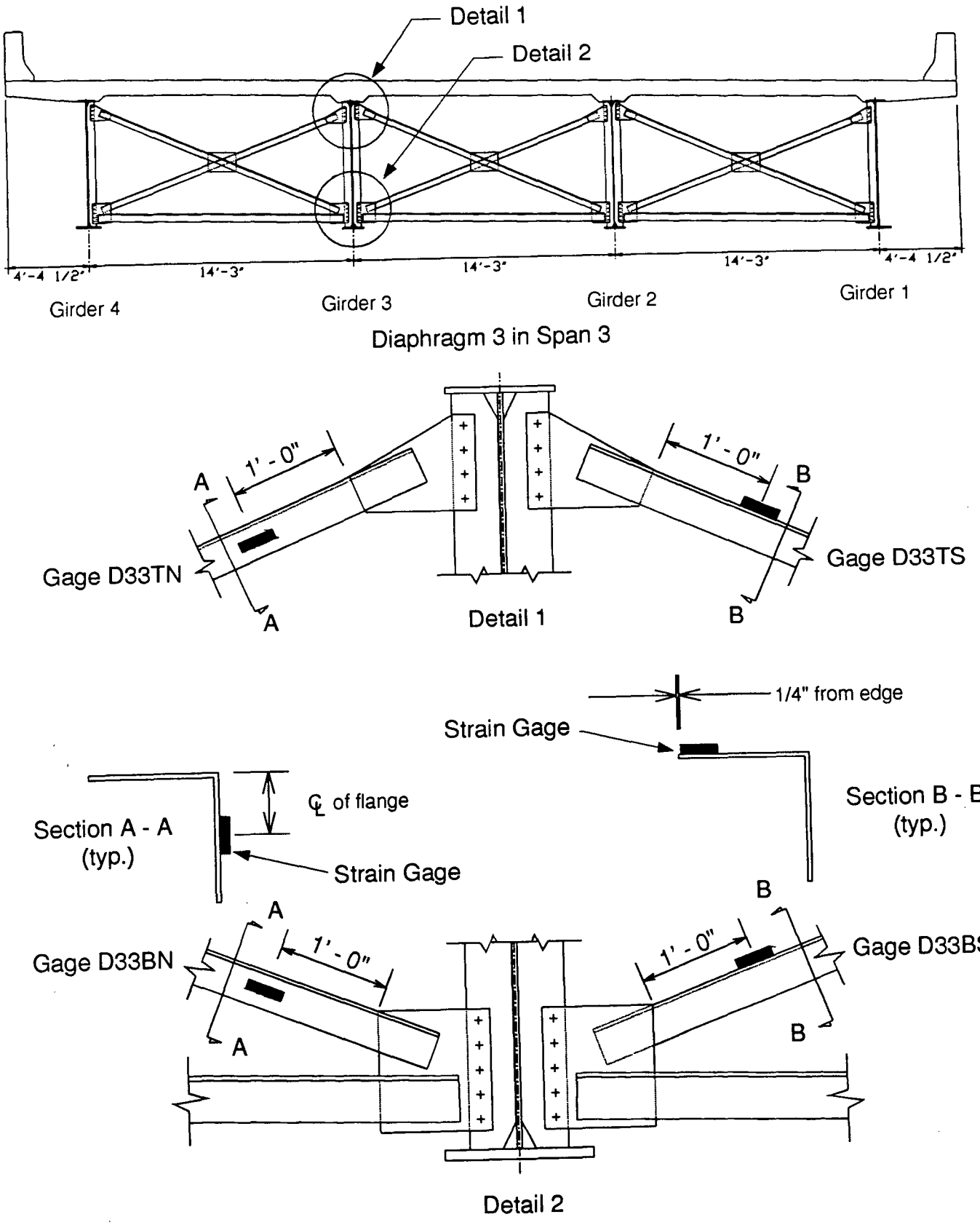

Fig. 2.12 (b) Diaphragm Gage Locations - Span 3

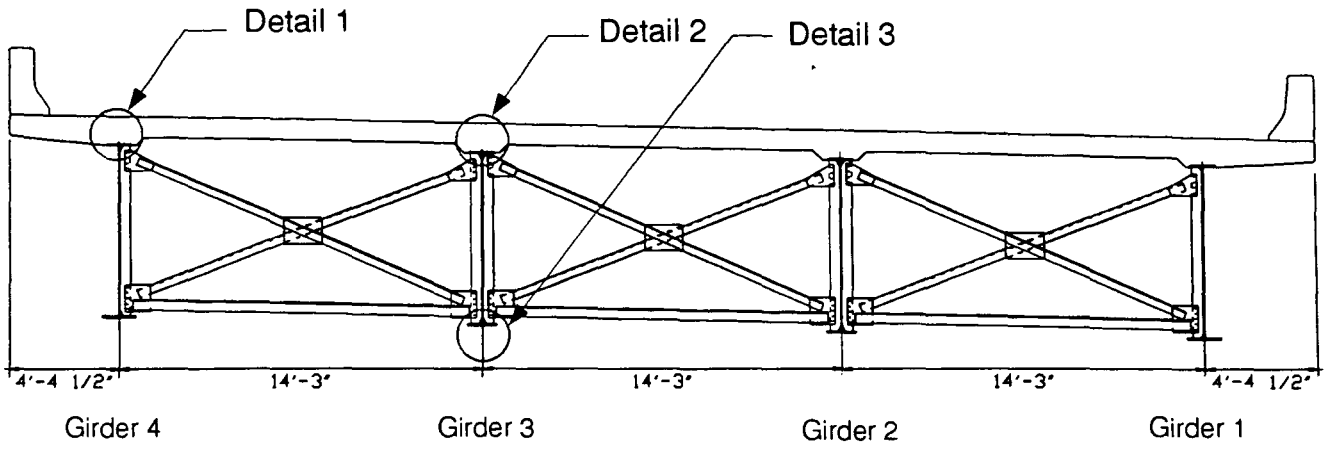

Diaphragm 3 in Span 3

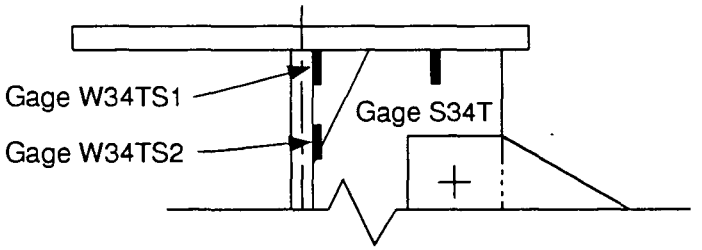

Detail 1

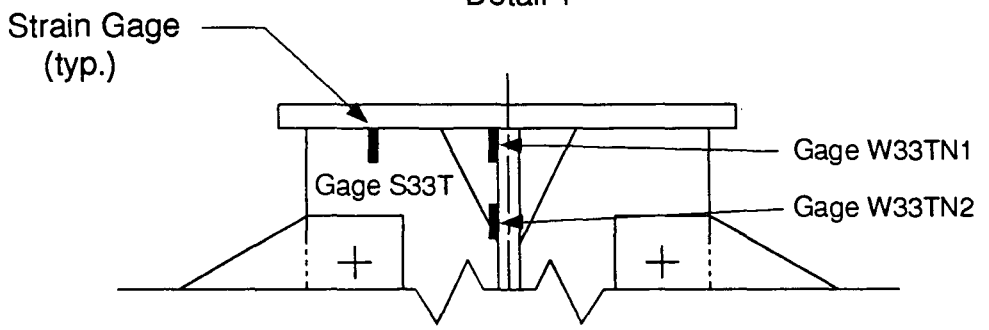

Detail 2

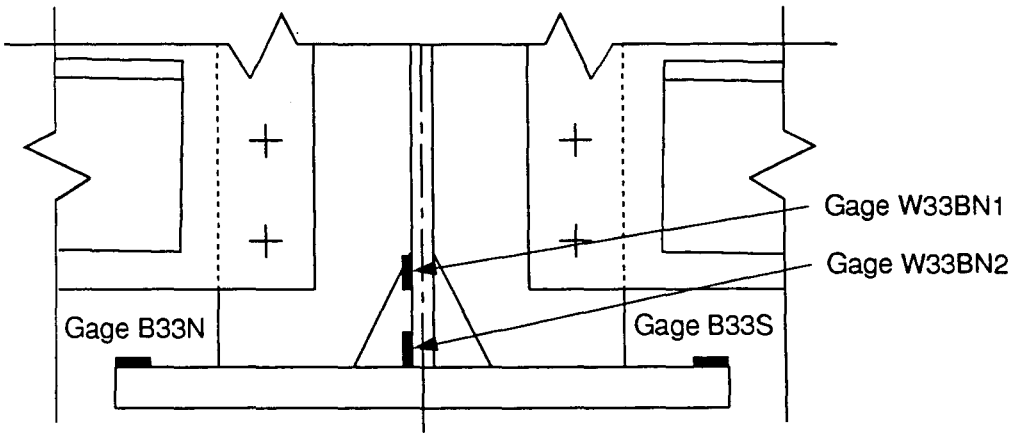

Detail 3

Fig. 2.12 (c) Diaphragm Gage Locations - Span 3

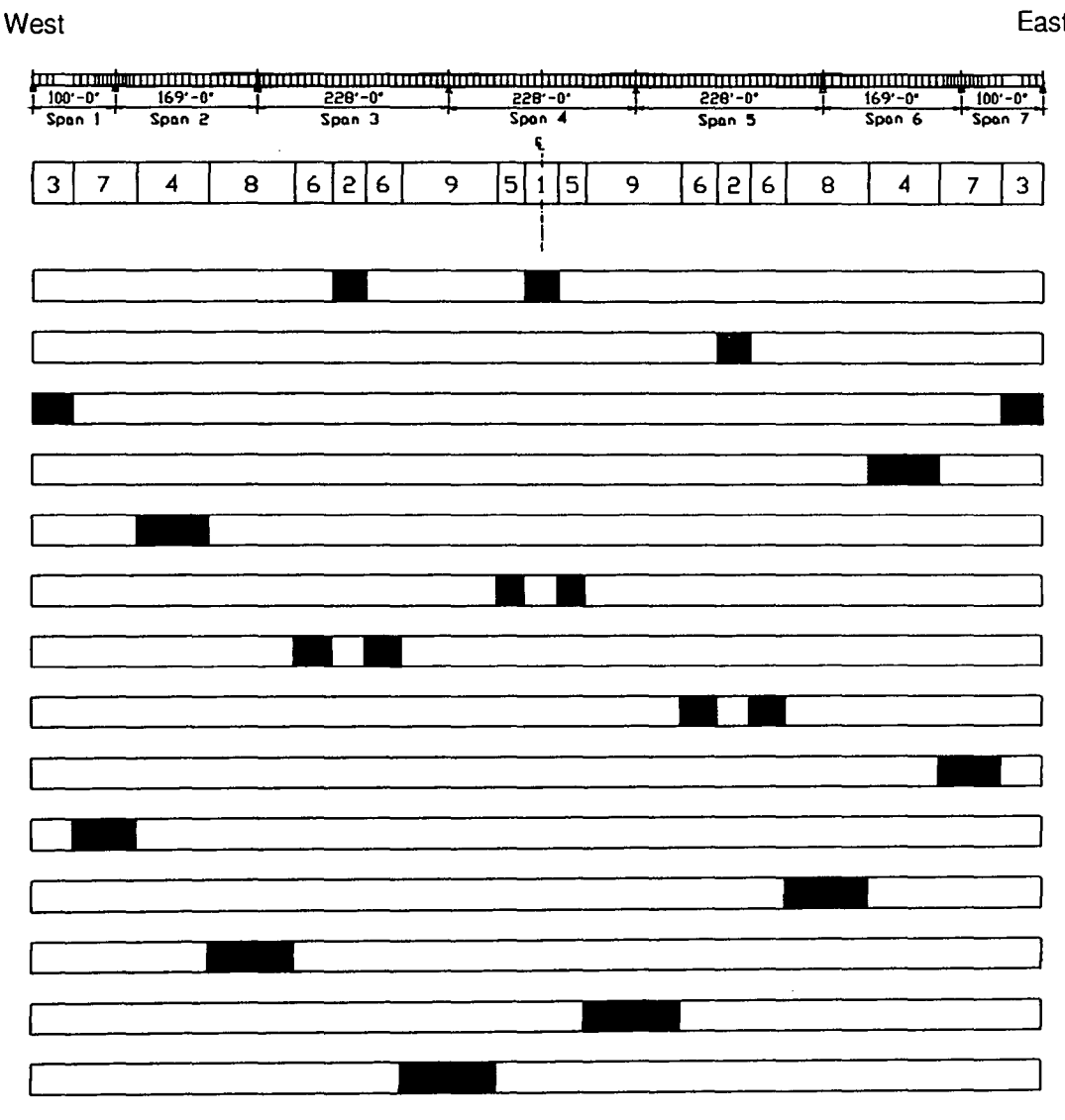

Slab Segment(s)	Placement Date
1,2W	Oct. 15
2E	Oct. 19
3W,3E	Oct. 20
4E	Oct. 21
4W	Oct. 22
5W,5E	Oct. 23
6W	Oct. 24
6E	Oct. 26
7E	Oct. 27
7W	Oct. 28
8E	Oct. 29
8W	Oct. 30
9E	Nov. 2
9W	Nov. 3

Elevation Reading No.	Date	Time (pm)
0	Oct. 14 (1987)	4:15-6:00
1	Oct. 15	4:00-5:30
2	Oct. 19	3:50-5:15
3	Oct. 20	4:00-5:00
4	Oct. 21	3:50-5:00
5	Oct. 22	4:00-5:15
6	Oct. 23	3:50-5:00
7	Oct. 25	3:00-4:30
8	Oct. 26	3:00-4:30
9	Oct. 28	3:00-4:00
10	Oct. 29	3:30-4:45
11	Oct. 30	3:15-4:30
12	Nov. 2	3:30-4:50
13	Nov. 5	3:35-5:00
14	Aug. 12 (1988)	3:20-5:00

Fig. 3.1 Time Table for Slab Placement/Deflection Readings

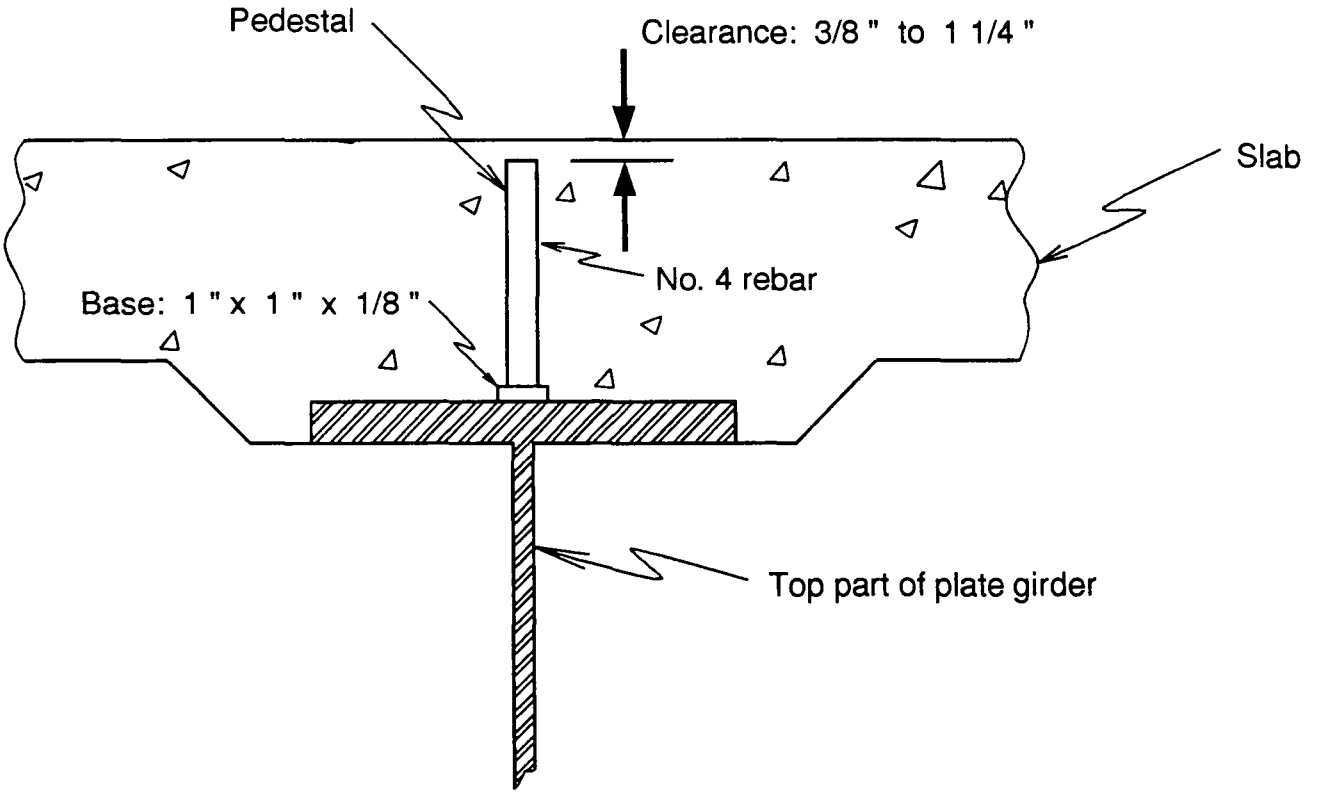

Fig. 3.2 Detail of Pedestal

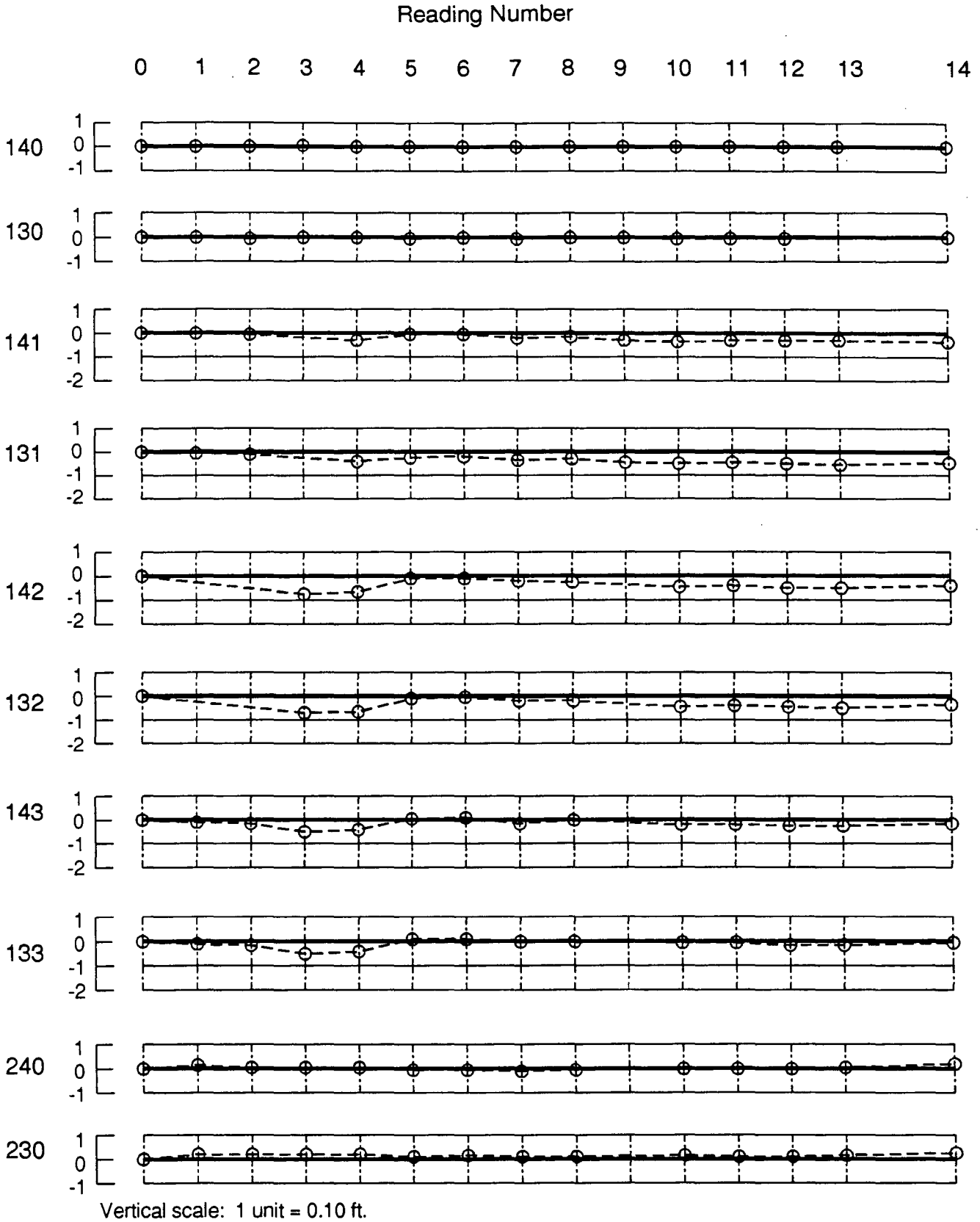

Fig. 3.3 Measured Deflections due to Slab Placement - Span 1

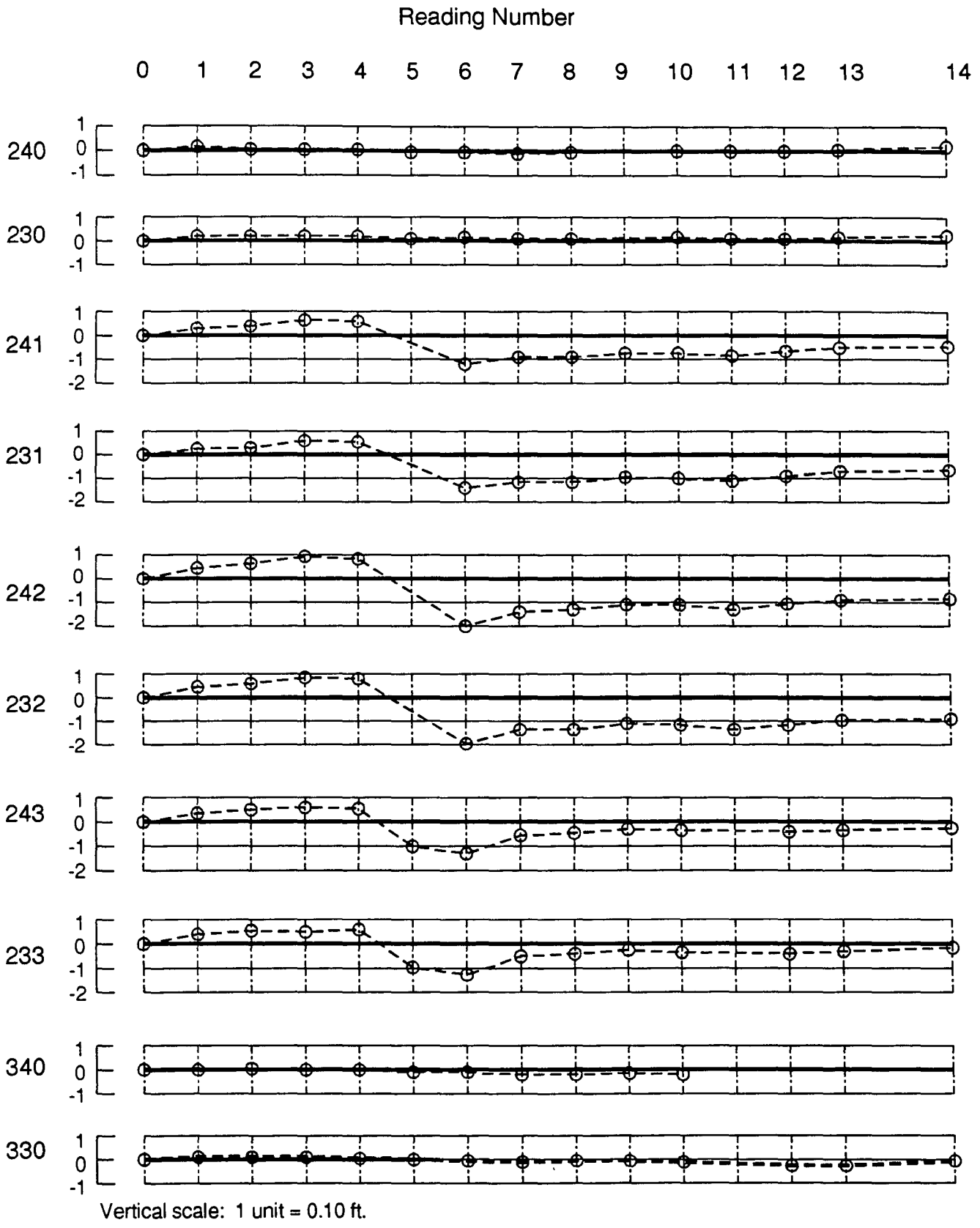

Fig. 3.4 Measured Deflections due to Slab Placement - Span 2

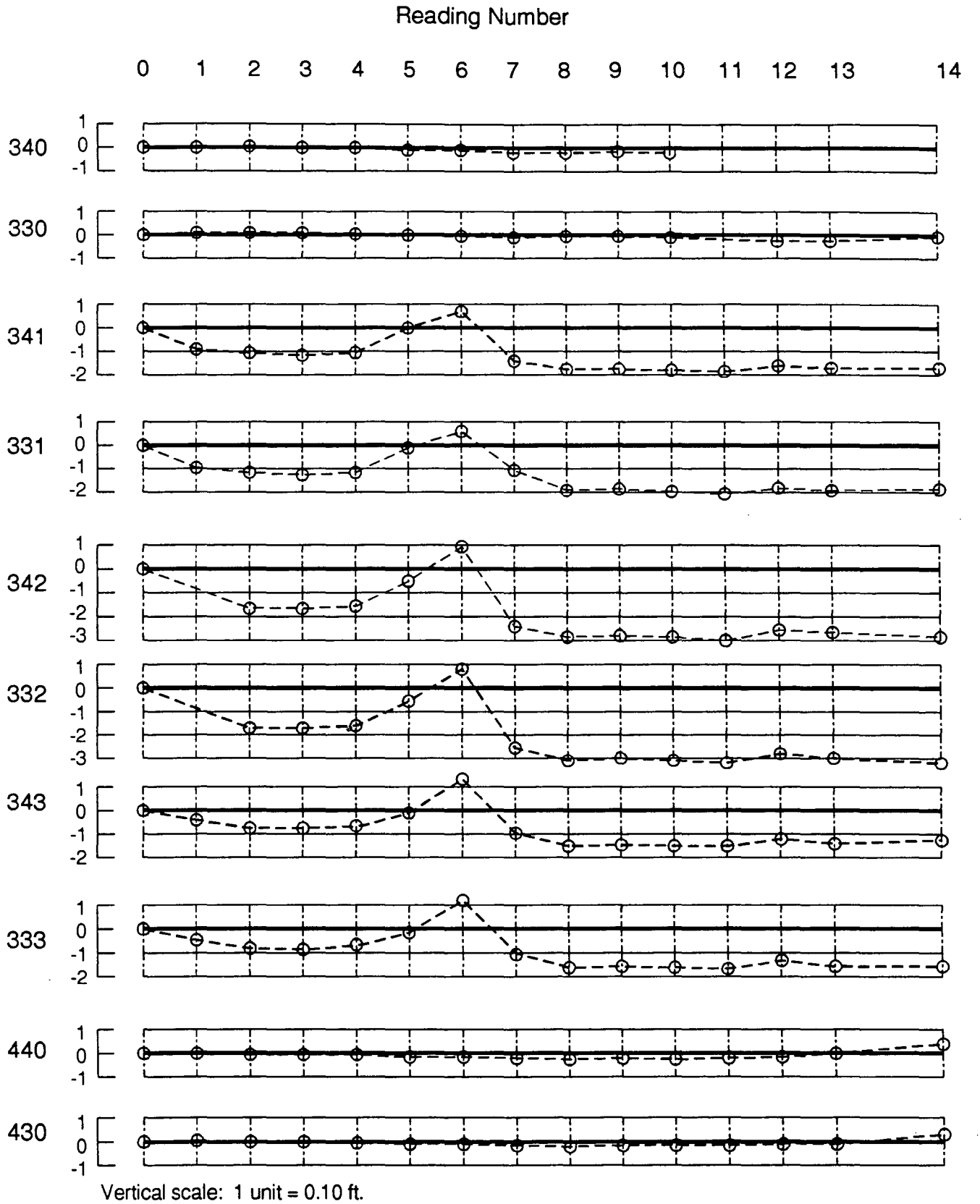

Fig. 3.5 Measured Deflections due to Slab Placement - Span 3

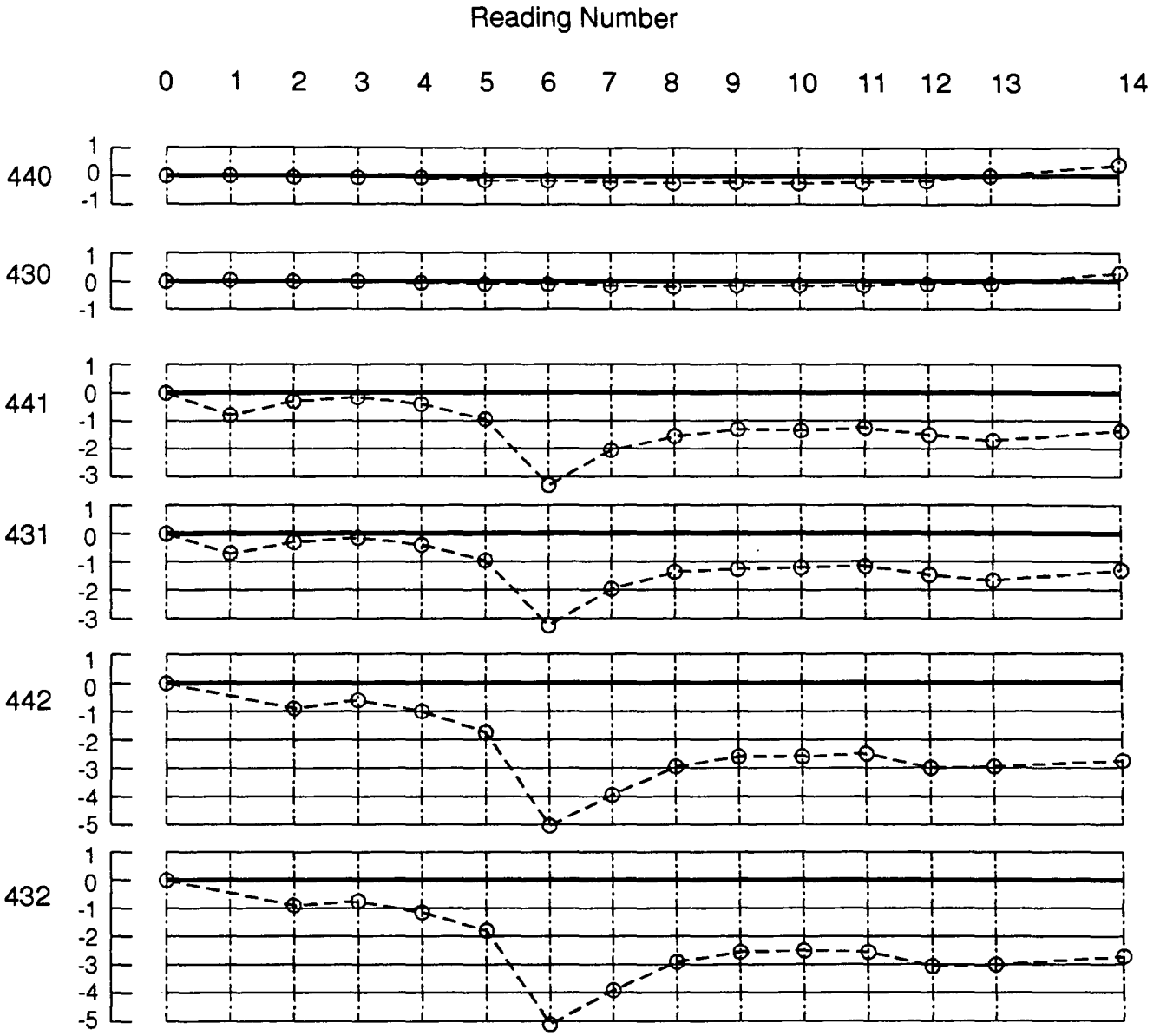

Vertical scale: 1 unit = 0.10 ft.

Fig. 3.6 Measured Deflections due to Slab Placement - Half Span 4

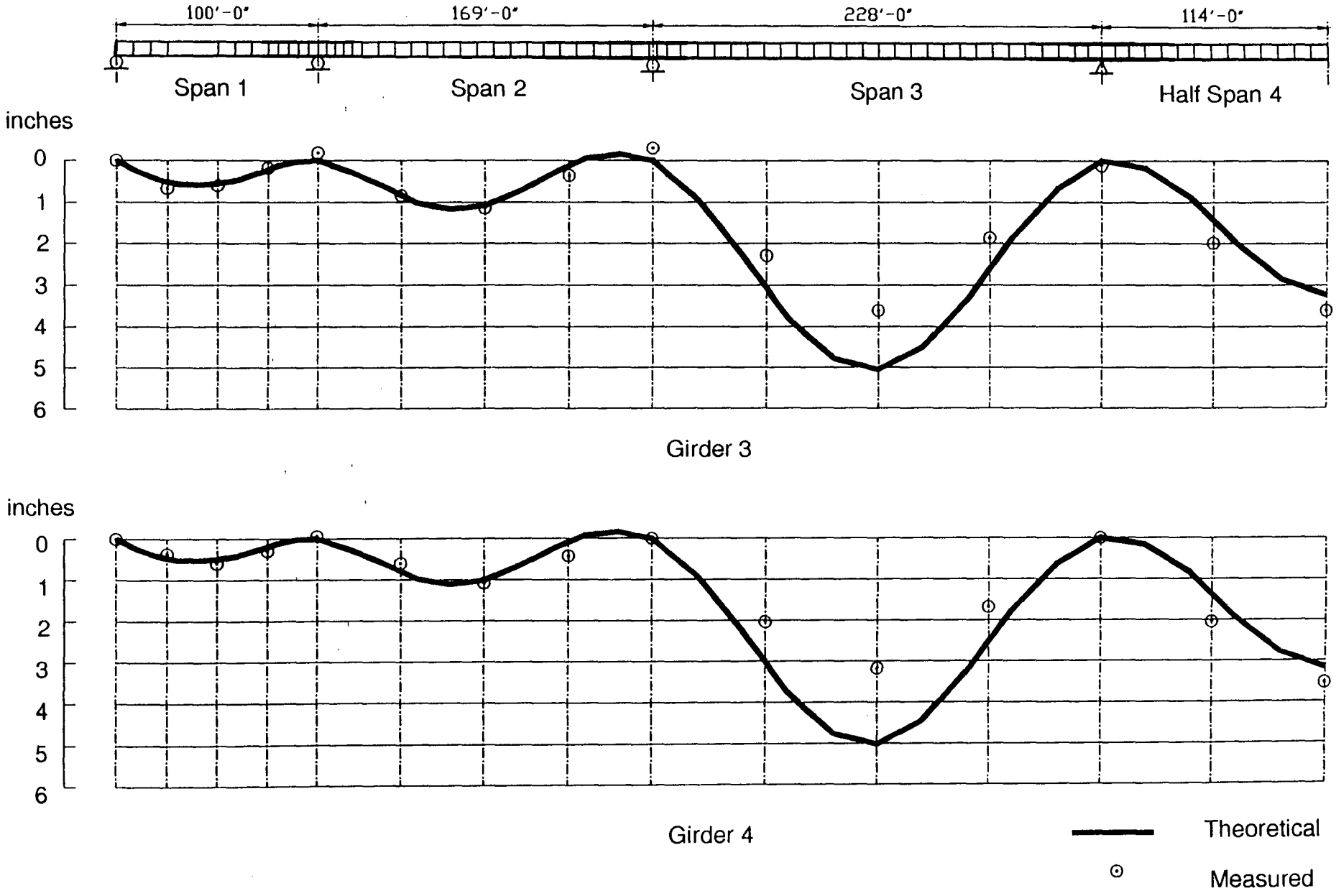

Fig. 3.7 Girder Deflections due to Slab Placement

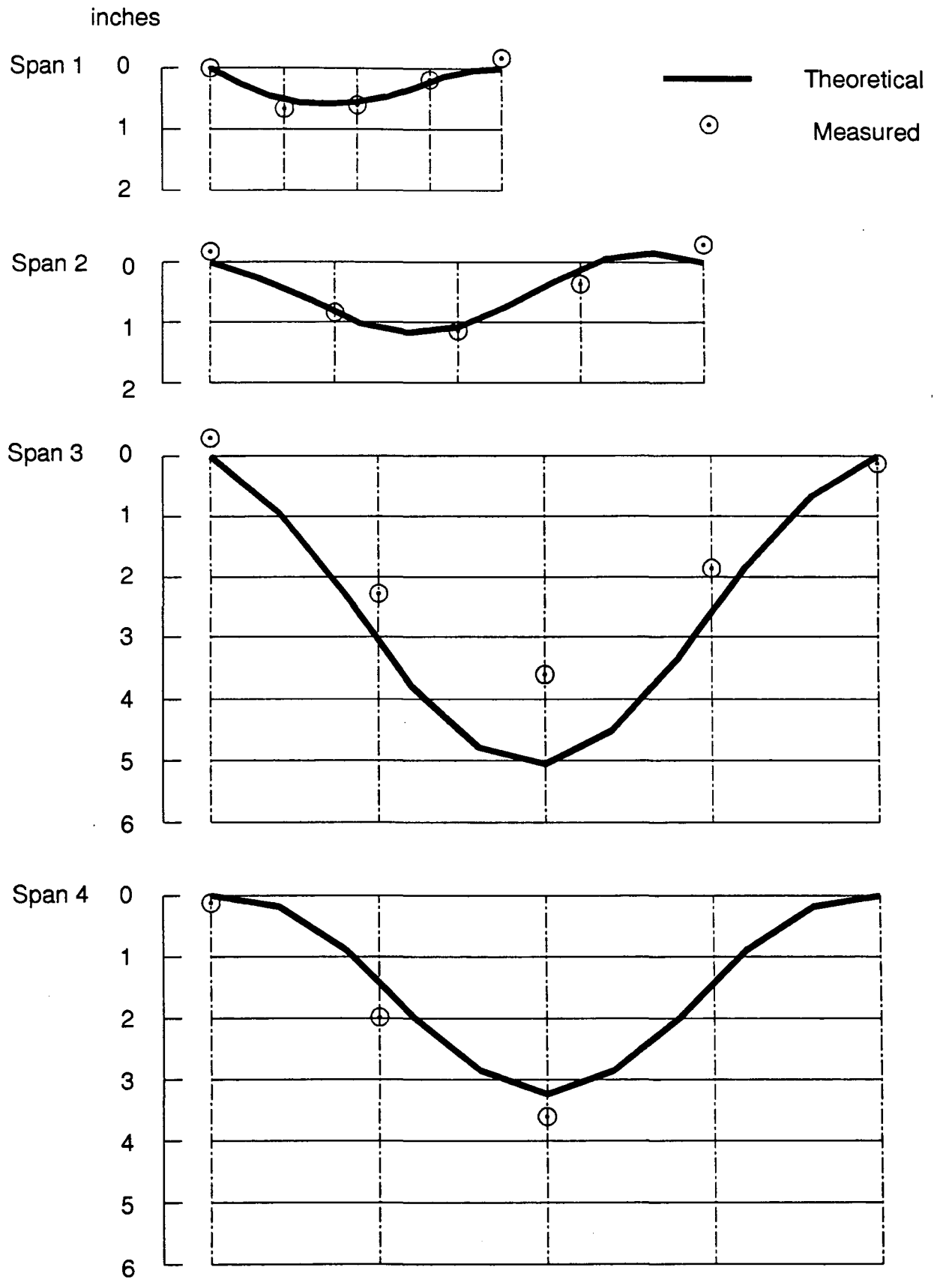

Fig. 3.8 Girder Deflections due to Slab Placement - Girder 3

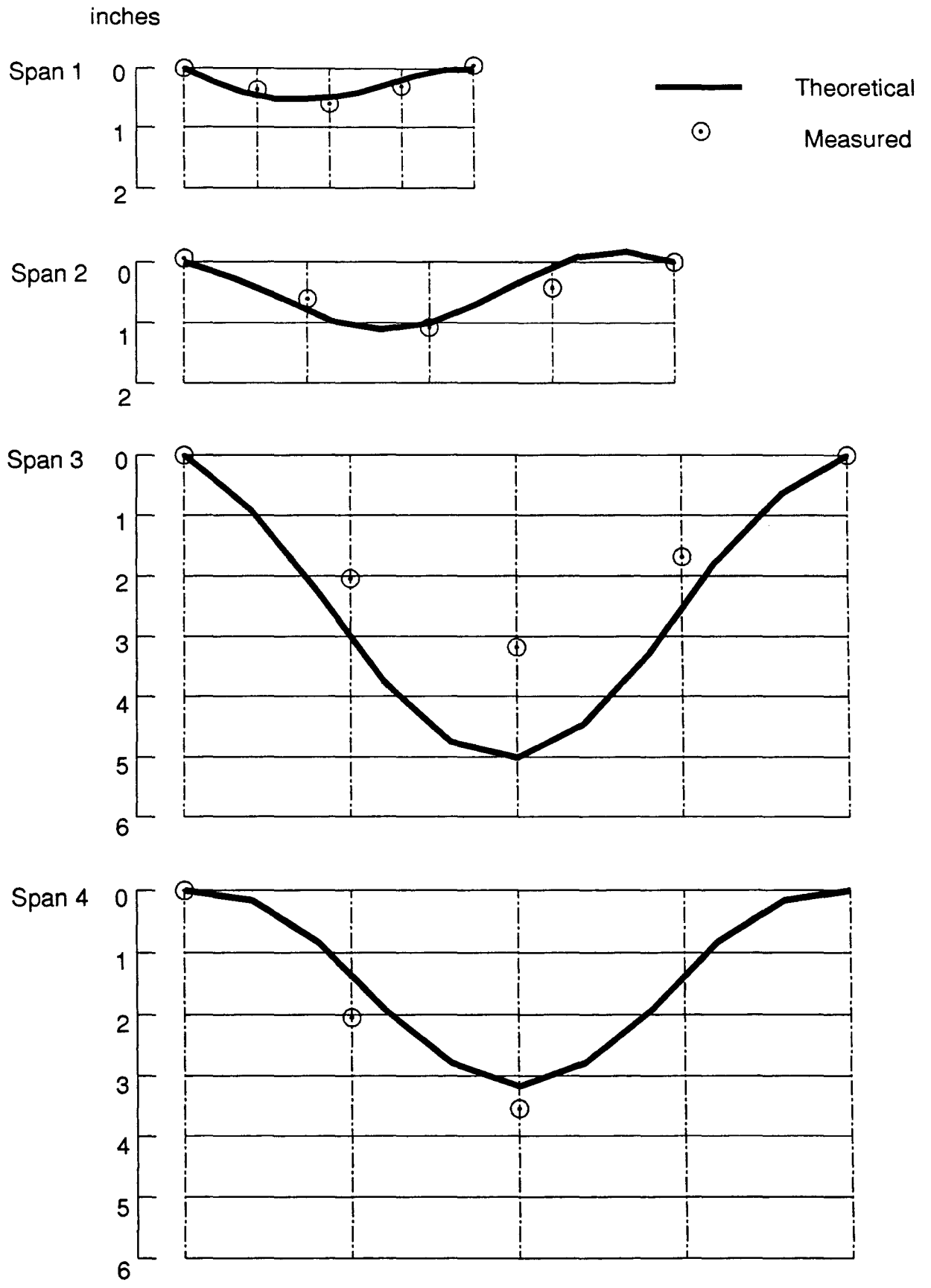

Fig. 3.9 Girder Deflections due to Slab Placement - Girder 4

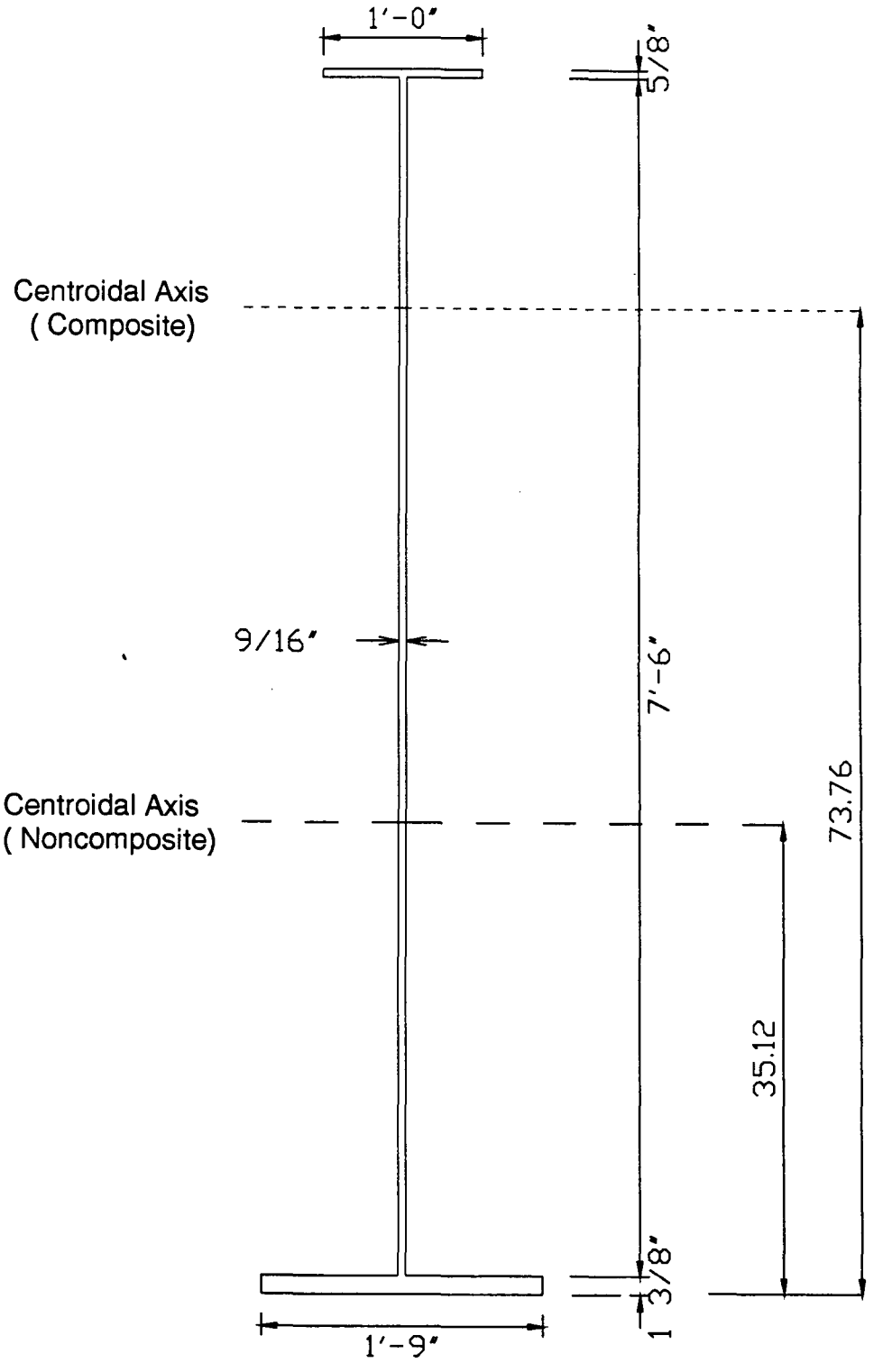

Fig. 4.1 Girder Cross Section at Location 432

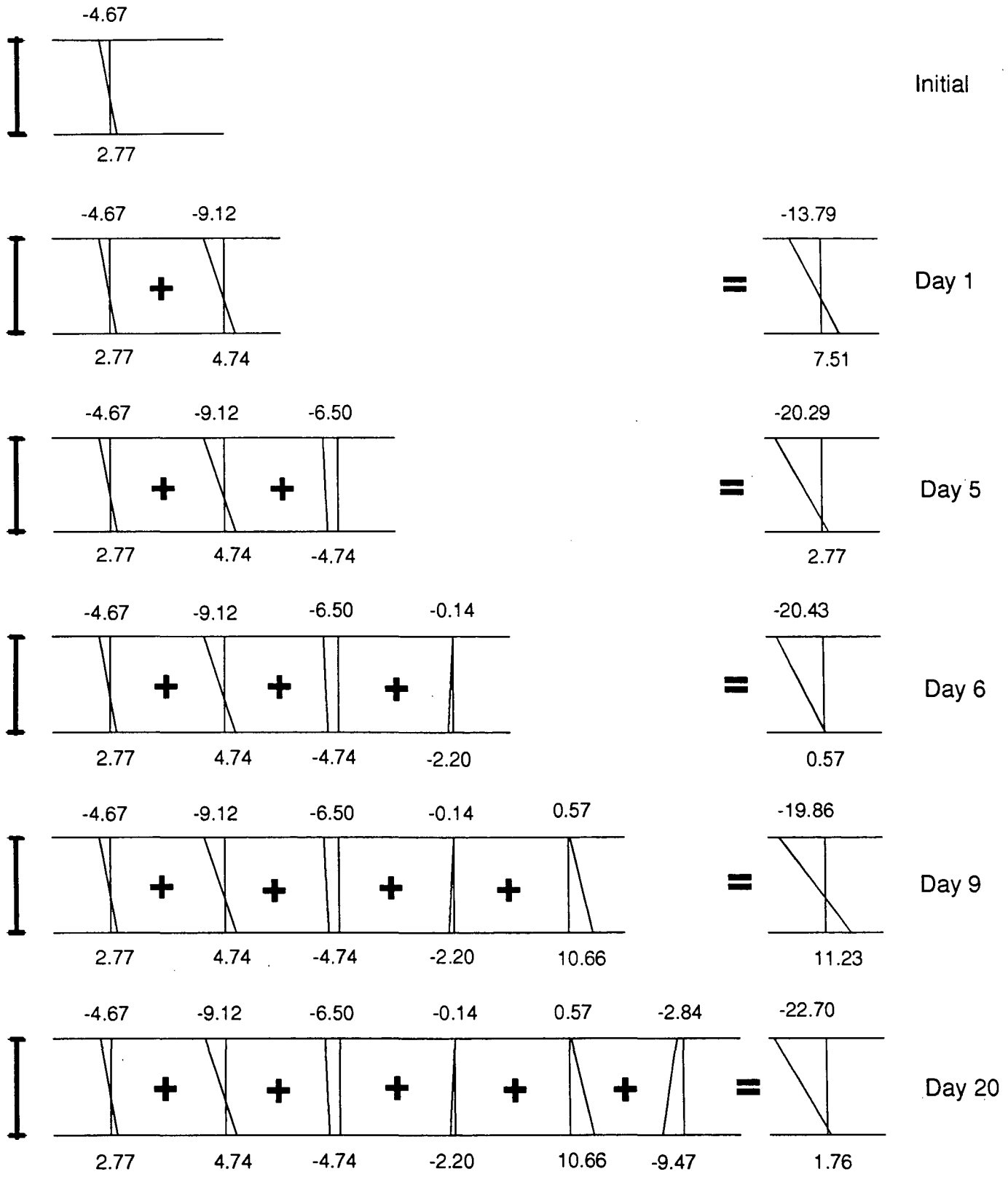

All stresses in ksi

Fig. 4.2 Stress Distributions and Increments of Stresses - Location 432

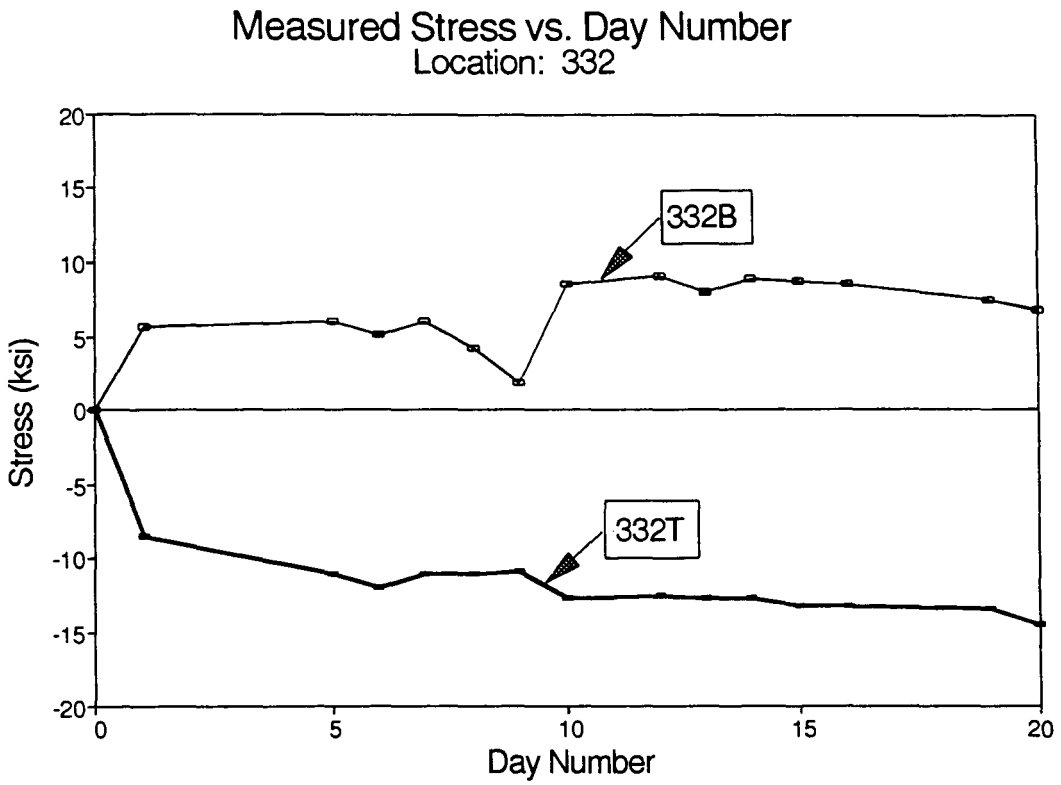

Day Number	Location 332T Measured (ksi)	Location 332B Measured (ksi)
1	-8.485	5.710
5	-11.075	6.080
6	-11.915	5.170
7	-10.990	6.080
8	-10.920	4.230
9	-10.765	1.810
10	-12.590	8.570
12	-12.505	9.070
13	-12.740	7.960
14	-12.705	8.840
15	-13.210	8.630
16	-13.215	8.570
19	-13.470	7.460
20	-14.565	6.750

Fig. 4.3 Variation of Stresses in Girder Flanges during Construction at Location 332

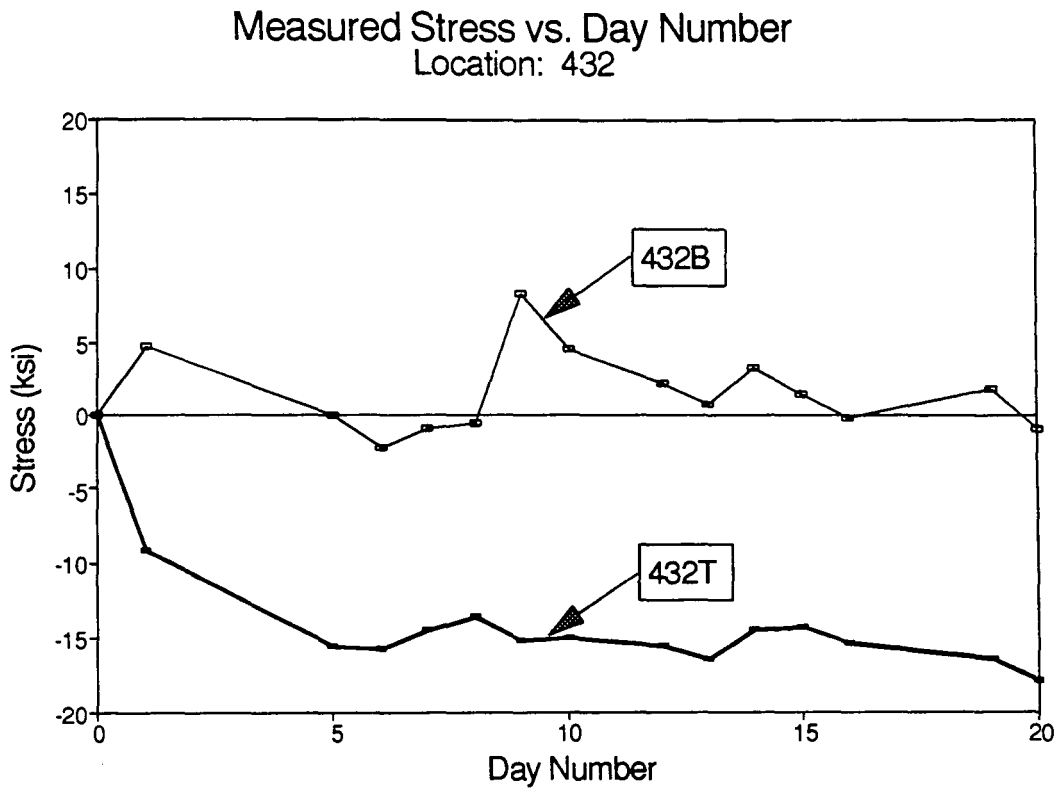

Day Number	Location 432T Measured (ksi)	Location 432B Measured (ksi)
1	-9.120	4.740
5	-15.620	0.000
6	-15.760	-2.200
7	-14.510	-0.890
8	-13.575	-0.510
9	-15.190	8.460
10	-15.100	4.570
12	-15.535	2.120
13	-16.510	0.640
14	-14.520	3.220
15	-14.275	1.400
16	-15.355	-0.210
19	-16.415	1.820
20	-18.025	-1.010

Fig. 4.4 Variation of Stresses in Girder Flanges during Construction at Location 432

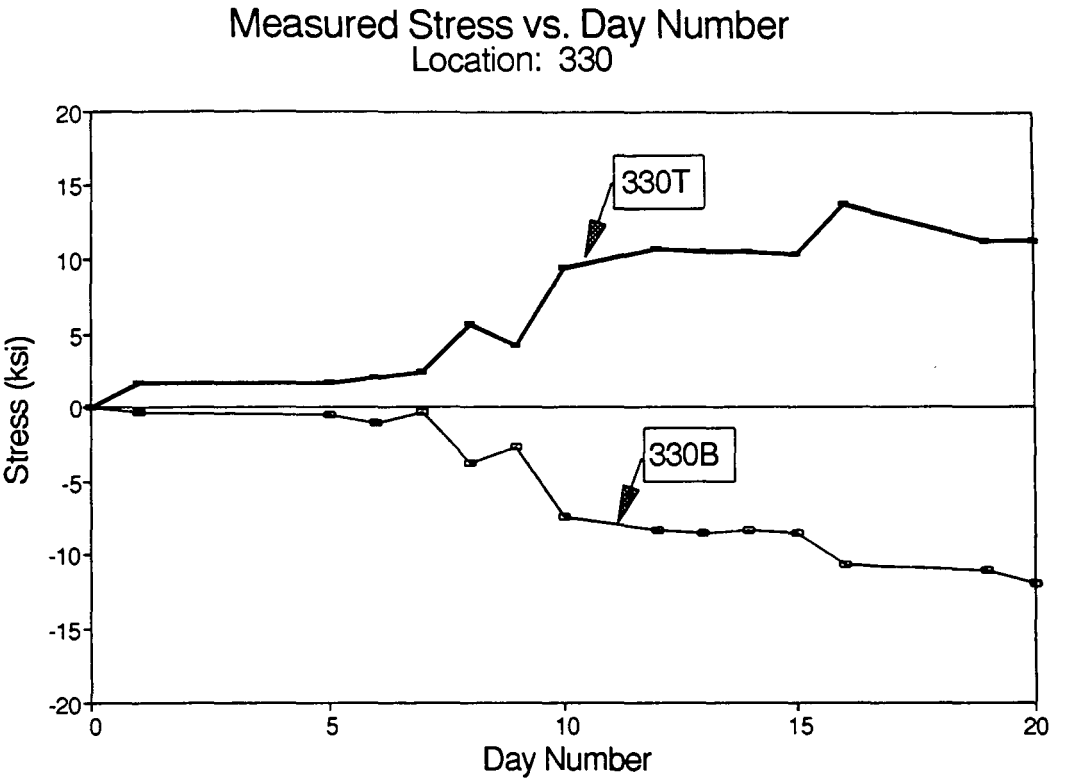

Day Number	Location 330T Measured (ksi)	Location 330B Measured (ksi)
1	1.600	-0.280
5	1.695	-0.570
6	2.045	-1.100
7	2.295	-0.310
8	5.590	-3.710
9	4.160	-2.700
10	9.505	-7.380
12	10.730	-8.320
13	10.465	-8.510
14	10.555	-8.390
15	10.415	-8.450
16	13.810	-10.680
19	11.235	-10.930
20	11.295	-11.940

Fig. 4.5 Variation of Stresses in Girder Flanges during Construction at Location 330

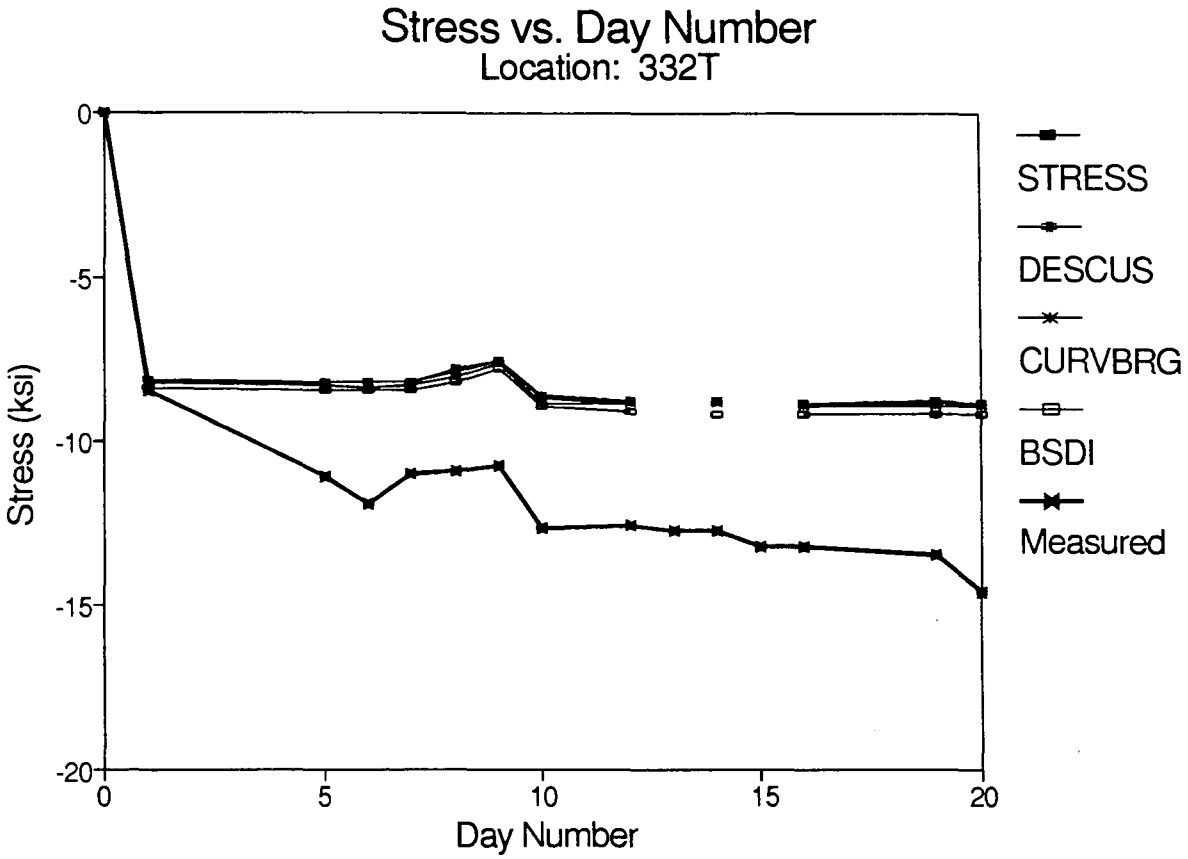

Day Number	Analysis Program				Measured (ksi)
	STRESS (ksi)	DESCUS (ksi)	CURVBRG (ksi)	BSDI (ksi)	
0	0.00	0.00	0.00	0.00	0.000
1	-8.15	-8.09	-8.26	-8.37	-8.485
5	-8.23	-8.16	-8.32	-8.45	-11.075
6	-8.26	-8.19	-8.35	-8.48	-11.915
7	-8.23	-8.16	-8.32	-8.46	-10.990
8	-7.91	-7.84	-8.00	-8.17	-10.920
9	-7.57	-7.50	-7.66	-7.79	-10.765
10	-8.69	-8.64	-8.81	-8.99	-12.590
12	-8.82	-8.77	-8.91	-9.15	-12.505
13					-12.740
14	-8.84	-8.79	-8.92	-9.16	-12.705
15					-13.210
16	-8.87	-8.82	-8.96	-9.21	-13.215
19	-8.84	-8.79	-8.93	-9.16	-13.470
20	-8.88	-8.85	-8.99	-9.19	-14.565

Fig. 4.6 Computed and Measured Stress Variation during Construction - Location 332T

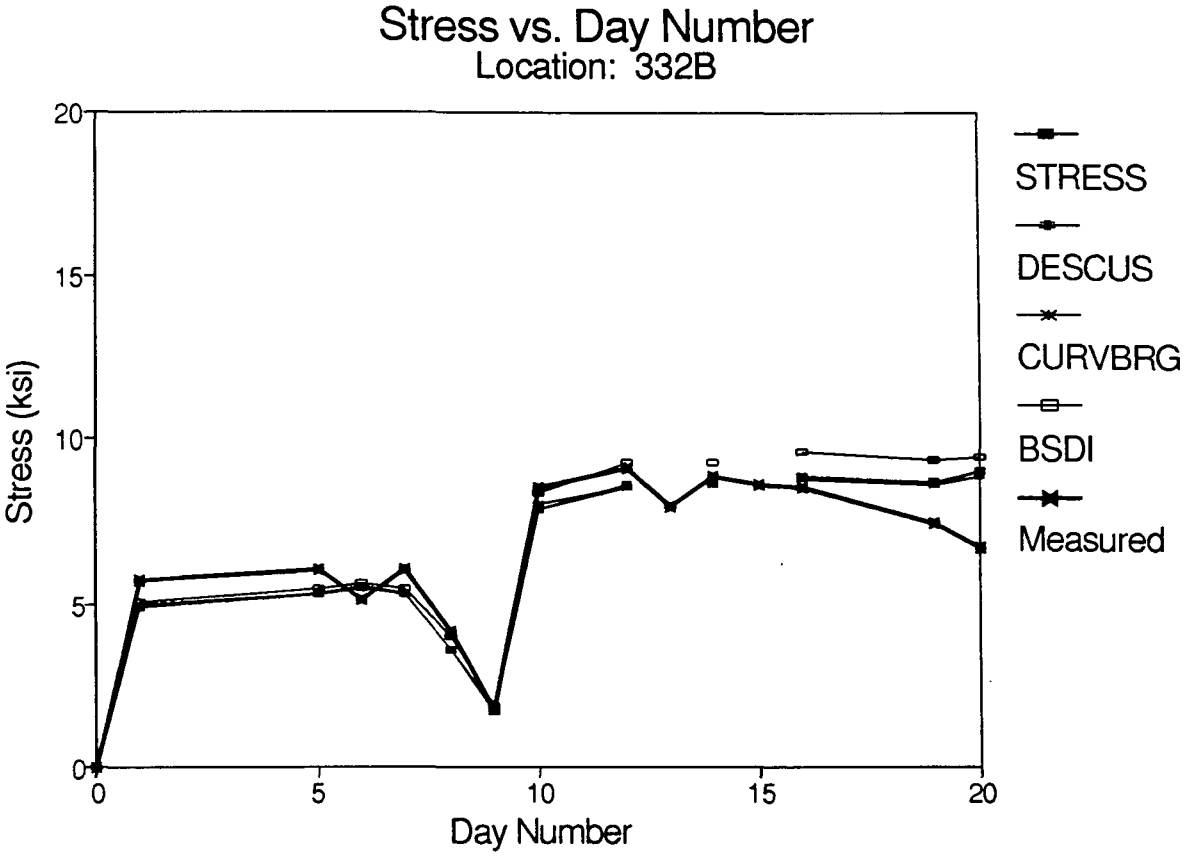

Day Number	Analysis Program				Measured (ksi)
	STRESS (ksi)	DESCUS (ksi)	CURVBRG (ksi)	BSDI (ksi)	
0	0.00	0.00	0.00	0.00	0.000
1	4.94	4.90	5.00	5.07	5.710
5	5.35	5.30	5.35	5.48	6.080
6	5.54	5.48	5.53	5.64	5.170
7	5.36	5.30	5.35	5.51	6.080
8	3.63	3.58	3.65	3.97	4.230
9	1.80	1.75	1.83	1.91	1.810
10	7.82	7.87	8.02	8.38	8.570
12	8.55	8.59	8.55	9.24	9.070
13					7.960
14	8.63	8.67	8.61	9.28	8.840
15					8.630
16	8.79	8.83	8.82	9.58	8.570
19	8.63	8.67	8.64	9.31	7.460
20	8.87	8.97	8.97	9.45	6.750

Fig. 4.7 Computed and Measured Stress Variation during Construction - Location 332B

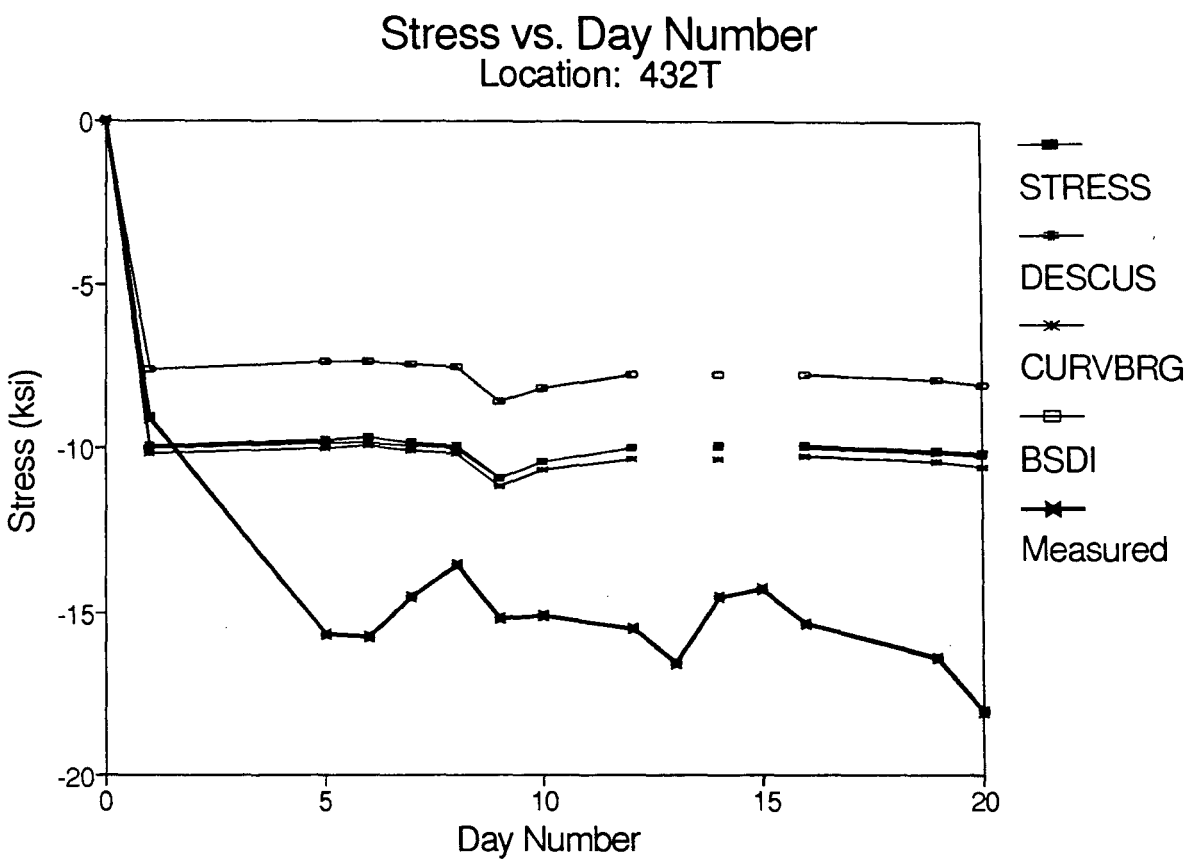

Day Number	Analysis Program				Measured (ksi)
	STRESS (ksi)	DESCUS (ksi)	CURVBRG (ksi)	BSDI (ksi)	
0	0.00	0.00	0.00	0.00	0.000
1	-10.03	-9.95	-10.14	-7.58	-9.120
5	-9.83	-9.75	-9.97	-7.39	-15.620
6	-9.81	-9.73	-9.95	-7.38	-15.760
7	-9.90	-9.82	-10.04	-7.44	-14.510
8	-10.00	-9.92	-10.14	-7.54	-13.575
9	-10.95	-10.89	-11.12	-8.65	-15.190
10	-10.46	-10.40	-10.63	-8.19	-15.100
12	-10.03	-9.97	-10.31	-7.79	-15.535
13					-16.510
14	-10.02	-9.96	-10.31	-7.79	-14.520
15					-14.275
16	-10.01	-9.95	-10.30	-7.77	-15.355
19	-10.13	-10.07	-10.43	-7.94	-16.415
20	-10.26	-10.20	-10.57	-8.10	-18.025

Fig. 4.8 Computed and Measured Stress Variation during Construction - Location 432T

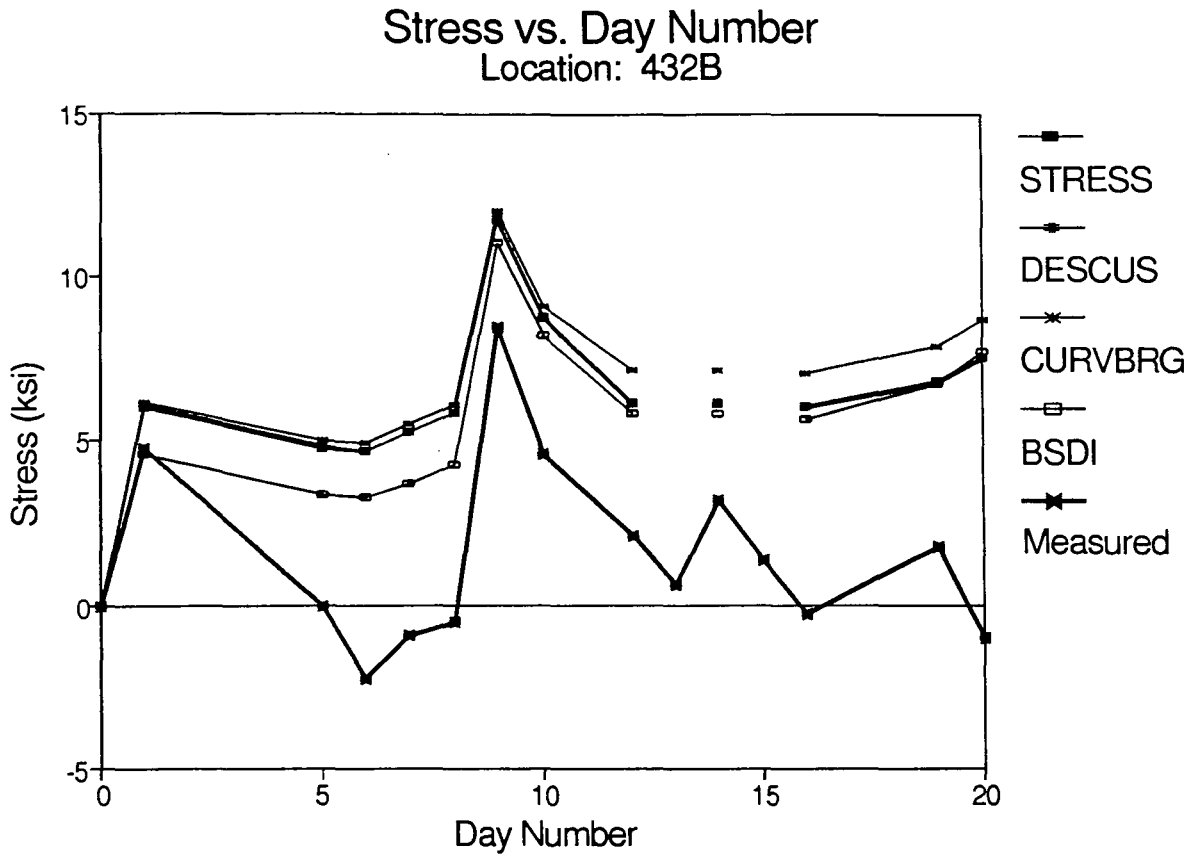

Day Number	Analysis Program				Measured (ksi)
	STRESS (ksi)	DESCUS (ksi)	CURVBRG (ksi)	BSDI (ksi)	
0	0.00	0.00	0.00	0.00	0.000
1	6.01	5.97	6.08	4.55	4.740
5	4.79	4.76	5.02	3.34	0.000
6	4.68	4.65	4.92	3.28	-2.200
7	5.23	5.20	5.46	3.66	-0.890
8	5.84	5.81	6.06	4.25	-0.510
9	11.68	11.74	12.06	11.07	8.460
10	8.69	8.76	9.09	8.23	4.570
12	6.05	6.14	7.13	5.81	2.120
13					0.640
14	6.01	6.10	7.10	5.80	3.220
15					1.400
16	5.95	6.04	7.01	5.68	-0.210
19	6.71	6.80	7.83	6.69	1.820
20	7.50	7.57	8.71	7.69	-1.010

Fig. 4.9 Computed and Measured Stress Variation during Construction - Location 432B

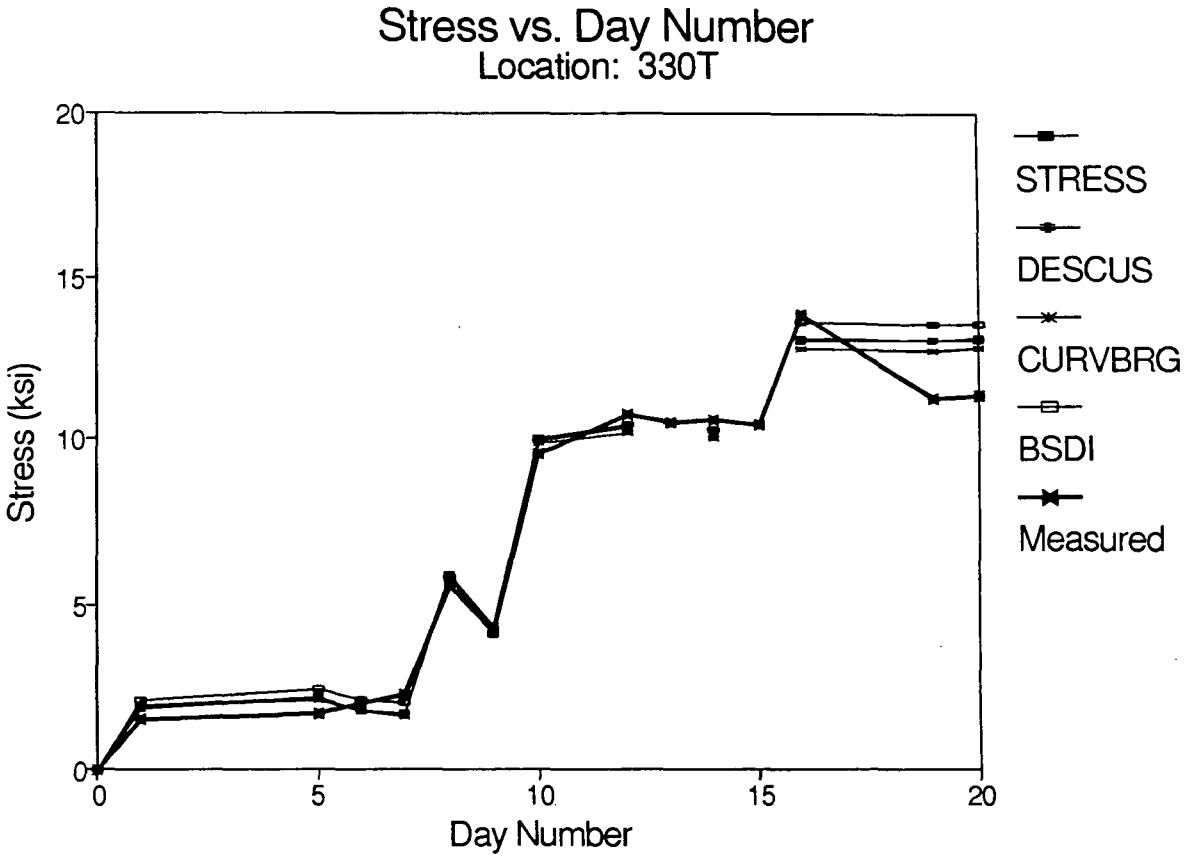

Day Number	Analysis Program				Measured (ksi)
	STRESS (ksi)	DESCUS (ksi)	CURVBRG (ksi)	BSDI (ksi)	
0	0.00	0.00	0.00	0.00	0.000
1	1.94	1.92	1.93	2.18	1.600
5	2.22	2.20	2.17	2.49	1.695
6	1.84	1.83	1.81	2.12	2.045
7	1.71	1.70	1.69	2.02	2.295
8	5.91	5.84	5.86	5.80	5.590
9	4.36	4.30	4.35	4.07	4.160
10	9.99	9.91	9.87	9.93	9.505
12	10.37	10.29	10.14	10.35	10.730
13					10.465
14	10.21	10.13	10.02	10.26	10.555
15					10.415
16	13.09	13.03	12.76	13.57	13.810
19	13.06	13.00	12.73	13.52	11.235
20	13.09	13.04	12.78	13.53	11.295

Fig. 4.10 Computed and Measured Stress Variation during Construction - Location 330T

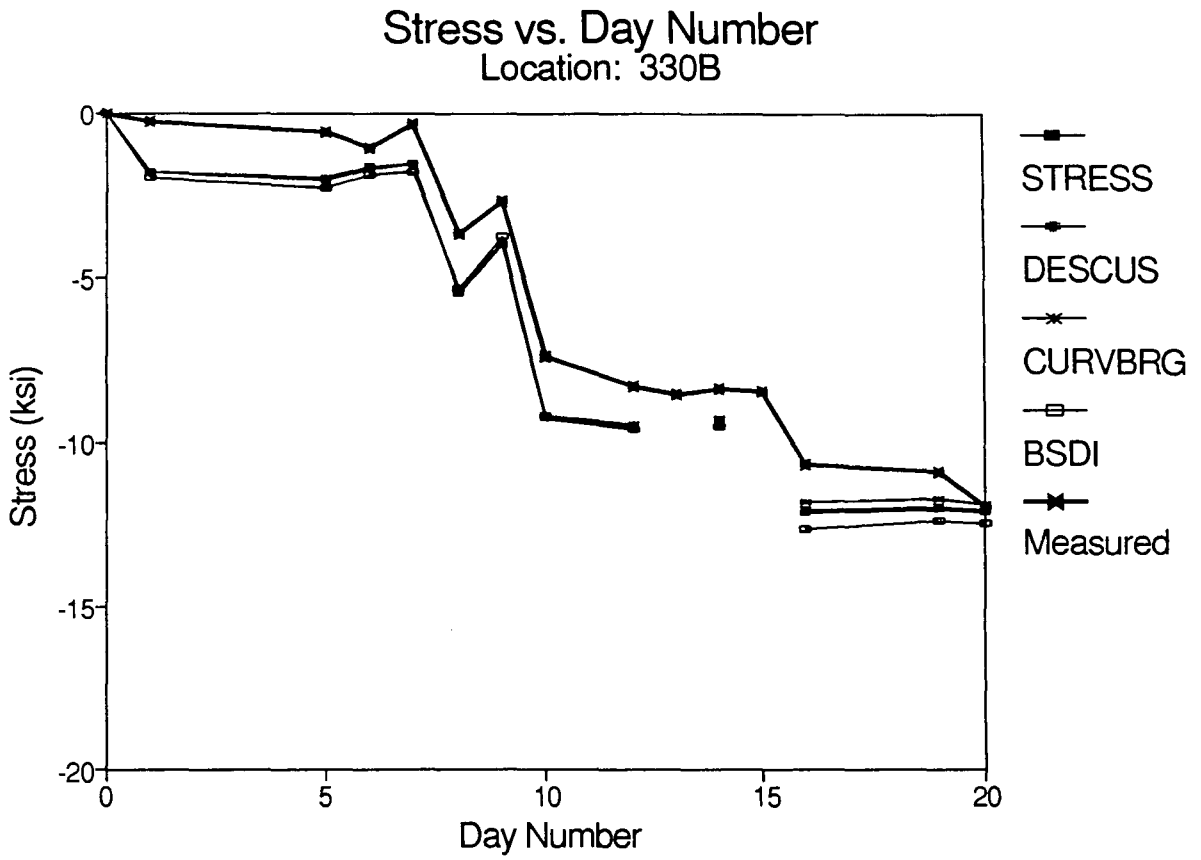

Day Number	Analysis Program				Measured (ksi)
	STRESS (ksi)	DESCUS (ksi)	CURVBRG (ksi)	BSDI (ksi)	
0	0.00	0.00	0.00	0.00	0.000
1	-1.80	-1.78	-1.79	-2.02	-0.280
5	-2.06	-2.04	-2.01	-2.31	-0.570
6	-1.71	-1.69	-1.68	-1.96	-1.100
7	-1.59	-1.57	-1.57	-1.87	-0.310
8	-5.49	-5.41	-5.44	-5.38	-3.710
9	-4.05	-3.98	-4.04	-3.77	-2.700
10	-9.27	-9.18	-9.16	-9.20	-7.380
12	-9.62	-9.53	-9.41	-9.59	-8.320
13					-8.510
14	-9.47	-9.38	-9.30	-9.51	-8.390
15					-8.450
16	-12.14	-12.07	-11.84	-12.58	-10.680
19	-12.03	-11.96	-11.72	-12.38	-10.930
20	-12.14	-12.11	-11.90	-12.44	-11.940

Fig. 4.11 Computed and Measured Stress Variation during Construction - Location 330B

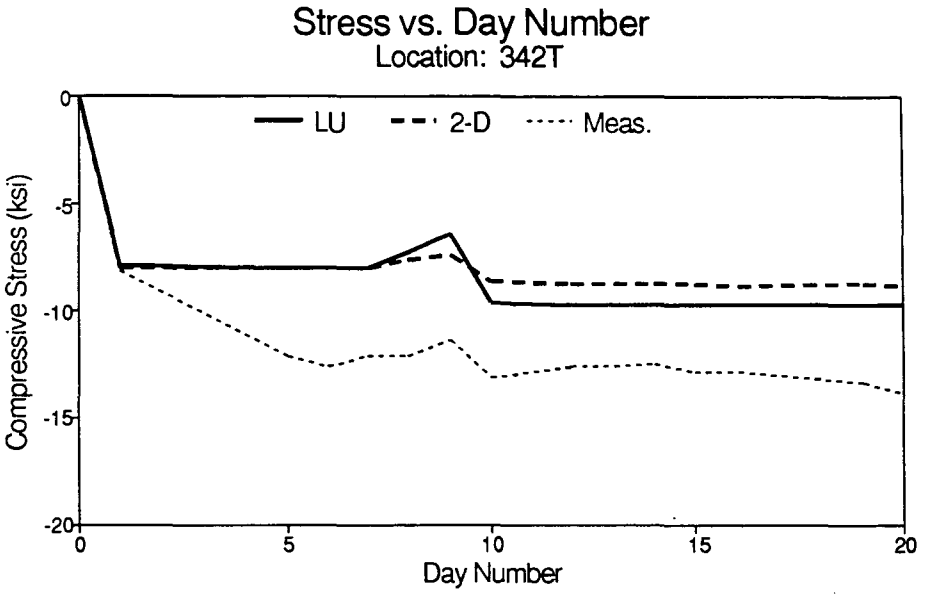

Day Number	LU (ksi)	2-D (ksi)	Measured (ksi)
1	-7.913	-7.97	-8.160
5	-8.015	-8.05	-12.200
6	-8.101	-8.09	-12.665
7	-8.054	-8.05	-12.200
8	-7.204	-7.71	-12.115
9	-6.426	-7.35	-11.400
10	-9.696	-8.62	-13.135
12	-9.717	-8.76	-12.700
13	-9.717		-12.615
14	-9.732	-8.78	-12.580
15	-9.732		-12.875
16	-9.755	-8.82	-12.855
19	-9.735	-8.79	-13.365
20	-9.795	-8.84	-13.880

Fig. 4.12 Comparison of Stresses at Location 342T (Shrinkage Excluded)

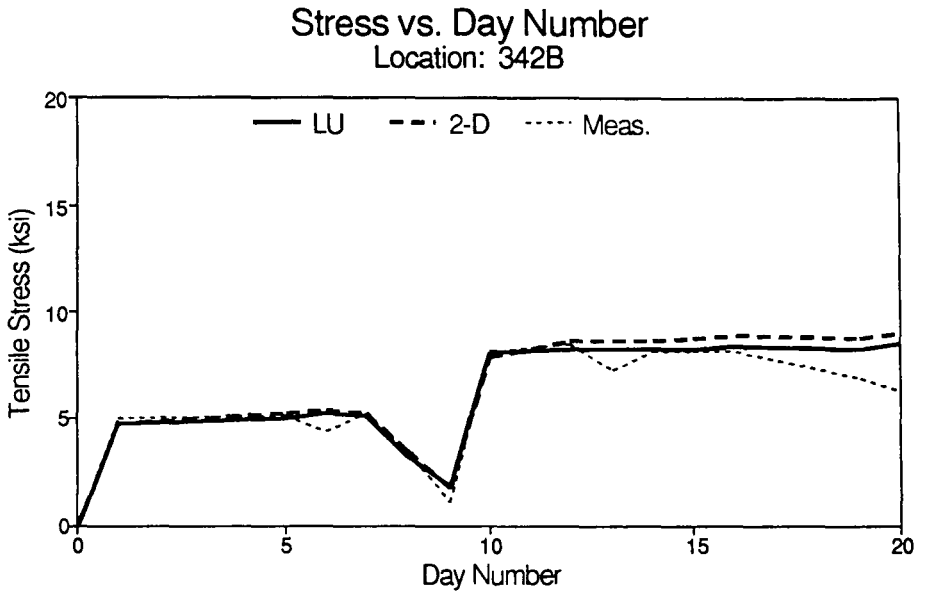

Day Number	LU (ksi)	2-D (ksi)	Measured (ksi)
1	4.768	4.73	4.940
5	4.945	5.12	5.070
6	5.128	5.30	4.340
7	5.044	5.12	5.170
8	3.270	3.41	3.400
9	1.848	1.63	1.100
10	8.069	7.89	8.070
12	8.163	8.59	8.400
13	8.164		7.240
14	8.232	8.67	8.100
15	8.232		8.140
16	8.330	8.85	8.040
19	8.244	8.69	6.800
20	8.525	8.95	6.200

Fig. 4.13 Comparison of Stresses at Location 342B (Shrinkage Excluded)

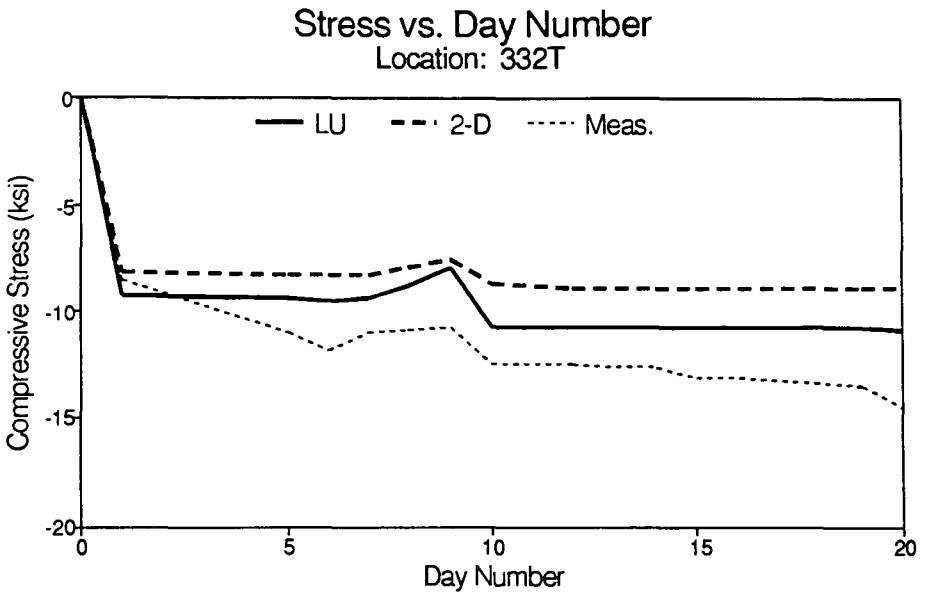

Day Number	LU (ksi)	2-D (ksi)	Measured (ksi)
1	-9.303	-8.15	-8.485
5	-9.417	-8.23	-11.075
6	-9.489	-8.26	-11.915
7	-9.440	-8.23	-10.990
8	-8.733	-7.91	-10.920
9	-7.947	-7.57	-10.765
10	-10.805	-8.69	-12.590
12	-10.826	-8.82	-12.505
13	-10.826		-12.740
14	-10.839	-8.84	-12.705
15	-10.839		-13.210
16	-10.852	-8.87	-13.215
19	-10.834	-8.84	-13.470
20	-10.880	-8.88	-14.565

Fig. 4.14 Comparison of Stresses at Location 332T (Shrinkage Excluded)

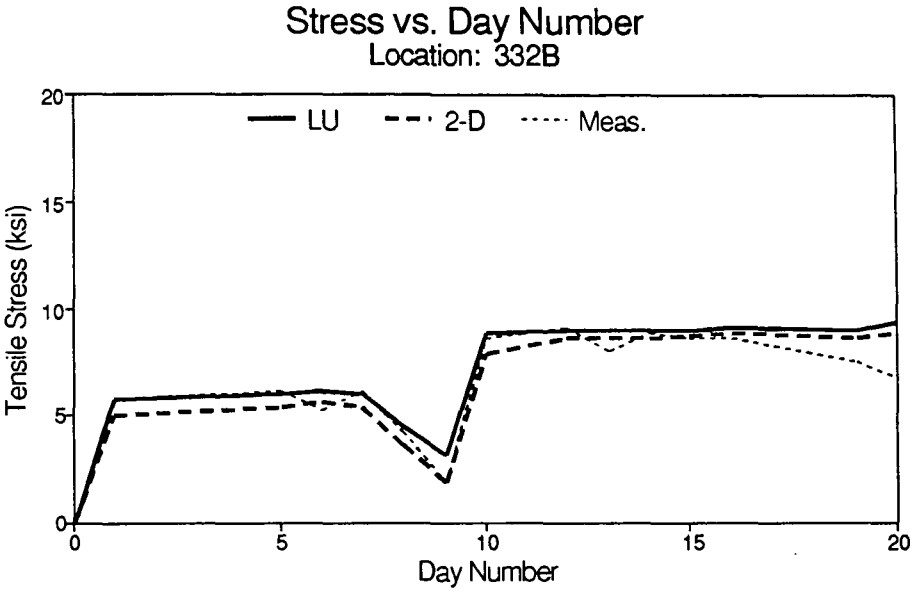

Day Number	LU (ksi)	2-D (ksi)	Measured (ksi)
1	5.721	4.94	5.710
5	5.924	5.35	6.080
6	6.078	5.54	5.170
7	5.992	5.36	6.080
8	4.409	3.63	4.230
9	3.036	1.80	1.810
10	8.854	7.82	8.570
12	8.957	8.55	9.070
13	8.958		7.960
14	9.023	8.63	8.840
15	9.024		8.630
16	9.097	8.79	8.570
19	9.005	8.63	7.460
20	9.356	8.87	6.750

Fig. 4.15 Comparison of Stresses at Location 332B (Shrinkage Excluded)

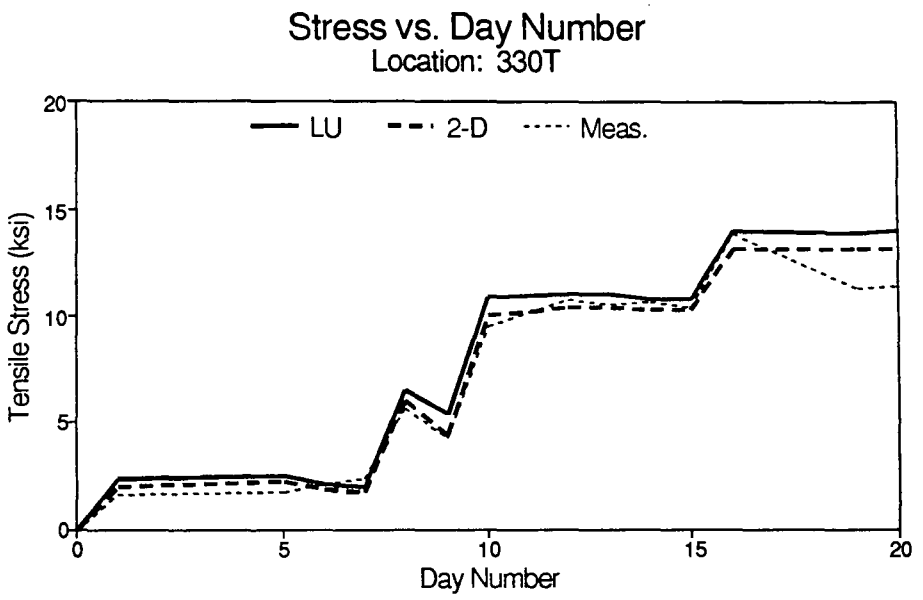

Day Number	LU (ksi)	2-D (ksi)	Measured (ksi)
1	2.328	1.94	1.600
5	2.470	2.22	1.695
6	2.019	1.84	2.045
7	1.955	1.71	2.295
8	6.539	5.91	5.590
9	5.365	4.36	4.160
10	10.858	9.99	9.505
12	10.916	10.37	10.730
13	10.916		10.465
14	10.767	10.21	10.555
15	10.767		10.415
16	13.936	13.09	13.810
19	13.910	13.06	11.235
20	13.969	13.09	11.295

Fig. 4.16 Comparison of Stresses at Location 330T (Shrinkage Excluded)

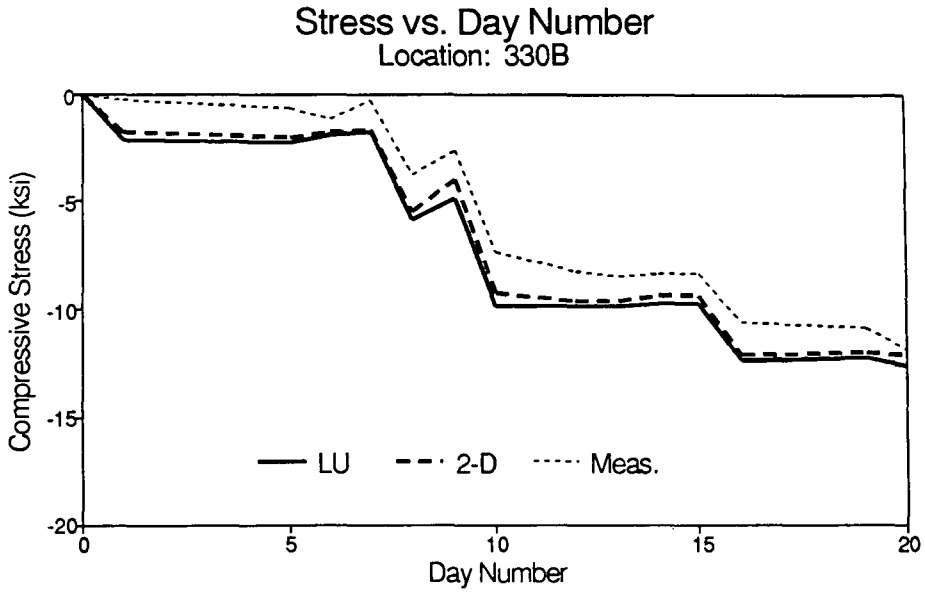

Day Number	LU (ksi)	2-D (ksi)	Measured (ksi)
1	-2.110	-1.80	-0.280
5	-2.239	-2.06	-0.570
6	-1.828	-1.71	-1.100
7	-1.771	-1.59	-0.310
8	-5.966	-5.49	-3.710
9	-4.896	-4.05	-2.700
10	-9.879	-9.27	-7.380
12	-9.931	-9.62	-8.320
13	-9.931		-8.510
14	-9.794	-9.47	-8.390
15	-9.795		-8.450
16	-12.445	-12.14	-10.680
19	-12.369	-12.03	-10.930
20	-12.636	-12.14	-11.940

Fig. 4.17 Comparison of Stresses at Location 330B (Shrinkage Excluded)

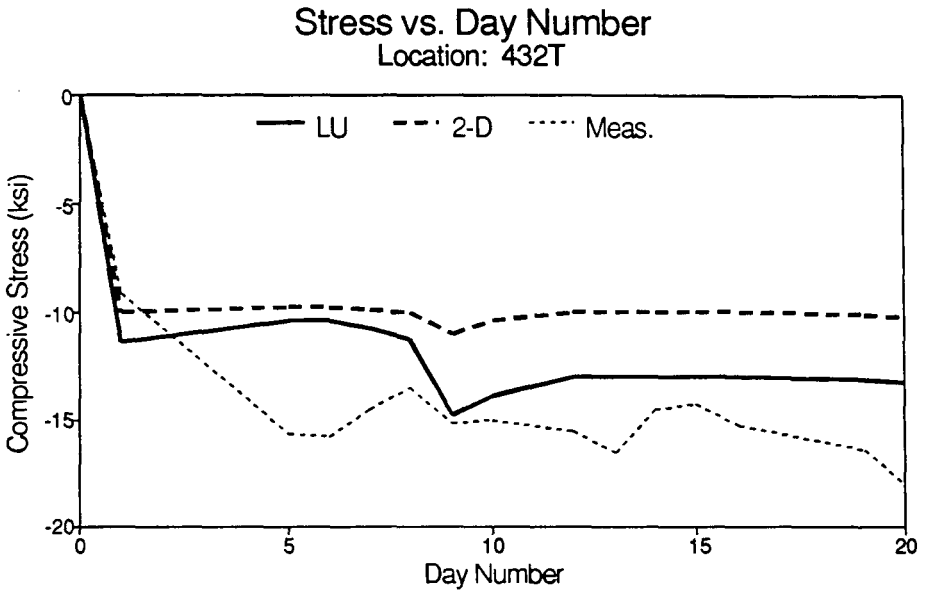

Day Number	LU (ksi)	2-D (ksi)	Measured (ksi)
1	-11.404	-10.03	-9.120
5	-10.446	-9.83	-15.620
6	-10.362	-9.81	-15.760
7	-10.806	-9.90	-14.510
8	-11.239	-10.00	-13.575
9	-14.808	-10.95	-15.190
10	-13.911	-10.46	-15.100
12	-13.020	-10.03	-15.535
13	-13.014		-16.510
14	-13.008	-10.02	-14.520
15	-13.004		-14.275
16	-12.998	-10.01	-15.355
19	-13.184	-10.13	-16.415
20	-13.300	-10.26	-18.025

Fig. 4.18 Comparison of Stresses at Location 432T (Shrinkage Excluded)

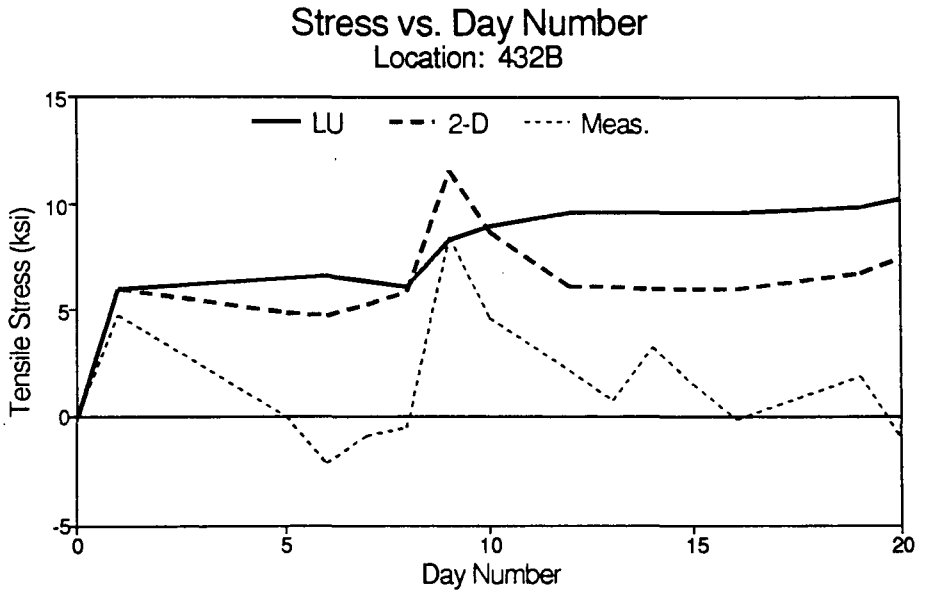

Day Number	LU (ksi)	2-D (ksi)	Measured (ksi)
1	5.950	6.01	4.740
5	6.500	4.79	0.000
6	6.532	4.68	-2.200
7	6.357	5.23	-0.890
8	6.183	5.84	-0.510
9	8.336	11.68	8.460
10	8.950	8.69	4.570
12	9.552	6.05	2.120
13	9.555		0.640
14	9.559	6.01	3.220
15	9.562		1.400
16	9.565	5.95	-0.210
19	9.919	6.71	1.820
20	10.273	7.50	-1.010

Fig. 4.19 Comparison of Stresses at Location 432B (Shrinkage Excluded)

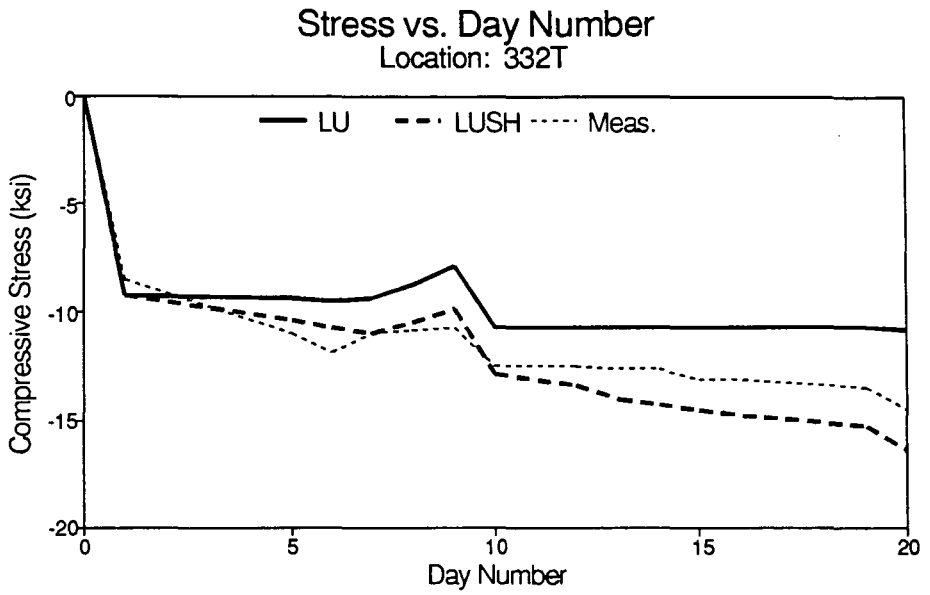

Day Number	LU (ksi)	LUSH (ksi)	Measured (ksi)
1	-9.303	-9.303	-8.485
5	-9.417	-10.473	-11.075
6	-9.489	-10.811	-11.915
7	-9.440	-11.029	-10.990
8	-8.733	-10.589	-10.920
9	-7.947	-9.948	-10.765
10	-10.805	-12.967	-12.590
12	-10.826	-13.414	-12.505
13	-10.826	-14.004	-12.740
14	-10.839	-14.257	-12.705
15	-10.839	-14.508	-13.210
16	-10.852	-14.756	-13.215
19	-10.834	-15.218	-13.470
20	-10.880	-16.466	-14.565

Fig 4.20 Comparison of Stresses at Location 332T (Shrinkage Included)

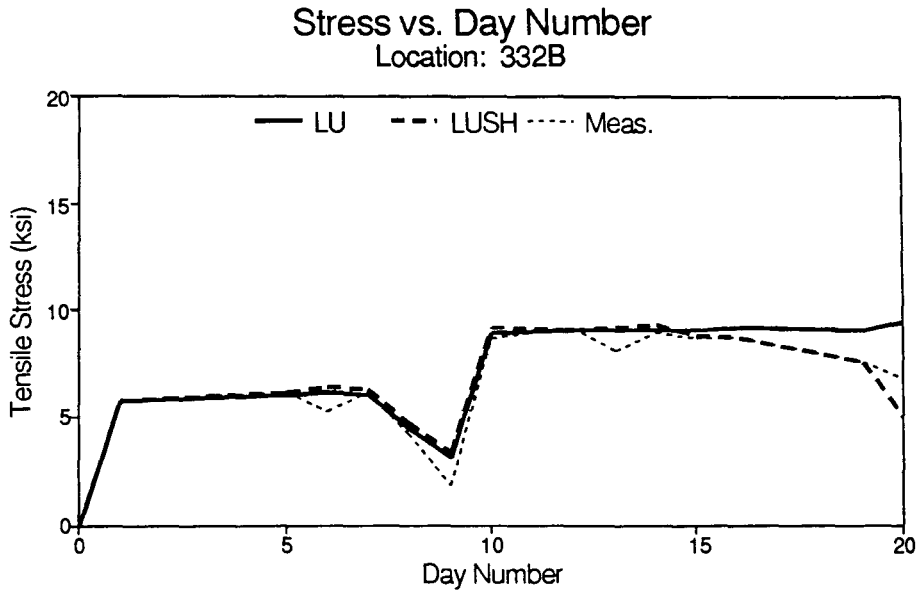

Day Number	LU (ksi)	LUSH (ksi)	Measured (ksi)
1	5.721	5.721	5.710
5	5.924	6.071	6.080
6	6.078	6.263	5.170
7	5.992	6.216	6.080
8	4.409	4.672	4.230
9	3.036	3.307	1.810
10	8.854	9.078	8.570
12	8.957	8.971	9.070
13	8.958	9.112	7.960
14	9.023	9.284	8.840
15	9.024	8.687	8.630
16	9.097	8.670	8.570
19	9.005	7.512	7.460
20	9.356	4.914	6.750

Fig. 4.21 Comparison of Stresses at Location 332B (Shrinkage Included)

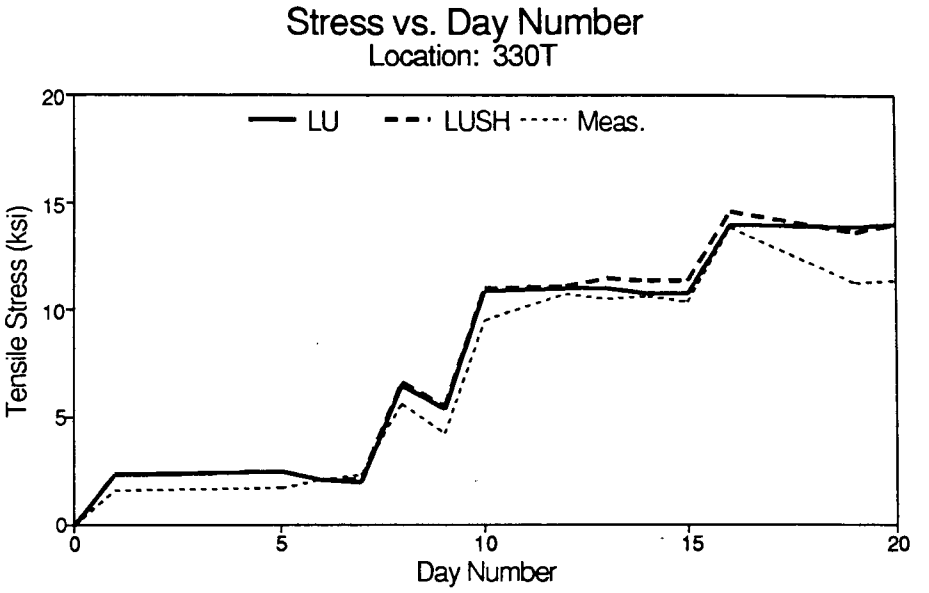

Day Number	LU (ksi)	LUSH (ksi)	Measured (ksi)
1	2.328	2.328	1.600
5	2.470	2.495	1.695
6	2.019	2.051	2.045
7	1.955	1.992	2.295
8	6.539	6.579	5.590
9	5.365	5.433	4.160
10	10.858	10.902	9.505
12	10.916	11.179	10.730
13	10.916	11.422	10.465
14	10.767	11.400	10.555
15	10.767	11.379	10.415
16	13.936	14.621	13.810
19	13.910	13.572	11.235
20	13.969	13.956	11.295

Fig. 4.22 Comparison of Stresses at Location 330T (Shrinkage Included)

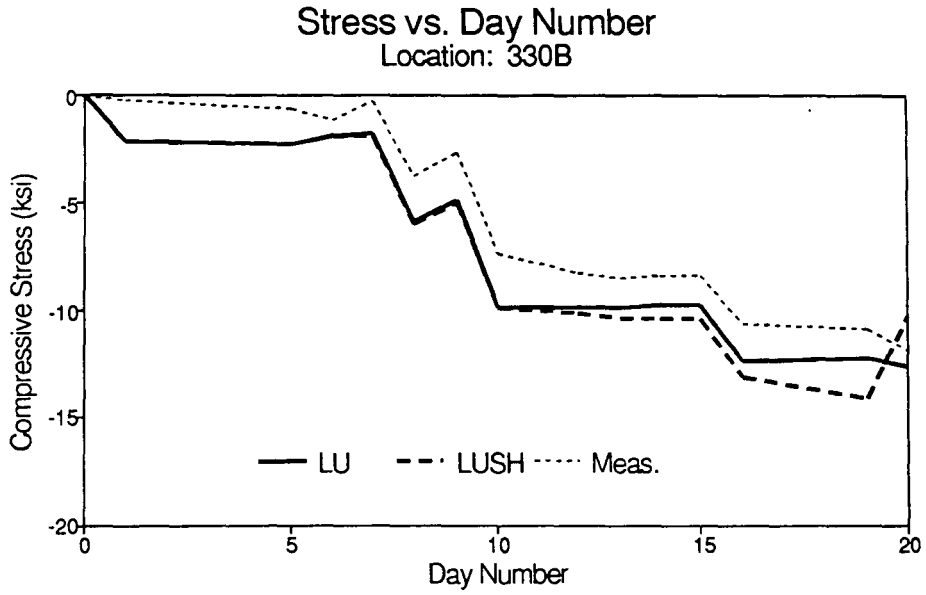

Day Number	LU (ksi)	LUSH (ksi)	Measured (ksi)
1	-2.110	-2.110	-0.280
5	-2.239	-2.263	-0.570
6	-1.828	-1.859	-1.100
7	-1.771	-1.805	-0.310
8	-5.966	-6.005	-3.710
9	-4.896	-4.959	-2.700
10	-9.879	-9.920	-7.380
12	-9.931	-10.171	-8.320
13	-9.931	-10.389	-8.510
14	-9.794	-10.367	-8.390
15	-9.795	-10.379	-8.450
16	-12.445	-13.101	-10.680
19	-12.369	-14.204	-10.930
20	-12.636	-10.271	-11.940

Fig. 4.23 Comparison of Stresses at Location 330B (Shrinkage Included)

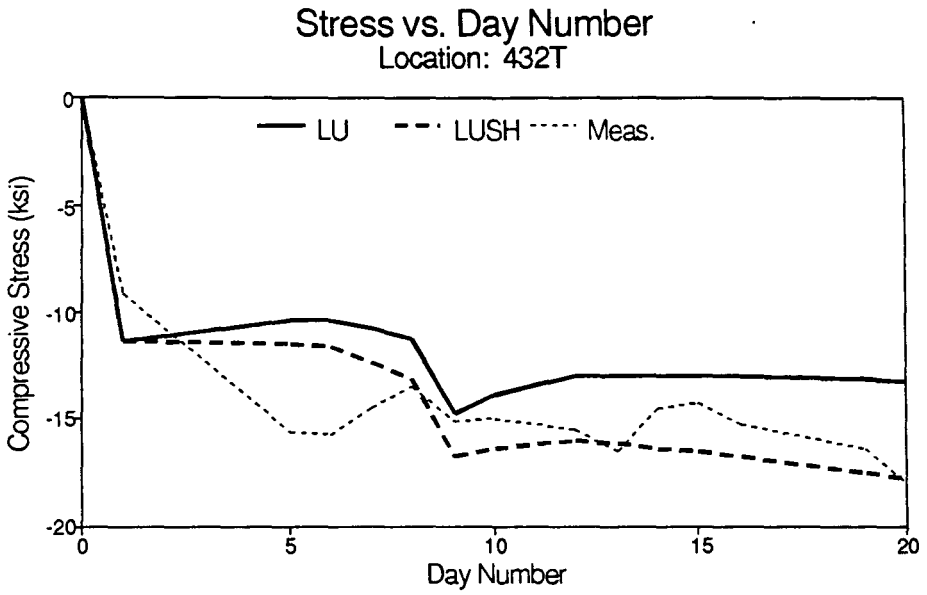

Day Number	LU (ksi)	LUSH (ksi)	Measured (ksi)
1	-11.404	-11.404	-9.120
5	-10.446	-11.521	-15.620
6	-10.362	-11.703	-15.760
7	-10.806	-12.414	-14.510
8	-11.239	-13.117	-13.575
9	-14.808	-16.830	-15.190
10	-13.911	-16.473	-15.100
12	-13.020	-16.025	-15.535
13	-13.014	-16.193	-16.510
14	-13.008	-16.376	-14.520
15	-13.004	-16.554	-14.275
16	-12.998	-16.750	-15.355
19	-13.184	-17.498	-16.415
20	-13.300	-17.726	-18.025

Fig. 4.24 Comparison of Stresses at Location 432T (Shrinkage Included)

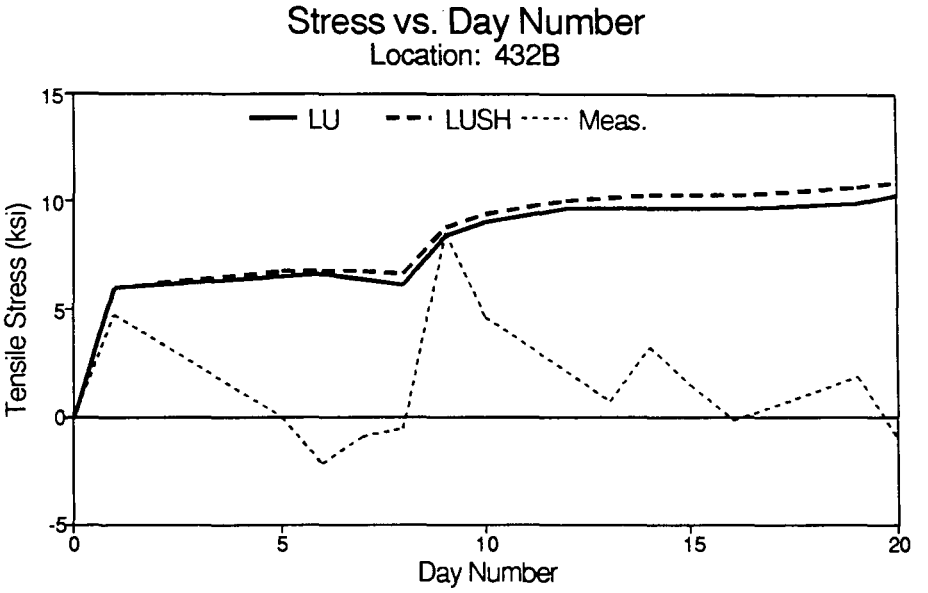

Day Number	LU (ksi)	LUSH (ksi)	Measured (ksi)
1	5.950	5.950	4.740
5	6.500	6.714	0.000
6	6.532	6.800	-2.200
7	6.357	6.679	-0.890
8	6.183	6.558	-0.510
9	8.336	8.737	8.460
10	8.950	9.384	4.570
12	9.552	10.065	2.120
13	9.555	10.128	0.640
14	9.559	10.174	3.220
15	9.562	10.200	1.400
16	9.565	10.245	-0.210
19	9.919	10.653	1.820
20	10.273	10.791	-1.010

Fig. 4.25 Comparison of Stresses at Location 432B (Shrinkage Included)

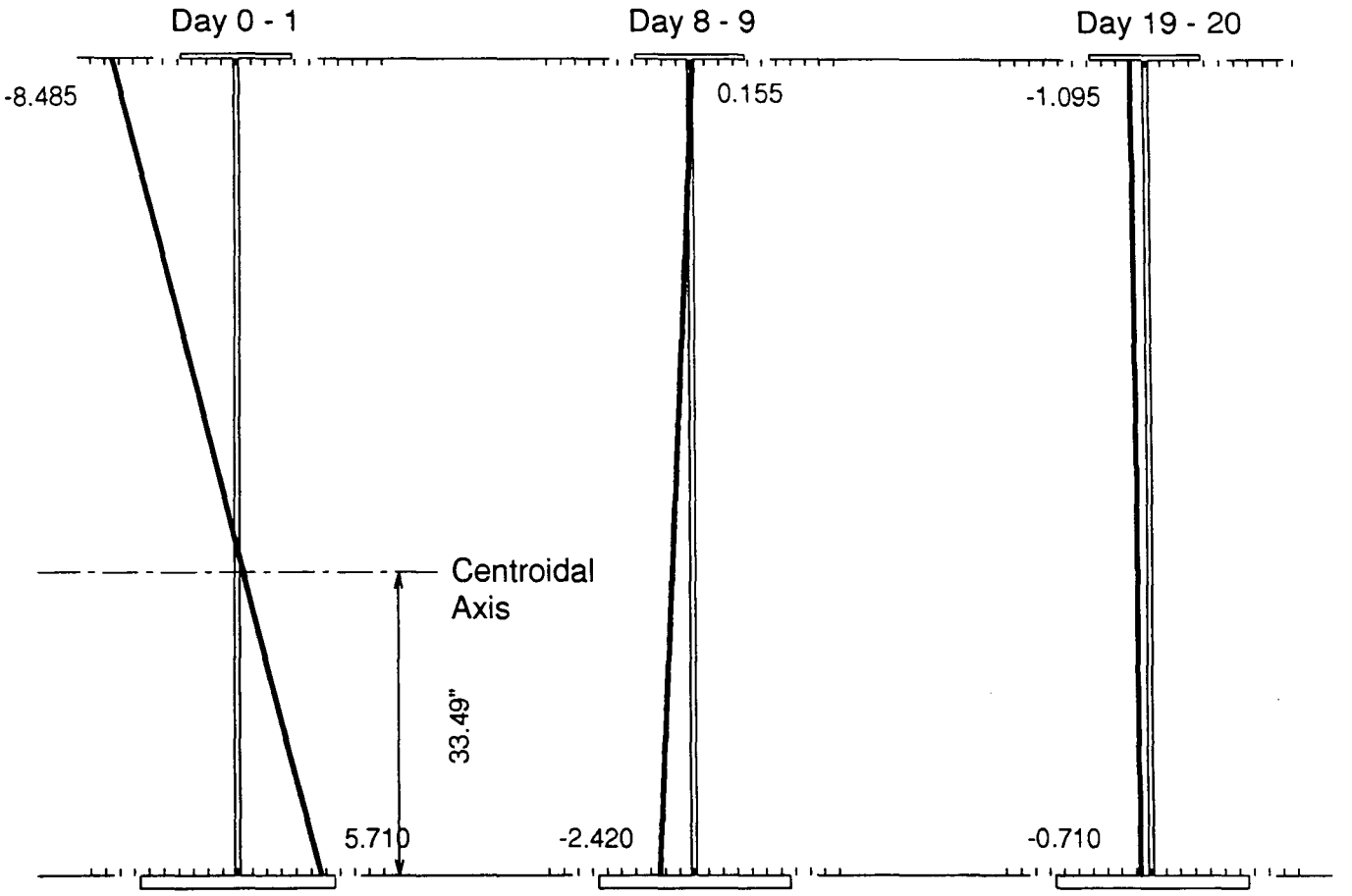

Measured Stress at Location 332				
Day	Top (ksi)	Bottom (ksi)	Top Incremental Difference (ksi)	Bottom Incremental Difference (ksi)
0	0.000	0.000		
1	-8.485	5.710	-8.485	5.710
8	-10.920	4.230		
9	-10.765	1.810	0.155	-2.420
19	-13.470	7.460		
20	-14.565	6.750	-1.095	-0.710

Fig. 4.26 Incremental Stresses in Cross Section 332 from Measurement

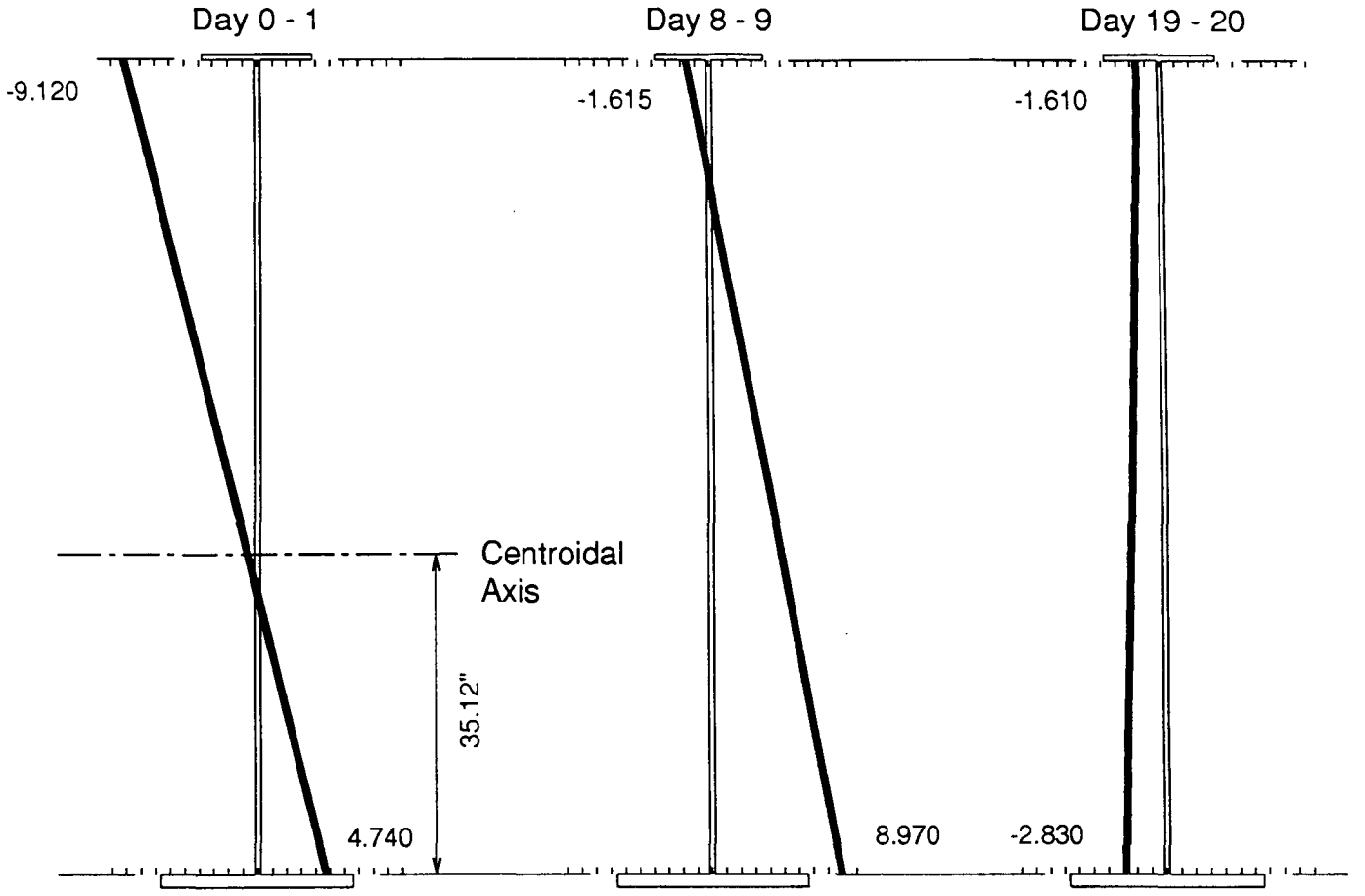

Measured Stress at Location 432				
Day	Top (ksi)	Bottom (ksi)	Top Incremental Difference (ksi)	Bottom Incremental Difference (ksi)
0	0.000	0.000		
1	-9.120	4.740	-9.120	4.740
8	-13.575	-0.510		
9	-15.190	8.460	-1.615	8.970
19	-16.415	1.820		
20	-18.025	-1.010	-1.610	-2.830

Fig. 4.27 Incremental Stresses in Cross Section 432 from Measurement

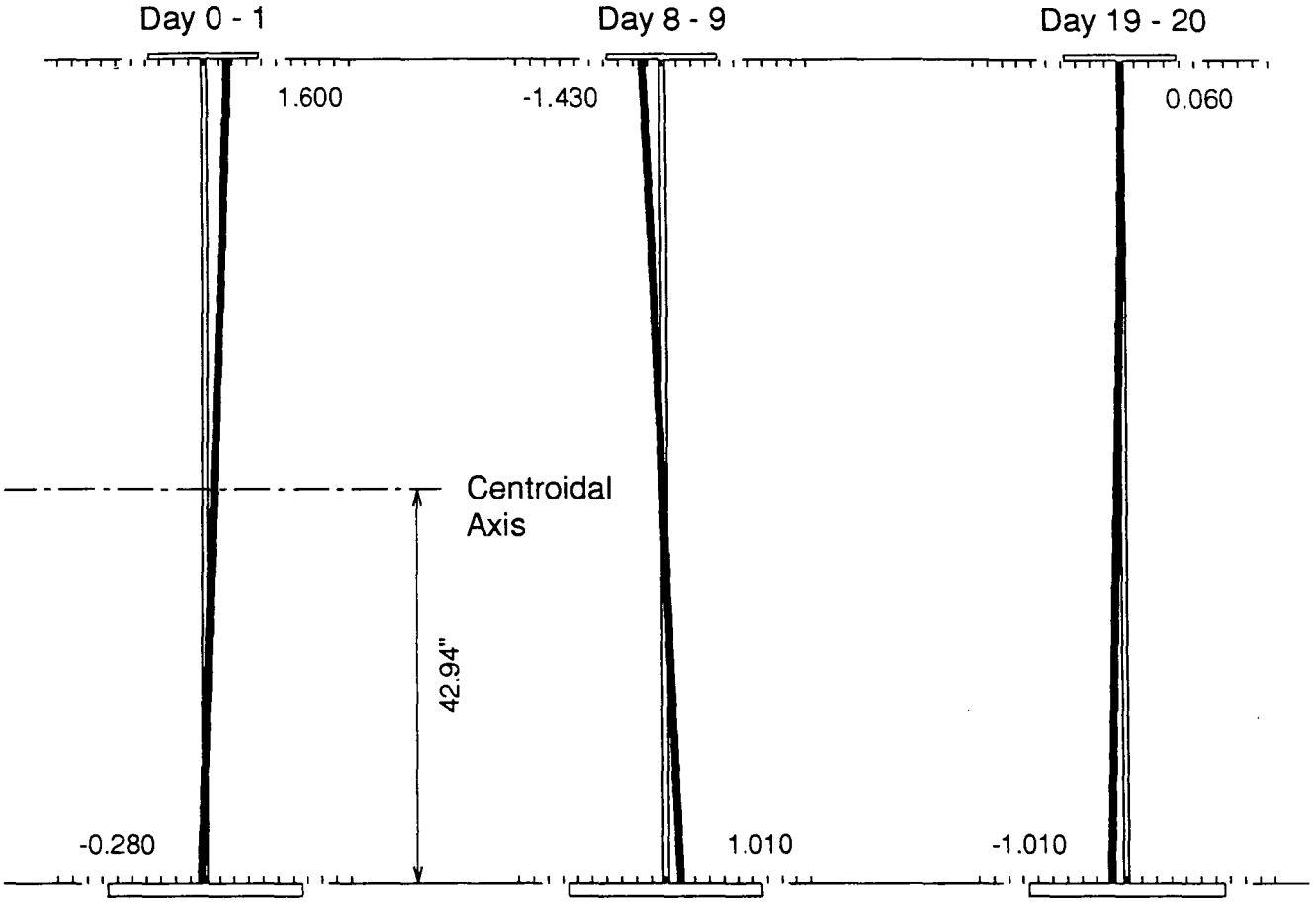

Measured Stress at Location 330				
Day	Top (ksi)	Bottom (ksi)	Top Incremental Difference (ksi)	Bottom Incremental Difference (ksi)
0	0.000	0.000		
1	1.600	-0.280	1.600	-0.280
8	5.590	-3.710		
9	4.160	-2.700	-1.430	1.010
19	11.235	-10.930		
20	11.295	-11.940	0.060	-1.010

Fig. 4.28 Incremental Stresses in Cross Section 330 from Measurement

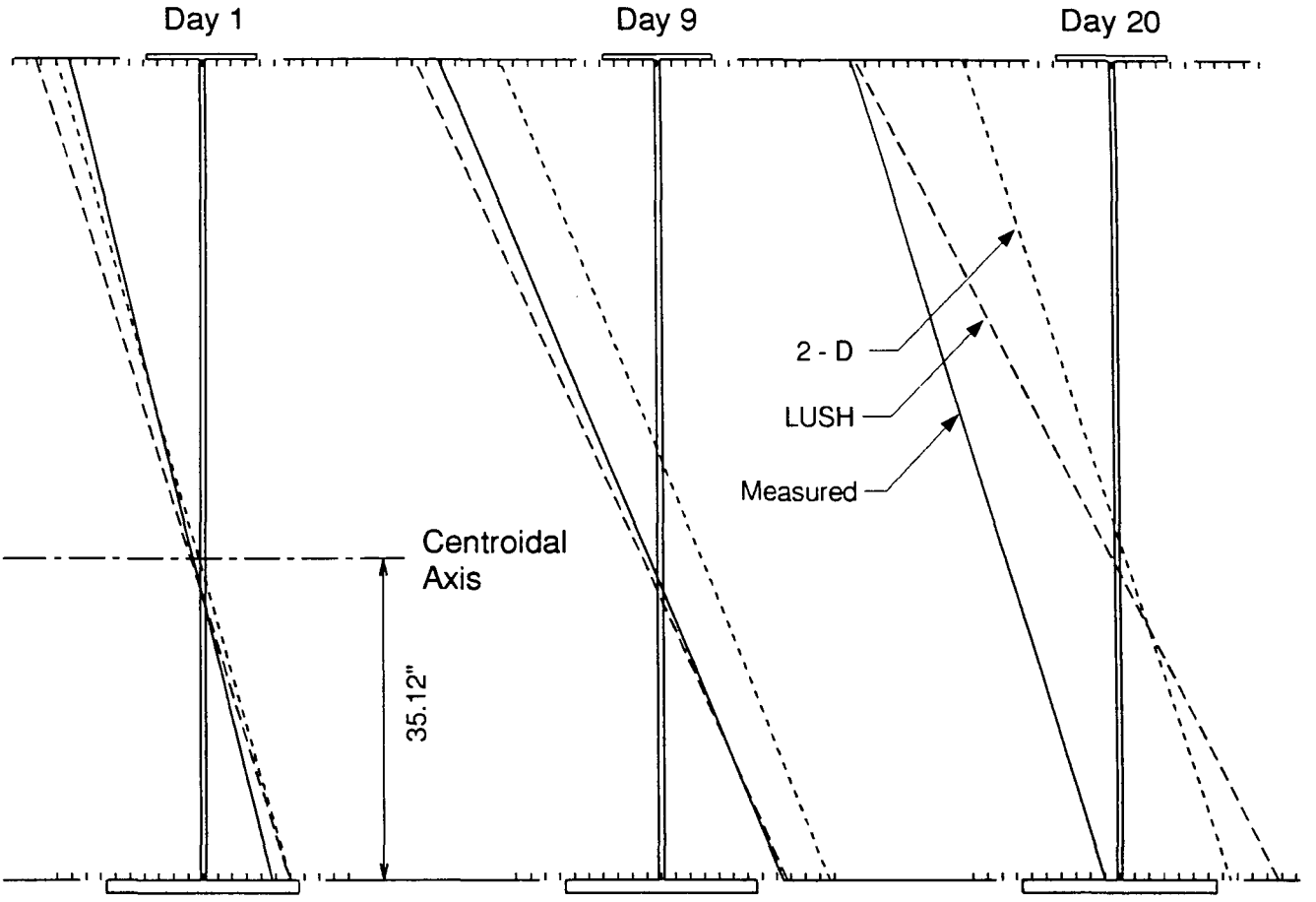

Location 432				
		2-D (ksi)	LUSH (ksi)	Measured (ksi)
Day 1	Top	-10.03	-11.404	-9.120
	Bottom	6.01	5.950	4.740
Day 9	Top	-10.95	-16.830	-15.190
	Bottom	11.68	8.737	8.460
Day 20	Top	-10.26	-17.726	-18.025
	Bottom	7.50	10.791	-1.010

Fig. 4.29 Cumulative Stresses due to Deck Weight at Cross Section 432

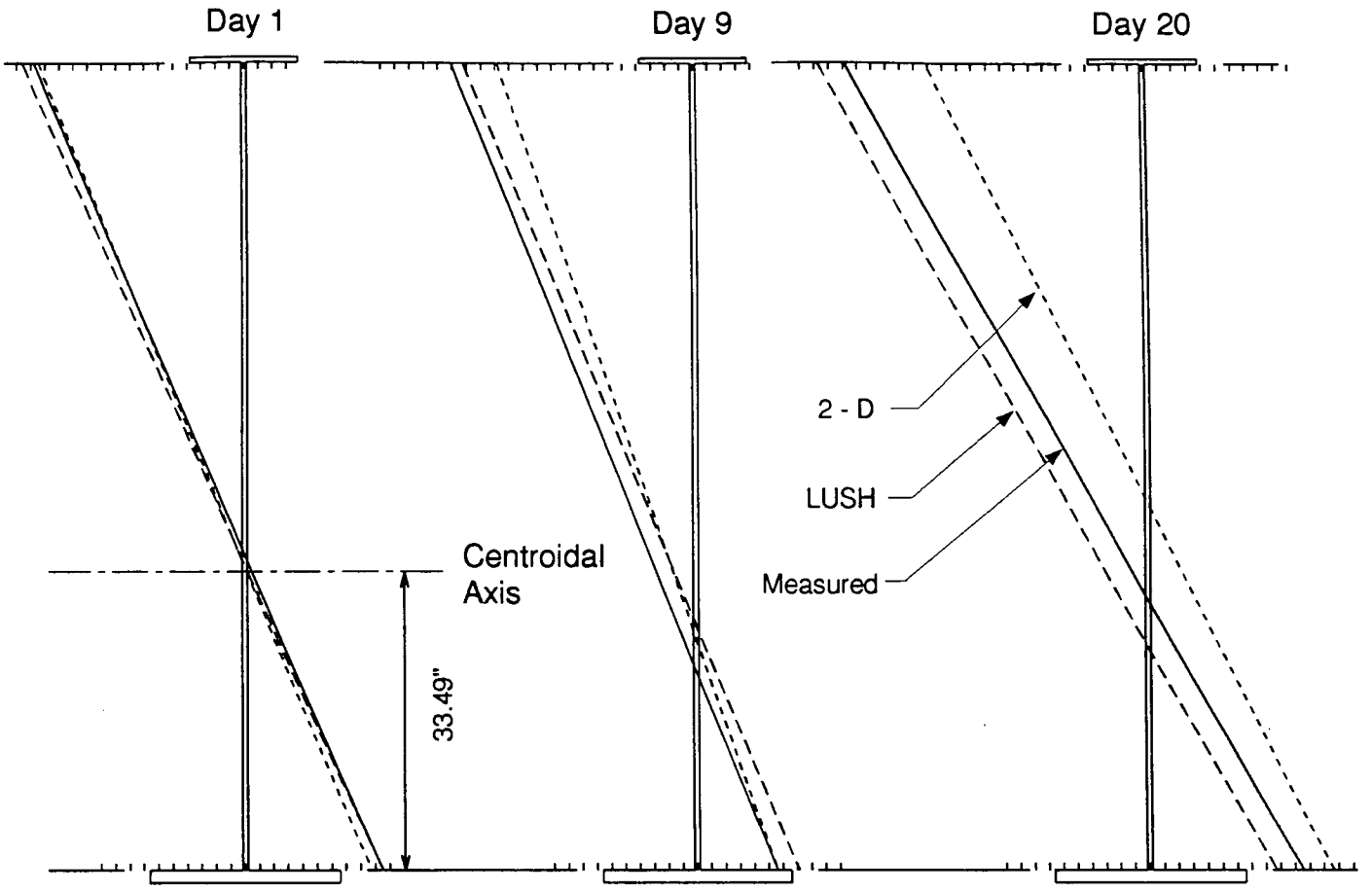

Location 332				
		2-D (ksi)	LUSH (ksi)	Measured (ksi)
Day 1	Top	-14.46	-15.61	-14.80
	Bottom	8.75	9.54	9.53
Day 9	Top	-13.87	-16.26	-17.08
	Bottom	5.61	7.13	5.63
Day 20	Top	-15.18	-22.78	-20.88
	Bottom	12.67	8.73	10.57

Fig. 4.30 Accumulated Dead Load Stresses in Cross Section 332

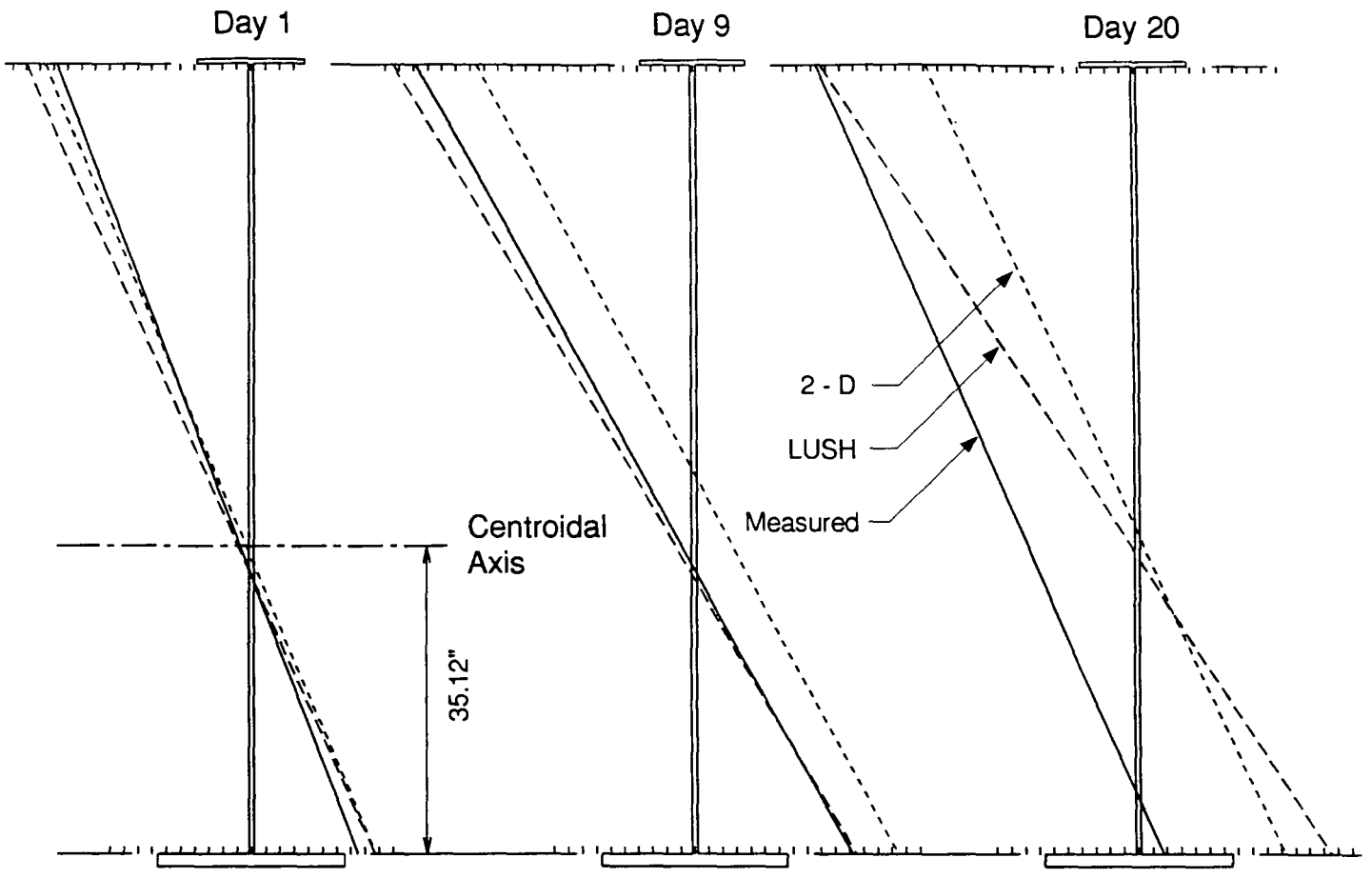

Location 432				
		2-D (ksi)	LUSH (ksi)	Measured (ksi)
Day 1	Top	-14.64	-16.02	-13.79
	Bottom	8.78	8.72	7.51
Day 9	Top	-15.57	-21.45	-19.86
	Bottom	14.46	11.51	11.23
Day 20	Top	-14.89	-22.35	-22.70
	Bottom	10.28	13.56	1.76

Fig. 4.31 Accumulated Dead Load Stresses in Cross Section 432

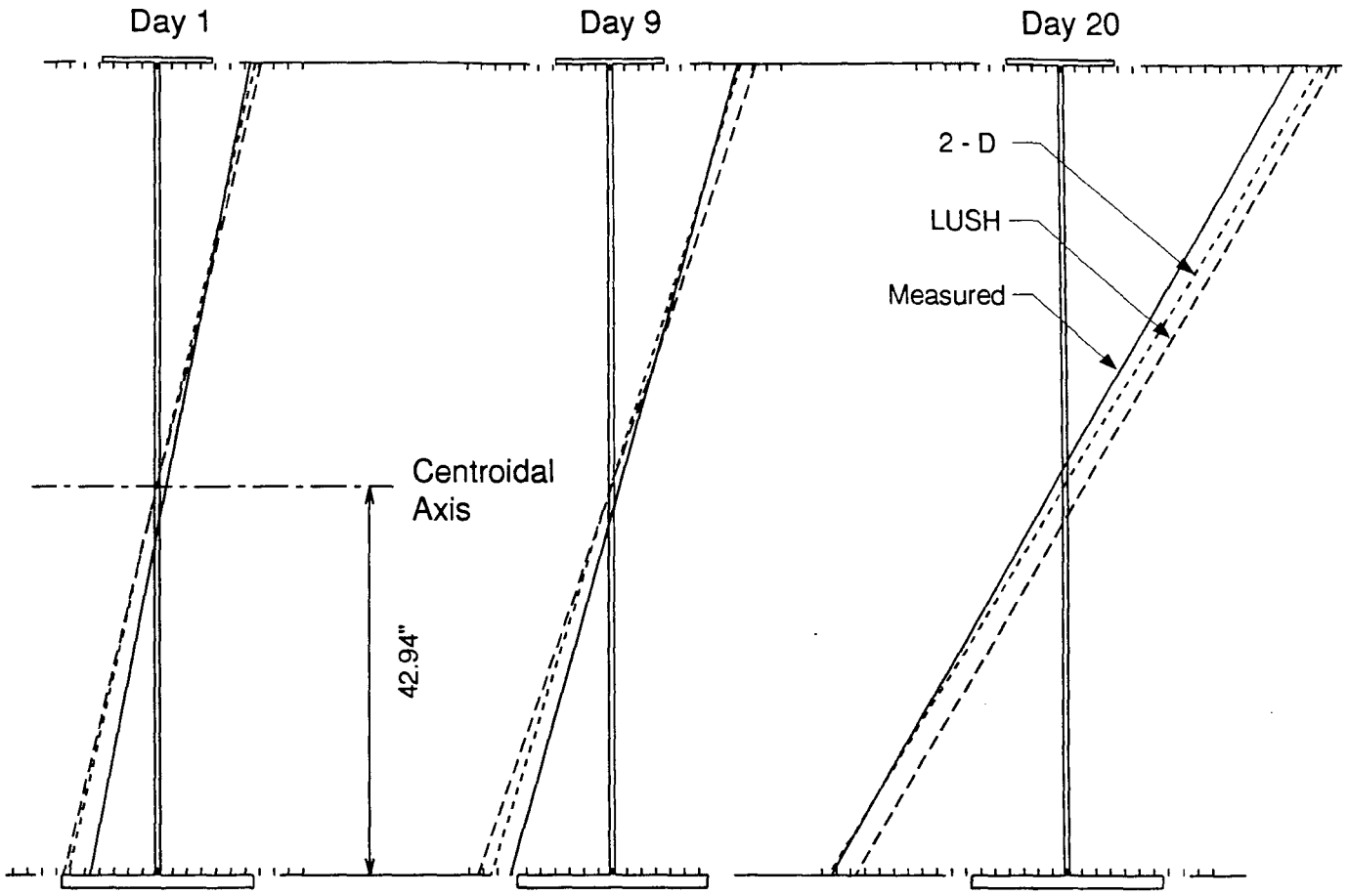

Location 330				
		2-D (ksi)	LUSH (ksi)	Measured (ksi)
Day 1	Top	6.72	7.11	6.38
	Bottom	-6.23	-6.54	-4.71
Day 9	Top	9.15	10.21	8.94
	Bottom	-8.48	-9.39	-7.13
Day 20	Top	17.88	18.74	16.08
	Bottom	-16.57	-14.70	-16.37

Fig. 4.32 Accumulated Dead Load Stresses in Cross Section 330

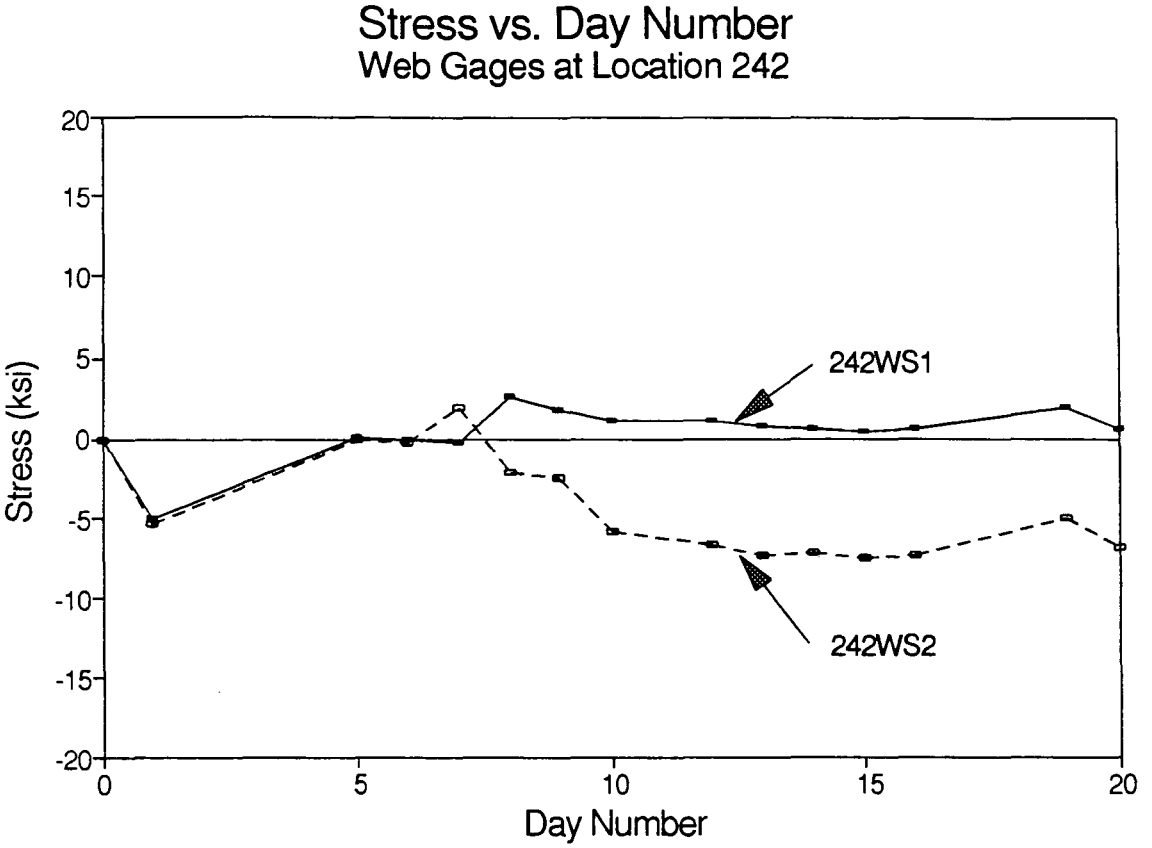

Day	Gage Number	
	242WS1 Stress (ksi)	242WS2 Stress (ksi)
0	0.00	0.00
1	-4.93	-5.18
5	0.14	-0.03
6	-0.10	-0.21
7	-0.24	1.86
8	2.56	-2.15
9	1.76	-2.45
10	1.00	-5.74
12	1.04	-6.53
13	0.73	-7.33
14	0.62	-7.09
15	0.42	-7.47
16	0.52	-7.26
19	1.82	-4.98
20	0.56	-6.74

Fig. 4.33 Vertical Stresses in Girder Web during Construction at Location 242

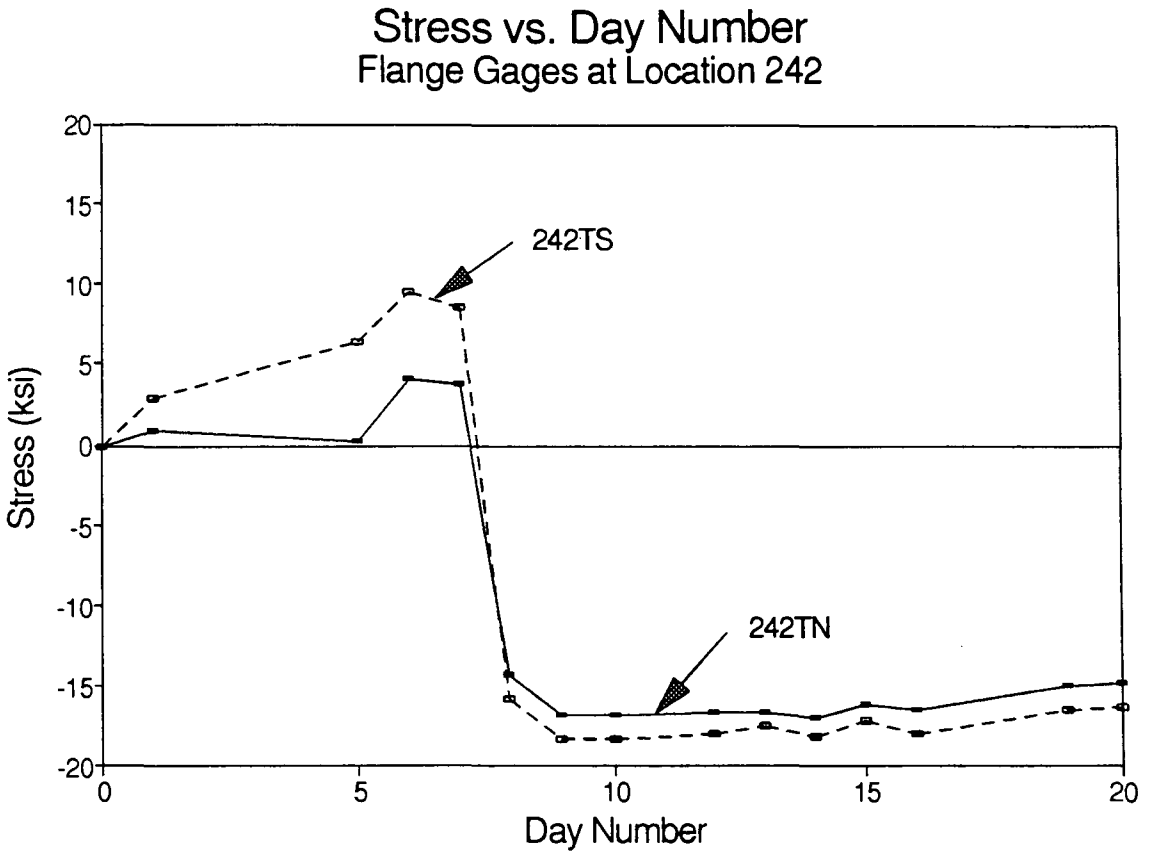

Day	Gage Number	
	242TN Stress (ksi)	242TS Stress (ksi)
0	0.00	0.00
1	0.79	2.83
5	0.24	6.42
6	4.07	9.58
7	3.62	8.61
8	-14.22	-15.74
9	-16.77	-18.25
10	-16.77	-18.29
12	-16.67	-17.89
13	-16.70	-17.47
14	-16.95	-18.14
15	-16.15	-17.10
16	-16.50	-17.98
19	-14.91	-16.49
20	-14.77	-16.35

Fig. 4.34 Stresses in Girder Flange during Construction at Location 242

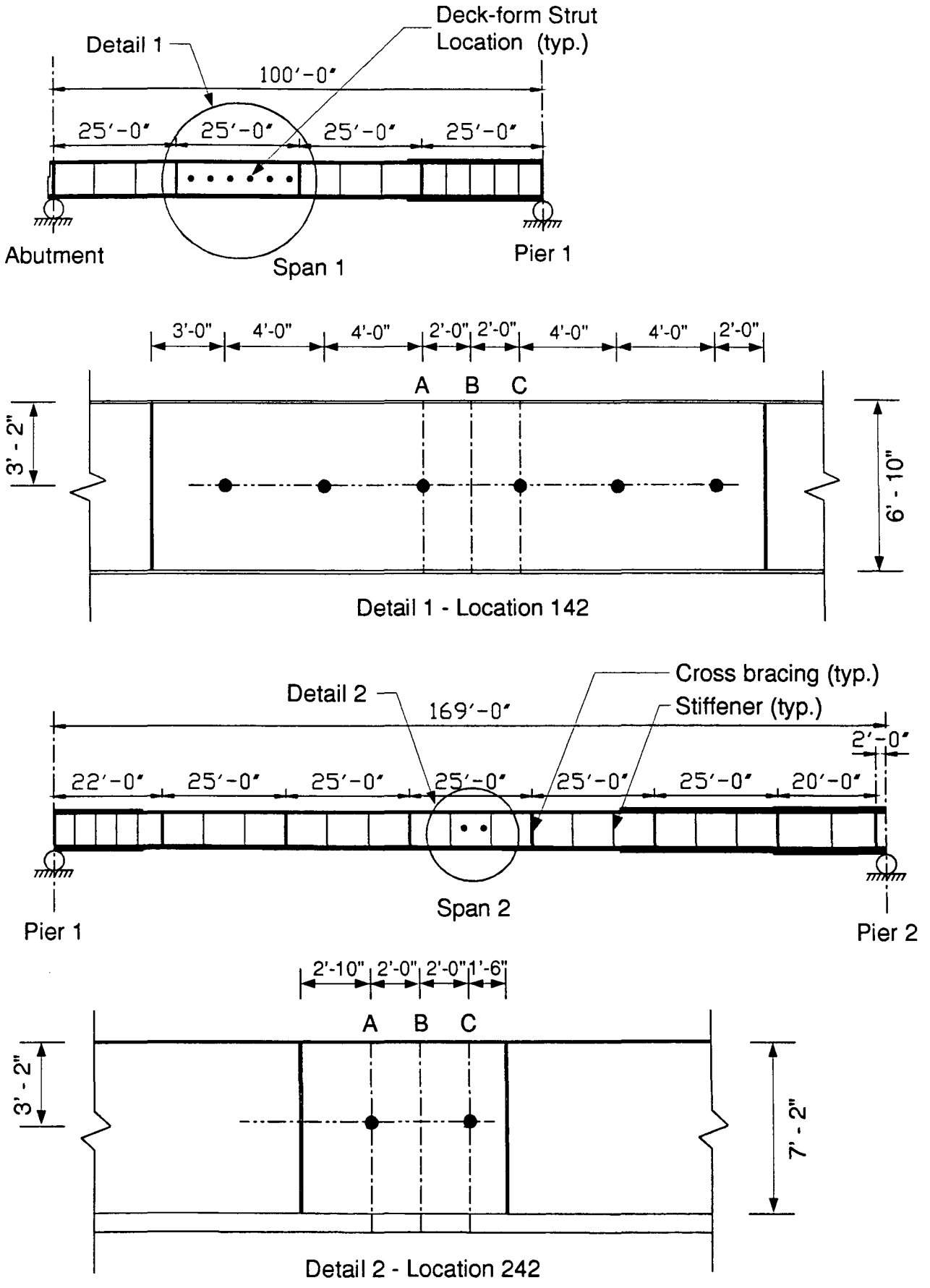

Fig. 4.35 Web Deflection Measurement at Locations 142 and 242

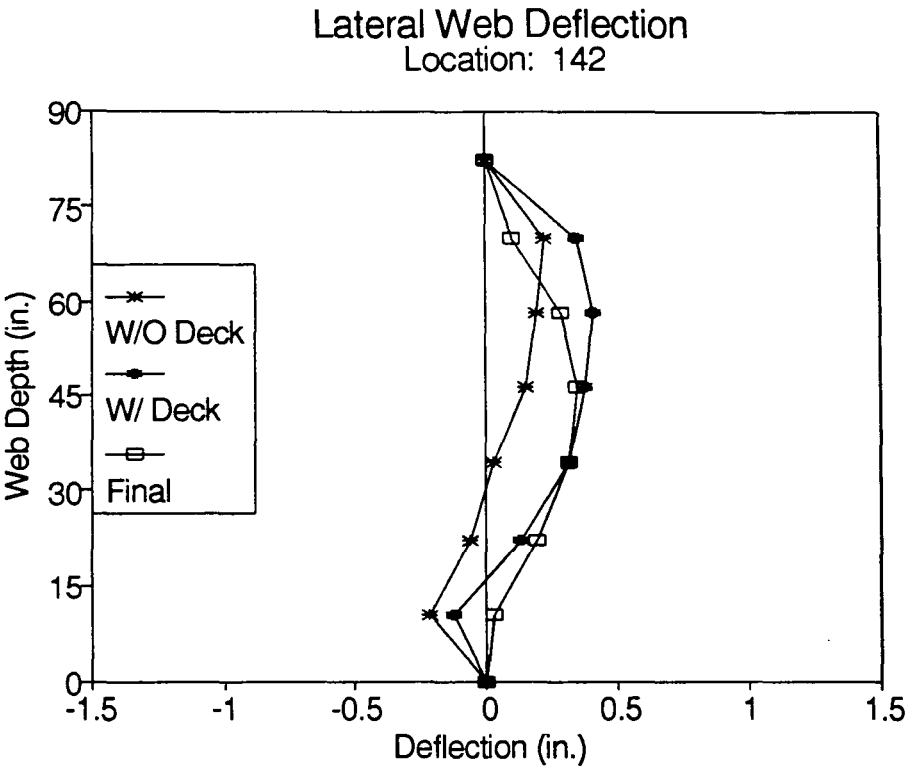

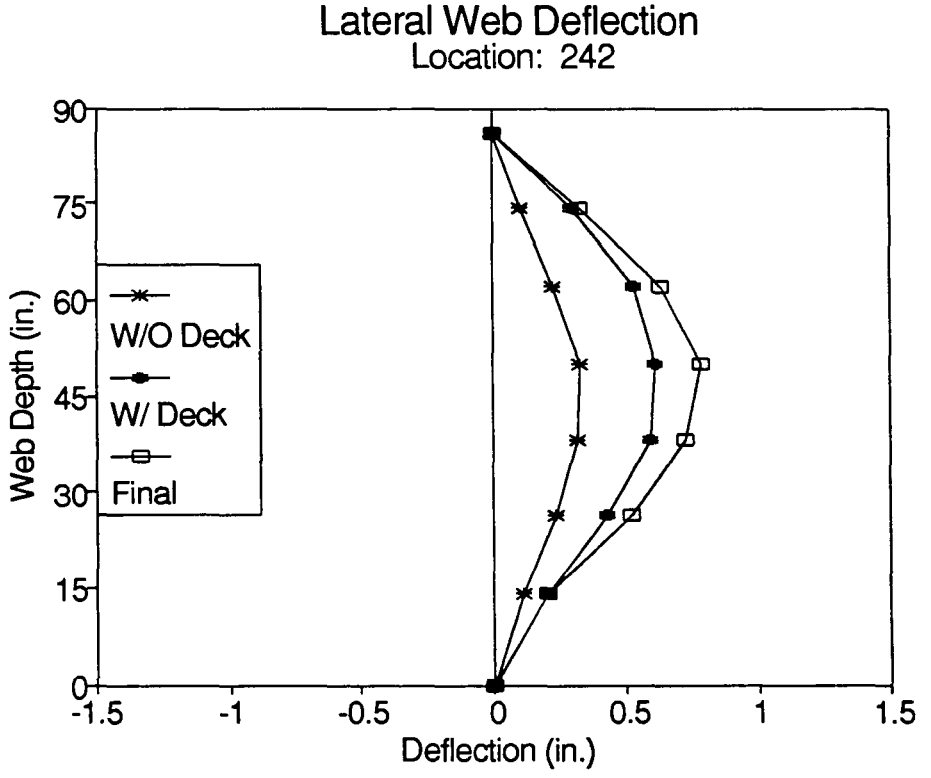

Fig. 4.36 Lateral Deflection of Web due to Deck Placement

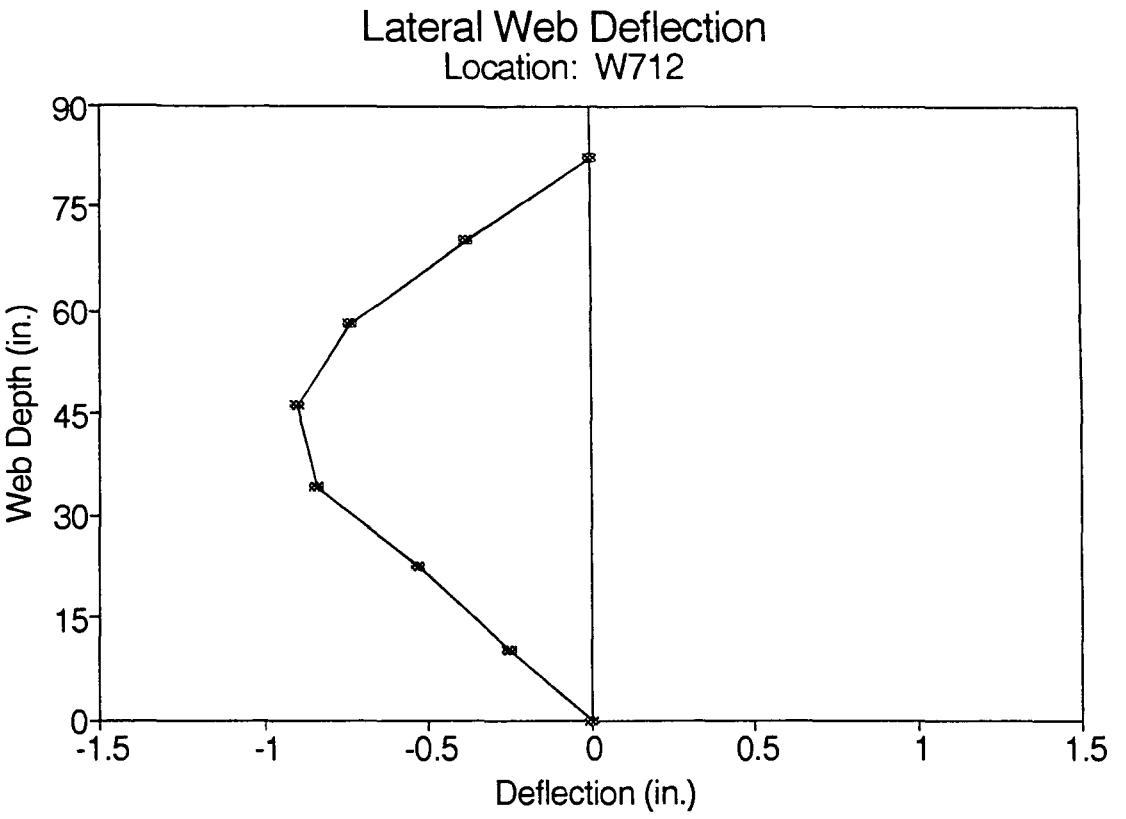

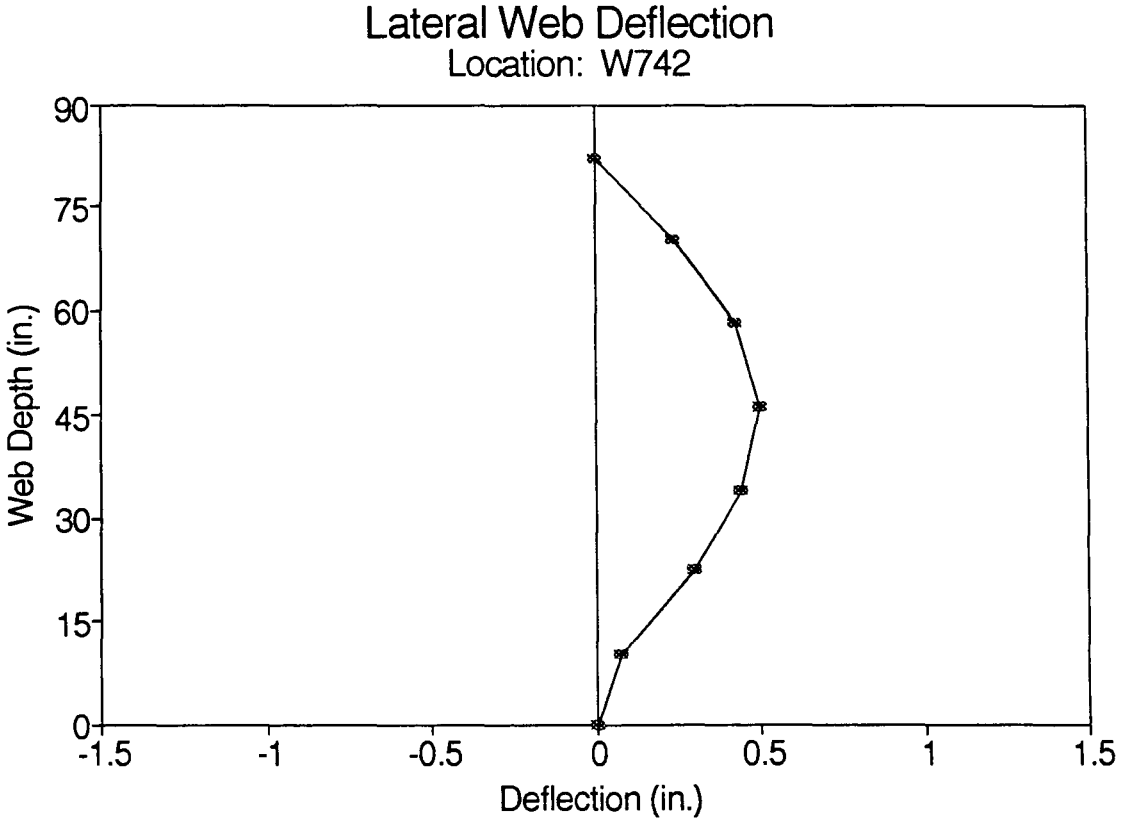

Fig. 4.37 Lateral Deflection of Web at Span W7 after Completion of Deck

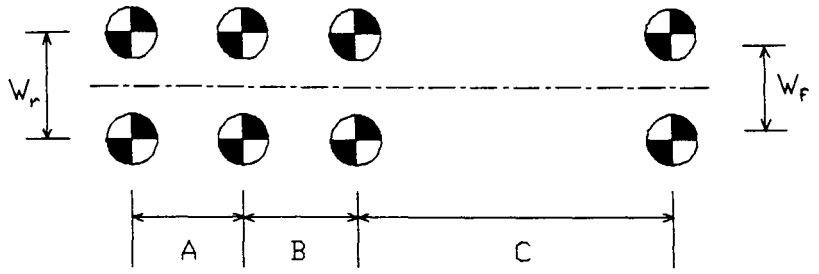

Truck No.	1	2	3	4	5	6
A	4'-3½"	4'-5½"	4'-7"	4'-2½"	4'-7"	4'-7"
B	4'-2"	4'-4½"	4'-5"	4'-3"	4'-0½"	4'-4½"
C	10'-10"	12'-2½"	10'-6"	10'-9"	9'-2"	10'-8"
W_r	5'-11"	6'-0"	6'-0½"	6'-0½"	5'-11"	6'-1"
W_f	6'-10"	6'-9"	6'-11"	6'-9"	6'-9"	6'-9"

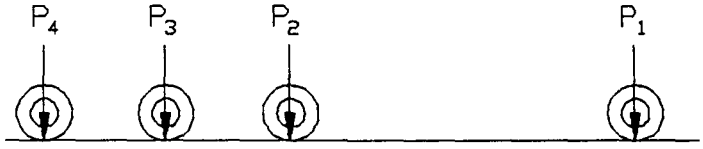

Truck No.	1	2	3	4	5	6
P_1	17.45^k	15.9^k	17.1^k	17.1^k	12.5^k	14.05^k
P_2	12.15^k	15.8^k	9.35^k	20.05^k	12.05^k	16.15^k
P_3	18.7^k	18.2^k	20.7^k	14.9^k	21.5^k	18.55^k
P_4	19.1^k	18.0^k	20.85^k	15.05^k	21.55^k	18.8^k
Total Load	67.4^k	67.9^k	68.0^k	67.1^k	67.6^k	67.55^k

Fig. 5.1 Dimensions and Axle Loads of Test Trucks

(A) Simulated HS - 25 Loading

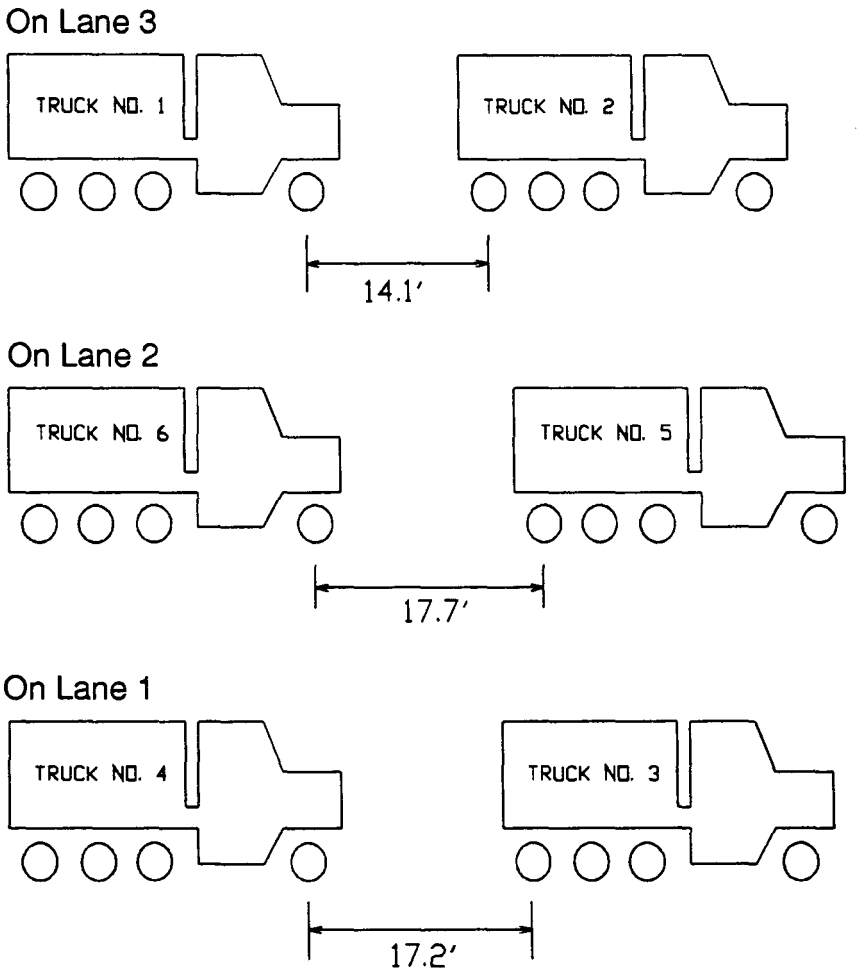

(B) Simulated 204K Permit Truck Loading

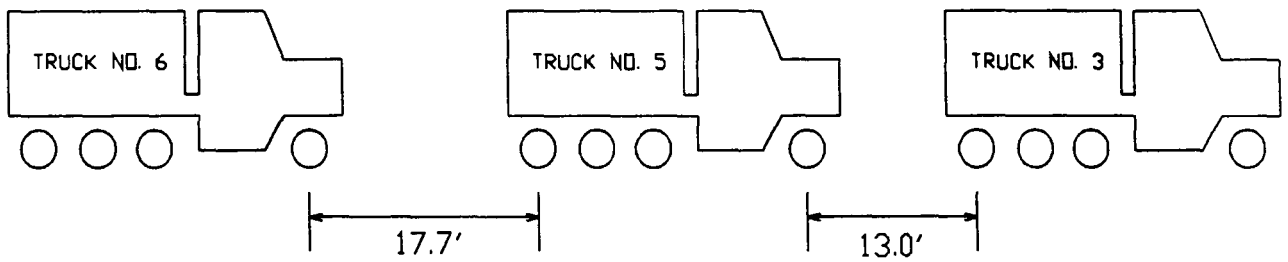

Fig. 5.2 Simulated HS - 25 and 204K Live Loads

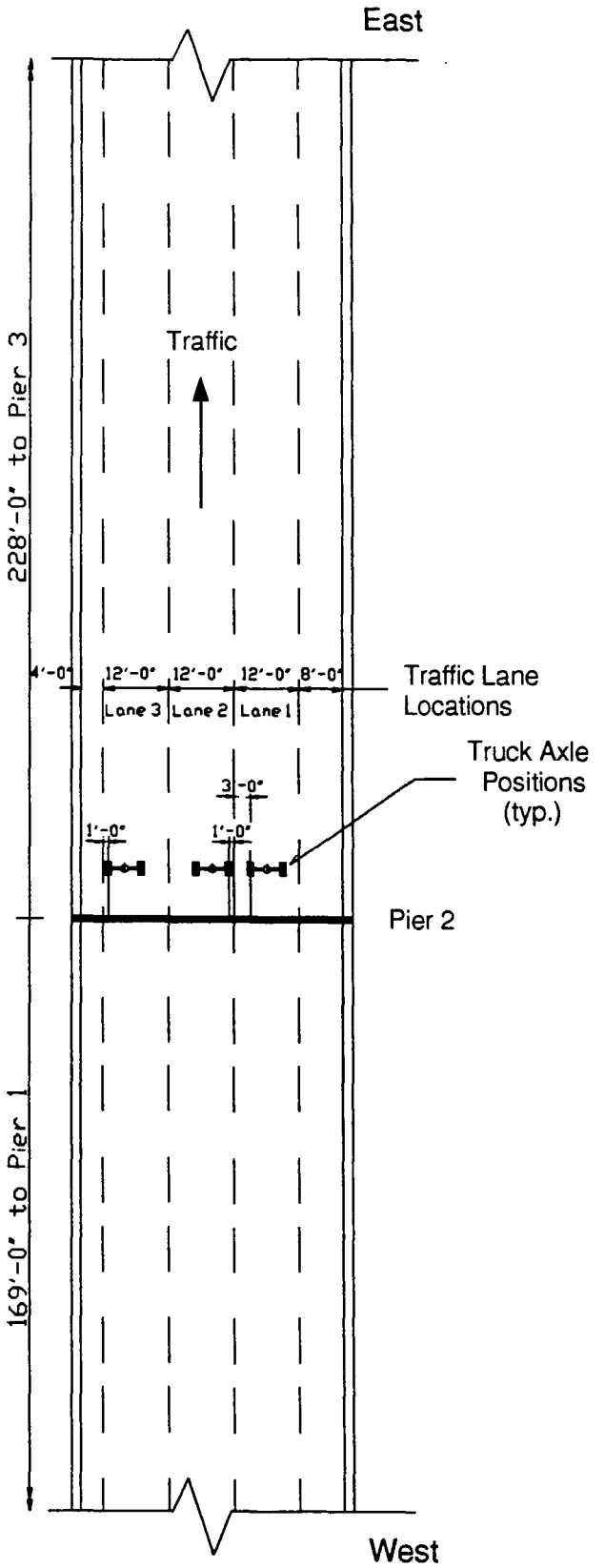

Fig. 5.3 Traffic Lanes and Test Truck Positions

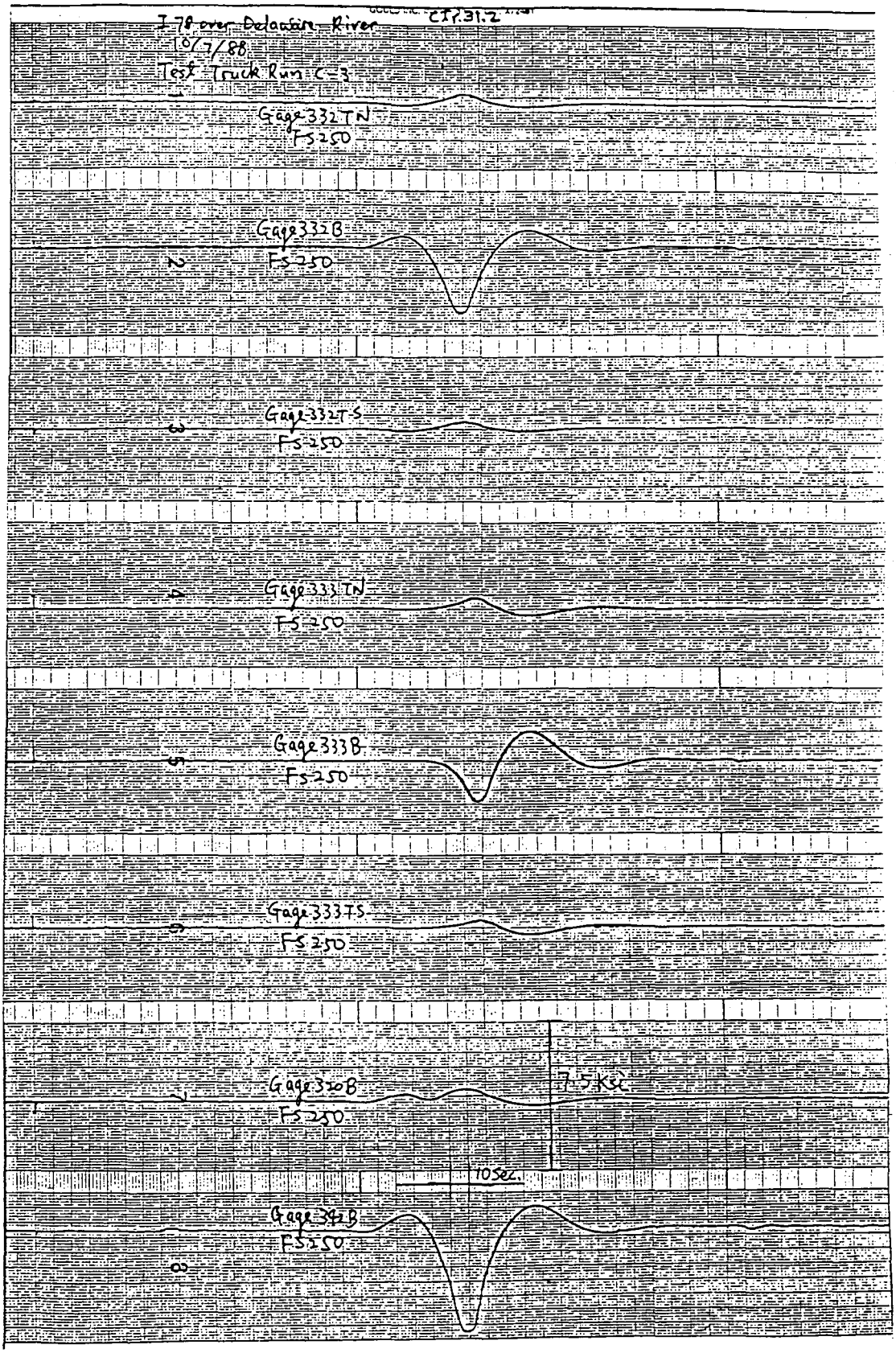

Fig. 5.4 Strain-Time Variations, Test Truck Run C3

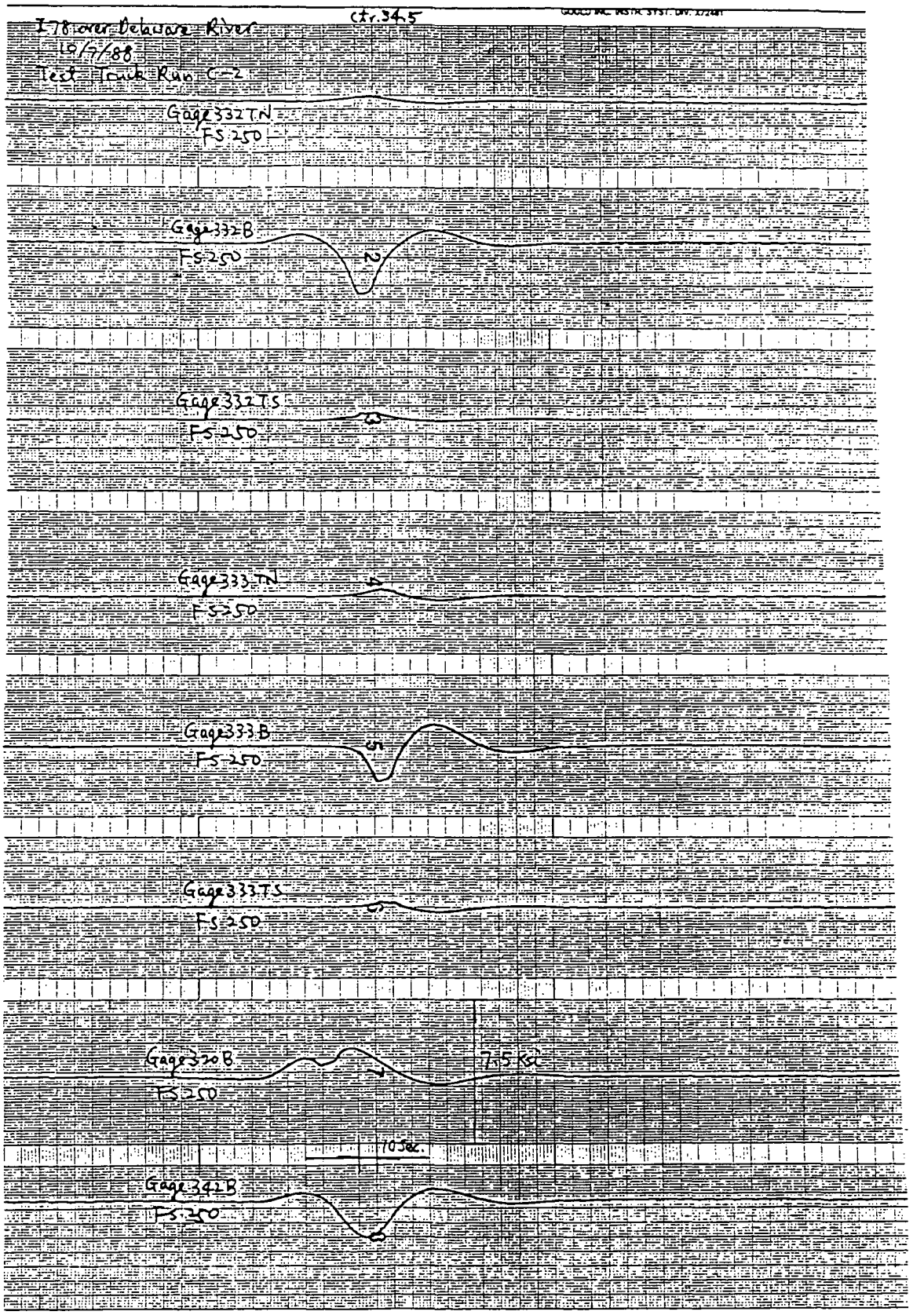

Fig. 5.5 Strain-Time Variations, Test Truck Run C2

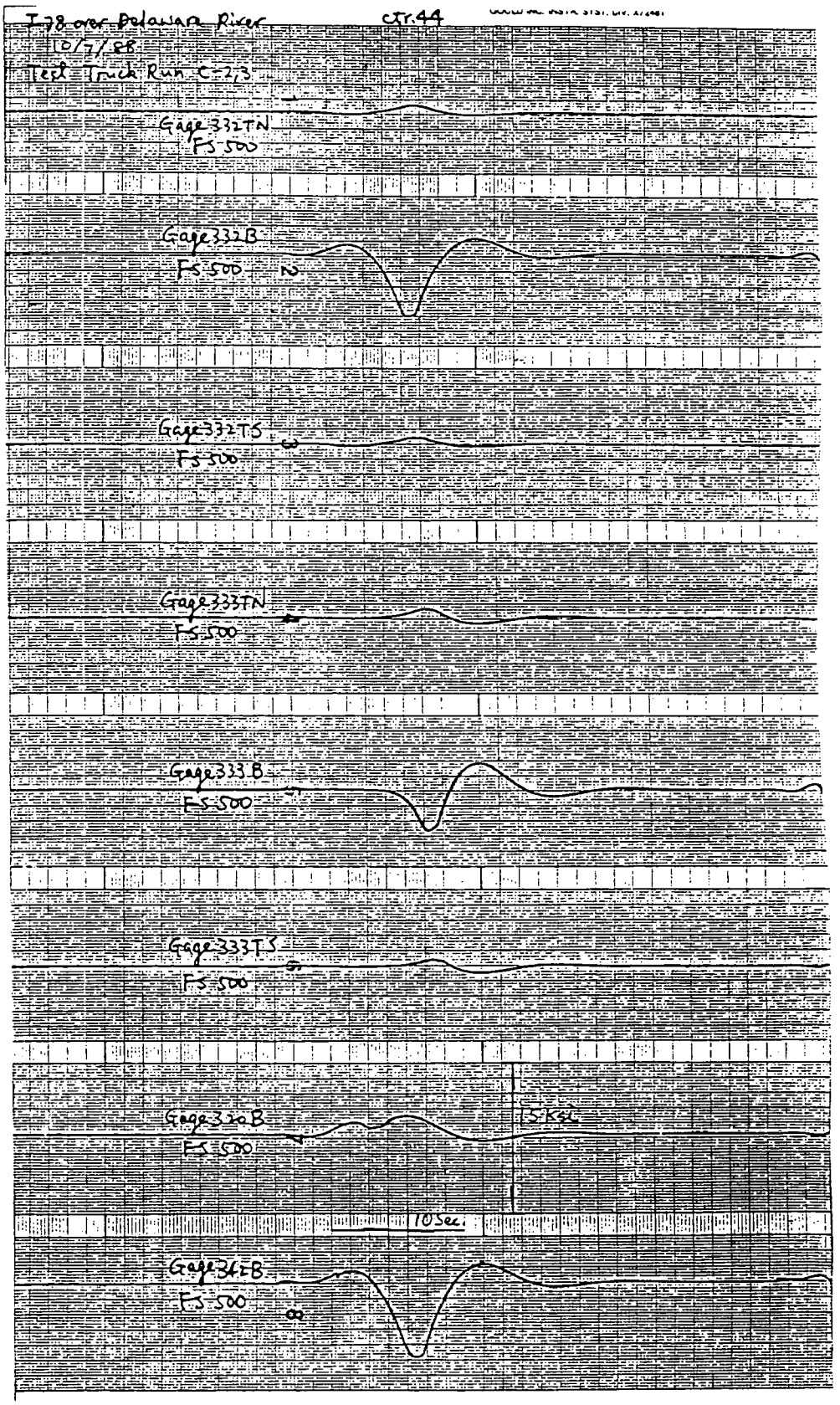

Fig. 5.6 Strain-time Variations, Test Truck Runs C2 and C3

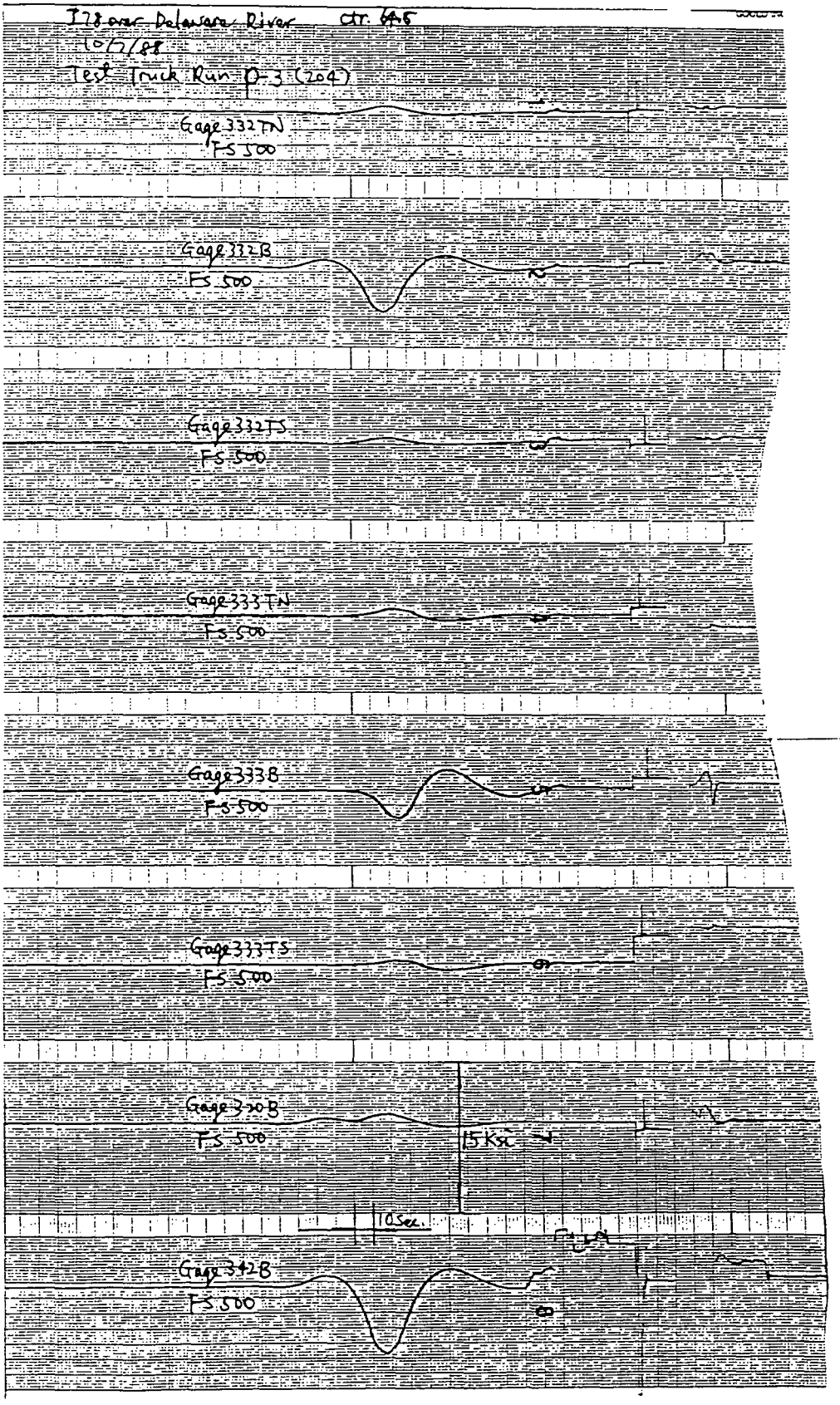

Fig. 5.7 Strain-Time Traces, Simulated Permit Truck (Run P3)

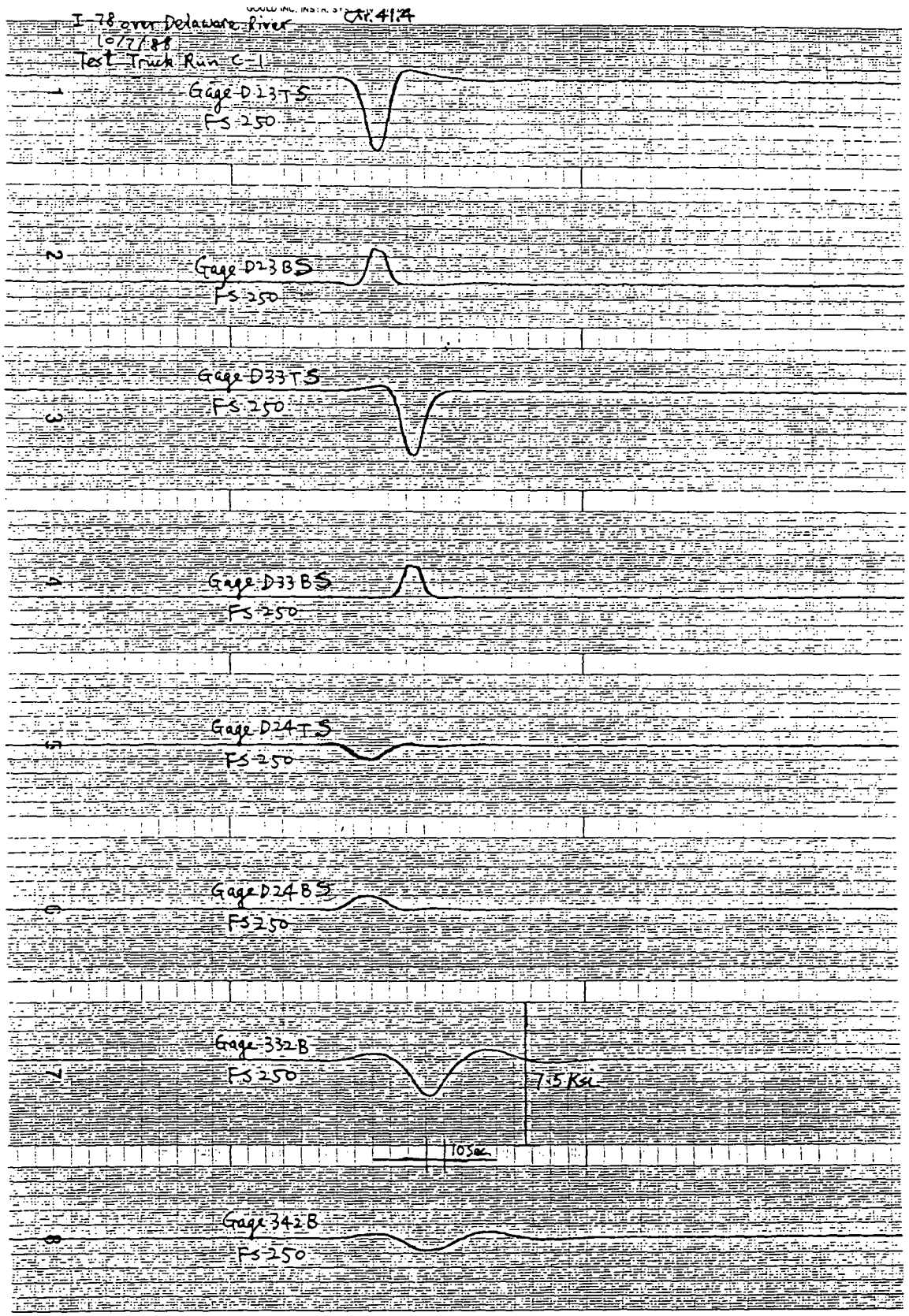

Fig. 5.8 Diaphragm Stresses, Test Truck Run C1

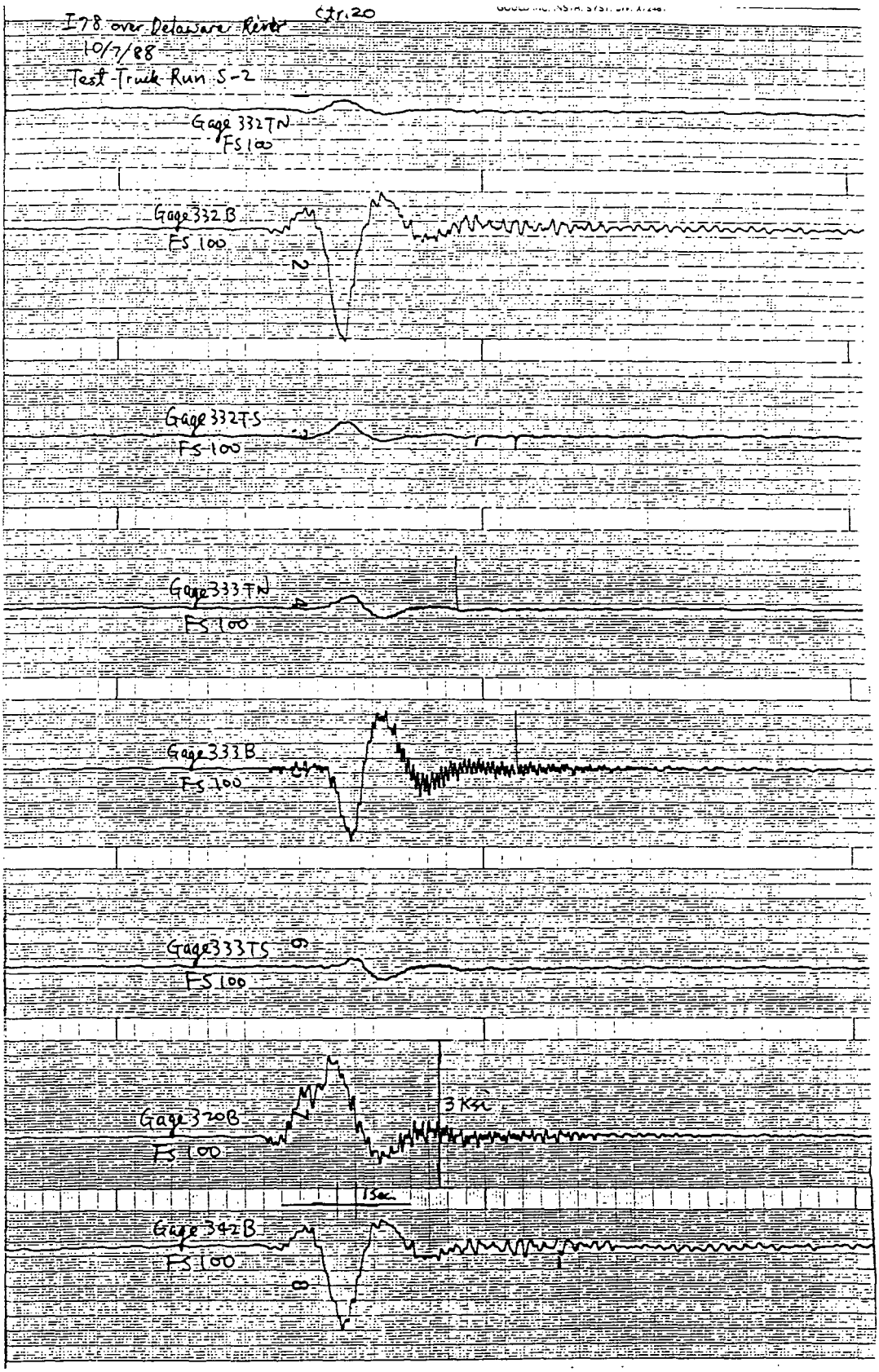

Fig. 5.9 Examples of Strain-Time Record, Test Truck Run S2

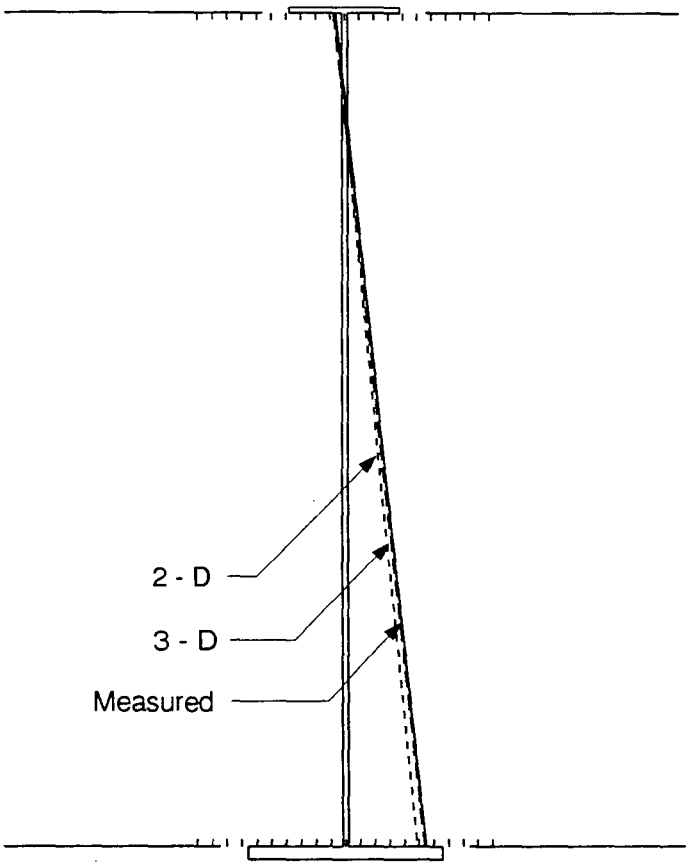

Location 242			
	2-D (ksi)	3-D (ksi)	Measured (ksi)
Top	-0.71	-0.78	-0.65
Bottom	4.87	5.37	5.47

Fig 5.10 HS25 Induced Maximum Stresses in Cross Section 242

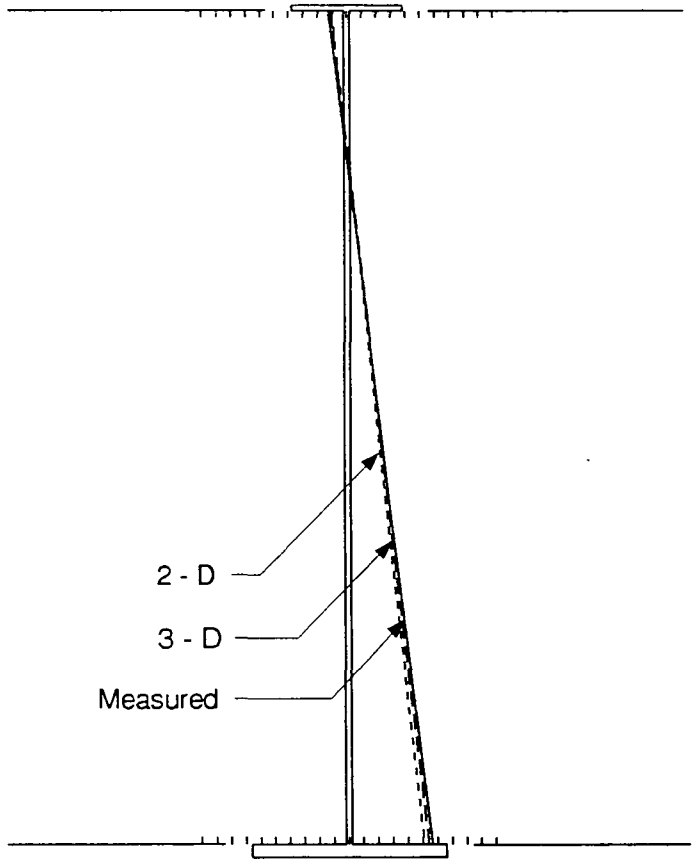

Location 342			
	2-D (ksi)	3-D (ksi)	Measured (ksi)
Top	-1.03	-1.09	-1.24
Bottom	5.08	5.41	5.62

Fig 5.11 HS25 Induced Maximum Stresses in Cross Section 342

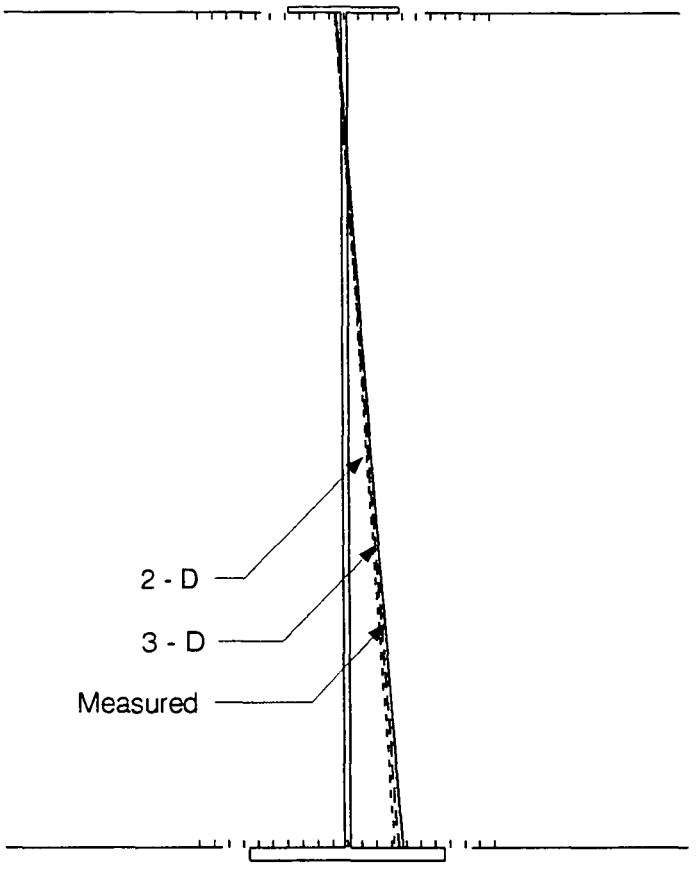

Location 332			
	2-D (ksi)	3-D (ksi)	Measured (ksi)
Top	-0.60	-0.65	-0.53
Bottom	3.21	3.48	3.76

Fig 5.12 HS25 Induced Maximum Stresses in Cross Section 332

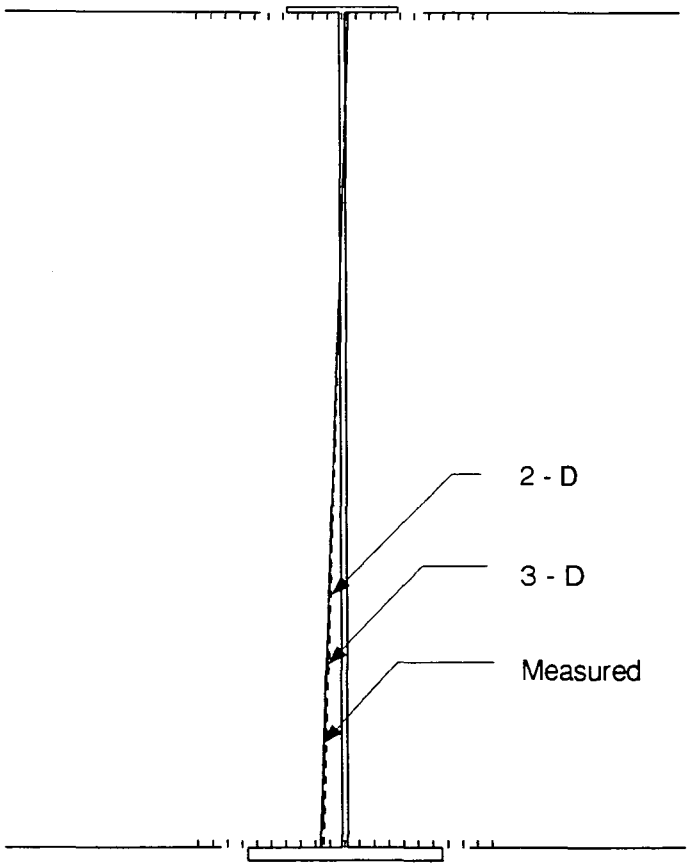

Location 330			
	2-D (ksi)	3-D (ksi)	Measured (ksi)
Top	0.37	0.40	0.44
Bottom	-1.47	-1.61	-1.68

Fig 5.13 HS25 Induced Maximum Stresses in Cross Section 330

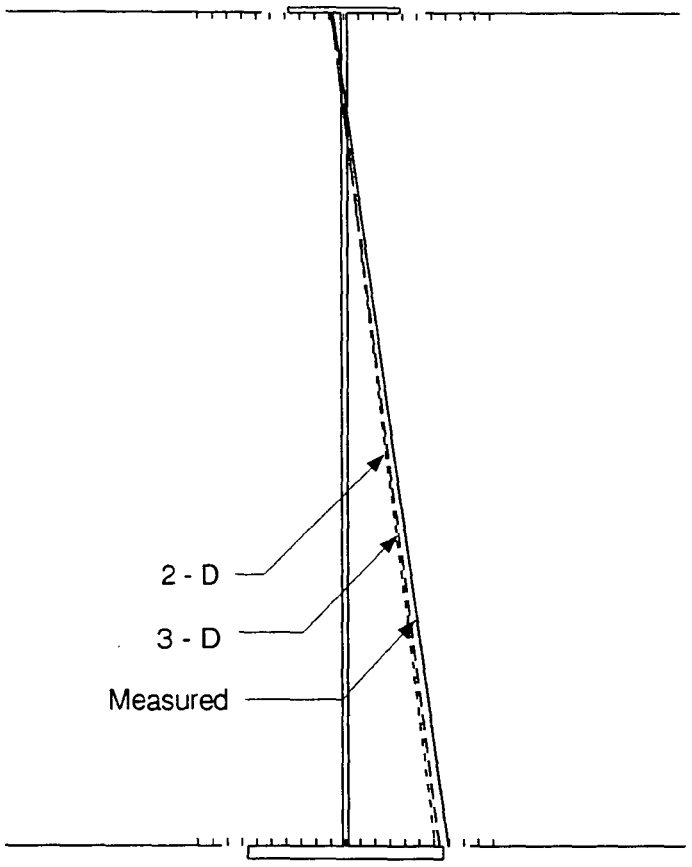

Location 242			
	2-D (ksi)	3-D (ksi)	Measured (ksi)
Top	-0.88	-0.92	-0.76
Bottom	6.09	6.38	6.98

Fig 5.14 204^{k} Induced Maximum Stresses in Cross Section 242

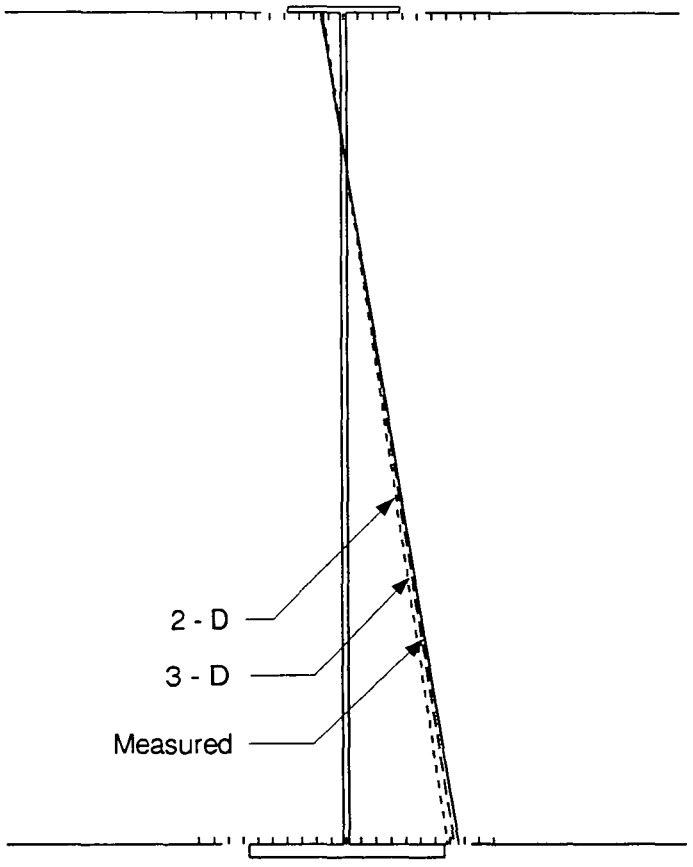

Location 342			
	2-D (ksi)	3-D (ksi)	Measured (ksi)
Top	-1.38	-1.47	-1.57
Bottom	6.81	7.27	7.57

Fig 5.15 204^{k} Induced Maximum Stresses in Cross Section 342

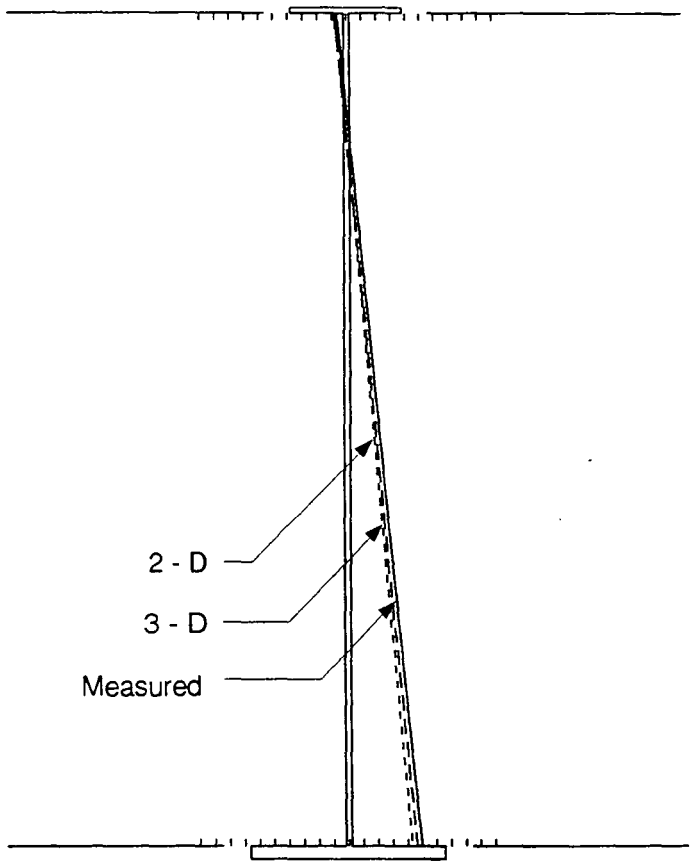

Location 332			
	2-D (ksi)	3-D (ksi)	Measured (ksi)
Top	-0.80	-0.86	-0.68
Bottom	4.33	4.65	4.98

Fig 5.16 204^{k} Induced Maximum Stresses in Cross Section 332

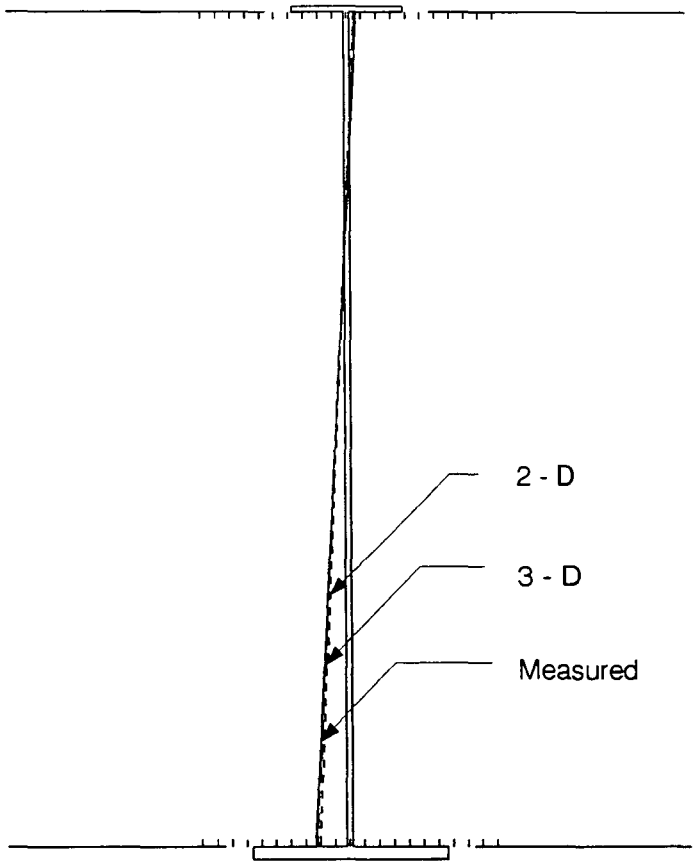

Location 330			
	2-D (ksi)	3-D (ksi)	Measured (ksi)
Top	0.51	0.57	0.66
Bottom	-2.04	-2.26	-2.33

Fig 5.17 204^{k} Induced Maximum Stresses in Cross Section 330

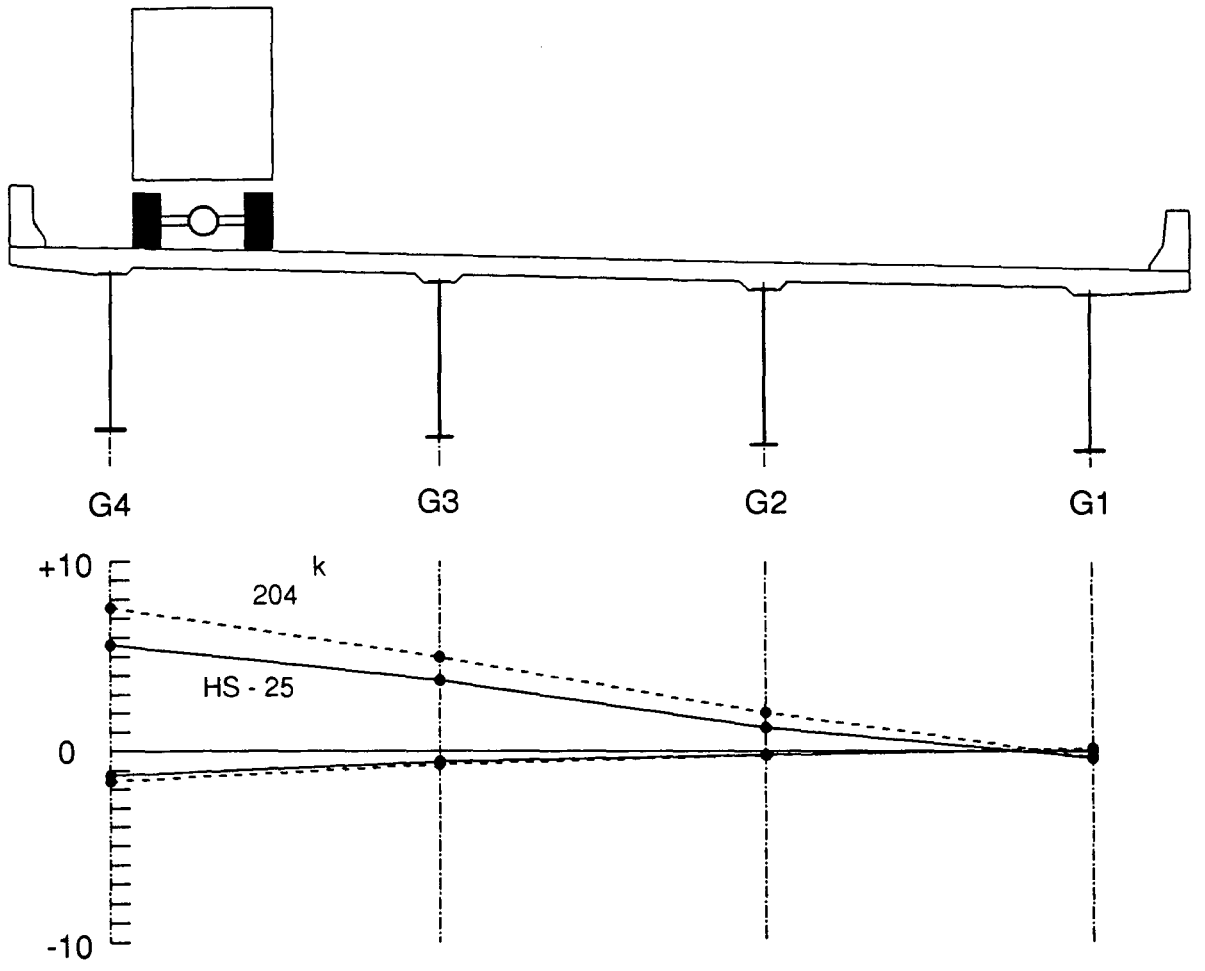

Simulated Truck	Flange	Location			
		342 (ksi)	332 (ksi)	322 (ksi)	312 (ksi)
HS-25	Top	-1.24	-0.53	-0.17	0.07
	Bottom	5.62	3.76	1.26	-0.34
k 204	Top	-1.57	-0.68	-0.20	0.18
	Bottom	7.57	4.98	2.06	-0.30

Fig. 5.18 Distribution of Stresses, Middle of Span 3 (3 X 2), C3 and P3

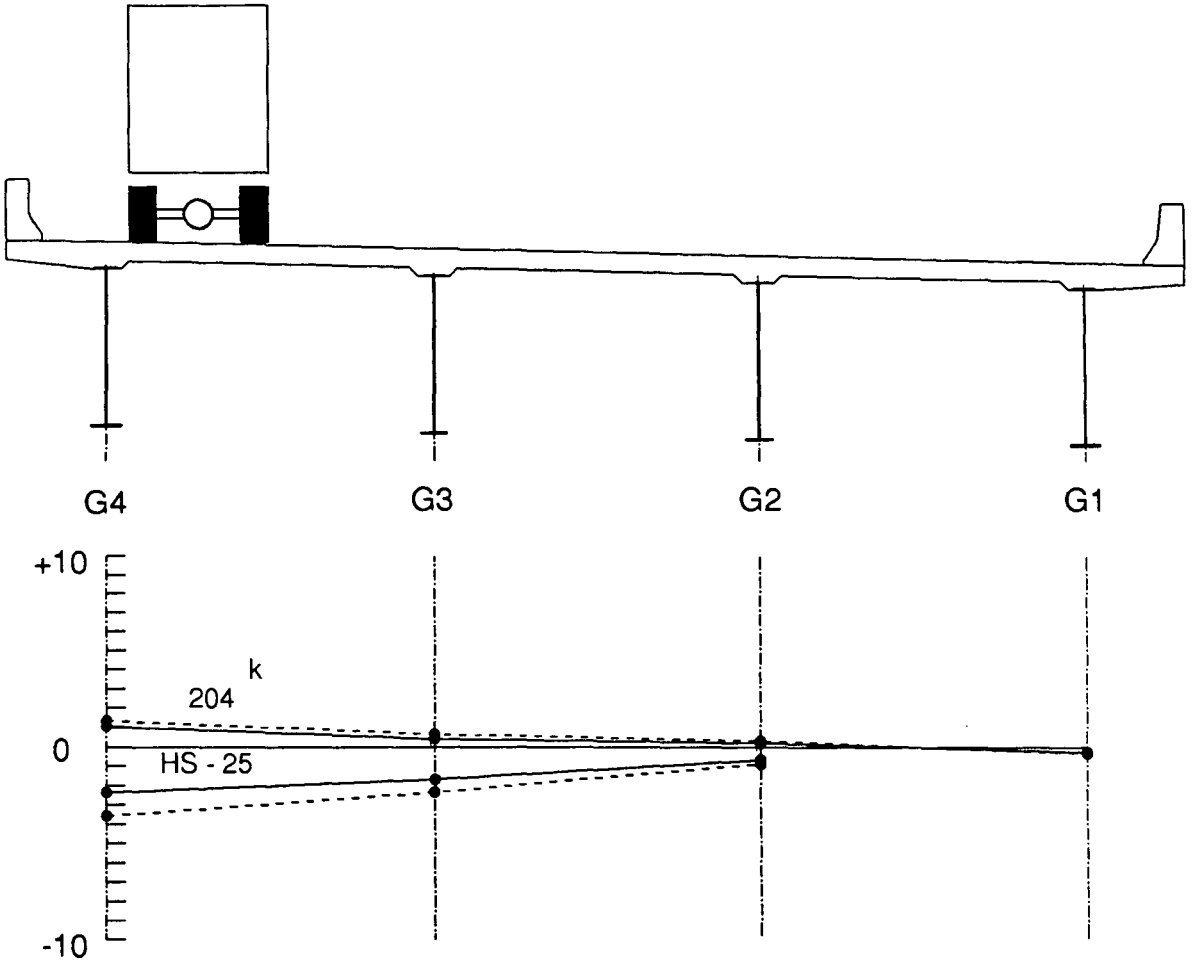

Simulated Truck	Flange	Location			
		340 (ksi)	330 (ksi)	320 (ksi)	310 (ksi)
HS-25	Top	1.08	0.44	0.22	-0.23
	Bottom	-2.35	-1.68	-0.65	---
k 204	Top	1.36	0.66	0.33	-0.31
	Bottom	-3.55	-2.33	-0.87	---

Fig. 5.19 Distribution of Stresses over Pier 2 (3 X 0) , C3 and P3

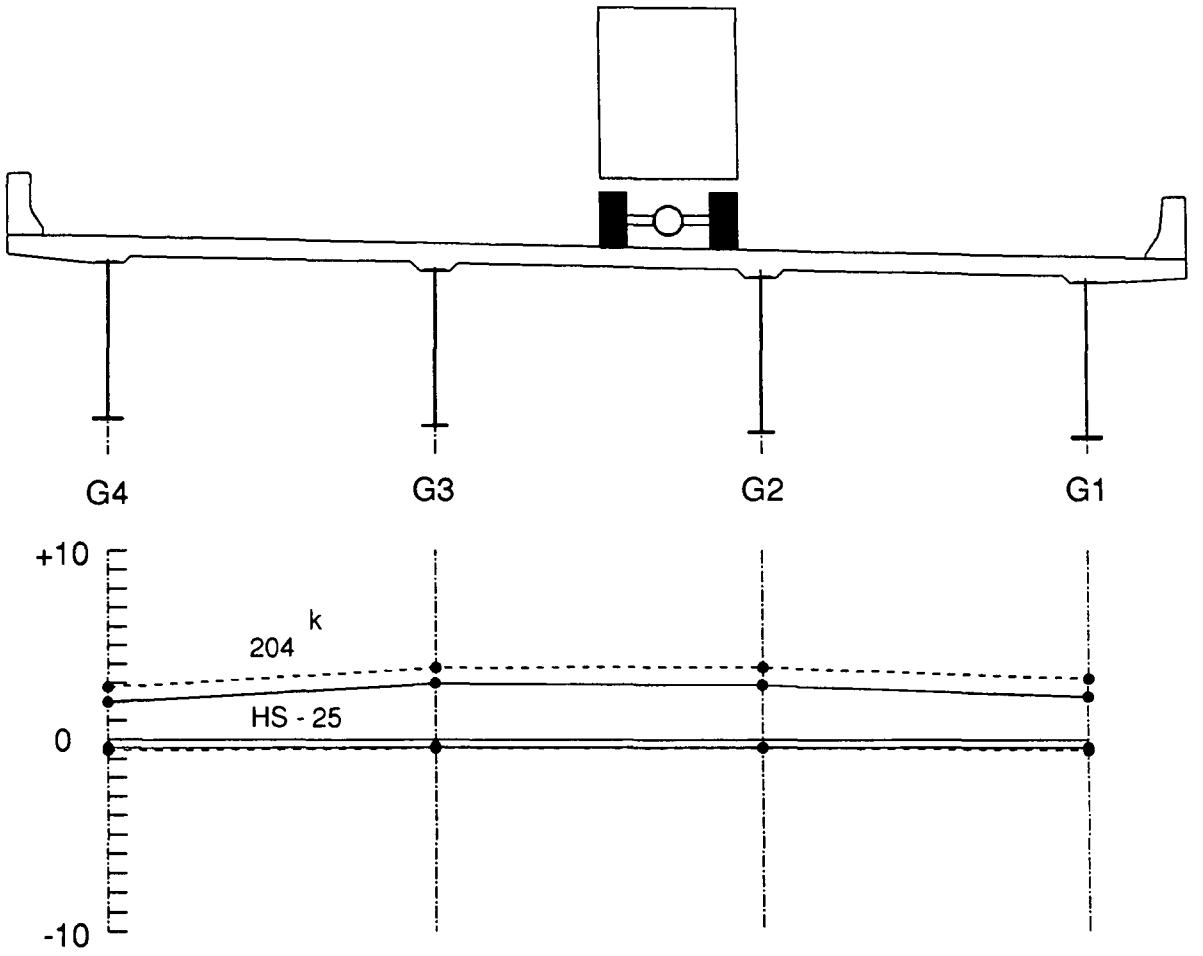

Simulated Truck	Flange	Location			
		342 (ksi)	332 (ksi)	322 (ksi)	312 (ksi)
HS-25	Top	-0.42	-0.37	-0.39	-0.39
	Bottom	1.98	2.99	2.89	2.28
k 204	Top	-0.56	-0.44	-0.42	-0.54
	Bottom	2.78	3.82	3.82	3.22

Fig. 5.20 Distribution of Stresses, Middle of Span 3 (3 X 2), C2 and P2

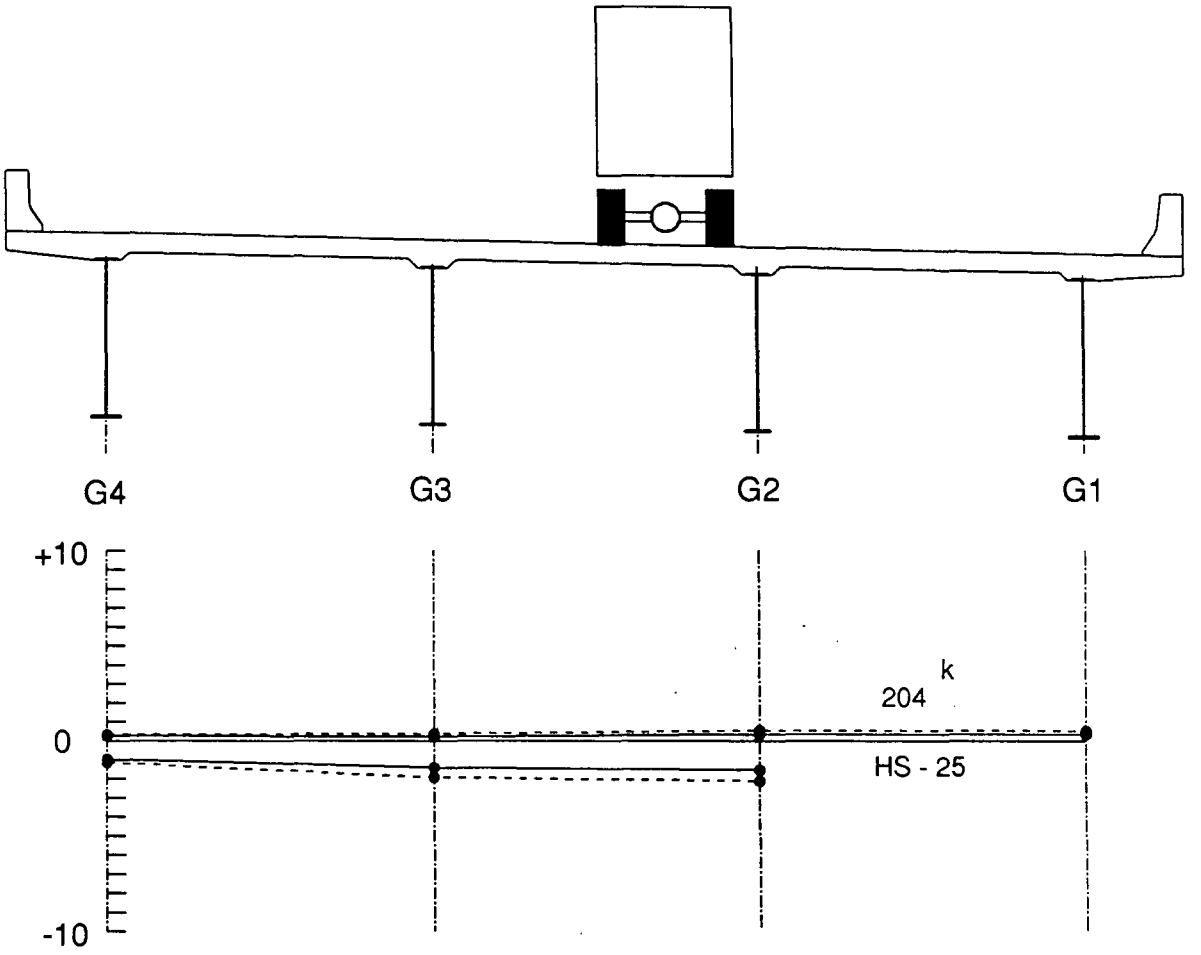

Simulated Truck	Flange	Location			
		340 (ksi)	330 (ksi)	320 (ksi)	310 (ksi)
HS-25	Top	0.30	0.24	0.38	0.36
	Bottom	-0.94	-1.40	-1.53	---
k 204	Top	0.34	0.38	0.55	0.53
	Bottom	-1.13	-1.93	-2.12	---

Fig. 5.21 Distribution of Stresses over Pier 2 (3 X 0) , C2 and P2

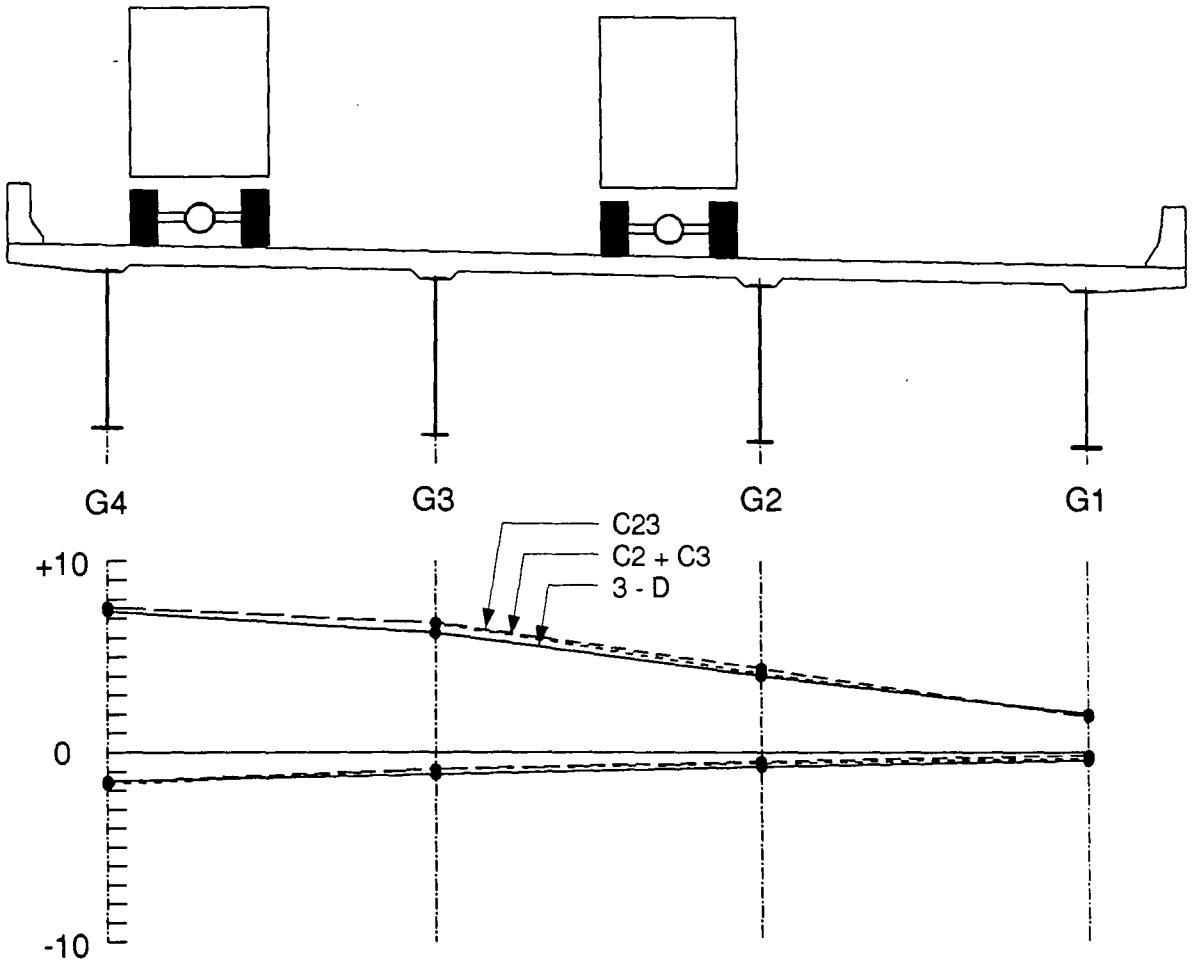

	Flange	Location			
		342 (ksi)	332 (ksi)	322 (ksi)	312 (ksi)
Measured C23	Top	-1.53	-0.86	-0.47	-0.14
	Bottom	7.60	6.78	4.42	1.88
Measured C2 + C3	Top	-1.66	-0.90	-0.56	-0.32
	Bottom	7.60	6.75	4.15	1.94
3 - D	Top	-1.49	-1.16	-0.75	-0.41
	Bottom	7.39	6.25	4.02	2.03

Fig. 5.22 Superposition of Loads, Middle of Span 3 (3 X 2) , C23

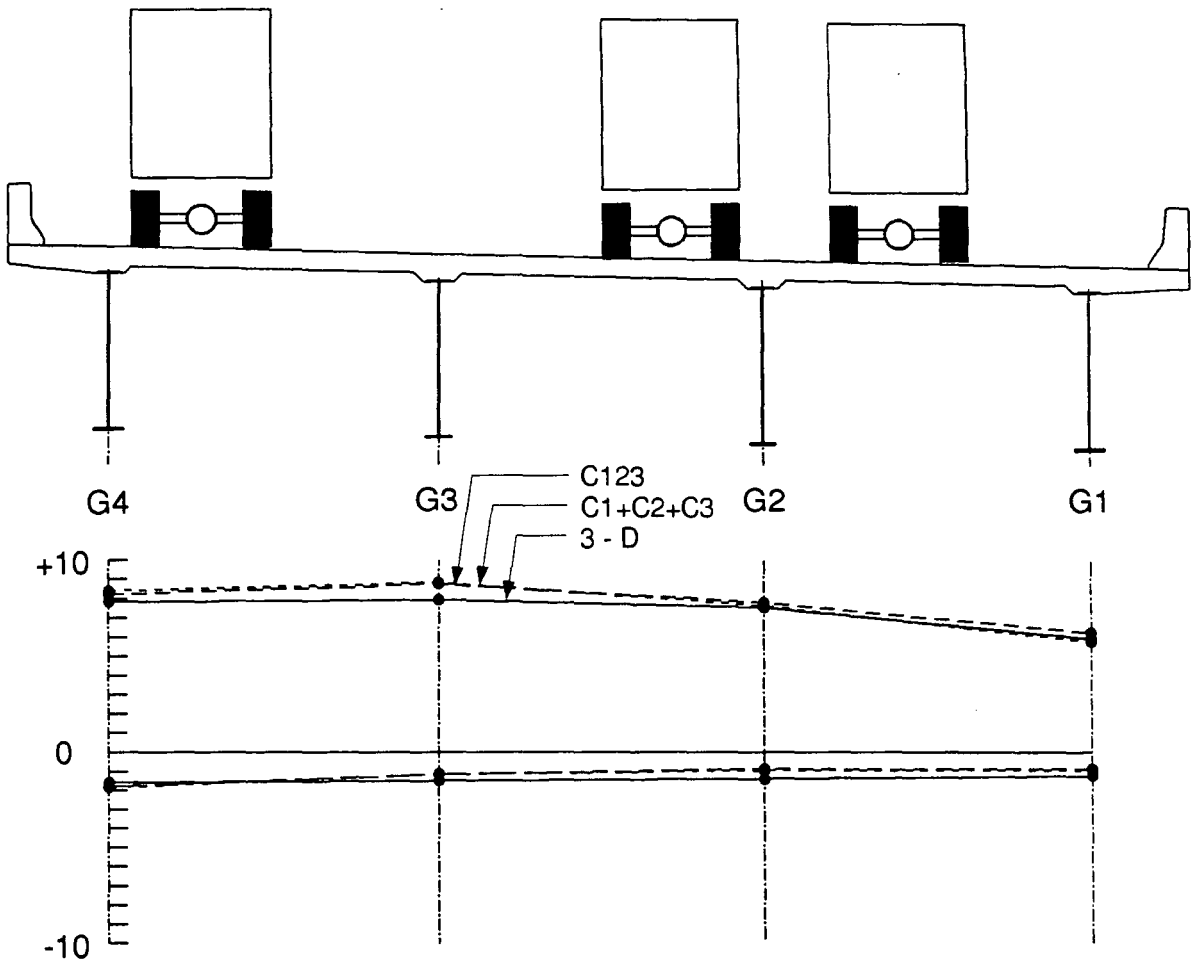

	Flange	Location			
		342 (ksi)	332 (ksi)	322 (ksi)	312 (ksi)
Measured C123	Top	-1.50	-1.12	-0.87	-0.86
	Bottom	8.23	8.77	7.80	6.27
Measured C1+C2+C3	Top	-1.84	-1.16	-0.96	-0.96
	Bottom	8.39	8.84	7.64	5.80
3 - D	Top	-1.58	-1.48	-1.40	-1.20
	Bottom	7.84	7.95	7.55	5.95

Fig. 5.23 Superposition of Loads, Middle of Span 3 (3 X 2) , C123

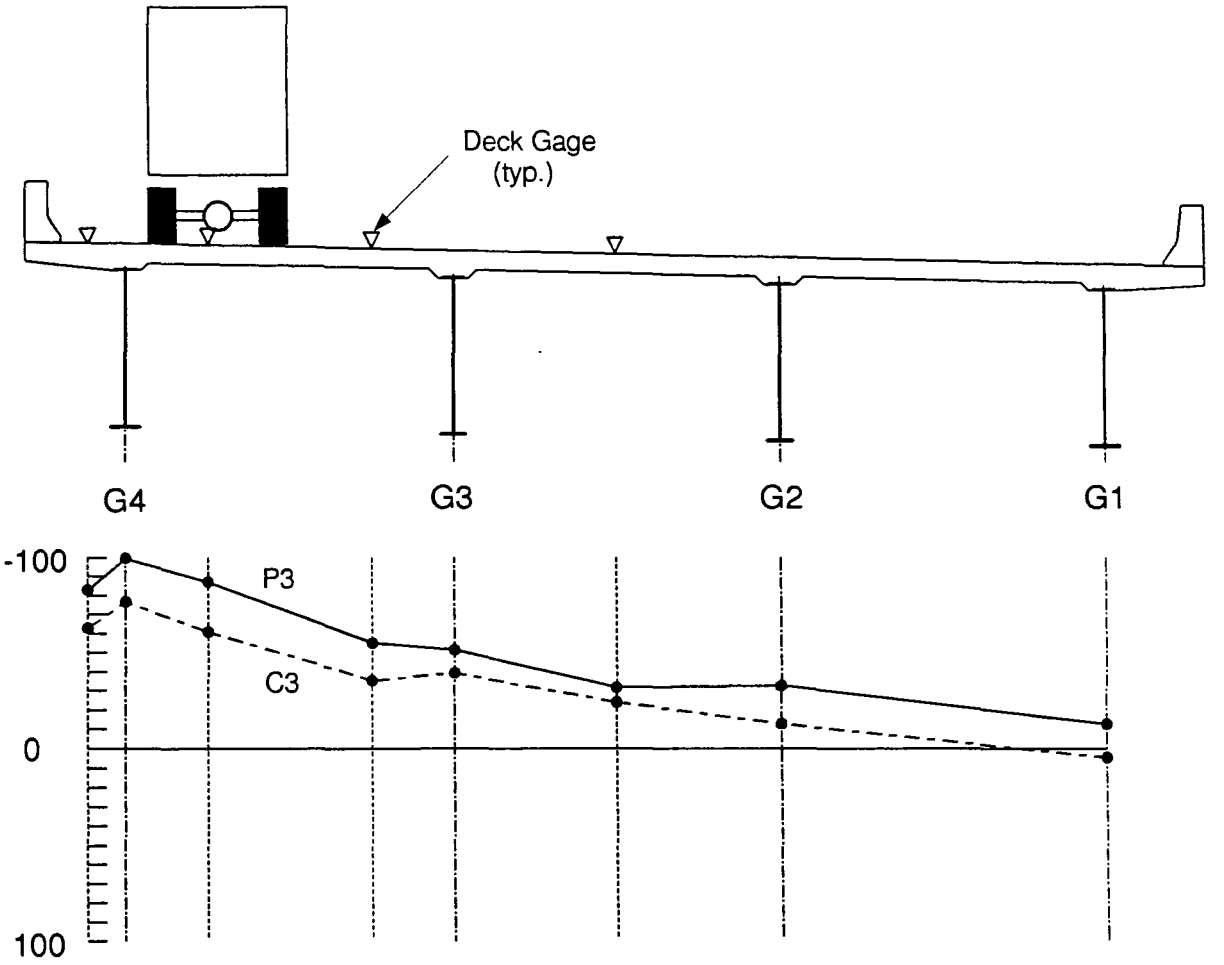

Run Designation	Location							
	342NL (μ in/in)	342 (μ in/in)	342SL (μ in/in)	332NL (μ in/in)	332 (μ in/in)	332SL (μ in/in)	322 (μ in/in)	312 (μ in/in)
C3	-63.0	-76.7	-60.9	-35.5	-39.3	-24.0	-12.9	4.5
P3	-82.9	-99.6	-87.1	-55.0	-51.4	-31.7	-32.7	-12.8

Fig. 5.24 Strain Distribution on Deck, Middle of Span 3 (3 X 2) , C3 and P3

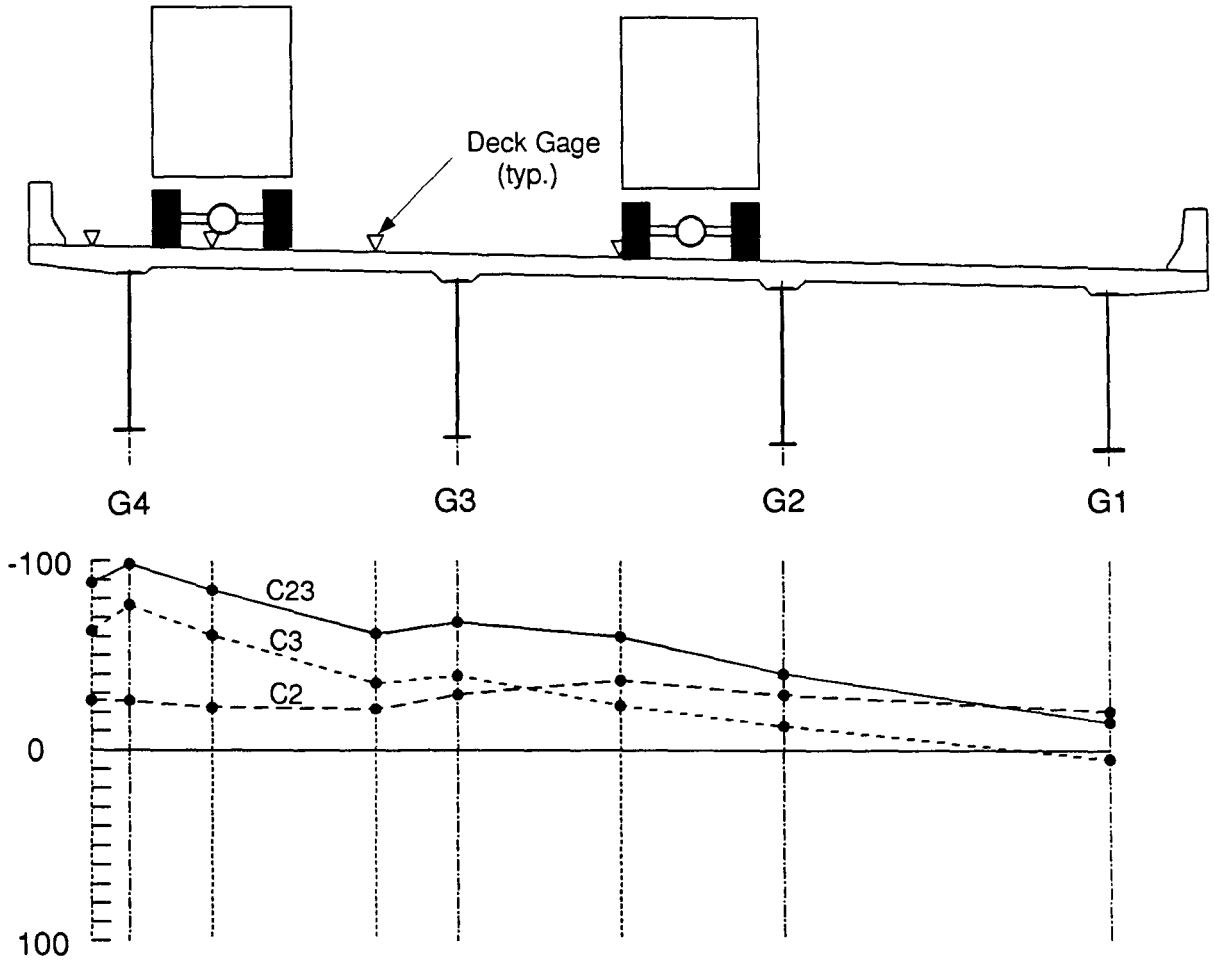

Run Designation	Location							
	342NL (μ in/in)	342 (μ in/in)	342SL (μ in/in)	332NL (μ in/in)	332 (μ in/in)	332SL (μ in/in)	322 (μ in/in)	312 (μ in/in)
C2	-26.5	-26.4	-22.9	-22.0	-29.6	-37.1	-29.5	-20.8
C3	-63.0	-76.7	-60.9	-35.5	-39.3	-24.0	-12.9	4.5
C23	-88.5	-98.4	-84.9	-61.6	-67.7	-60.0	-40.4	-15.0

Fig. 5.25 Strain Distribution on Deck, Middle of Span 3 (3 X 2) , C2, C3 and C23

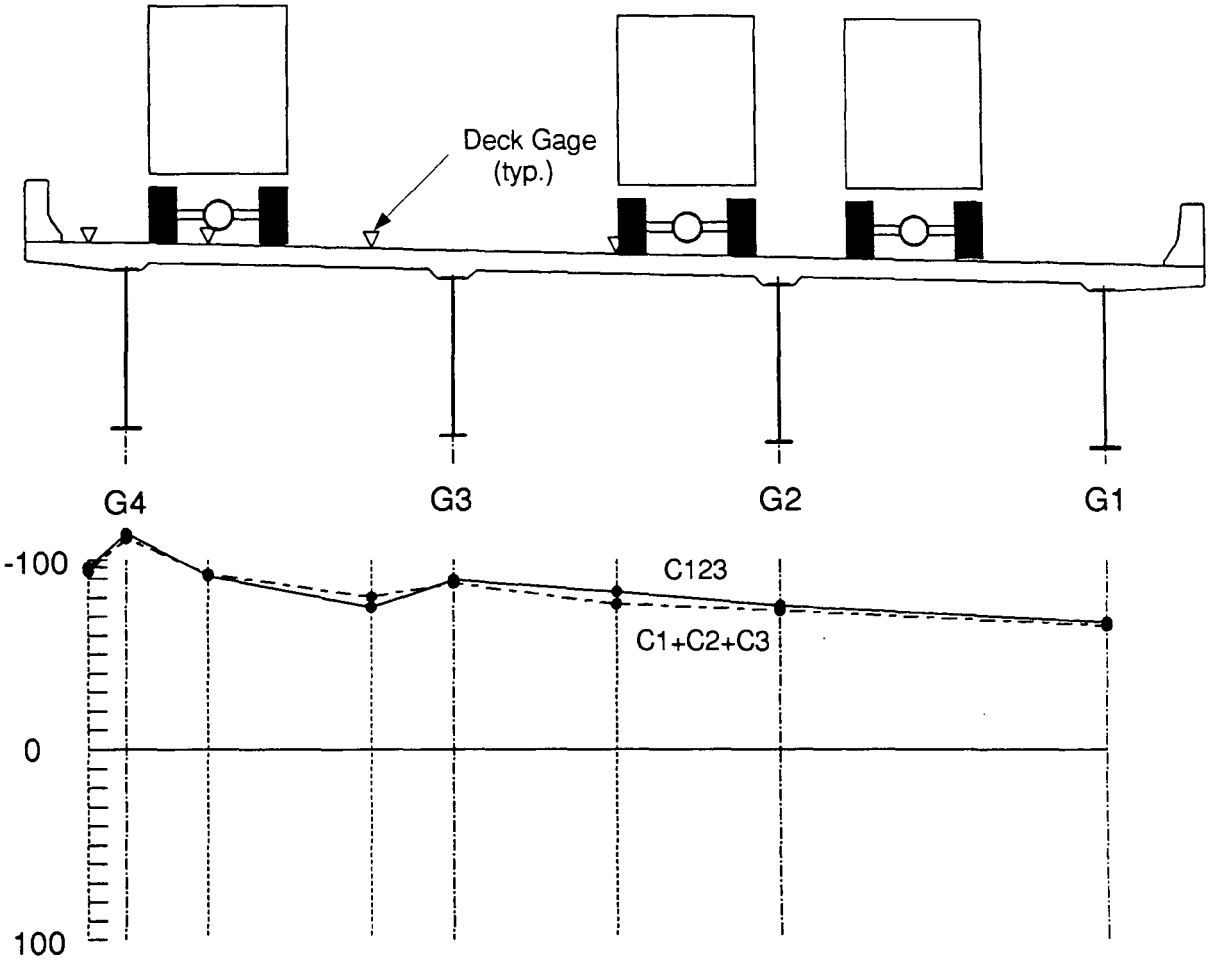

Run Designation	Location							
	342NL (μ in/in)	342 (μ in/in)	342SL (μ in/in)	332NL (μ in/in)	332 (μ in/in)	332SL (μ in/in)	322 (μ in/in)	312 (μ in/in)
C123	-94.0	-111.3	-92.5	-80.3	-87.6	-76.4	-73.0	-65.1
C1+C2+C3	-96.1	-113.9	-91.5	-74.8	-89.3	-82.9	-75.5	-66.9

Fig. 5.26 Strain Distribution on Deck, Middle of Span 3 (3 X 2) , C123

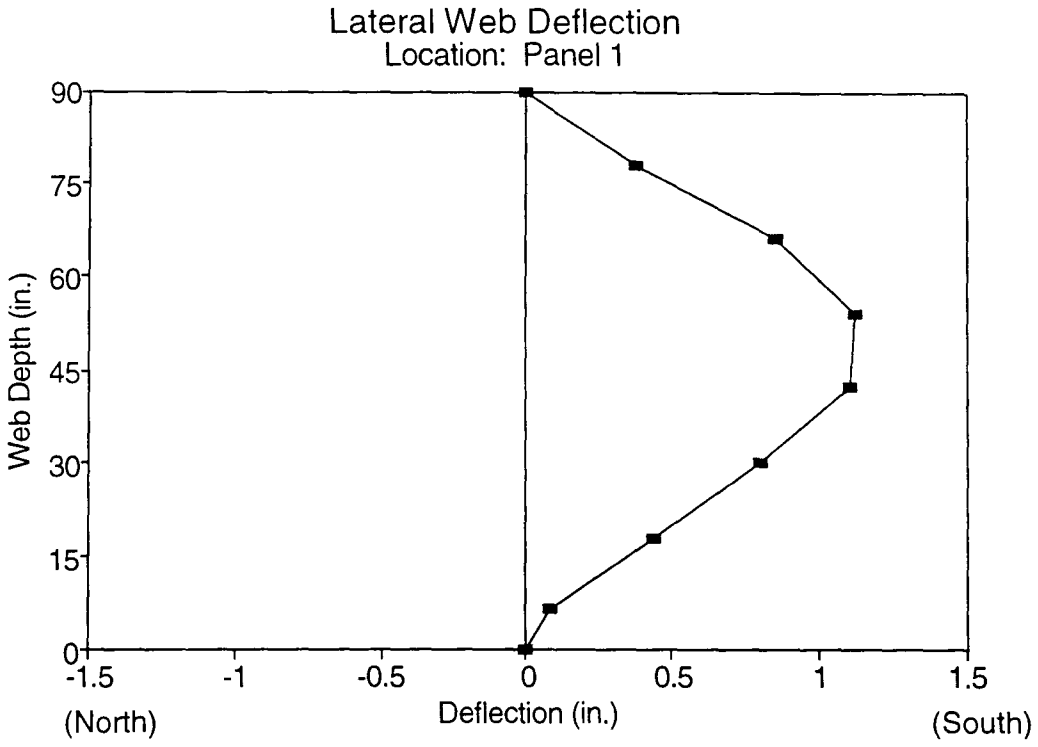

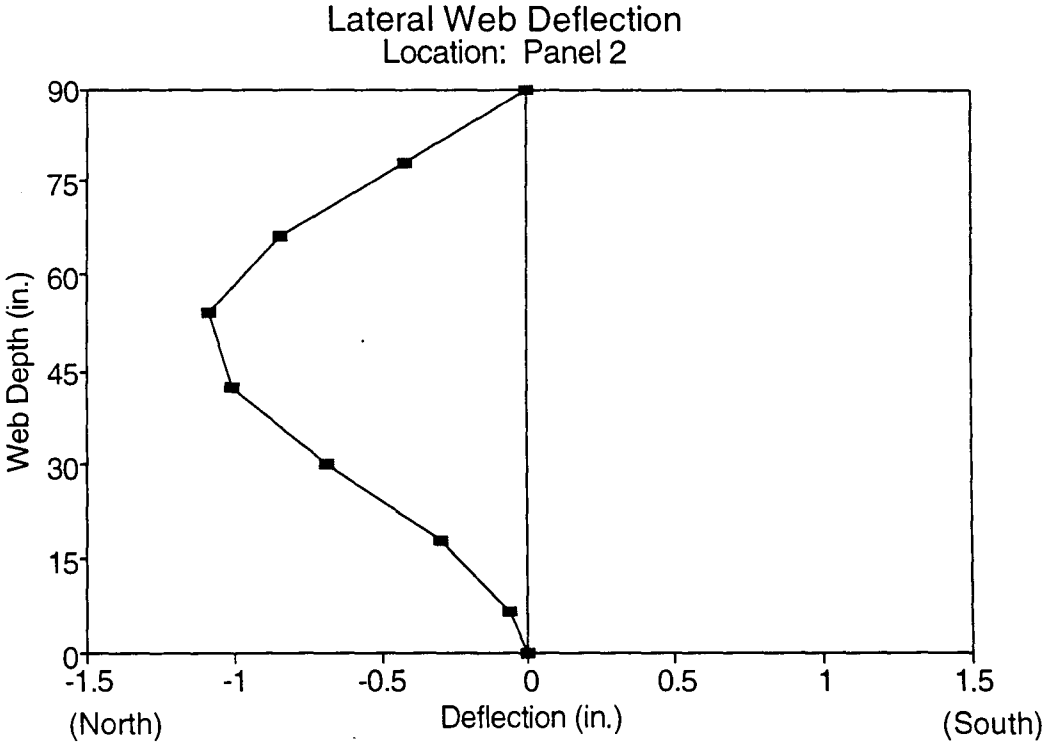

Fig. 5.27 Lateral Web Deflection under Dead Load, at Section 432

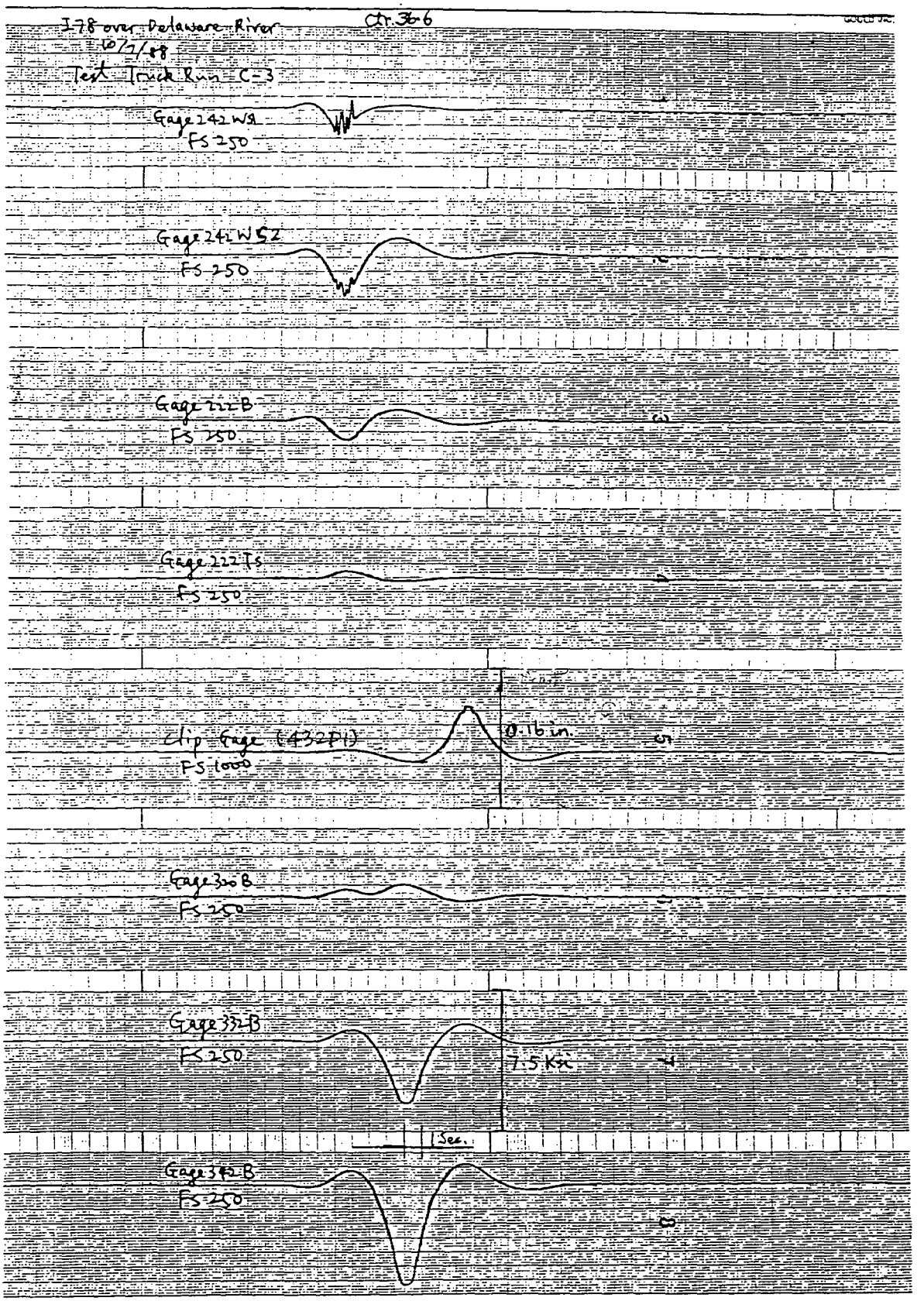

Fig. 5.28 Variation of Web Deflection (Chip Gage) and Strains, Test Truck Run C3

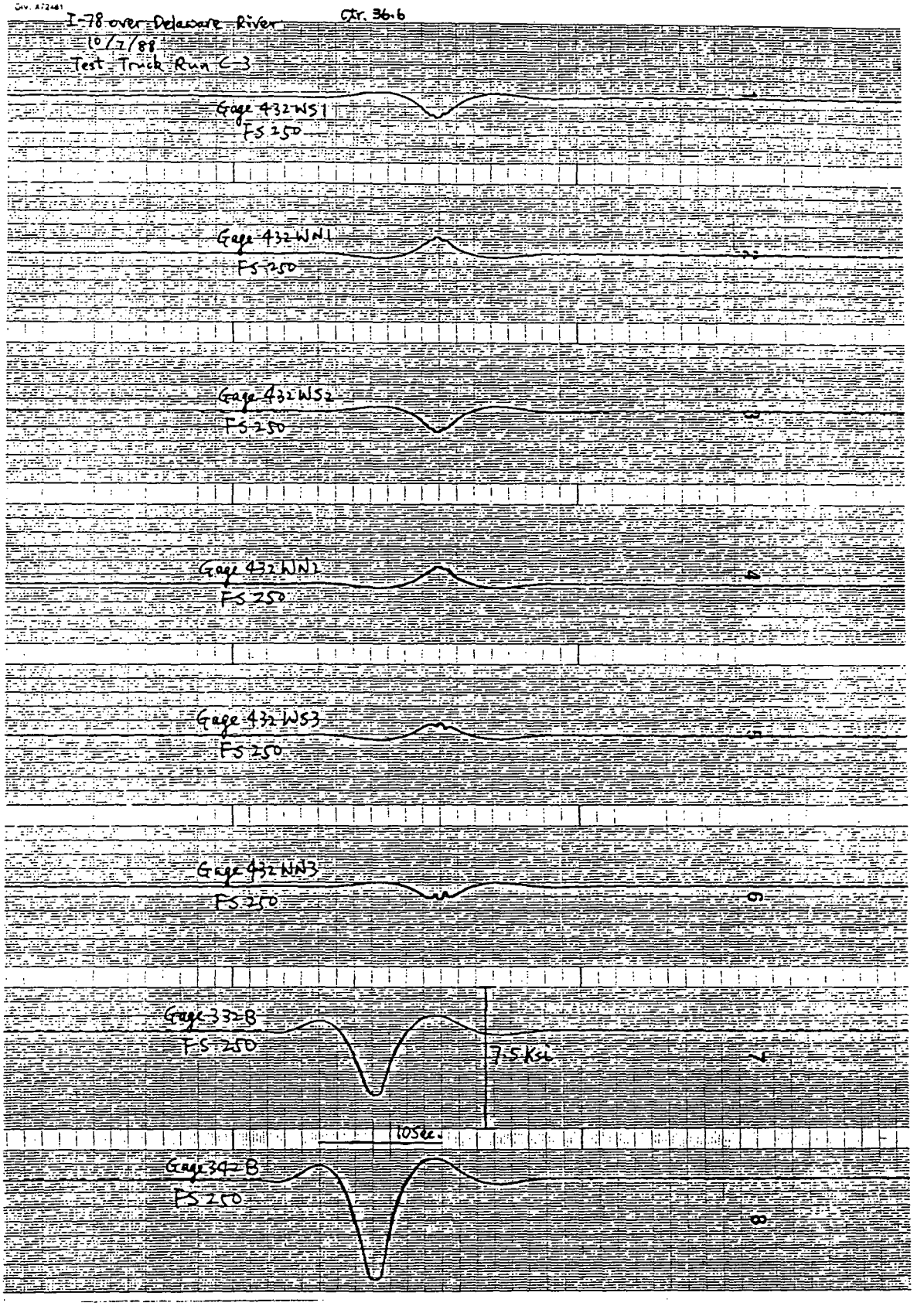

Fig. 5.29 Strain-Time Variation, Web Strain Gage Pairs at 432

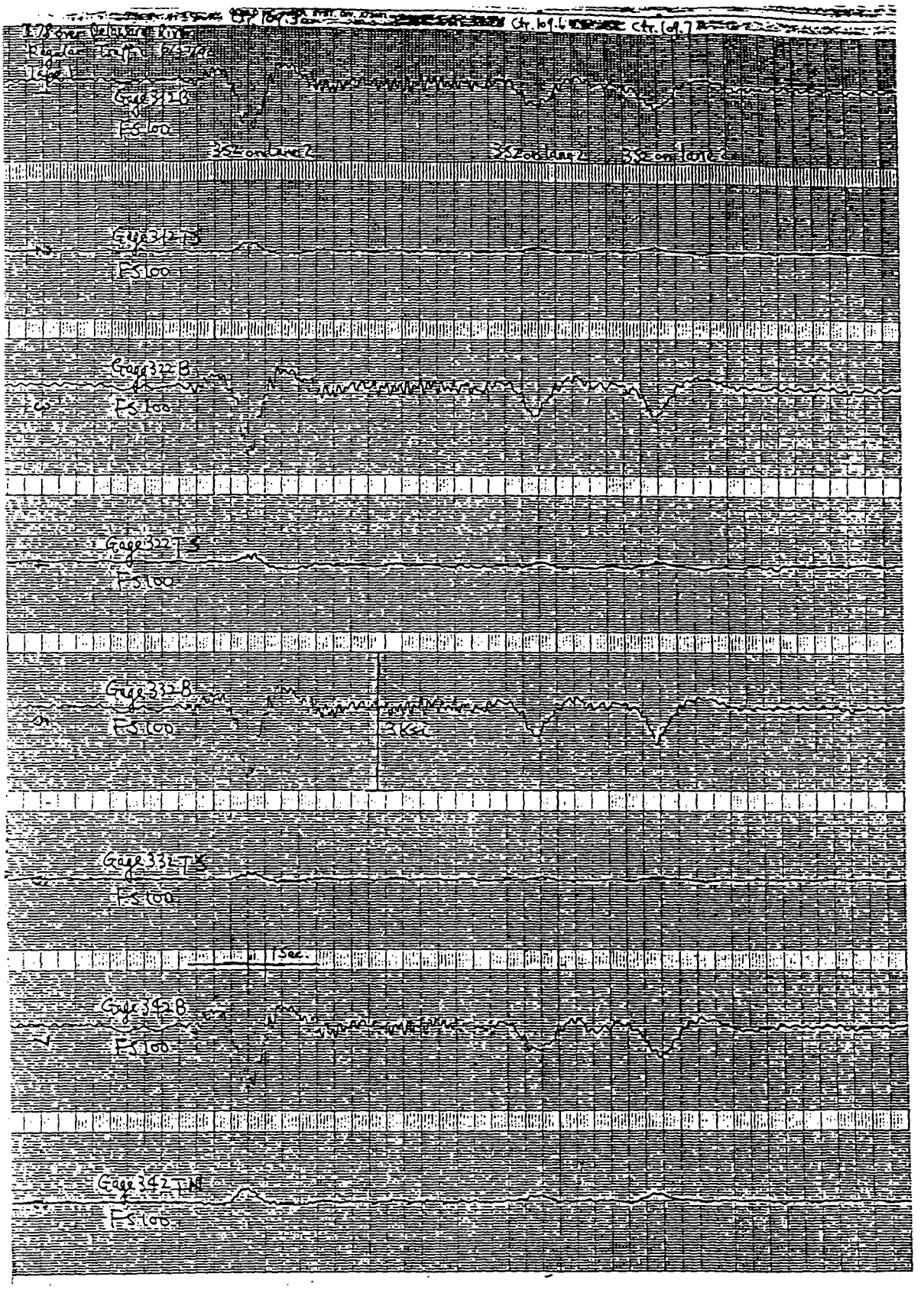

Fig. 6.1 Strain-Time Variation due to Regular 352 Trucks, at 3X2

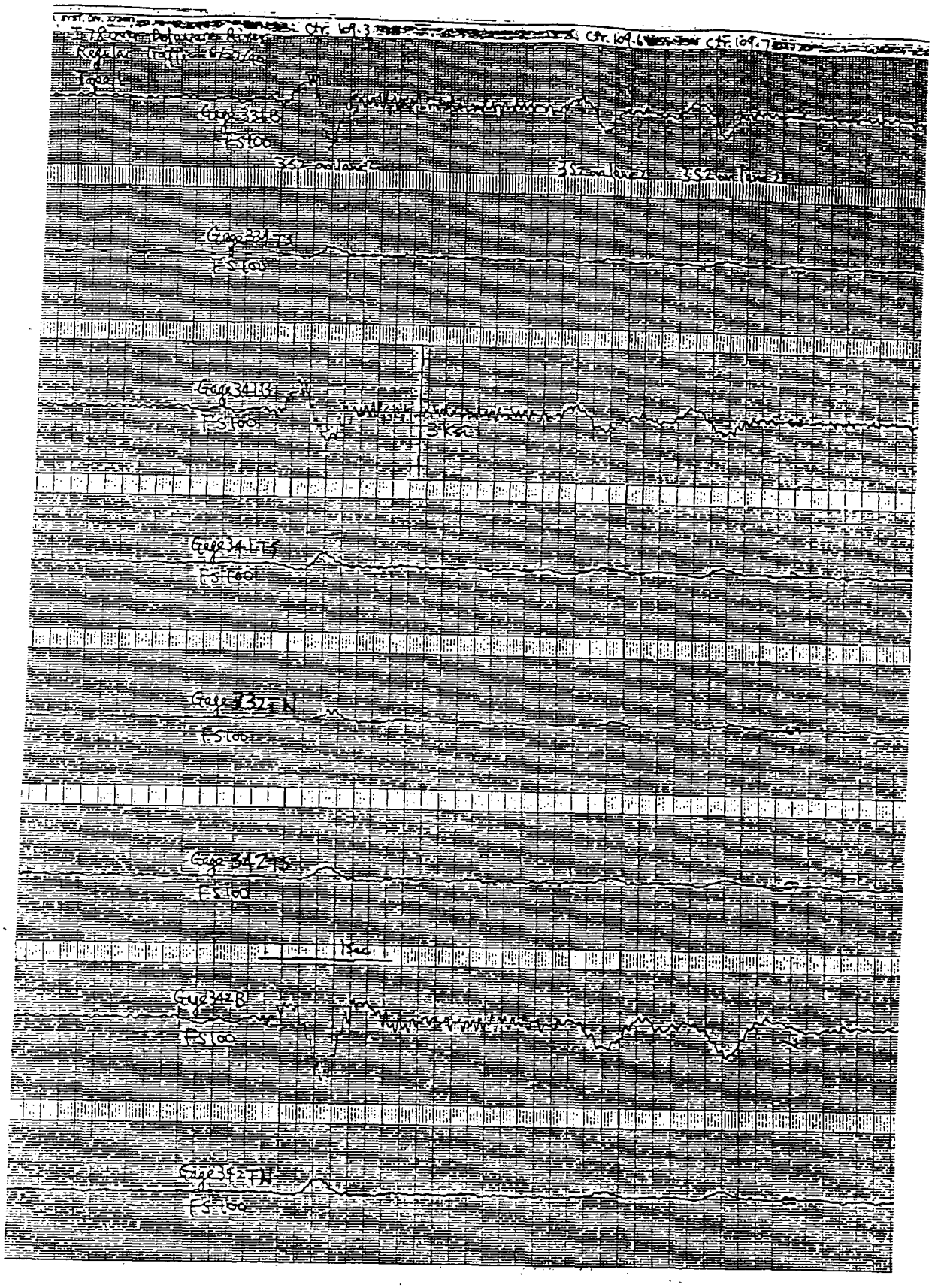

Fig. 6.2 Strain-Time Variation due to Regular 332 Trucks, at 3X1

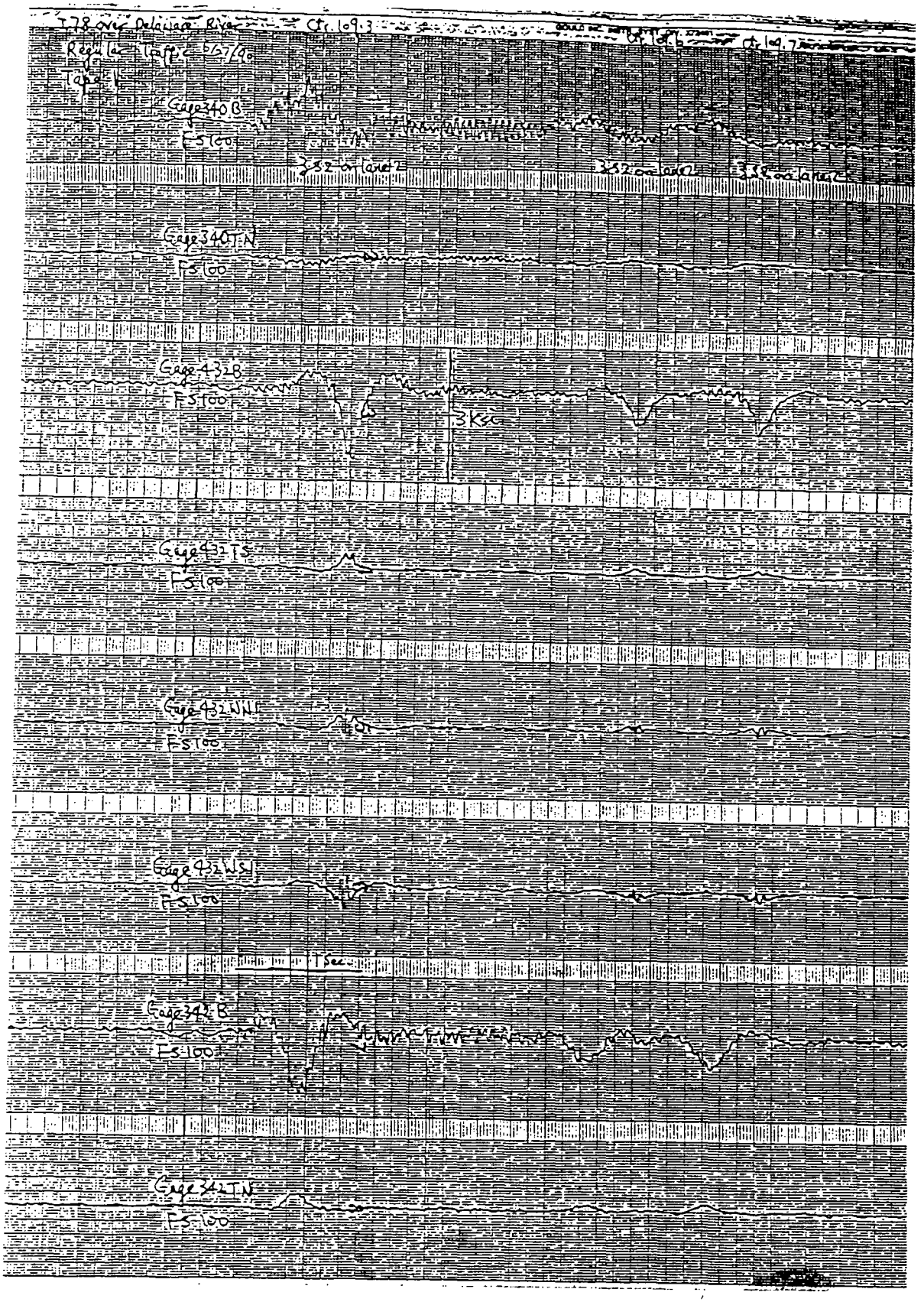

Fig. 6.3 Strain-Time Variation due to Regular 332 Trucks, at 432

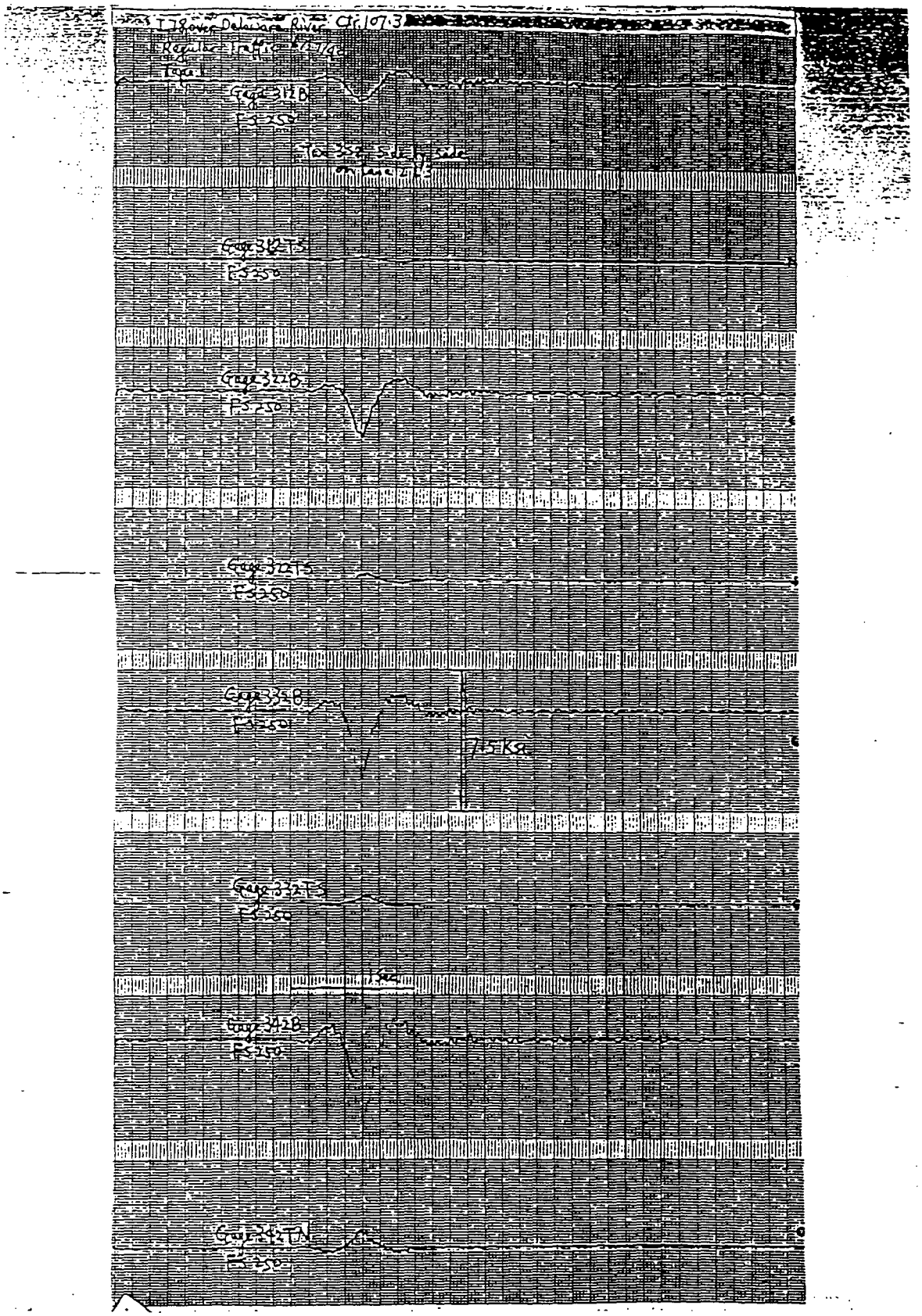

Fig. 6.4 Strain due to two 322 Trucks Side-by-Side, at 3X2

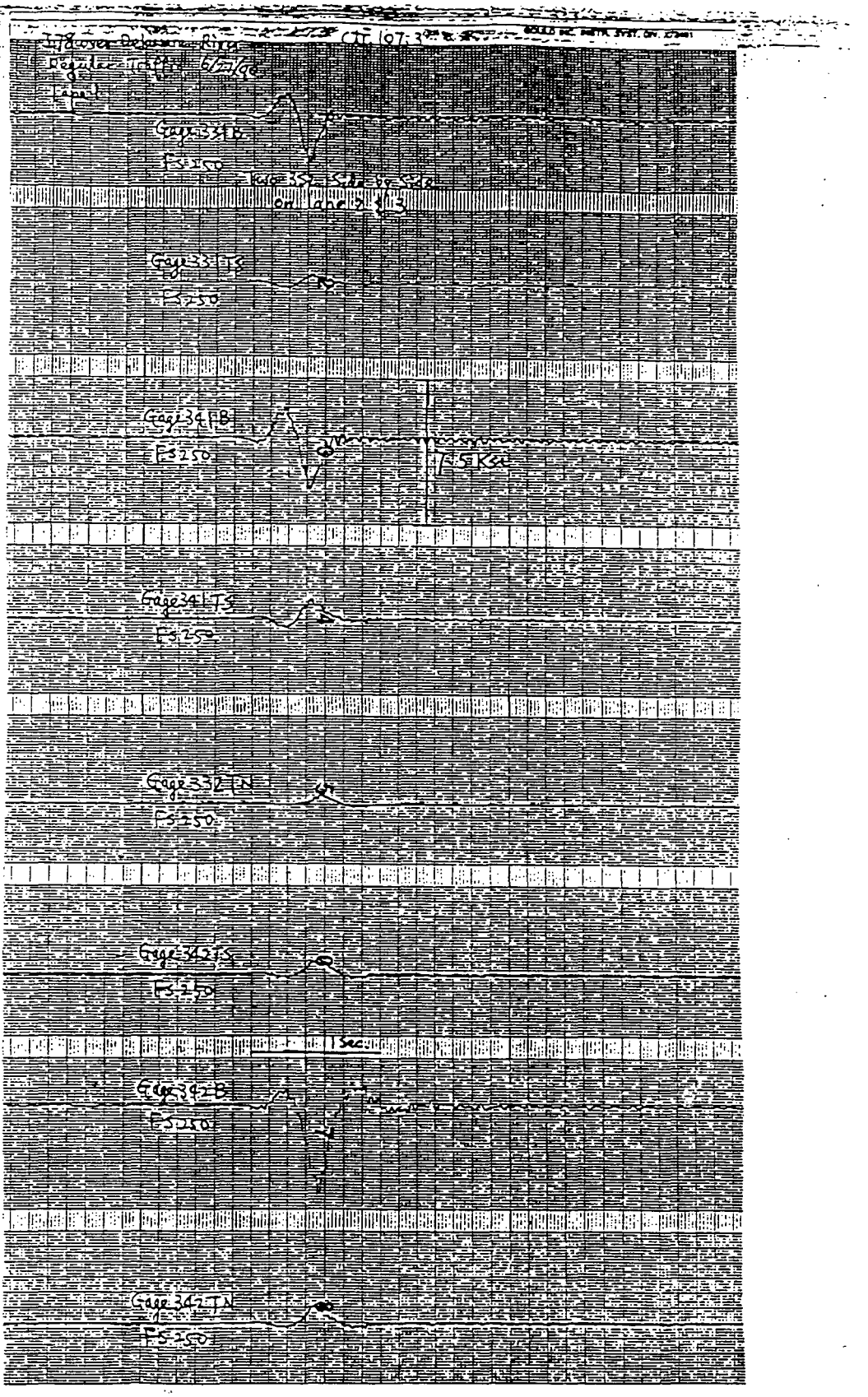

Fig. 6.5 Strain due to two 322 Trucks Side-by-Side, at 3X1

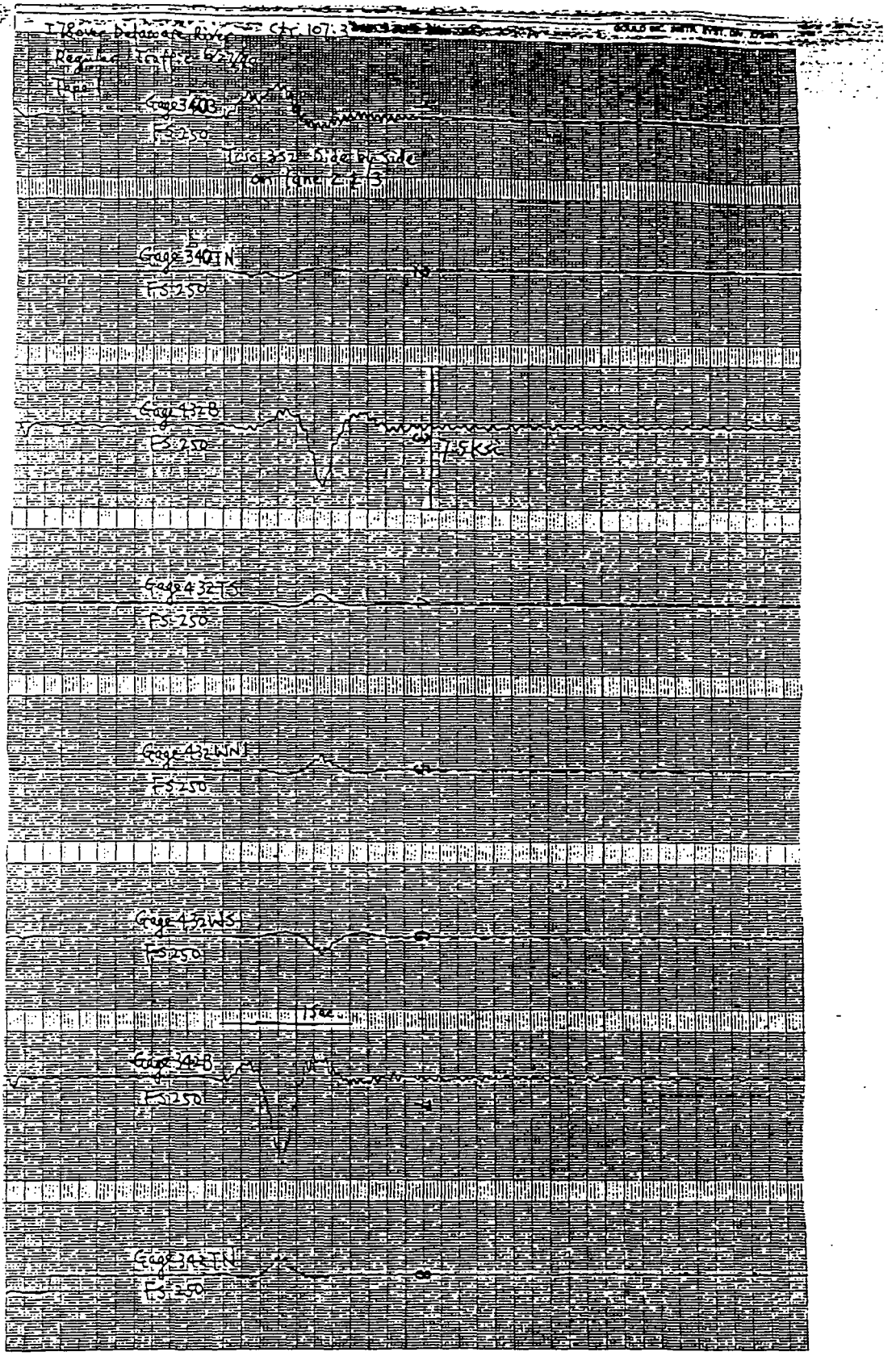

Fig. 6.6 Strain due to two 322 Trucks Side-by-Side, at 432

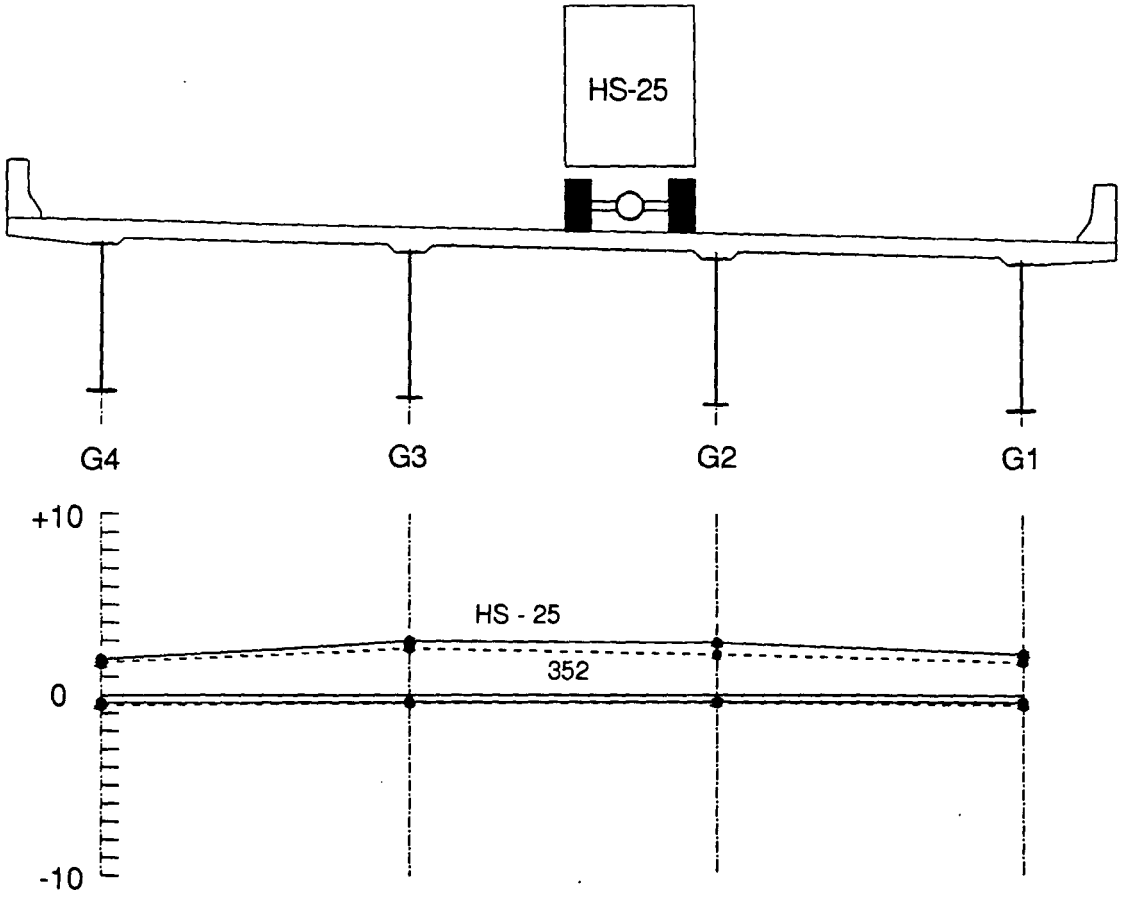

Truck	Flange	Location			
		342 (ksi)	332 (ksi)	322 (ksi)	312 (ksi)
Simulated HS-25	Top	-0.42	-0.37	-0.39	-0.39
	Bottom	1.98	2.99	2.89	2.28
352	Top	-0.39	-0.24	-0.34	-0.28
	Bottom	1.95	2.24	2.19	1.81

Fig. 6.7 Distribution of Stresses, Middle of Span 3 (3 X 2), C2 and R2

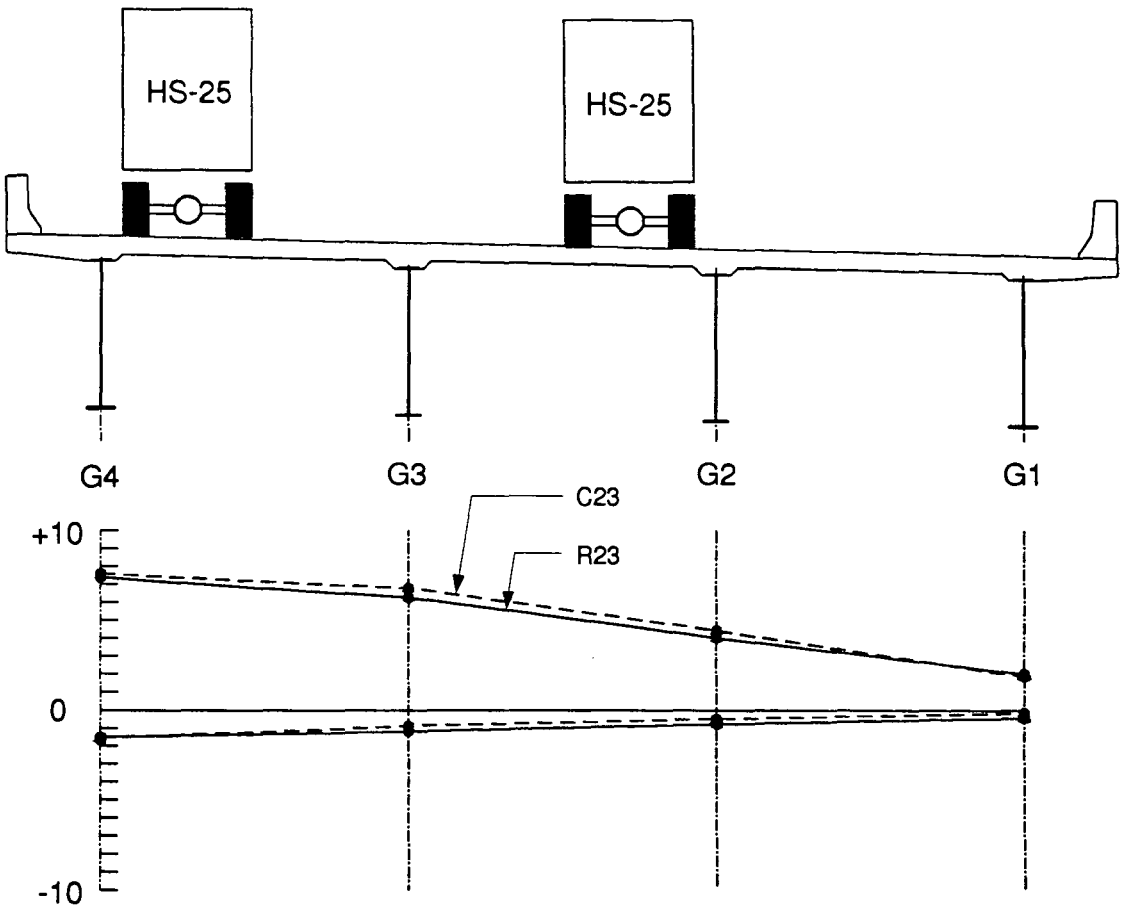

Truck Run	Flange	Location			
		342 (ksi)	332 (ksi)	322 (ksi)	312 (ksi)
C23	Top	-1.53	-0.86	-0.47	-0.14
	Bottom	7.60	6.78	4.42	1.88
R23	Top	-1.17	-0.52	-0.60	-0.28
	Bottom	6.17	5.09	3.51	1.91

Fig. 6.8 Distribution of Stresses, Middle of Span 3 (3 X 2) , C23 and R23

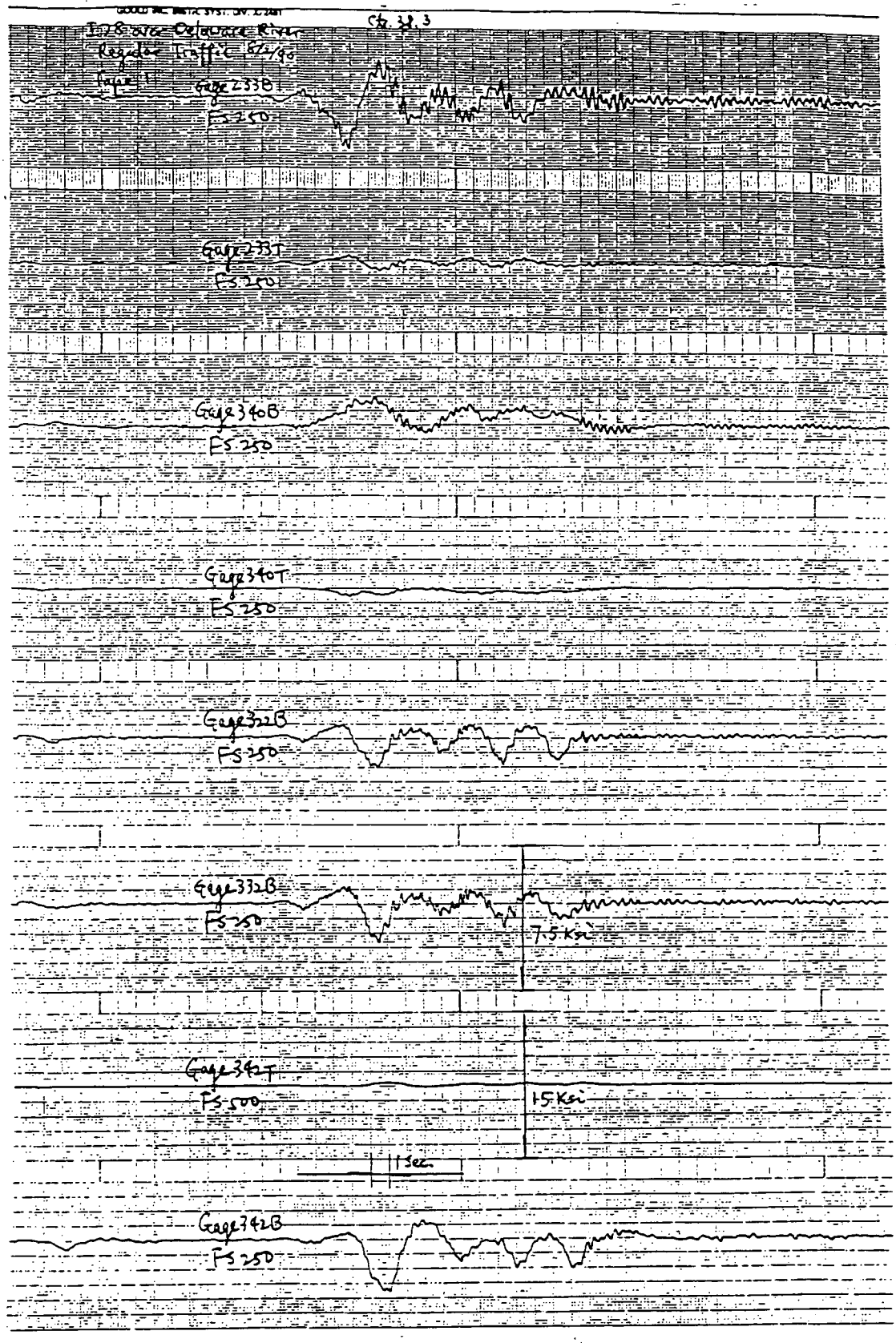

Fig. 6.9 Strain due to Trucks in Tandem, Spans 2 and 3

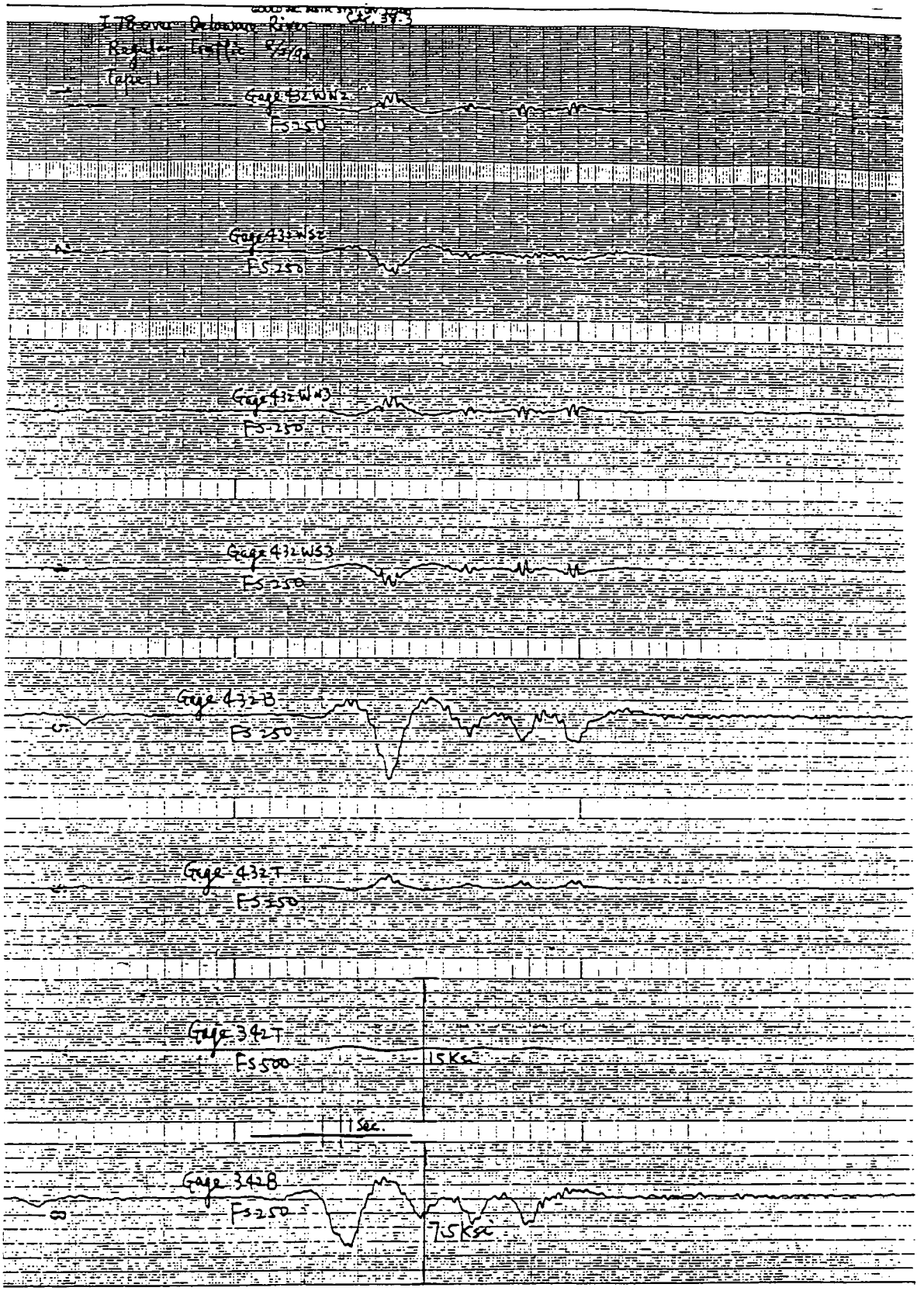

Fig. 6.10 Strains due to Trucks in Tandem, at 432

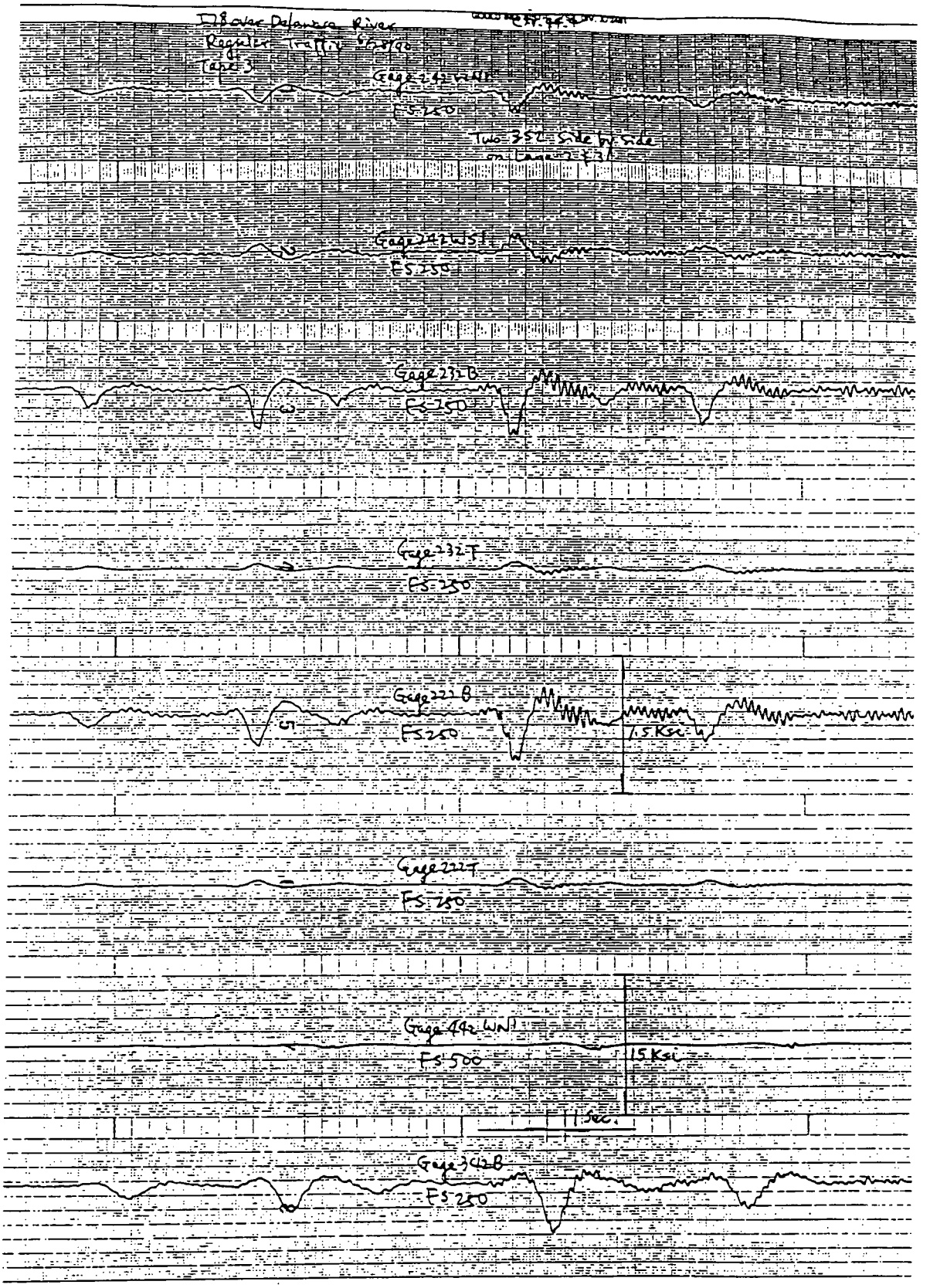

Fig. 6.11 Strain-Time Traces, Regular Traffic, Span 2

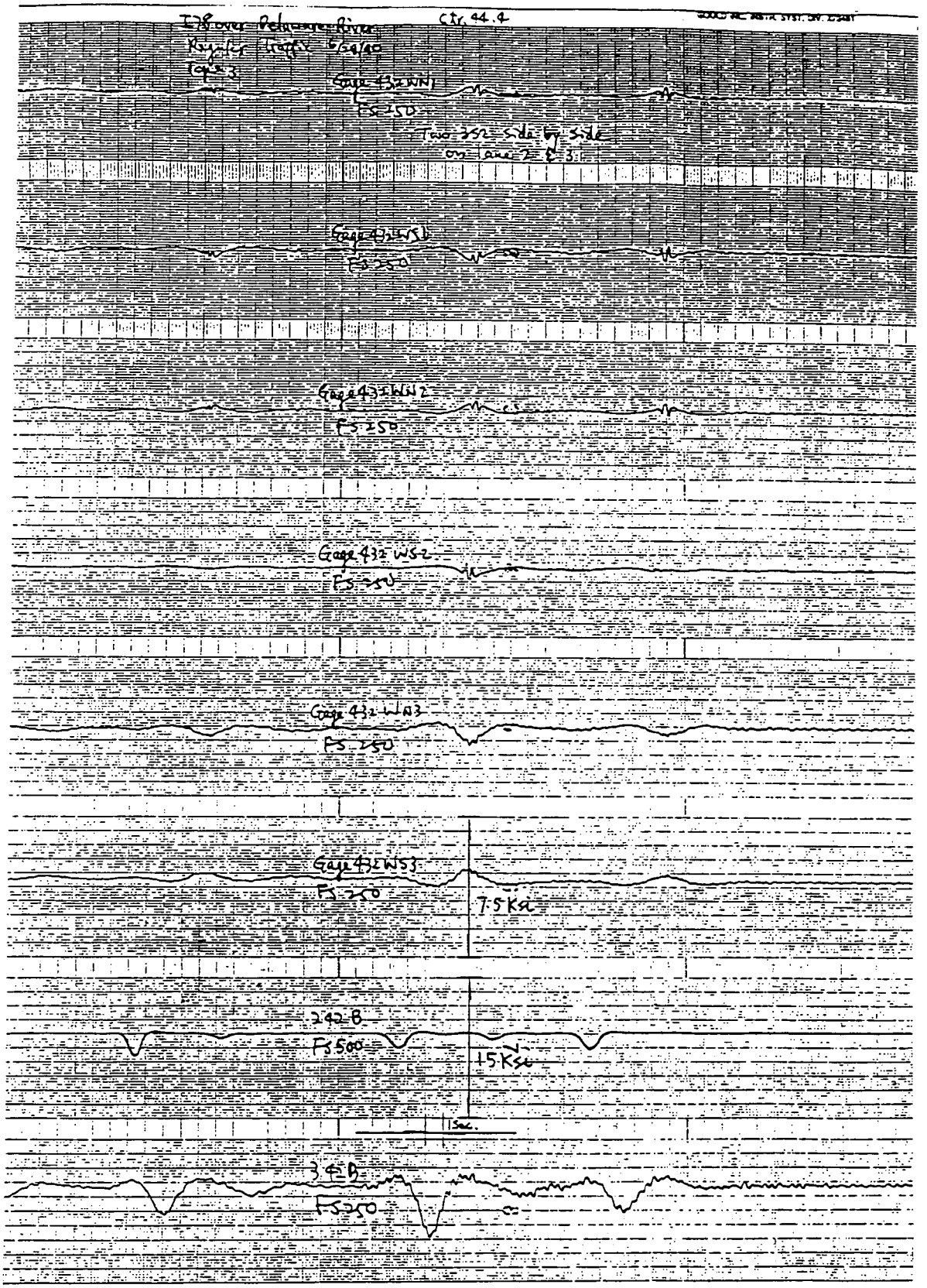

Fig. 6.12 Strain-Time Traces, Regular Traffic, Span 4

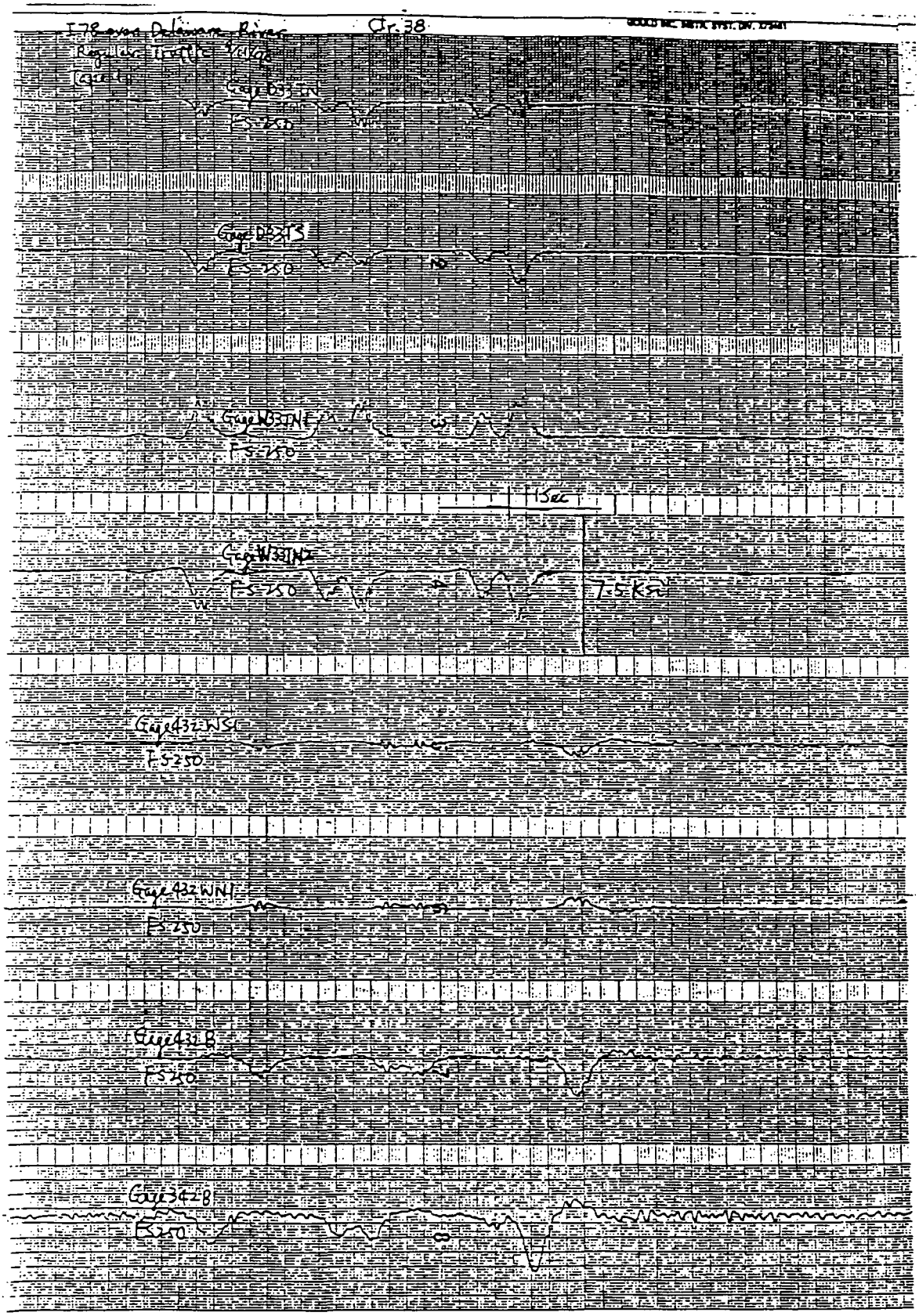

Fig. 6.13 Strain-Time Traces, Regular Traffic, Web Gages at 432

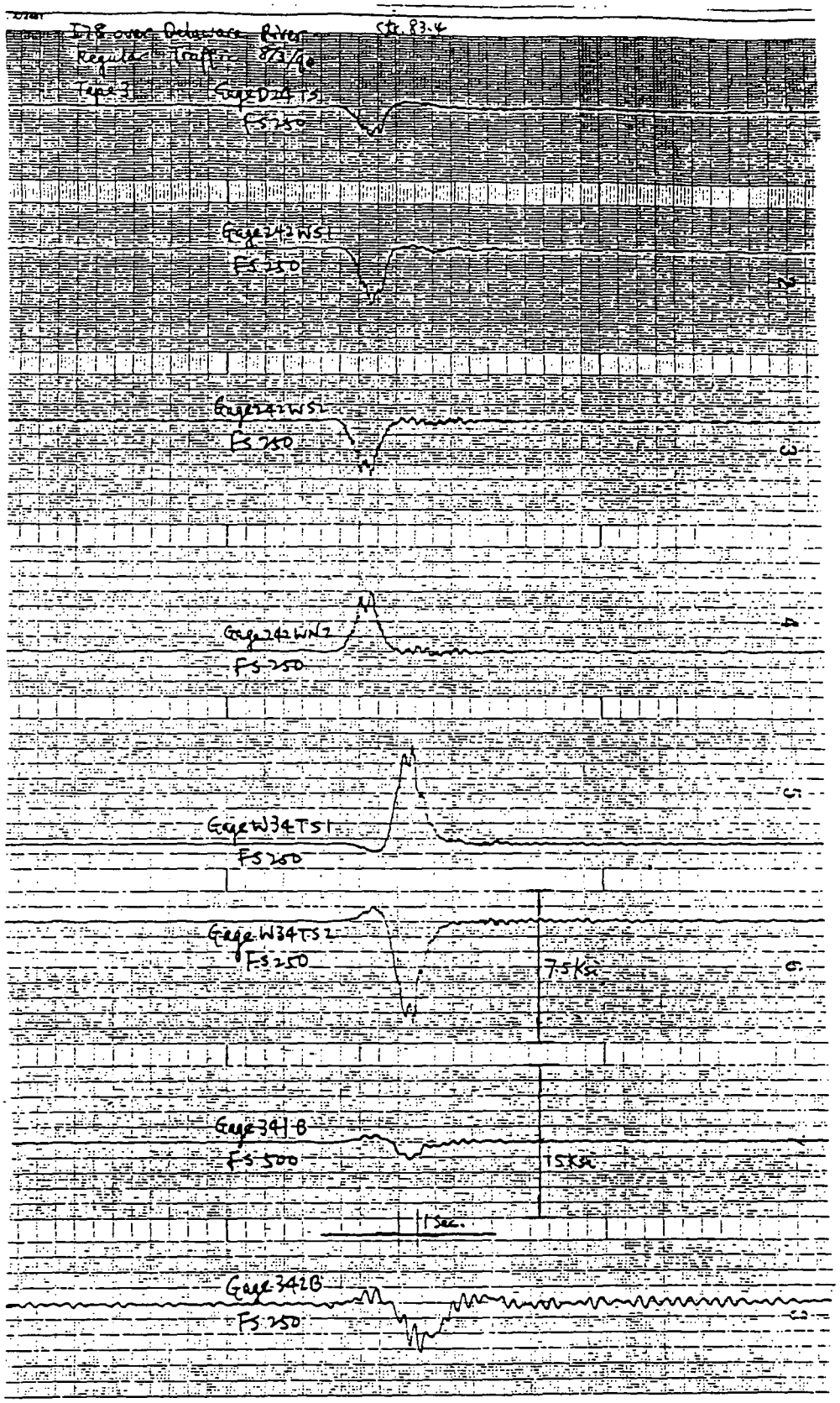

Fig. 6.14 Strain-Time Traces, Regular Traffic, Web Gages at 242

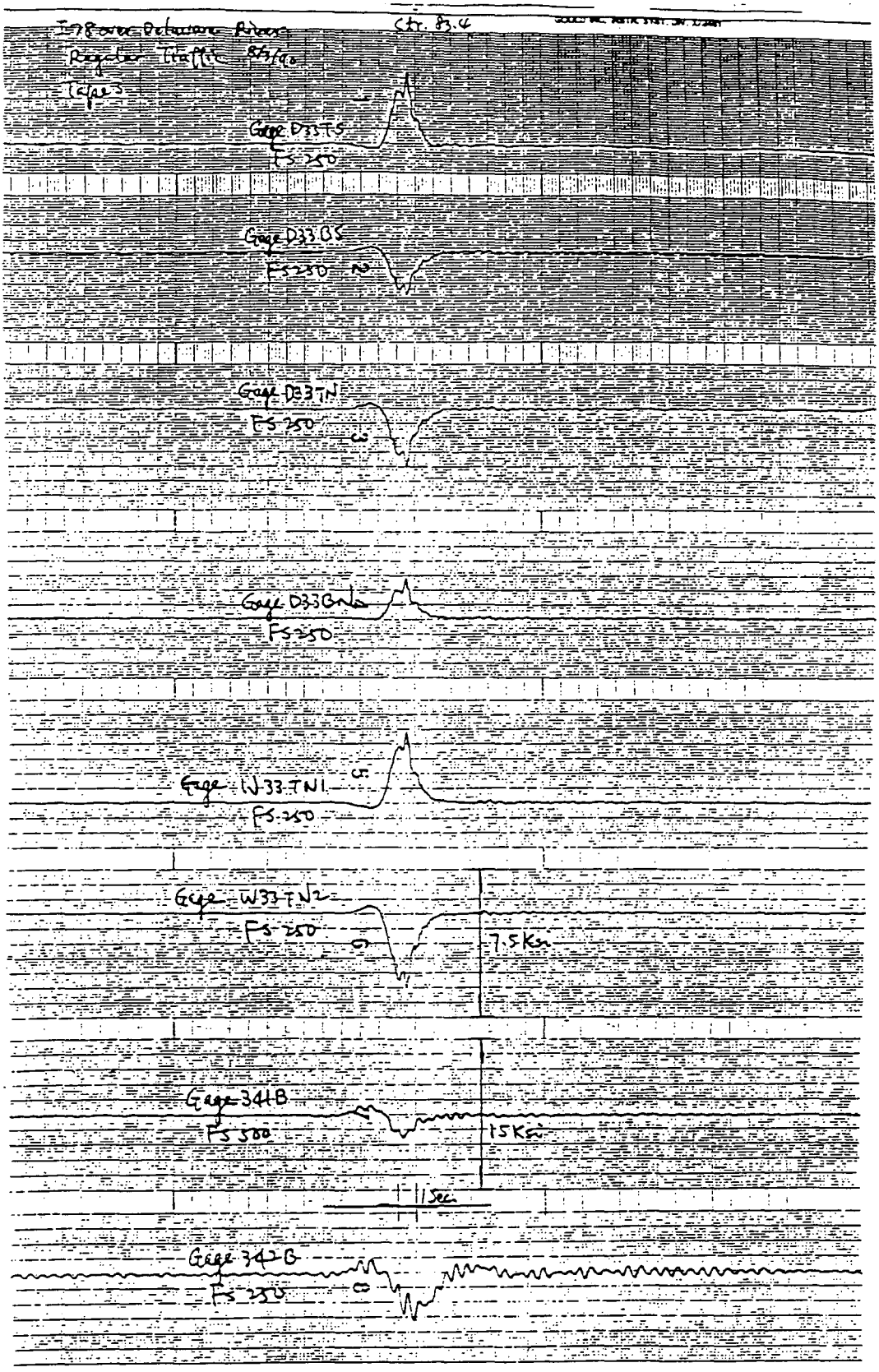

Fig. 6.15 Strain-Time Traces, Regular Traffic, Diaphragm and Web, Span 3

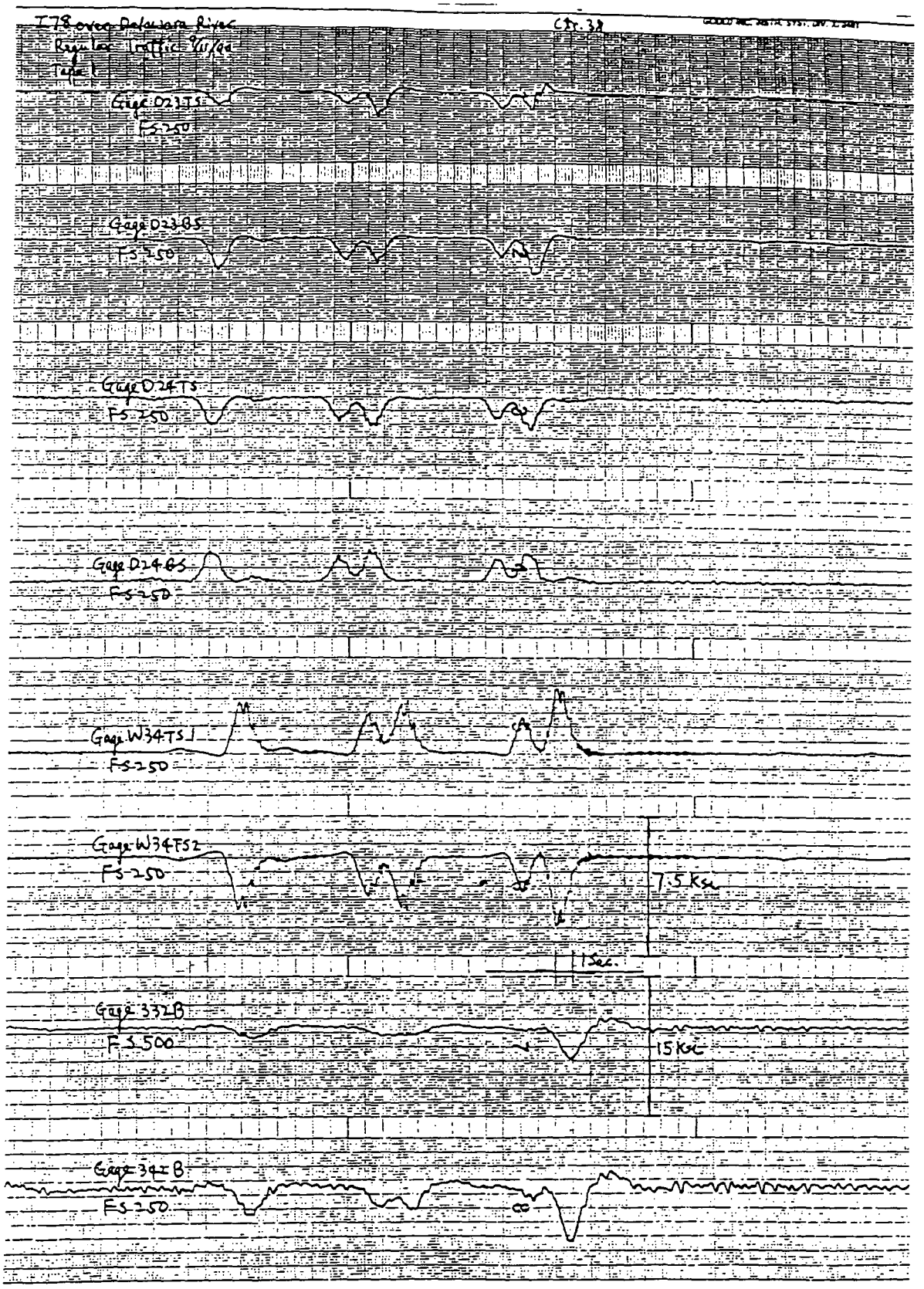

Fig. 6.16 Strain-Time Traces, Regular Traffic, Diaphragm and Web, Span 2

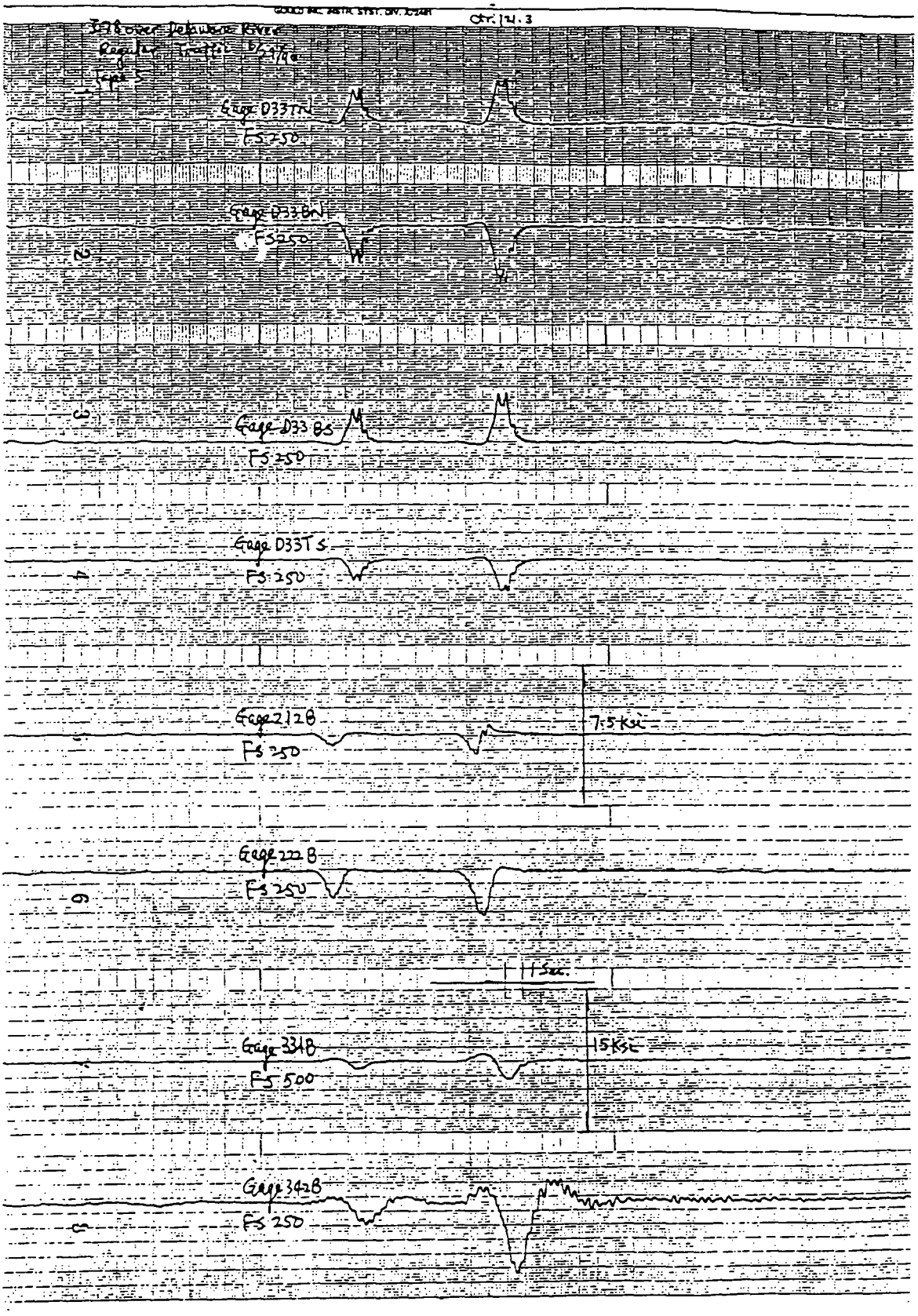

Fig. 6.17 Strain-Time Traces, Regular Traffic, Diaphragm Gages, Span 3

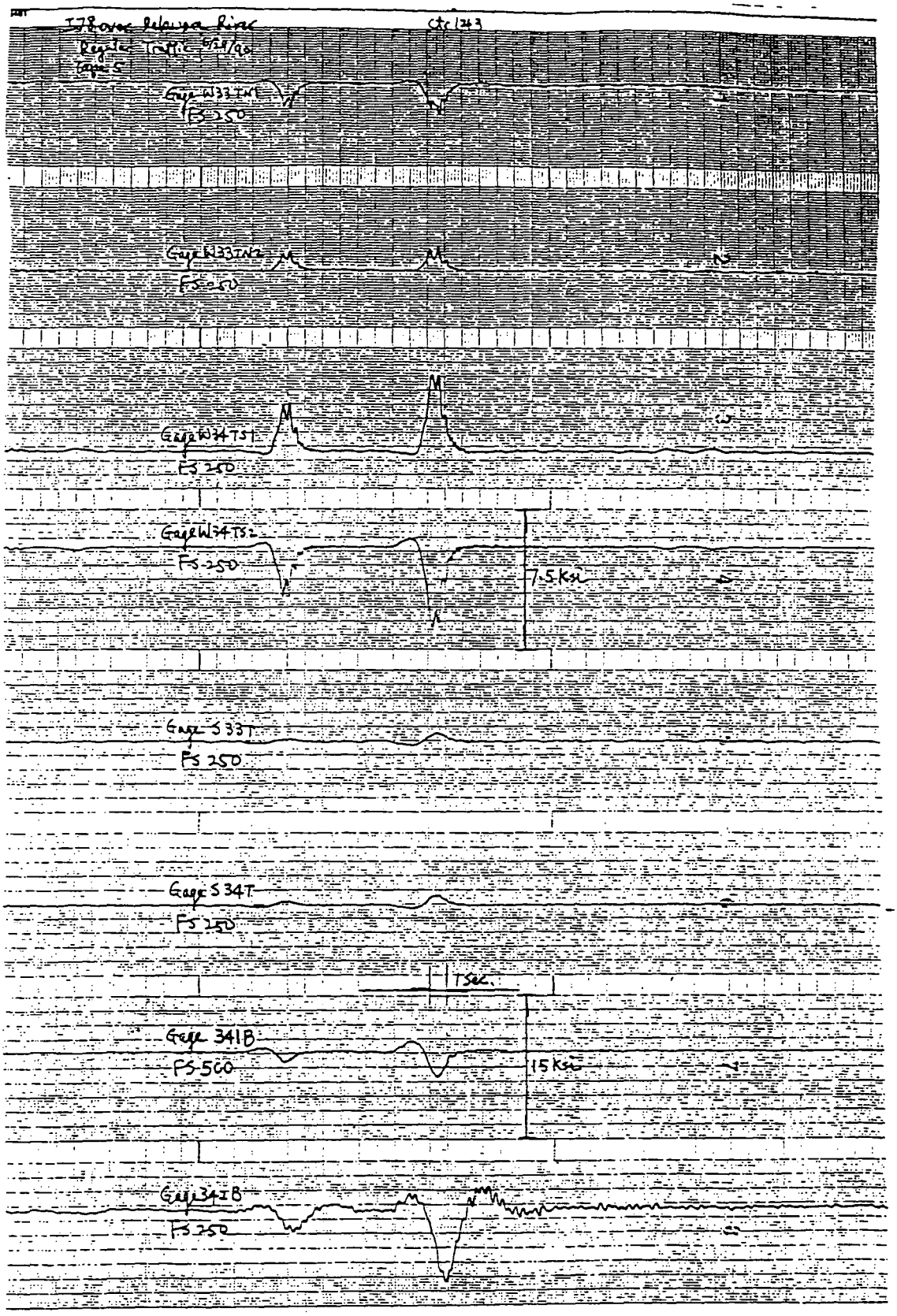

Fig. 6.18 Strain-Time Traces, Regular Traffic, Web Gages, Span 3

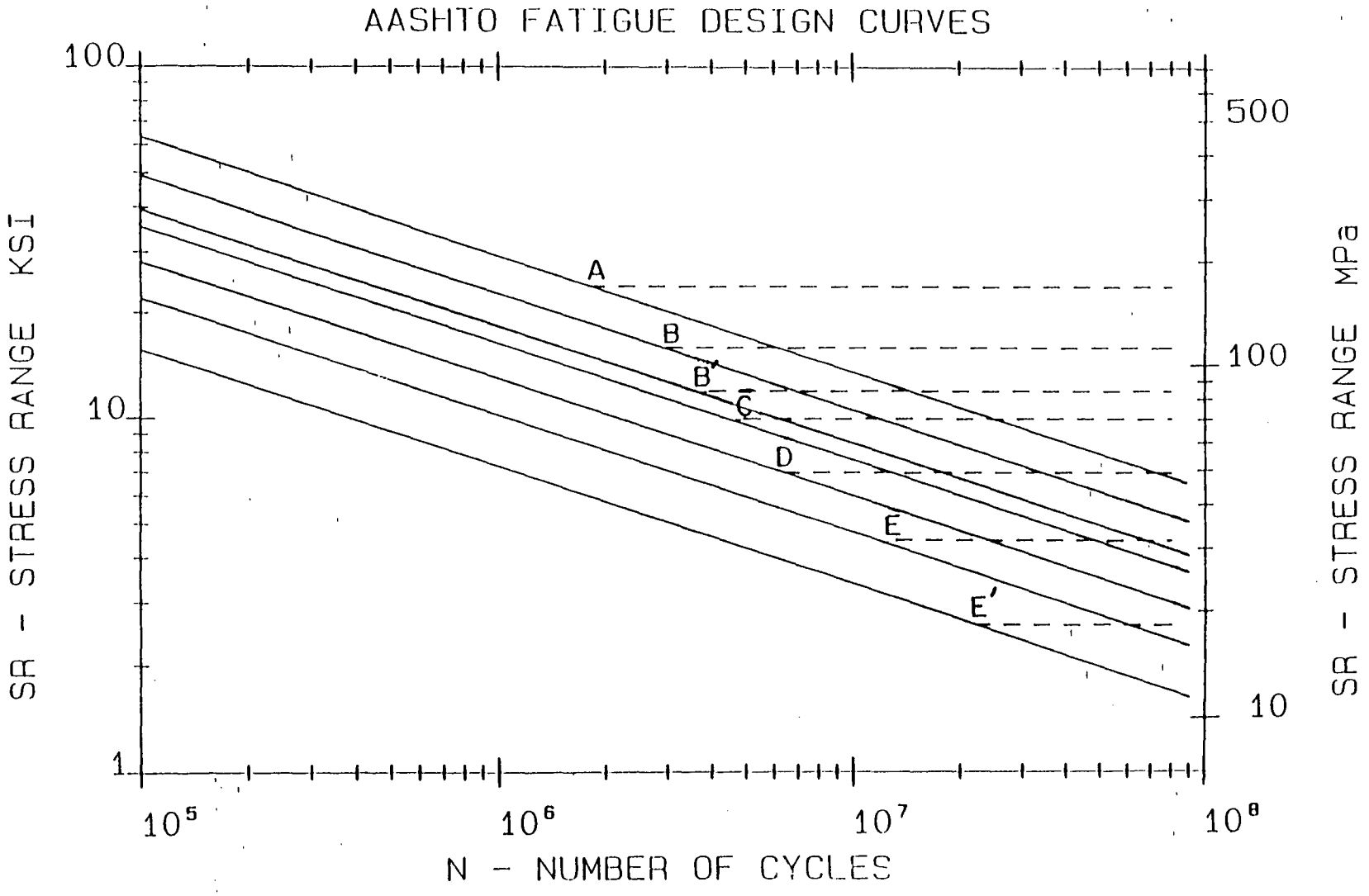

Fig. 7.1 AASHTO Allowable Fatigue Stress Ranges - Redundant Load Path

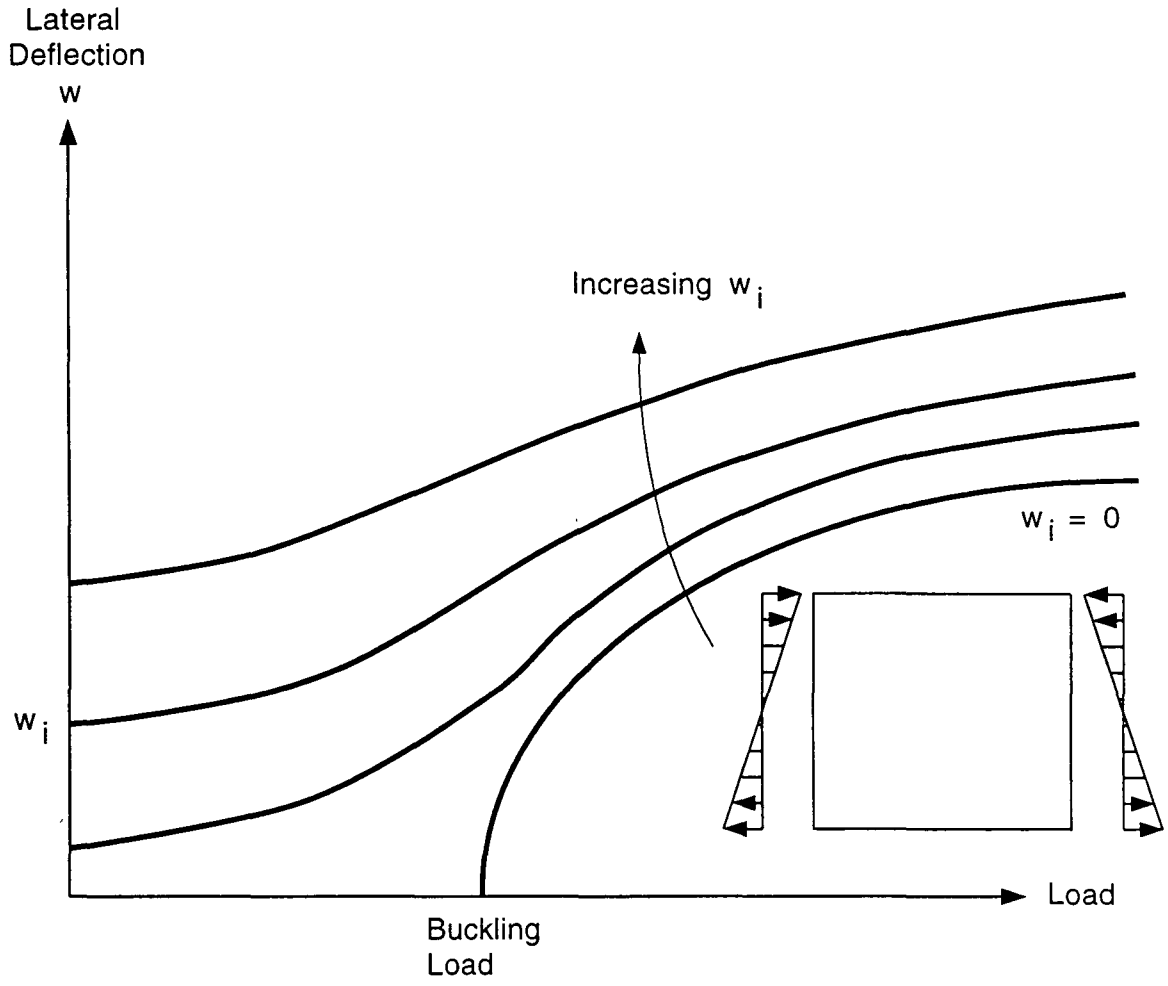

Fig. 7.2 Plate Buckling Load and Lateral Deflection

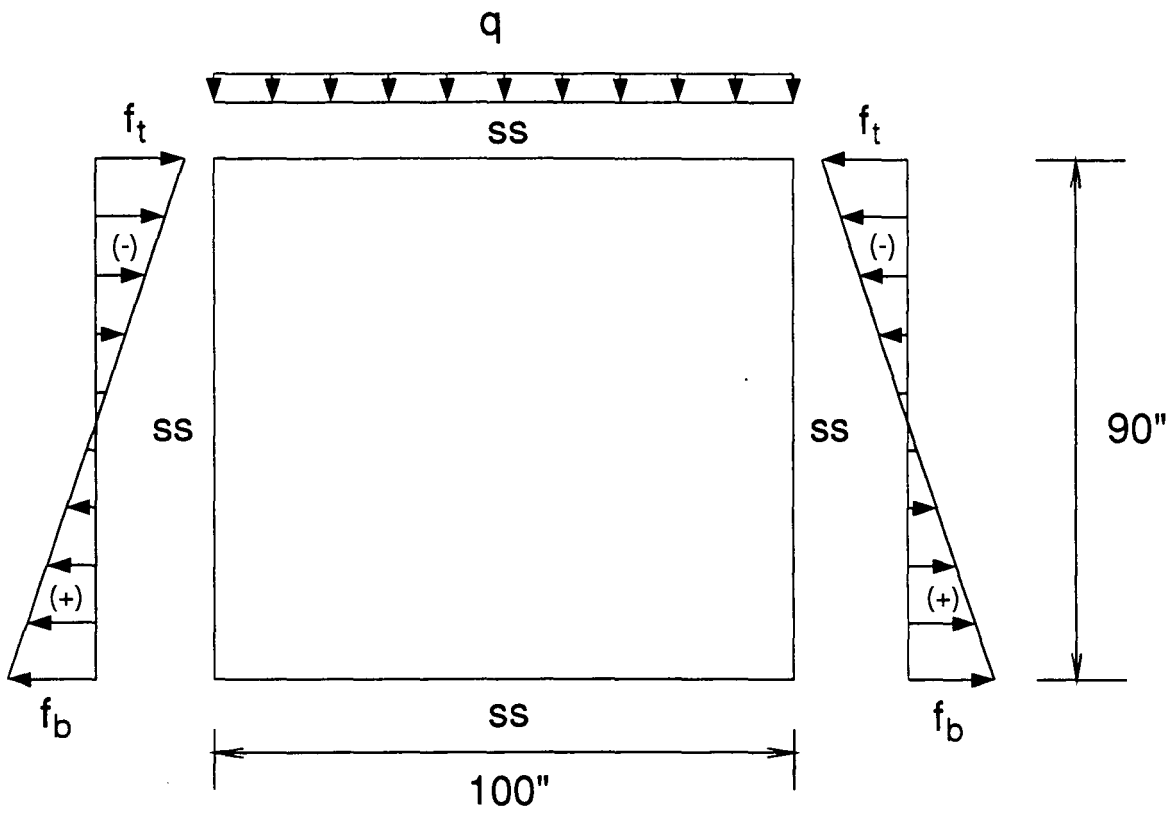

Fig. 7.3 Schematic Loading in Web Panel at Location 432

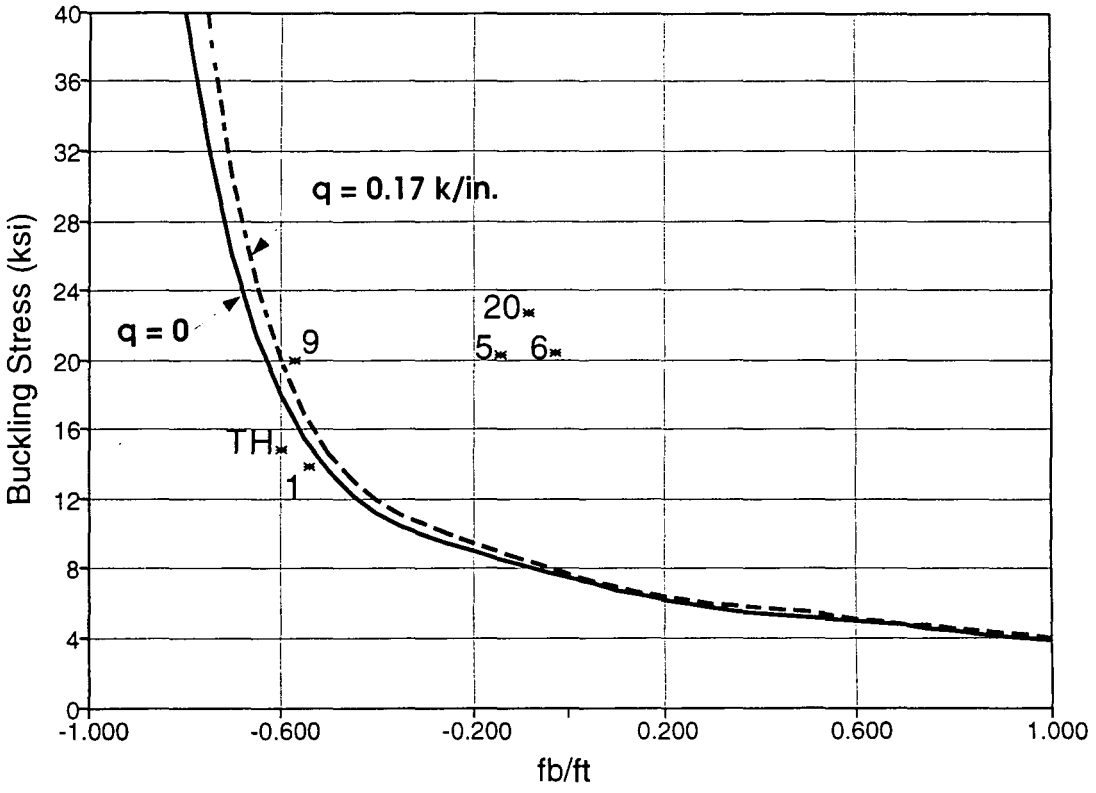

Fig. 7.4 Buckling Stresses

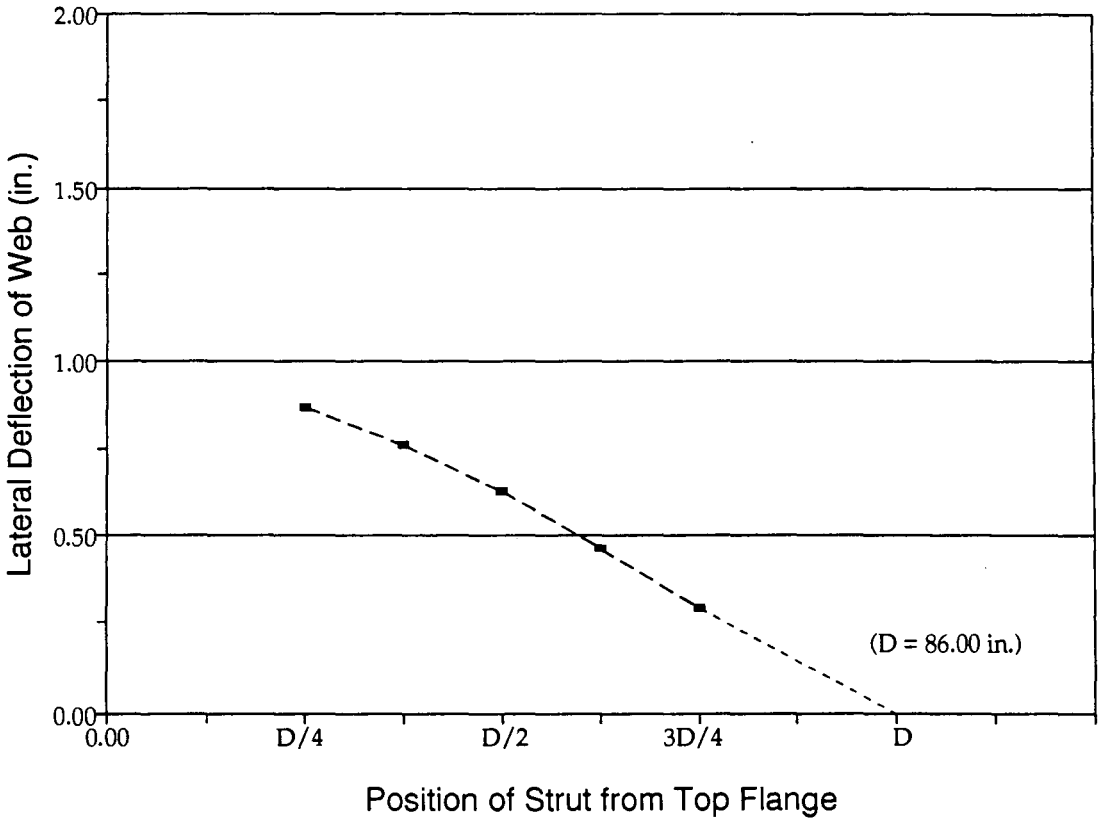

Fig. 7.5 Estimated Web Deflection and Strut Position at Location 242

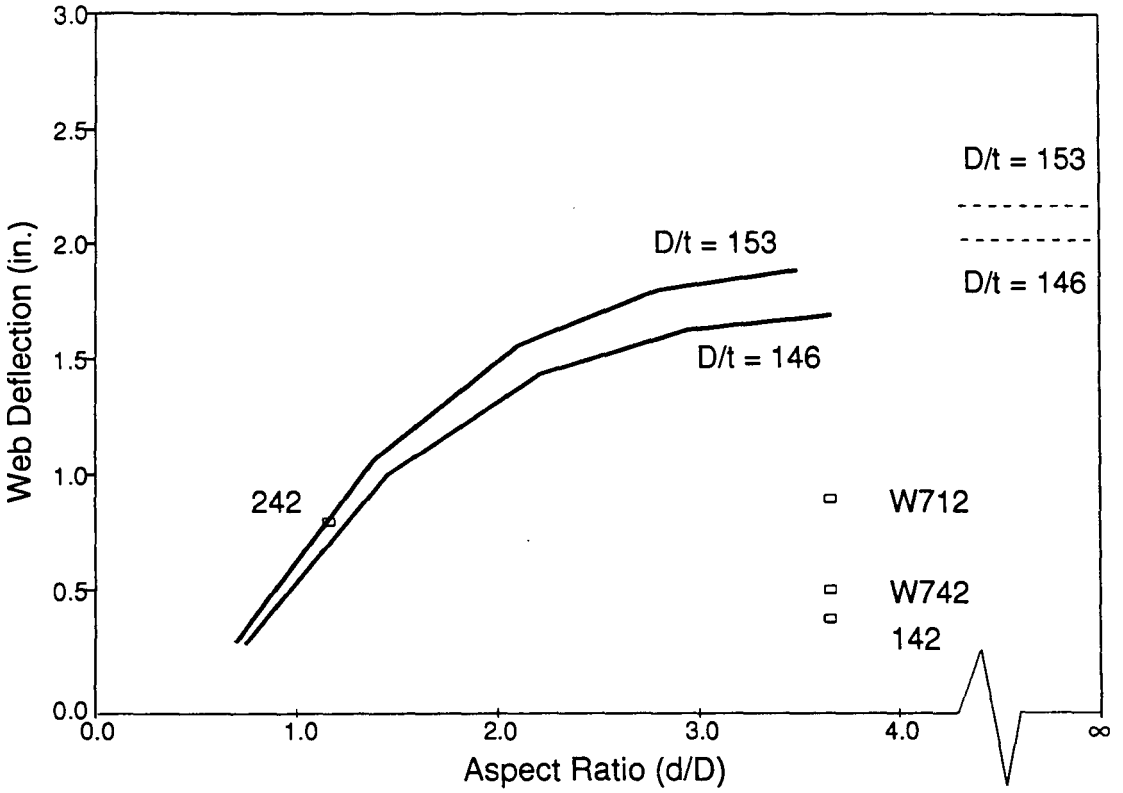

Fig. 7.6 Web Deflection and Panel Aspect Ratio

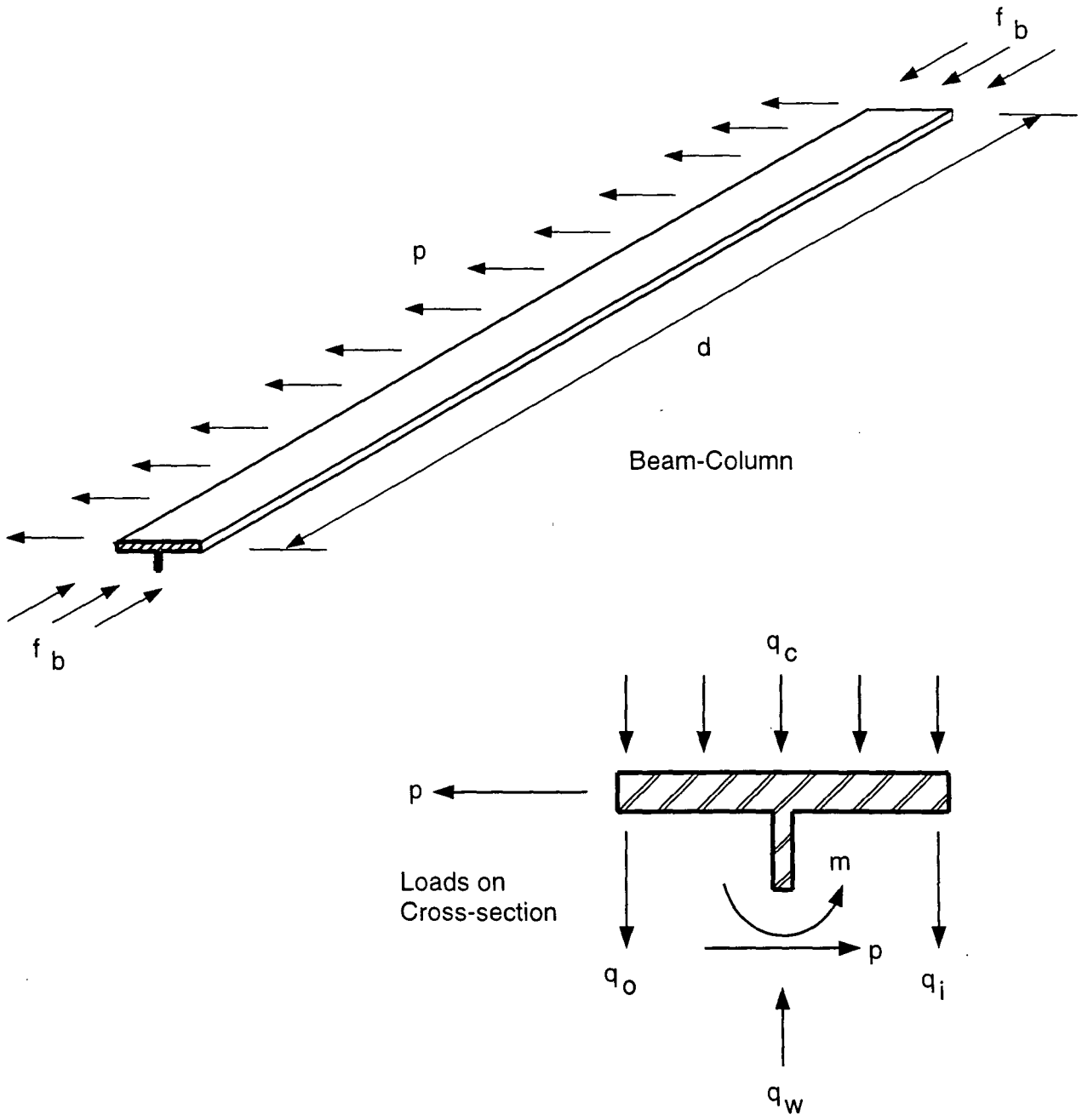

Fig. 7.7 Schematic of Compression Flange Beam-Column of Exterior Girder During Construction

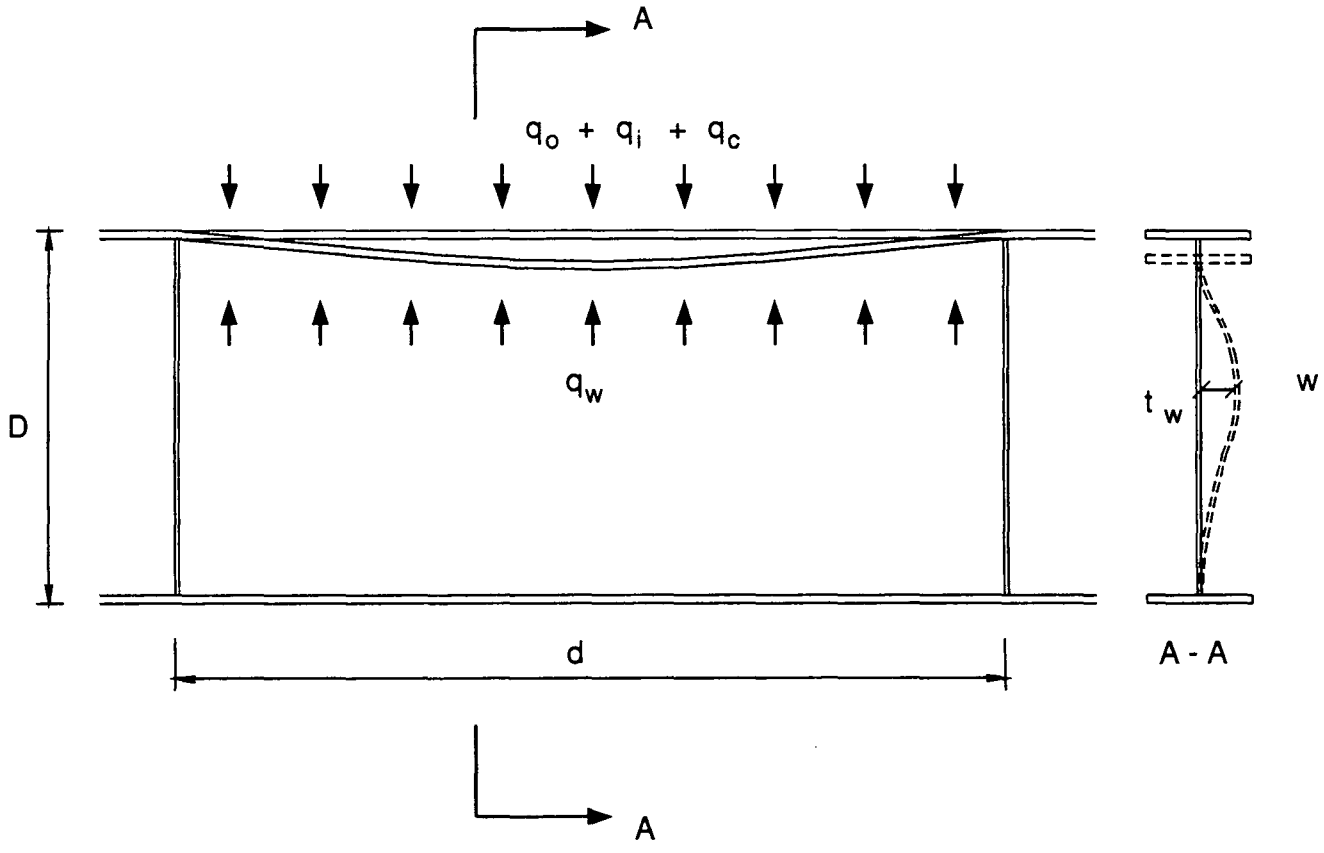

Fig. 7.8 Flange Bending and Web Deflection due to Vertical Loads

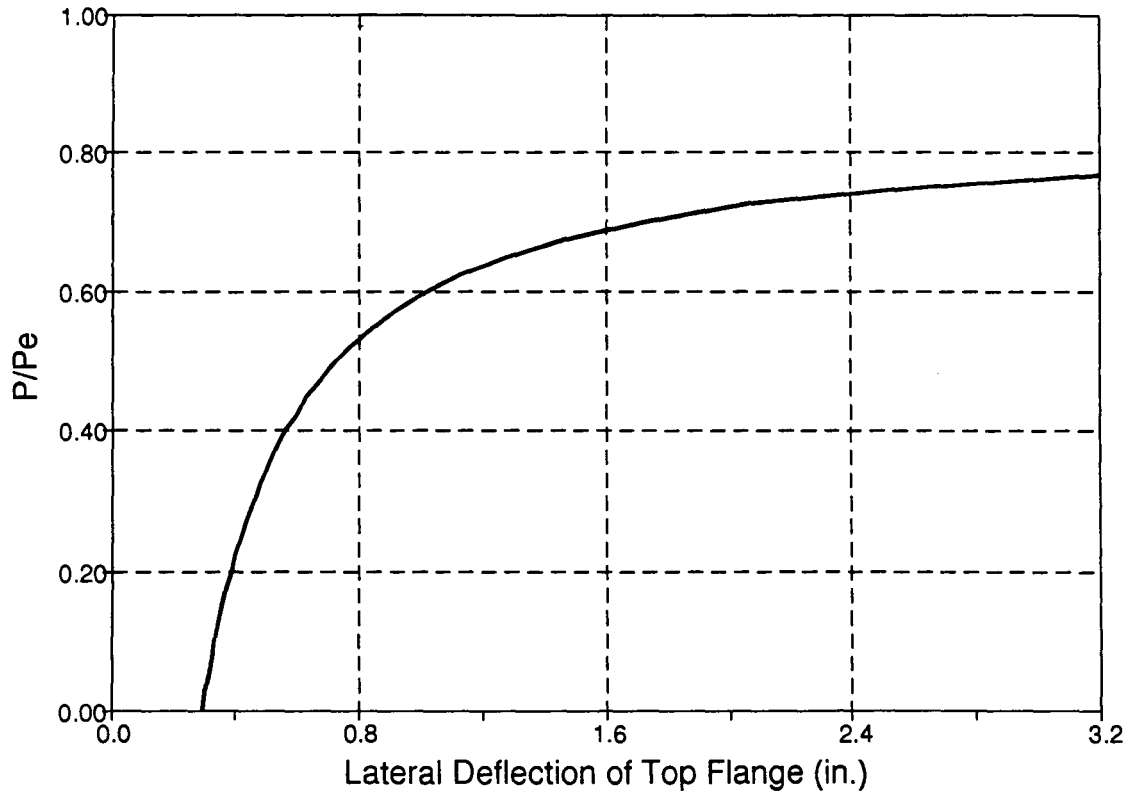

Fig. 7.9 Lateral Deflection of Top Flange as a Function of Normalized Buckling Load